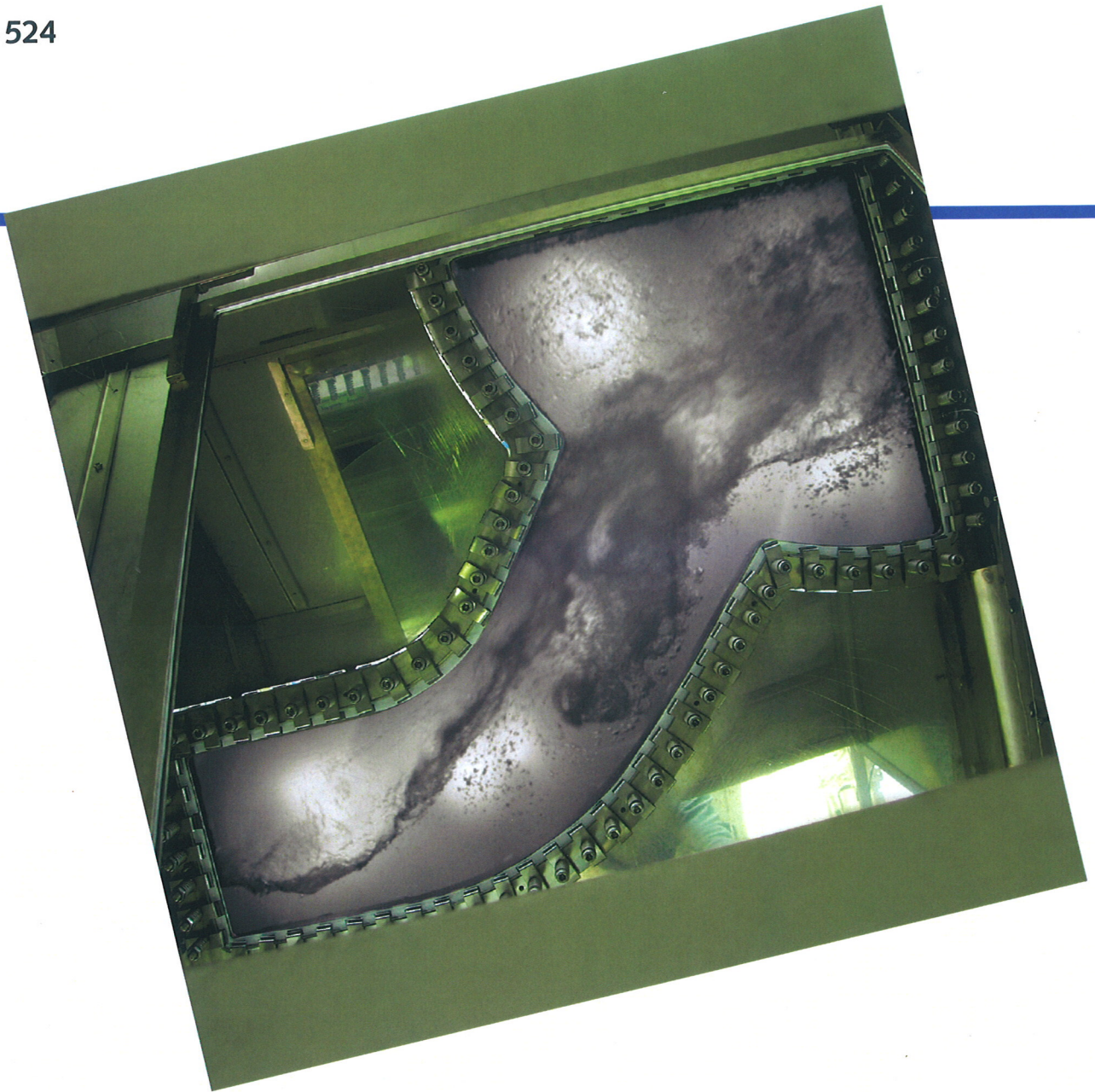


FZD-524



Wissenschaftlich - Technische Berichte
FZD-524 2009 · ISSN 1437-322X

ANNUAL REPORT 2008

INSTITUTE OF SAFETY RESEARCH



Forschungszentrum
Dresden Rossendorf

Wissenschaftlich-Technische Berichte
FZD-524
2009

Annual Report 2008

Institute of Safety Research

Editors:

Prof. Dr. rer. nat. Frank-Peter Weiss
Prof. Dr. rer. nat. habil. Udo Rindelhardt



Forschungszentrum
Dresden Rossendorf

Cover Picture: Steam/water flow in a model of the hot leg of a pressurised water reactor. Two-phase flow observed during the counter-current flow limitation of steam and water at 50 bar and 264°C. Photomontage of the test section with a high-speed camera picture of measurements performed at the TOPFLOW test facility.

Forschungszentrum Dresden - Rossendorf e.V.
Institut für Sicherheitsforschung

Postfach 51 01 19
D-01314 Dresden
Bundesrepublik Deutschland

Direktor	Prof. Dr. rer. nat. Frank-Peter Weiß
Telefon	+ 49 (3 51) 2 60 34 80
Telefax	+ 49 (3 51) 2 60 34 40
E-Mail	f.p.weiss@fzd.de
WWW	http://www.fzd.de/FWS

CONTENTS

Preface

Selected reports

Christophe Vallée, Tobias Seidel, Dirk Lucas, Matthias Beyer, Horst-Michael Prasser, Heiko Pietruske, Peter Schütz, and Helmar Carl Comparison of air/water and steam/water flooding experiments in a model of the hot leg of a PWR	3
Eckhard Krepper, Sören Alt, and Stefan Renger Influence of air entrainment on the liquid flow field caused by a plunging jet	10
Dana Veronica Danciu and Martin Schmidtke Empirical and numerical studies on gas entrainment by impinging jets	16
Marco Jose da Silva, Bartosz Matusiak, Krzysztof Grudzień, and Uwe Hampel Measurement of hydrodynamics in fixed beds with electrical capacitance tomography and capacitance wire mesh sensor	22
Christian Cierpka, Tom Weier, and Gunter Gerbeth Synchronized force and PIV measurements for active flow control by periodic electromagnetic forces on a NACA0015 profile – effects of excitation frequency	29
Frank Stefani, Gunter Gerbeth, Thomas Gundrum, Rainer Hollerbach, Janis Priede, Jacek Szklarsky, and Günther Rüdiger From PROMISE 1 to PROMISE 2: New experimental results on the helical magnetorotational instability	36
Andreas Cramer, Xiugang Zhang, and Gunter Gerbeth Thermoelectromagnetic convection – an alternative stirring technique in metallurgy	42
Sören Kliem, Yaroslav Kozmenkov, Siegfried Mittag, Ulrich Rohde, and Frank-Peter Weiss The influence of different thermal hydraulic models on the results of a DYN3D boron dilution transient calculation	48
Bruno Merk and Frank-Peter Weiß Analytical time dependent transport developments for the analysis of Accelerator Driven System (ADS) experiments	54
Siegfried Mittag and Sören Kliem Burning plutonium and minimizing radioactive waste in existing PWR	60
Frank Bergner, Uwe Birkenheuer, and Andreas Ulbricht Flux dependence of defect cluster formation in neutron irradiated weld materials	66

Matthias Werner, Eberhard Altstadt, Gerhard Brauer, Klaus Noack, and Reinhard Krause-Rehberg	
Finite element calculations for time-dependent thermal analysis of EPOS components	70
Cornelia Heintze, Carmen Recknagel, and Frank Bergner	
Nanoindentation of ion-irradiated Fe-Cr model alloys and ferritic/martensitic steels	76
Summaries of research activities	83
Accident Analysis of Nuclear Reactors	85
Materials and Components Safety	88
Thermal Fluid Dynamics of Multi-Phase Flows	90
Magneto-Hydrodynamics	93
Transient Two-Phase Flow Test Facility TOPFLOW	95
Publications	97
Publications in journals	99
Conference contributions and other oral presentations	108
Contributions to proceedings and other collected editions	125
FZD reports and other reports	138
Granted patents	142
PhD and diploma theses	143
Awards	145
Guests	146
Meetings and workshops	148
Seminars of the institute	149
Lecture courses	151
Departments of the institute	152
Personnel	153

Preface

The Institute of Safety Research (ISR) is one of the six Research Institutes of Forschungszentrum Dresden-Rossendorf e.V. (FZD), which is a member institution of the Wissenschaftsgemeinschaft Gottfried Wilhelm Leibniz (Leibnizgemeinschaft). Together with the Institutes of Radiochemistry and Radiation Physics, ISR implements the research programme „Nuclear Safety Research“, which is one of the three scientific programmes of FZD.

The research of ISR aims at assessing and enhancing the safety and efficiency of industrial plants and at improving the environmental sustainability of the processes involved. The applications are mainly related to nuclear power plants of present and future designs.

To achieve the goals mentioned, the institute performs research in nuclear reactor physics including transmutation of long lived waste, in thermal fluid dynamics including magneto-hydrodynamics (MHD), and in nuclear materials sciences. The different research projects we are dealing with, as well as our large scale thermal hydraulic test facility TOPFLOW (Transient Two-Phase Flow Test Facility) are listed in Table 1 together with the assignment to FZDs scientific programmes.

The activities in nuclear materials are related to the irradiation induced ageing of nuclear reactor components. The thermal fluid dynamics research work is essentially based on the experiments performed at the Transient Two-Phase Flow Test Facility, TOPFLOW. TOPFLOW is one of the large research and user facilities of FZD and represents the reference thermal hydraulic experiment of the so-called “German CFD (Computational Fluid Dynamics) Initiative” in nuclear reactor safety research. The development and validation of our reactor dynamics code DYN3D coupled to thermal hydraulic computation models for the safety analyses of current and future nuclear reactors is the decisive asset of our reactor physics portfolio. DYN3D became an integral part of the European software platform NURESIM for the numerical simulation of nuclear reactors. There are about 12 organisations using DYN3D in seven European countries and Russia.

By participating in the development and operation of the pulsed photo-neutron source at the radiation source ELBE (Electron linear accelerator for beams of high brilliance and low emittance), as well as in the interpretation of the measurements of neutron reaction cross sections with candidate materials for future nuclear reactors and with radioactive waste isotopes, we also contribute to the Transmutation project coordinated by the Institute of Radiation Physics. Beyond that, our Magneto-Hydrodynamics research is partly engaged in the “Advanced Materials” programme. There, it is devoted to the improvement of materials manufacturing technologies by optimising the involved flow processes of electrically conducting fluids through the application of external magnetic fields.

Table 1. Research projects and user facility of the Institute of Safety Research, 2008

Programme	Project / User Facility
Nuclear Safety Research	Accident Analysis of Nuclear Reactors
	Materials and Components Safety
	Thermal Fluid Dynamics of Multi-Phase Flows
	Magneto-Hydrodynamics
	Transmutation
	Transient Two-Phase Flow Test Facility TOPFLOW
Advanced Materials	Magneto-Hydrodynamics

Our work is financed through the basic funding of FZD, as well as by external funds from public research grants and from contracts with the industry. In 2008, 45 % (3.656 k€) of our total expenditure were covered by such external funds with 13 % from research grants of the Federal Government, 14 % originated from Deutsche Forschungsgemeinschaft, 6 % from the EU, and 12 % from research contracts mainly with the industry (see Fig.1). The deployment of the total budget on the different projects and the user facility TOPFLOW (see Table 1) is illustrated in Fig. 2.

Together with the Dresden Technical University, the Zittau University of Applied Sciences, and VKTA (Verein für Kernverfahrenstechnik und Analytik) Rossendorf, the ISR represents the East German Centre of Competence in Nuclear Technology (Kompetenzzentrum Ost für Kerntechnik) which in turn is a member of the German Alliance for Competence in Nuclear Technology (Kompetenzverbund Kerntechnik). As such, the ISR also takes care to keep and promote the expertise in nuclear engineering. For that end, a strategic partnership exists between Kompetenzzentrum Ost and Vattenfall Europe Nuclear Energy (VENE).

Beyond this, ISR in general cares for the next generation of young scientists by supervising PhD, Master, and Diploma students for example. The quality of the education at ISR is underlined by the prizes awarded to our PhD students. Christoph Vallée received a best paper award at the students competition of the 16th International Conference on Nuclear Engineering in Orlando, USA in 2008 for his presentation about new experiments on steam-water counter current flow limitation at the so called PWR hot leg experiment at TOPFLOW. Marco da Silva and Sebastian Thiele became best paper award winners at the 5th International Symposium on Process Tomography in Zakopane, Poland in 2008 for their paper on the development of a wire mesh sensor that is based on the measurement of the complex electrical impedance which allows flow measurements in mixtures of weakly electrically conducting fluids like oil and air.

Amongst the many excellent results obtained in 2008, some deserve particular reference.

Andreas Ulbricht and Frank Bergner studied the ageing of nuclear reactor pressure vessel (RPV) steels due to fast neutron irradiation. Relying on mechanical studies and small angle neutron scattering analyses they could show that the thermal annealing of aged RPV material leads to the dissolution of the irradiation induced microstructural defects and to an almost complete reconstitution of the former mechanical properties. Moreover, a lowered sensitivity to re-irradiation was observed. Additionally, they proved that different neutron fluxes resulted in different defect size distributions but in roughly the same integral volume content of irradiation induced defects at the same integral fluence. The underlying mechanism could be explained by rate theory modelling. The corresponding mechanical tests revealed no substantial difference in the fracture mechanical properties of the investigated materials exposed to the same integral fluence at different fluxes. This fact substantiated the hypothesis that the mechanical properties of the material under investigation are mainly determined by the integral volume content of the defects, whereas the defect sizes seem to be of minor influence. The systematic research and the results of far reaching consequence to the possible operational lifetime of nuclear reactor pressure vessels (see the related article in this report) were acknowledged with the Forschungspreis des Forschungszentrums Dresden-Rossendorf 2008.

Furthermore, I would like to highlight the Magneto-Hydrodynamics project of the ISR which forms a major part of the Collaborative Research Centre (SFB) 609 on “Electromagnetic flow

control in metallurgy, crystal growth, and electrochemistry". In autumn 2008, the German Science Foundation (DFG) decided to continue funding for another 4 years. This means a total funding period of 11 years for that innovative project pursued together with the Dresden Technical University as leading institution and other partners from research centres and universities in the vicinity of Dresden-Rossendorf.

Studies on the role of magnetic fields in astrophysics were also part of the former funding periods of SFB 609 as well as of a common project (Wettbewerbsprojekt der Leibnizgemeinschaft) of Astrophysikalisches Institut Potsdam (AIP) and the IRS. In the framework of all that, Frank Stefani (IRS) and Günther Rüdiger (AIP) succeeded in clarifying the role of magnetic fields in the creation of giant stars or black holes in the centre of cosmic accretion discs. For their pioneering work, they earned the highly prestigious "Society Needs Science 2008" award of the "Stifterverband für die Deutsche Wissenschaft" for their first experimental demonstration of the Magneto-Rotational Instability (MRI) effect in the PROMISE (Potsdam Rossendorf Magnetic Instability Experiment) experiment.

During the reporting period, the ISR organised important meetings and workshops with international participation, such as the international workshop on "Multi-Phase Flow: Simulation, Experiment and Application", which was jointly hosted by ISR and ANSYS/CFX[®], and which continues the series of meetings on that topic in Dresden-Rossendorf. Moreover, we organised the International Symposium on Computational Electro-Magneto-Hydro-Dynamics which was held in Venice, Italy.

Meetings such as these underline the national and international scientific reputation of the Institute of Safety Research.

In July 2008, the German Council of Science and Humanities (Deutscher Wissenschaftsrat) published its recommendations resulting from the evaluation of FZD in 2007. The evaluation report acknowledges the quality of the research at FZD and underlines the complexity and long term character of our research topics. Based on this assessment, the Council recommended that the FZD, presently being a Leibniz institute, should become a member of the Helmholtz Association. According to the present schedule, FZD will step into the Helmholtz Association at the beginning of 2011.

I would like to thank all staff members of the institute for their high quality work and for making the year 2009 another successful one for ISR.



F.-P. Weiß

Rossendorf, 7 April 2009

Fig. 1: Funding sources 2008

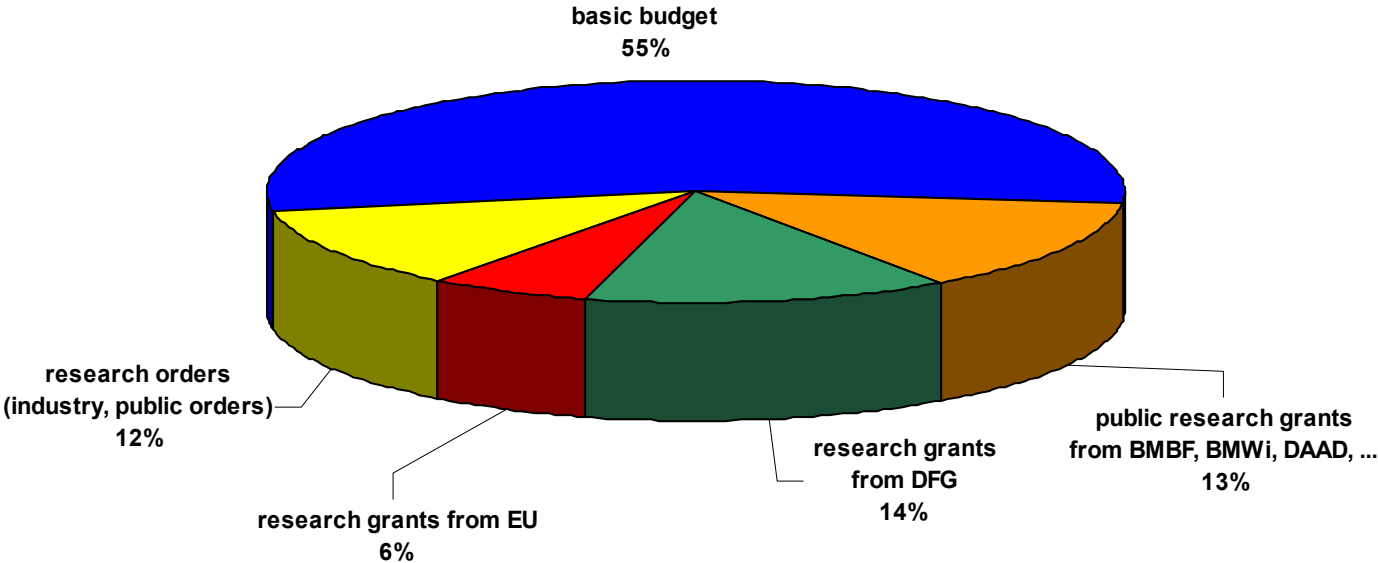
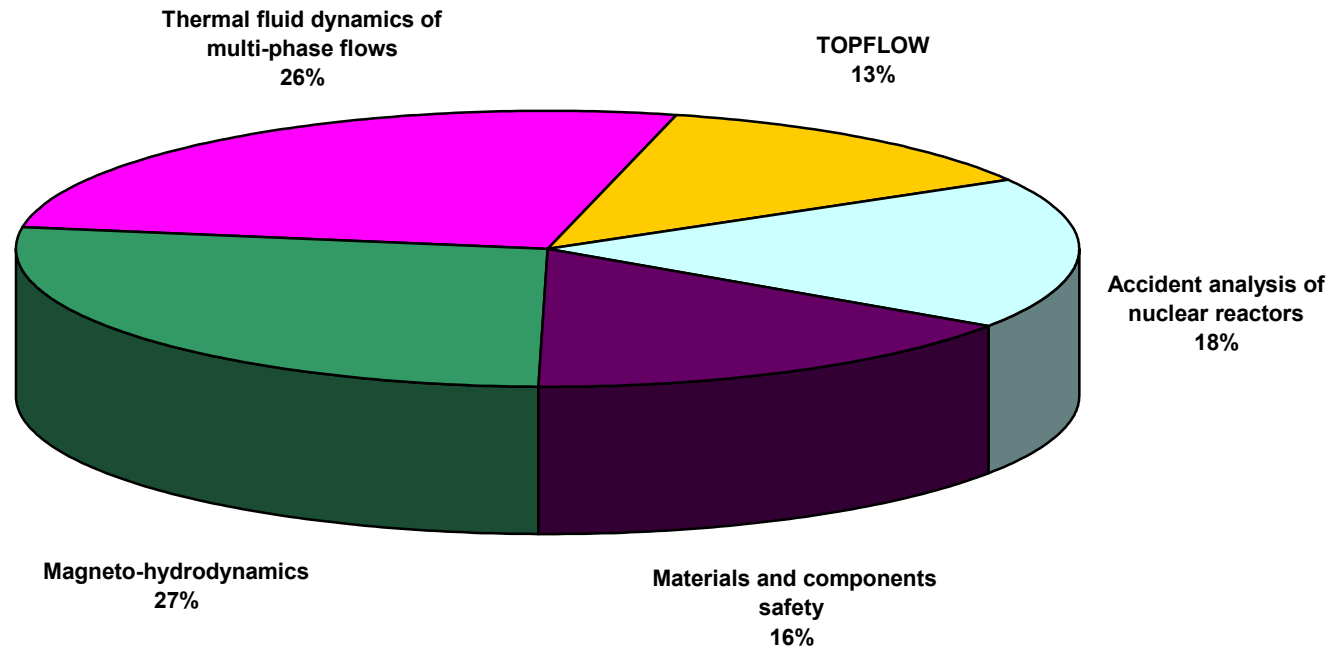


Fig. 2: Deployment of funding on the projects and user facilities 2008



Selected reports

COMPARISON OF AIR/WATER AND STEAM/WATER FLOODING EXPERIMENTS IN A MODEL OF THE HOT LEG OF A PWR

Christophe Vallée, Tobias Seidel, Dirk Lucas, Matthias Beyer, Horst-Michael Prasser¹, Heiko Pietruske, Peter Schütz, and Helmar Carl

1. Introduction

In pressurised water reactors (PWR), different scenarios of small break Loss Of Coolant Accident (LOCA) lead to the reflux-condenser mode in which steam enters the hot leg from the reactor pressure vessel (RPV) and condenses in the steam generator. A part of the condensate flows back towards the RPV in counter current to the steam. During the reflux-condenser mode, a counter-current flow limitation (CCFL) should be prevented because this might affect the core cooling. The simulation of CCFL conditions, which is dominated by 3D effects, requires the use of computational fluid dynamics (CFD) methods. These methods are not yet mature for two-phase flows and have to be validated before they can be applied to nuclear reactor safety. Therefore, dedicated experimental data is needed with high resolution in space and time.

In order to investigate the two-phase flow behaviour in a complex reactor-typical geometry and to supply suitable data for CFD code validation, a model of the hot leg of a pressurised water reactor (PWR) was built at Forschungszentrum Dresden-Rossendorf (FZD). Counter-current flow limitation (CCFL) experiments were performed with air and water at room temperature and pressures up to 3.0 bar as well as with steam and water at pressures up to 50 bar and the corresponding saturation temperature of 264°C. One selected 50 bar experiment is presented here. High-speed camera images are shown as well as the flooding curves obtained from the different experimental runs in terms of the Wallis parameter, which is commonly used in the literature. However, using this non-dimensional parameter, a discrepancy is observed between the air/water experiment on one hand and the steam/water experiments on the other hand. Therefore, a modified Wallis parameter is proposed, which takes into account the effect of the fluid viscosities on the CCFL.

2. The hot leg model

The hot leg model (Figures 1 and 2) is devoted to optical measurement techniques. Therefore, a flat test section design was chosen with a width of 50 mm. The test section outlines represent the hot leg of the German *Konvoi* PWR at a scale of 1:3, which corresponds to a channel height of 250 mm in the straight part of the hot leg. The test section is mounted between two separators, one simulating the reactor pressure vessel (RPV) and the other is connected to the steam generator (SG) inlet chamber. This allows to perform co-current as well as counter-current flow experiments. Moreover, the hot leg model is installed in the pressure vessel of the TOPFLOW facility of FZD (Figure 2), which is used to perform high-pressure experiments under pressure equilibrium with the inside atmosphere of the vessel. Therefore, the test section can be designed with thin materials and equipped with large windows like in the hot leg model. The presented two-phase flow experiments focus on the flow structure occurring in the region of the riser and of the steam generator inlet chamber during counter-current flow before and around the onset of flooding.

¹ ETH Zürich, Department of Mechanical and Process Engineering, Zürich (Switzerland)

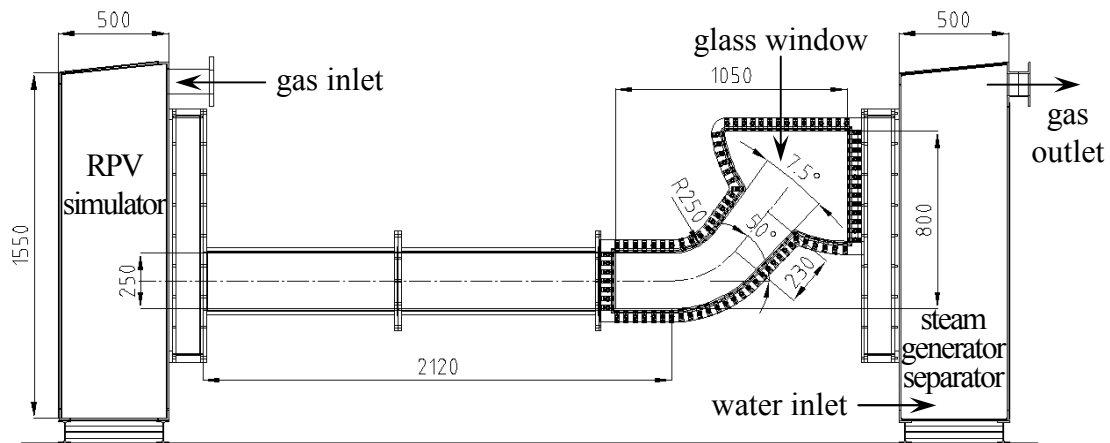


Fig. 1: Schematic view of the hot leg model test section (dimension in mm)

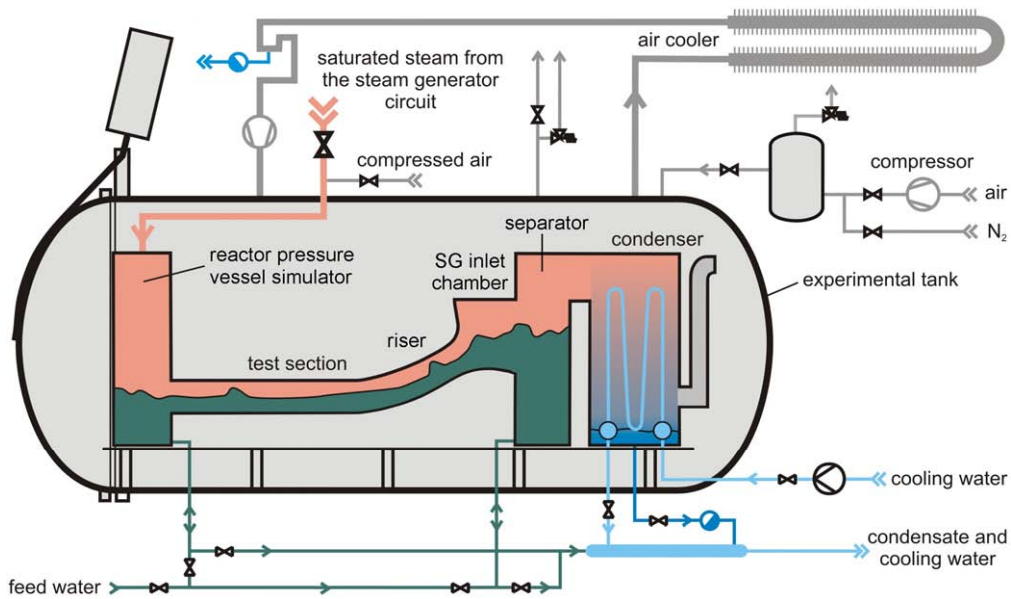


Fig. 2: Schematic view of the experimental apparatus

3. Experiments and results

3.1. Experimental procedures and phenomenological analysis of a typical experiment

During the experiments, a constant water flow rate was injected into the SG separator, while the gas flow rate injected into the RPV simulator was stepwise increased to reach the flooding conditions. Global parameters were measured, including the injected flow rates of gas and water, the system pressure, the water levels inside both separators, and the pressure drop over the test section. These signals were acquired at 1 Hz on a PC and synchronised with a high-speed video camera for visual observations of the flow structure. One of the experiments was chosen here to describe the observed phenomena and to explain the methodology used to analyse the measured data. This run was performed at the following boundary conditions: a system pressure of 50.0 bar, a temperature of about 262°C, and a water flow rate of 0.72 kg/s. The analysis of the evolution of the global parameters over time (Figure 3) allows to characterise the flow behaviour. Especially the water levels measured in the separators and the pressure difference between them give indication of the flow regime. Furthermore, the increase of the water level in the RPV simulator allows to measure the water flow rate

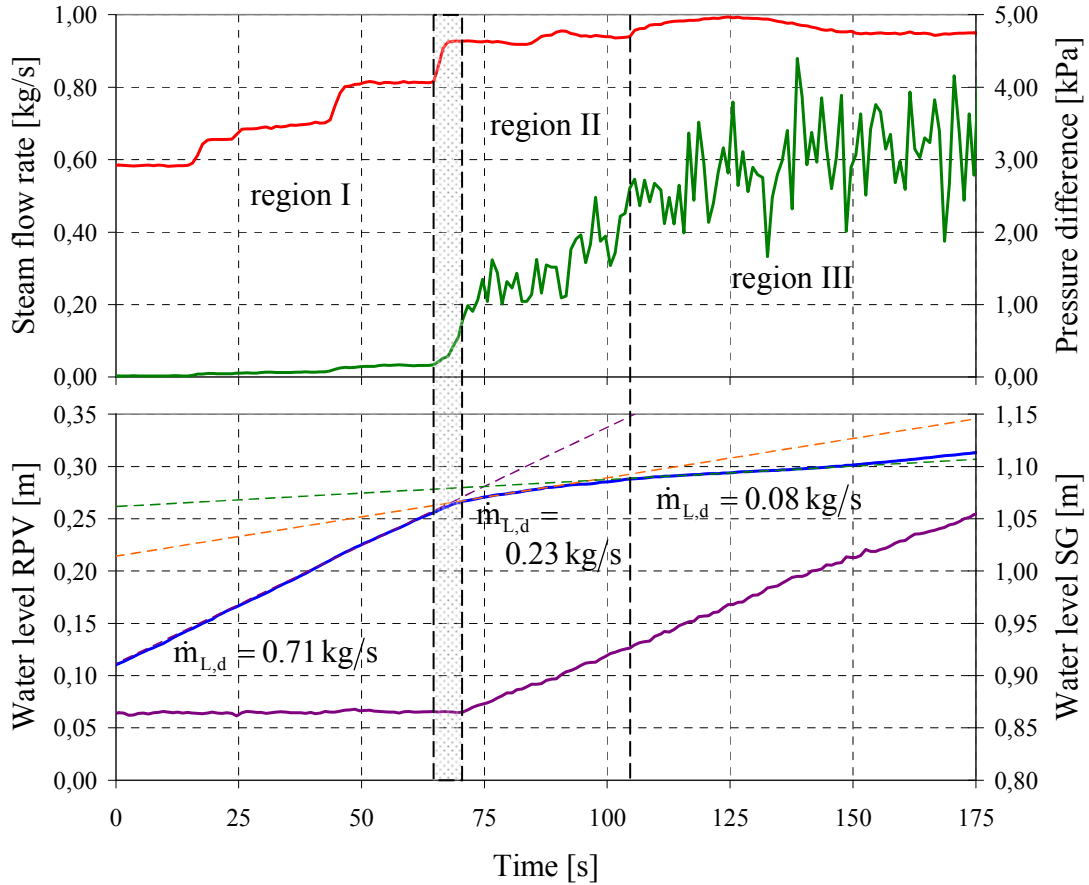


Fig. 3: Steam mass flow rate (top diagram, red curve), pressure drop over the test section (top diagram, green curve), water level in the RPV simulator (bottom diagram, blue curve) and in the SG separator (bottom diagram, purple curve) during the CCFL experiment at 50 bar

streaming through the test section (discharge flow). This indicates the onset of flooding and the intensity of the counter-current flow limitation. Therefore, linear interpolation lines were added to the measured water level in Figure 3. Based on the trend indicated by these lines, the experiment was divided into 3 regions:

I. For a steam flow rate lower than 0.82 kg/s ($t < 65$ s), the water level in the SG separator is constant and the slope of the water level increase in the RPV simulator corresponds to a water flow rate of 0.71 kg/s, which is very close to the injected mass flow rate. This indicates a stable counter-current flow, confirmed by the camera images (Figure 4-a), which is characterised by a constant and very low pressure drop over the test section (< 0.2 kPa).

II. At $t = 65$ s, the steam flow rate is increased to about 0.94 kg/s (± 0.02). Immediately, the pressure difference between the separators increases, indicating the beginning of the counter-current flow limitation. With a delay of about 5 s, the slope of the water level in the RPV simulator decreases to a discharge water flow of 0.23 kg/s. Consequently, the water level in the SG separator increases significantly. Furthermore, the pressure difference between the separators becomes unstable and fluctuates between 1 and 2.5 kPa due to the slugs generated in the hot leg (Figure 4-b).

III. For $105 < t < 150$ s, the steam flow rate is slowly increased to values up to 0.99 kg/s. This further reduces the discharge water flow to a minimum of 0.08 kg/s and the pressure drop over the test section increases up to values higher than 4 kPa. The camera pictures (Figure 4-c) reveal a highly mixed two-phase flow: big slugs are observed which flow up the riser and transport water into the SG separator where it accumulates.

The slight decrease of the steam flow rate at the end of the experiment leads to a decreasing CCFL intensity after $t = 150$ s, which is similar to the processes observed during deflooding experiments. The flow conditions described here are similar to those observed during the air/water experiments reported in Deendarlianto et al. (2008).

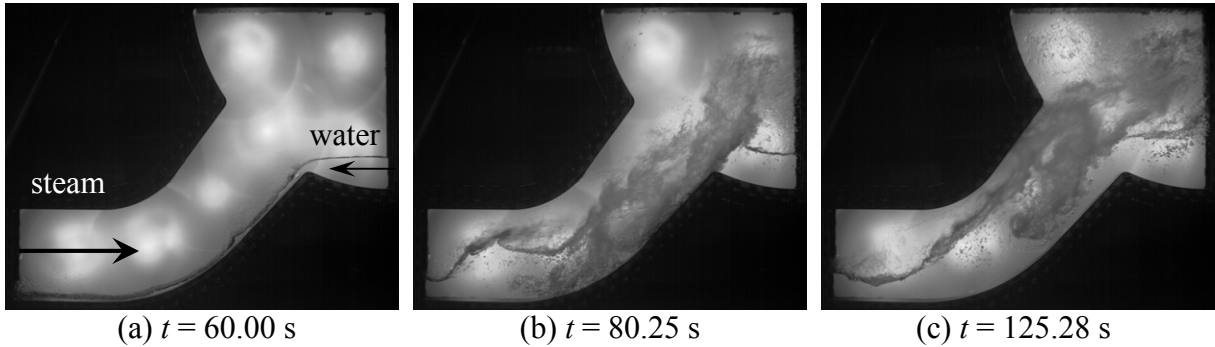


Fig. 4: Flow behaviour during steam/water counter-current flow at $\dot{m}_L = 0.72$ kg/s and $p = 50.0$ bar

3.2. Flooding characteristics of the hot leg model

The plot of the gas flow rate versus the discharge water flow rate during CCFL is called the flooding characteristics. In order to automatise the arrangement of the flooding diagram, a data treatment routine was developed. This includes a low-pass filter for the calculation of the water level gradient in the RPV simulator in order to obtain the discharge water flow rate. Finally, only the quasi-stationary points obtained after the onset of flooding were selected for the flooding curve. Commonly, the results of CCFL experiments are presented in terms of the non-dimensional superficial velocity J_i^* (also called Wallis parameter) For the phase i , this was defined by Wallis & Dobson (1973) for near horizontal channels with rectangular cross-section as follows:

$$J_i^* = j_i \cdot \sqrt{\frac{1}{g \cdot H} \cdot \frac{\rho_i}{\rho_L - \rho_G}} \quad (1)$$

where j is the superficial velocity and ρ the density of the fluid (indicated by L for the liquid and G for the gas), g the gravitational acceleration and H the height of the channel. The Wallis parameter takes into account the effect of the pressure on the fluid densities. In the past, the Wallis parameter was used by many researchers to correlate CCFL data obtained in hot leg typical geometries (i.e. a horizontal tube connected to a riser): among others Richter et al. (1978) and Ohnuki (1986) who performed experiments at reduced scales, as well as Weiss & Hertlein (1988) who published results obtained at original power plant scale in the Upper Plenum Test Facility (UPTF).

For all the experiments (see details in Table 1), the points belonging to the flooding curve were plotted in terms of the Wallis parameter in Figure 5. The figure shows the typical decreasing trend of the experimental points, indicating that after the onset of flooding an increase of the gas flow rate induces a decrease of the discharge water flow rate. Furthermore, Figure 5-a reveals a clear separation between the air/water experiments on one hand and steam/water experiments on the other hand. The zero penetration point (interception of the flooding curve with the ordinate axis) occurs at higher non-dimensional gas superficial velocities for the steam/water experiments compared to the air/water experiments.

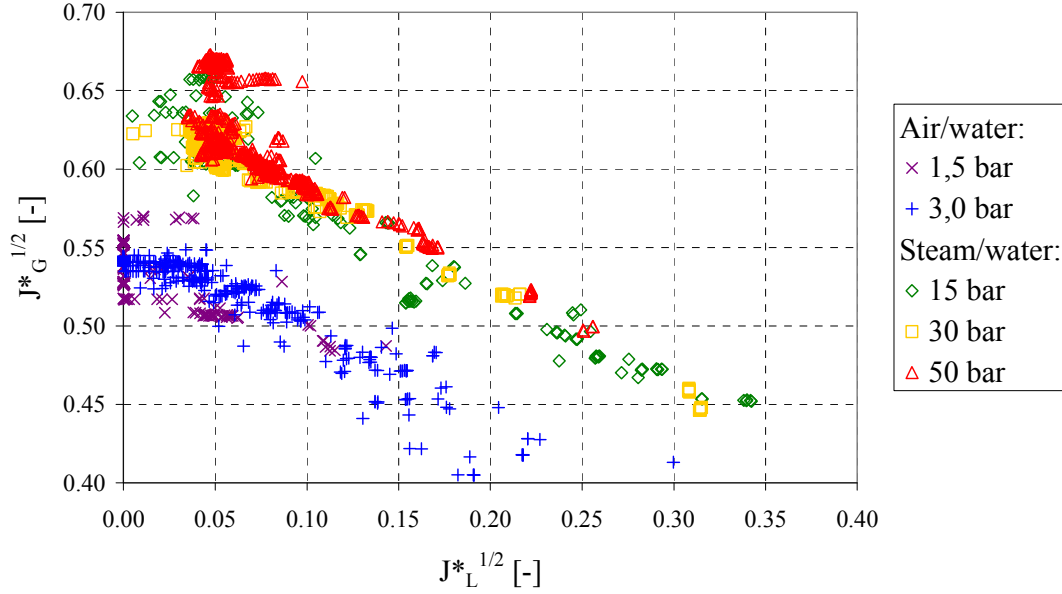


Fig. 5: Flooding characteristics of the hot leg model plotted in terms of the Wallis parameter

Table 1: Overview on the CCFL experiments

Gas [-]	Air	Air	Steam	Steam	Steam	Total number
Pressure [bar]	1.5	3.0	15.0	30.0	50.0	of runs
Temperature [°C]	18-24	18-24	197	232	262	[-]
Flooding runs	5	7	3	2	4	21
Deflooding runs	1	8	3	2	2	16

3.3. Proposition of a viscosity correction term for the Wallis parameter

As shown in the previous sections, our flooding data could not be described with one single correlation while using the classical Wallis parameter. One possible reason explaining this discrepancy between the air/water experiments on one hand and steam/water experiments on the other hand could be an overestimation of the real steam flow rate due to condensation. However, this would mean that about 30% of the measured steam mass flow rate (i.e. about 0.3 kg/s at 50 bar) have condensed before arriving to the test section. Such a condensation amount can be excluded because during other experimental series, steam flow rates down to 0.075 kg/s were injected and steam also reached the test section.

Therefore, the effect should be of physical nature and a non-dimensional group may be found to correlate the data and explain this discrepancy. From a dimensional analysis of the fluid properties, it was found that apart from the gas density, the viscosity of the liquid water varies significantly with the boundary conditions: from 1.0×10^{-4} Pa·s at 264°C to 1.2×10^{-3} Pa·s at 13°C. Since the Wallis parameter does not include the viscosity, different other non-dimensional parameters containing it (like the Reynolds and Ohnesorge number) or combinations of these parameters were tested, without success. Finally, a dynamic viscosity ratio correction term was multiplied with the Wallis parameter as follows:

$$X_i^* = J_i^* \cdot \left(\frac{\mu_i}{\mu_k} \right)^n \quad \text{with } k \neq i \quad (2)$$

The exponent n was determined empirically in order to best correlate the data to $-0,2$. The result shown in Figure 6 demonstrates that with this correction term, a good correlation can be achieved between the low pressure air/water experiments and the high-pressure steam/water experiments. No comparable experiments performed in one and the same facility were published in the past. Only experiments at atmospheric pressure conditions for both fluid combinations were found (e.g. Ohnuki, 1986), where the viscosity varies only over a factor of about 3. Because the flooding characteristics depend also strongly on the test section geometry, the effect of the viscosity of the liquid water on the counter-current flow limitation was not isolated in such details before.

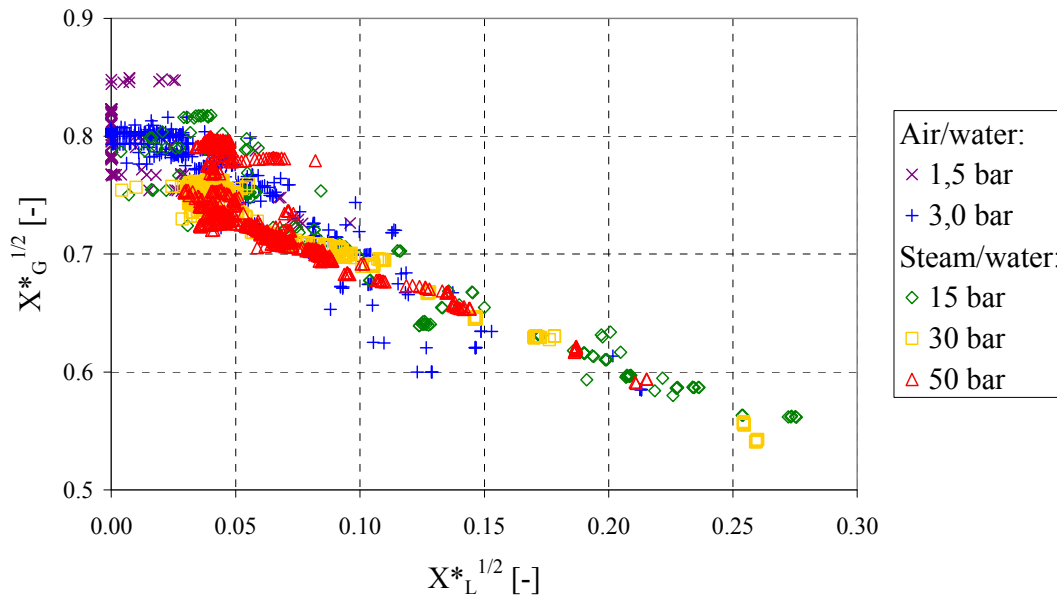


Fig. 6: Flooding characteristics of the hot leg model plotted in terms of the modified Wallis parameter

4. Summary and conclusions

The counter-current flow limitation was investigated in a flat model of the hot leg of a pressurised water reactor. Experiments were performed with air and water at low pressure and room temperature and with steam and saturated water at reactor typical pressure conditions. As an example, one experiment was presented and analysed. High-speed video observations show that the flow structures observed during flooding do not differ qualitatively between both series of experiments.

Furthermore, a numerical data processing method was developed and the resulting flooding curves were plotted in terms of the classical Wallis parameter. Using this non-dimensional parameter, the flooding was obtained at higher non-dimensional gas superficial velocities with steam and water compared to the air/water experiments. In order to explain this discrepancy, a correction term for the Wallis parameter is proposed, which takes into account the effect of the fluid viscosities on the flooding. This parameter allowed a good correlation between the experiments performed at 5 different pressure levels ranging from 1.5 to 50 bar and temperatures of 18 to 264°C.

The higher gaseous Wallis parameter needed to reach flooding with steam and water compared to air and water indicates that the correlations currently implemented in the one dimensional system codes like RELAP5, principally based on air/water experimental data, are

conservative. Therefore, the found discrepancies show that the safety margin before flooding taken into account in the actual reactor safety analyses is probably bigger than intended.

References

- [1] Deendarlianto, C. Vallée, D. Lucas, M. Beyer, H. Pietruske, H. Carl (2008). Experimental study on the air/water counter-current flow limitation in a model of the hot leg of a pressurised water reactor. *Nuclear Engineering and Design* 238/12, 3389-3402.
- [2] G. B. Wallis & J. E. Dobson (1973). The onset of slugging in horizontal stratified air-water flow. *Int. J of Multiphase Flow* 1, 173-193.
- [3] H. J. Richter, G. B. Wallis, K. H. Carter, S. L. Murphy (1978). Deentrainment and counter-current air-water flow in a model PWR hot leg. NRC-0193-9.
- [4] A. Ohnuki (1986). Experimental study of counter-current two-phase flow in horizontal tube connected to inclined riser. *Journal of Nuclear Science and Technology*, 23/3, 219-232.
- [5] P. A. Weiss & R. J. Hertlein (1988). UPTF test results: First three separate effect tests. *Nuclear Engineering and Design* 108/1-2, 249-263.
- [6] H. Y. Kim & H. C. No (2002). Assessment of RELAP5/MOD3.2.2 γ against flooding database in horizontal-to-inclined pipes. *Annals of Nuclear Energy* 29, 835-850.

Acknowledgments

This work is carried out in the frame of a current research project funded by the German Federal Ministry of Economics and Technology, project number 150 1329.

The authors would like to thank the TOPFLOW team for their work on the test facility and the preparation of the experiments, by name Klaus Lindner, Heiko Rußig, Marko Tamme and Steffen Weichelt.

INFLUENCE OF AIR ENTRAINMENT ON THE LIQUID FLOW FIELD CAUSED BY A PLUNGING JET

Eckhard Krepper, Sören Alt¹, and Stefan Renger¹

1. Introduction

The paper presents the role of plunging jets in the context of the strainer clogging issue. During a LOCA debris of thermal insulation might be released near the break. Fractions of the released insulation fibers can be transported into the reactor sump, where they may block the sump sieves and perturb the emergency core cooling systems. According to the considered scenario, the water ejected by the anticipated break falls several meters on to the sump water surface. On its way, the jet is mixed with air. Furthermore, air bubbles are entrained by the impinging jet below the water surface. The entrained gaseous bubbles will rise and have an additional influence on the flow field. The jet-induced flow sensitively influences the fiber transport.

2. Basic investigations of the plunging jet

To investigate the influence of a plunging jet on the water flow field, experiments were performed in a Plexiglas tank of about 1*1*1 m at the University of Applied Sciences Zittau/Görlitz. High-speed video techniques enable the measurement of the bubble entrainment plume. For the presented CFD model approach, the phenomenon of the air entrainment by the jet was not modeled but, given as boundary condition. The focus of the presented calculations emphasizes the influence of the entrained gas on the liquid flow field. Correlations on gas entrainment at a plunging jet were published by different authors, e.g. by Bin (1993).

For the parameters in the range of interest here, Bin calculates the volume flow rate of entrained air Q_G as

$$Q_G = 0.04Q_W Fr^{0.28} \left(\frac{H}{d_{OF}} \right)^{0.4} \quad (1)$$

where Fr is the Froude number defined by

$$Fr = \frac{V_{OF}^2}{gd_{OF}} \quad (2)$$

The penetration depth is estimated as:

$$Z_{Bin} = 0.42V_{OF}^{4/3} d_{OF} Q_G^{-1/4} \quad (3)$$

Q_W is the water volume flow, H the distance of the jet outlet nozzle from the tank surface, d_{OF} the impact diameter of the jet and V_{OF} the jet velocity at the water surface. Q_G is the volume flow rate of entrained gaseous bubbles. Assuming a jet impact velocity of 3 m/s and an impingement diameter on the surface of 0.05 m, the volumetric flow rate of entrained air, Q_G , calculated according to equation (1) amounts to $0.2Q_W$. The corresponding maximum gas penetration depth was calculated by equation (3) to be in the range of 0.5 m.

¹ University of Applied Sciences Zittau/Görlitz

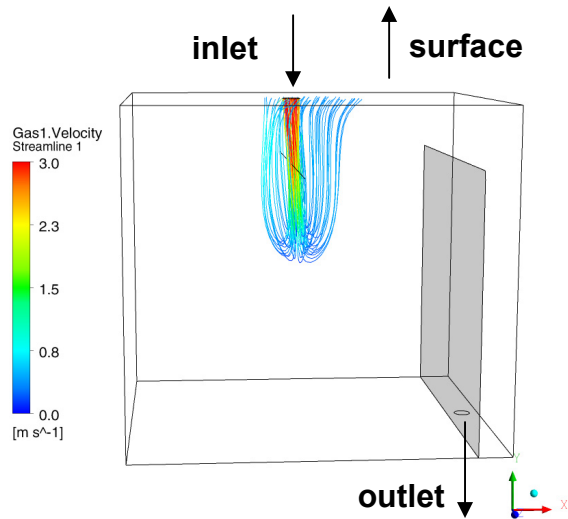


Fig. 1: CFD simulation of the jet experiment

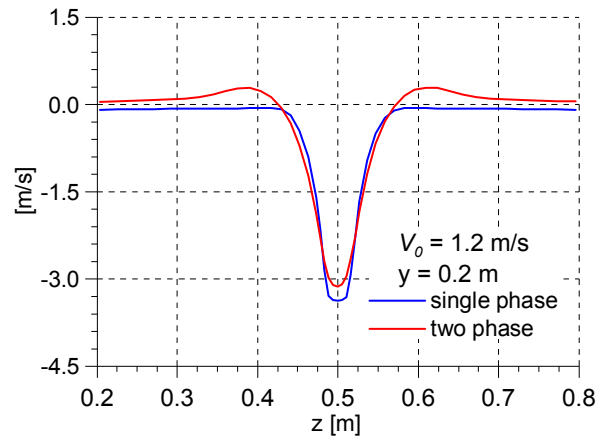


Fig. 2: Influence of the air entrainment on the liquid velocity profile

Fig. 1 gives a sketch of the situation calculated by the CFD code. In the 3D simulation using a grid of 120000 cells, an Euler/Eulerian approach was applied. The liquid phase was simulated using a shear stress turbulence model. For the gaseous phase, a bubble diameter of 4 mm was assumed. In the momentum exchange between the phases the drag force, the turbulent dispersion force and the lift force were considered. The water and gas velocity and the gas volume fraction α at the inlet were set as a boundary condition. The injected amount of water is drained via the outlet at the bottom. The gas leaves the tank via the surface of the tank. Fig 1 shows the gas streamlines of the calculated gas velocity field.

The maximum gas penetration depth of ca. 0.5 m predicted by eq. (3) is confirmed by the CFD calculations. Fig. 2 presents profiles of the vertical liquid velocity in a depth of 0.2 m (marked in Fig. 1). For the cases without and with air entrainment, the influence of the gas entrainment on the liquid velocity field near the jet can be seen. The entrained bubbles near the jet rise and reduce the water velocities.

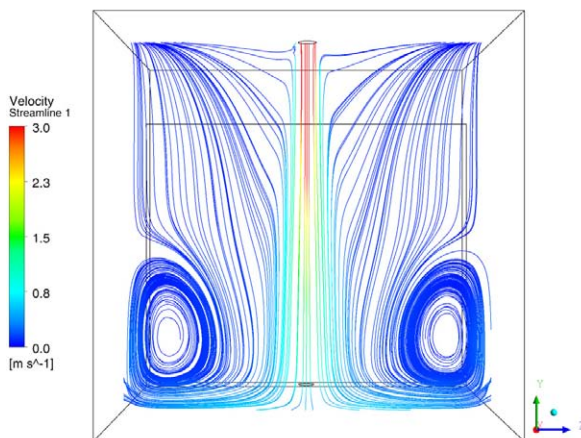


Fig. 3: Water streamlines neglecting the air entrainment

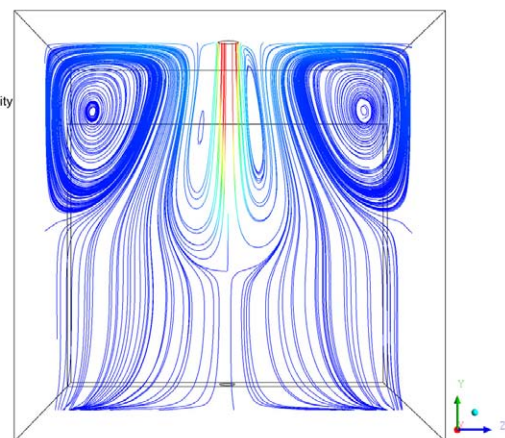


Fig. 4: Water streamlines considering the air entrainment

This phenomenon influences the water flow field in the whole tank. Figures 3 and 4 show the water streamlines projected on a middle plane. In the single-phase case (Fig. 3), two vortices emerge near the bottom. In the two-phase case (Fig. 4), the rising air bubbles move the water upward. The vortices are shifted upward and point in the direction opposite to the one phase situation.

3. Flow phenomena in a 6 m pool

3.1. Influence on the water field

The gas entrainment of the impinging jet even influences the flow field observed in a larger pool having the dimensions equivalent to containment sump geometries. The experiments referred to were performed at the “Zittauer Strömungswanne” (length of 6 m, a depth of 1 m and a water height of 2.6 m) at the University of Applied sciences in Zittau.

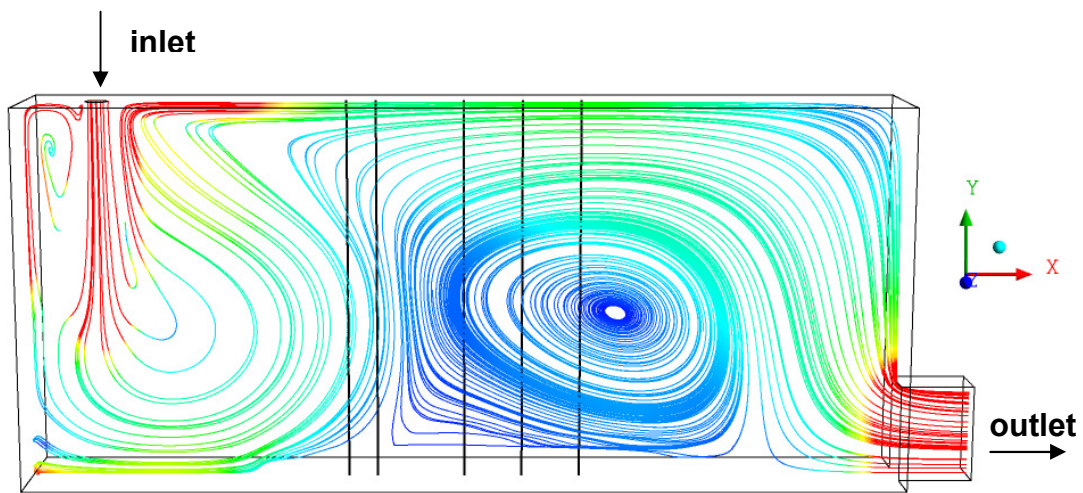


Fig. 5: Water streamlines projected on a middle plane. The black lines mark the measurement position of the water profiles of horizontal velocity (see Fig. 6)

For the 3D simulation, a grid of about 750000 cells and the same model options were applied as in the investigations presented in section 2. The water jet was injected at the marked inlet position at the upper left side. Leaving a tube with 3 m/s the jet has a velocity of ca. $V_{OF} = 5$ m/s at the water surface. The jet diameter at the water surface was assumed to be 0.15 m. In the calculations where air entrainment was considered, a gas volume fraction of $Q_G / (Q_W + Q_G)$ at the inlet of about 0.2 was applied. The water is drained at the lower right side. Air moves into the pool down to a depth of 1.7 m, rises again and degasses via the water surface. Fig. 5 shows the resulting flow field represented by water streamlines projected on a mid-plane. A large swirl was established, which rotated in the clockwise direction.

During the experiments, the horizontal velocity (x-direction) was measured by a vane wheel at different positions marked by the lines in Fig. 5. The measured und calculated vertical profiles are compared in Fig. 6. Whereas in the lower region a backward flow is seen, in the upper regions a positive flow was found towards the drain outlet, which was of the same order of magnitude as in the calculations. The occurrence of the large clockwise rotating swirl was clearly reflected by the calculations. Small differences in the profiles might be caused by an insufficient reproduction of the location of the swirl centre.

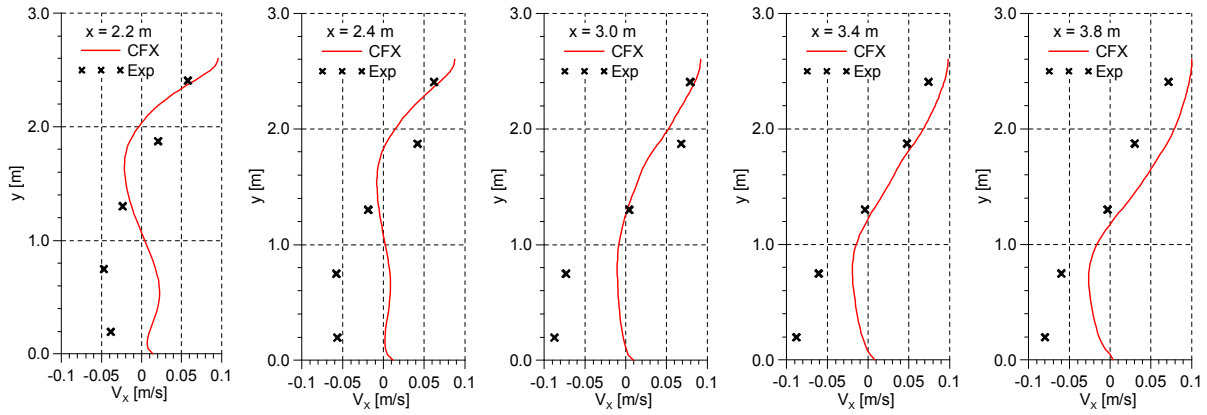


Fig. 6: Measured and calculated profiles of horizontal water velocity at different positions (compare Fig. 5)

In Fig. 6 the influence of the jet velocity on the establishment of the large swirl direction was investigated by experiments. Whereas for jet velocities lower than 1.5 m/s a swirl in counter clockwise direction was determined, for higher jet velocities the swirl in clockwise direction was found.

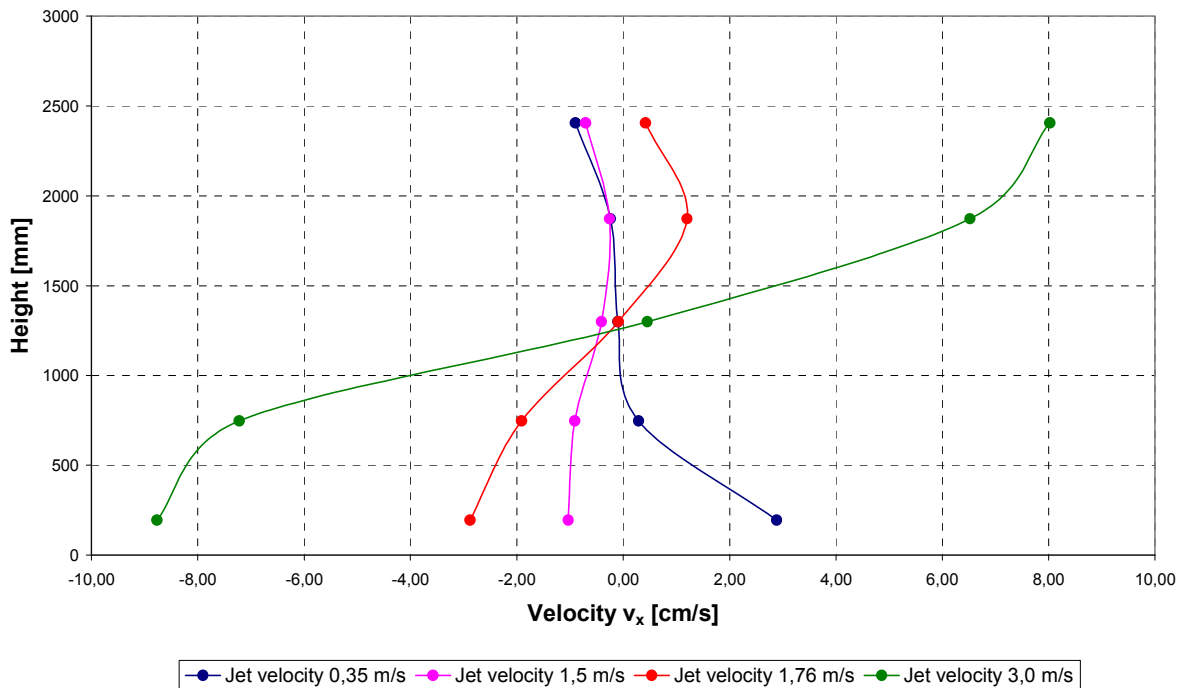


Fig. 7: Measured horizontal water velocity at different heights at the position $x = 3.0$ m for different jet velocities

3.2. Effect on the fiber transport

CFD calculations also reveal the consequences of air entrainment upon the fiber transport. About 1.6 kg fibers were added to the jet injection over a certain period of time (between 5 and 35 s in the simulations described here). The fibers were modeled as a dispersed phase of

virtual particles as described by Krepper et al. (2008). The water swirl moves the injected fibers backward to the region just below the plunging point. Large amounts of fibers are accumulated in the swirl and hold in the pool before they reach the outlet (see Fig. 8a). This behavior however depends on the flow situation. A different flow picture is found with a lower water injection velocity V_{OF} of only 1.5 m/s, presented in Fig. 8b). For this case, the gas volume fraction at the inlet was set to 0.1 instead of 0.2 as for the 5 m/s case. The same integral fiber mass was injected for the same time period. In this case, the entrained air reaches a depth of only 0.7 compared to 1.7 m in the case of 8a). The large water swirl now rotates in the counter clock direction. The fibers move directly to the outlet.

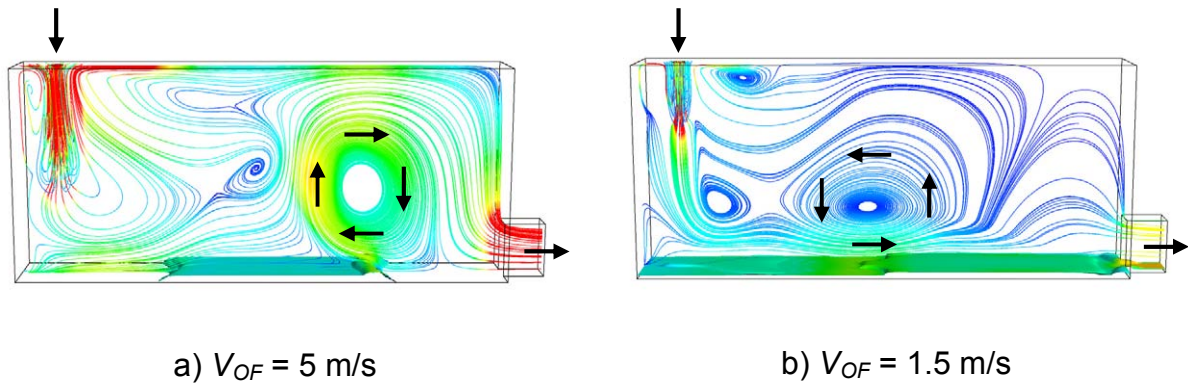


Fig. 8: Water streamlines projected on a middle plane for different jet inlet velocity V_{OF} . Deposited fibers at the bottom of the pool are shown as isosurface of the fiber phase

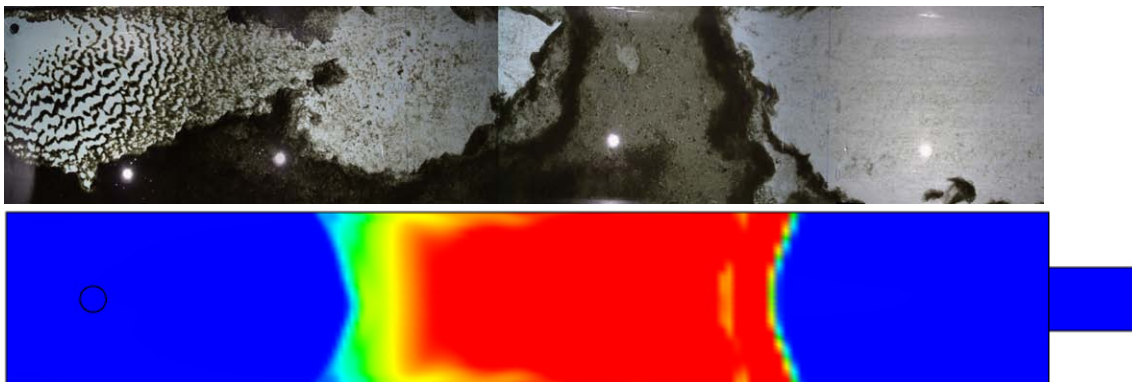


Fig. 9: Observed (upper) and calculated (lower picture) fiber distribution at the bottom of the pool after an experiment with $V_{OF} = 5 \text{ m/s}$ jet (compare Fig. 7a)

The upper picture of Fig. 9 shows the observed fiber deposition after an experiment at the facility in Zittau. The lower picture of the calculations shows that the same characteristics of fiber deposition could be found. Directly below the jet, marked by a circle in the calculated picture, a zone free of fibers is established. Most of the fibers are accumulated in the middle of the tank.

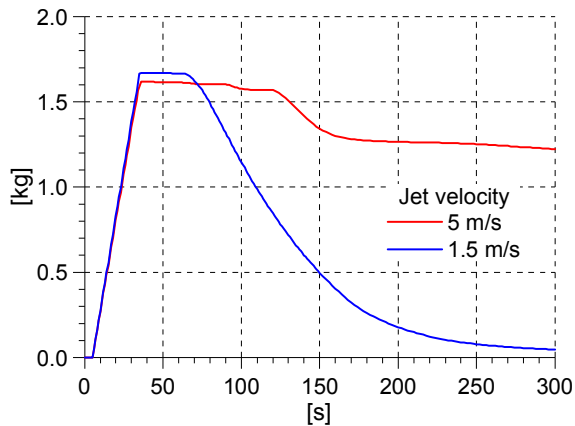


Fig. 10: Integral amount of fibers in the pool

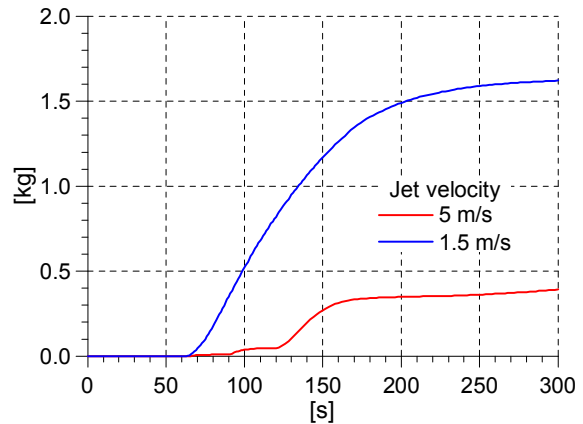


Fig. 11: Integral amount of fibers, which left the pool respective are deposited at the strainers

Fig. 10 shows the integral fiber content in the pool for the two cases of jet velocity. In the case $V_{OF} = 1.5$ m/s the fibers are transported directly to the outlet. Almost all fibers left the pool after 300 seconds and are respectively deposited at the strainers (see Fig. 11). In the case of $V_{OF} = 5$ m/s large amounts of fibers are accumulated in the pool for a longer time. This accumulation was caused by the clockwise rotating swirl. Consequently the fiber mass left the pool respective deposited at the strainers is much lower (see Fig. 11).

4. Summary and outlook

CFD is able to calculate the main flow characteristics during plunging jet situations. The establishment of the large swirl caused by the entrained air and its consequences on the fiber deposition pattern could be measured in the experiments and calculated in the simulations.

Applying CFD methods for the described problem gives at least a qualitative description of the flow phenomena and the determination of resulting consequences on the fiber transport is possible. The CFD-simulation of real sump scenarios however during an anticipated accident has to consider thousands of problem seconds and therefore may fail due to the large computational effort required.

References

- [1] Bin, A. K. (1993): Gas entrainment by plunging liquid jets, Chem. Eng. Sci. Vol. 48, pp. 3585-3630
- [2] Krepper, E.; Cartland-Glover, G.; Grahn, A.; Weiss, F.-P.; Alt, S.; Hampel, R.; Kästner, W.; Seeliger, A., (2008): Numerical and experimental investigations for insulation particle transport phenomena in water flow, Annals of Nuclear Energy 35 (2008), 1564–1579
- [3] Krepper, E., Cartland-Glover, G.; Grahn, A., (2009): CFD Modellierung einer partikelbelasteten Kühlmittelströmung im Sumpf und in der Kondensationskammer, Report FZD-521, Aug. 2009

Acknowledgement

The work is funded by the German Federal Ministry of Economics and Labour under the contract Nos. 1501270 and 1501307.

EMPIRICAL AND NUMERICAL STUDIES ON GAS ENTRAINMENT BY IMPINGING JETS

Dana Veronica Danciu and Martin Schmidtke

1. Introduction

This work concerns experiments as well as CFD simulations on the gas entrainment for the impinging jet configuration. A water jet impinging on a free surface of a pool causes air entrainment as soon as the jet velocity is high enough (inception velocity). A swarm of bubbles appears below the surface as result of the impingement. Impinging jets may be applied in industrial processes and also of relevance to nuclear reactor safety. One example is the emergency core cooling (ECC) injection into a partially filled cold leg, which occurs in some scenarios of loss of coolant accidents at Pressurized Water Reactors. In this case, the injected cold water impinges as a jet on the surface of the hot water. Depending on the velocity of the jet, steam bubbles may be entrained below the surface by the impinging jet. These bubbles contribute to heat exchange and mixing of the fluids. Heat transfer between cold and hot water and mixing in the cold leg play an important role since the mixed water enters the reactor pressure vessel and may cause high temperature gradients at the wall of the vessel (pressurized thermal shock). Another scenario for the occurrence of plunging jet phenomena can be found in the case of a pipe break. The water released from the break can fall as a jet into the reactor sump and transport insulation material towards the sump strainers. Many experiments have been carried out on impinging jets. The comprehensive overview by Bin, 1993, reveals that the results depend critically on the individual setup (e.g. the nozzle geometry) and it is difficult to draw general conclusions. Data with high resolution in space and time are required for the qualification of Computational Fluid Dynamics (CFD) models for such flow situations. Therefore a new experimental setup was designed and first CFD simulations were done for these experiments.

2. The experiment

Figure 1 shows a schematic of the experimental setup. The experiments were carried out in a 0.3m x 0.3m x 0.5m water tank constructed from transparent acrylic walls for visualization purposes. The water level in the tank was kept constant at 0.28 m throughout the experiments. Tap water was pumped out of the tank and re-injected through a smooth 6 mm diameter, 50 mm long steel pipe used as nozzle to produce a vertical falling round jet. A rotameter was used for the measurement of the flow rate. Images of the impact region between the jet and the water pool were captured by a high-speed camera. For each experimental condition, a sequence of images of the region below the surface was taken. The camera was operated with a frame rate of 200 frames per second. Backlighting with high luminosity LED panels was used during the experiments in order to have a proper exposure at the required image rate. Experiments were performed for different nozzle heights (L_j in Figure 1) and volumetric flow rates, with both tap- and de-ionized water. The velocity of the jet ranged between 0.9 m/s and 2.5 m/s at the nozzle exit and the jet length was varied between 0.01 m and 0.2 m. For a given water velocity v_0 inside the pipe which is used as nozzle one obtains the impact velocity v_j by assuming free fall over the full jet length L_j .

$$v_j = \sqrt{v_0^2 + 2g L_j} \quad (1)$$

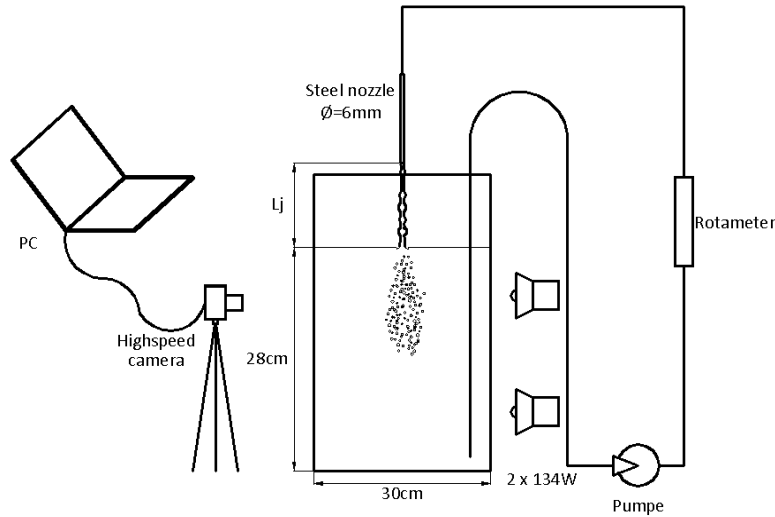


Fig. 1: Experimental setup

A nozzle Reynolds number is calculated based on v_0 , the pipe diameter (6 mm) and the material data of water. In the experiments described below the nozzle velocity v_0 is varied between 1.1 and 1.8 m/s. Thereby the pipe Reynolds number based on its diameter varies in the range $6500 < Re < 11000$, so that the liquid flow inside the nozzle can be expected to be fully turbulent. In general, one expects that the gas entrainment increases with the turbulence generated inside the nozzle (i.e. the nozzle Reynolds number) and with the impact velocity of the jet v_j .

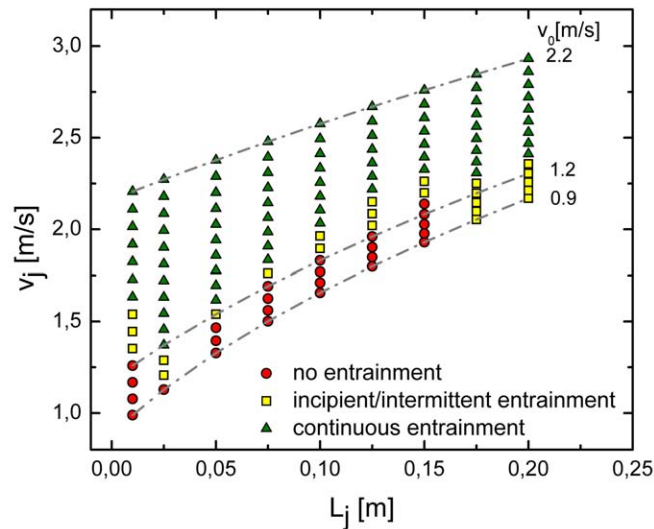
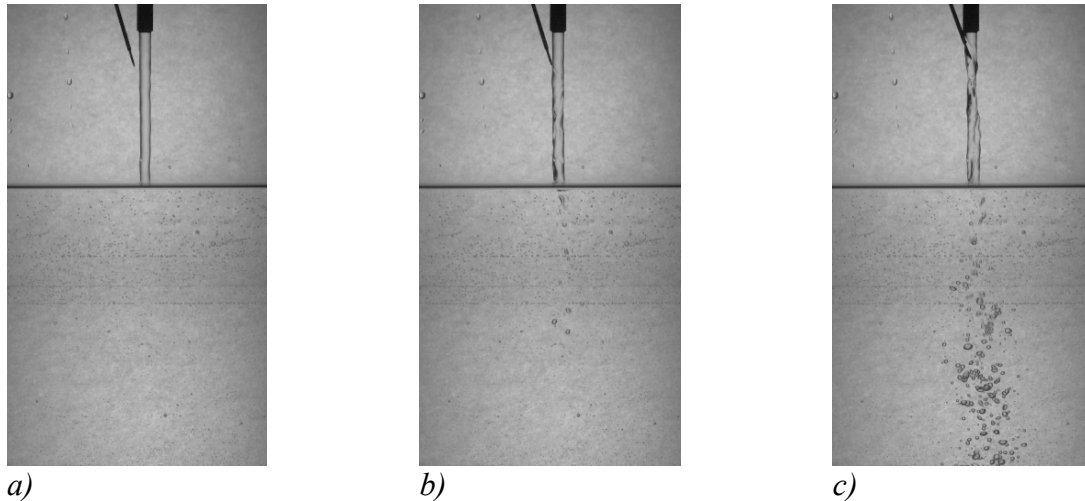


Fig. 2: Test matrix. Entrainment regime in dependency of the jet length L_j and the impact velocity v_j . Dashed lines: Series for constant nozzle exit velocity v_0

Fig. 2 shows the test matrix of the experiments performed at the Forschungszentrum Dresden-Rossendorf. In the literature [2], different entrainment regimes have been noted: No entrainment, incipient/intermittent entrainment (i.e. one bubble or a bubble pack only over a period of several seconds) and continuous entrainment. Remarkable is the fact that if v_0 is kept constant and the jet length is increased, a non-monotonous entrainment behavior can occur. This is most obvious for $v_0 = 1.2$ m/s, where no entrainment is observed for $L_j = 1.5$ cm, some entrainment for L_j between 2.5 cm and 5 cm, no entrainment again for

higher jet length, etc. (see corresponding dashed line in Fig. 2). Varying the jet length at a constant v_0 changes the jet diameter at the impact point and the momentum transfer from the jet into the pool.

The “roughness” of the jet plays an important role in the occurrence of air entrainment. To prove the importance of the jet surface disturbances in the entrainment process, our experiments include tests where a 7.5 cm long jet which did not entrain air was disturbed with a thin needle. Due to the appearance of waves and thus an increase of the surface roughness of the jet, air entrainment takes place. We also observed that if the tip of the needle barely touches the jet, only a small number of bubbles appears (Fig. 3).



*Fig. 3: Sequence presenting the influence of jet surface disturbances on air entrainment
a): undisturbed jet; b): superficial disturbance; c): deep disturbance*

The amount of entrained bubbles does not increase monotonously with the jet length or the impact velocity (c.f. the data series for $v_0 = 1.2$ m/s discussed above). This indicates that different mechanisms contribute to gas entrainment. Particularly uneven surface structures of the jet can trigger bubble generation [3]. Due to Rayleigh instabilities surface waves may arise, which propagate downwards. These waves grow with the jet length. On the other hand, the turbulence of the liquid inside the nozzle also contributes to the “surface roughness” of the jet. This turbulence decreases along the jet due to eddy dissipation. The exact reason of the non-monotonous entrainment cannot be identified in this experiment, since turbulence parameters are not measured. However, if the jet length L_j is kept constant and the nozzle Reynolds number is increased step by step then gas entrainment increases monotonously – either due to increasing turbulence generated inside the nozzle or due to the increasing impact velocity v_j . If the impact velocity is higher than 2.2 m/s or the nozzle exit velocity v_0 is higher than 1.4 m/s, entrainment is observed in any case (c.f. Fig. 2).

For a more quantitative description of the gas entrainment the geometry of the gas plume is measured. The so-called “penetration depth” of a plume is the distance of the lowest bubbles to the surface. Due to the fact that the plume fluctuates, one cannot refer to the penetration depth at a certain moment. Therefore, images are subdued to background subtraction, removal of the small air bubbles at the walls and averaging. Our algorithm averages over 2000 frames, corresponding to a time interval of 10 s. It is noticeable in the averaged images that the lower tip of the bubble plume rarefies; meaning that only a small amount of bubbles travels that deep. Integrals of the grey values are calculated on horizontal lines across the time

averaged plume image. The height, where the integral value falls below 10% of its maximum is defined as penetration depth. Fig. 4 shows an example of the penetration depth variation for two different nozzle exit velocities, but identical impact velocity, $v_j = 2.5$ m/s. The penetration depth of the plume decreases with the amount of gas entrained. The difference between the two cases is obvious. The plume becomes denser with increasing velocity v_0 . Due to the bubble drag the water jet below the water is decelerated and the plume retracts towards the surface of the water.

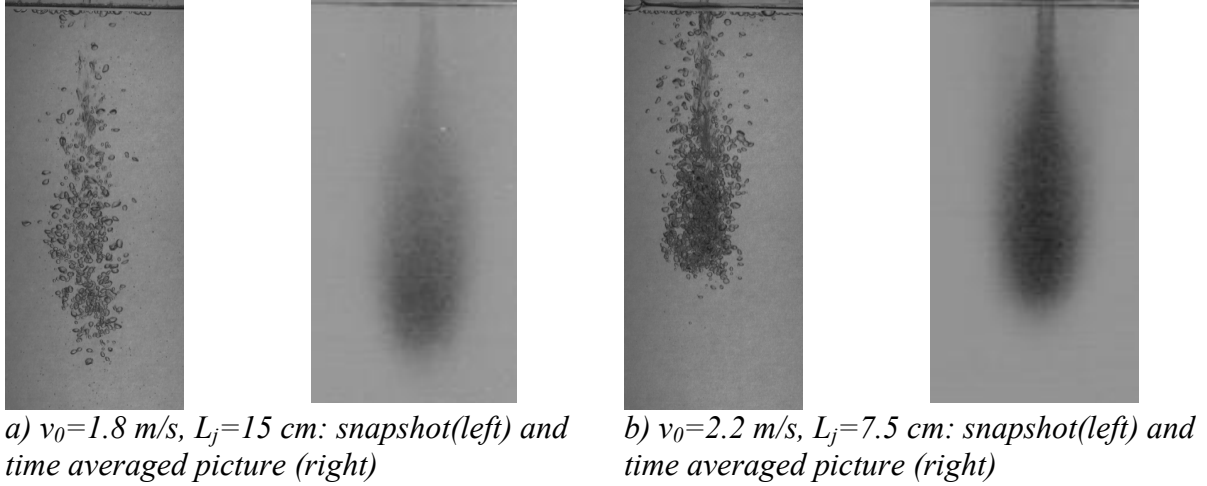


Fig. 4: Example of the penetration depth variation for constant impact velocity $v_j = 2.5$ m/s, for two different nozzle exit velocities and jet lengths.

According to Bin [1], the penetration depth H_p can be calculated as

$$H_p = 2.1v_j^{0.775}d_0^{0.67} \quad (2)$$

where d_0 is the nozzle exit diameter. This means that for constant impact velocity, the penetration depth should be constant, (e.g. $H_p = 14$ cm for $v_j = 2.5$ m/s and $d_0=6$ mm). The experimental values of the penetration depth are found in the range given by Bins' formula, whereas different penetration depths were observed for identical impact velocity and nozzle diameter at different nozzle velocities and jet lengths (e.g. $H_p = 17.2$ cm obtained for the jet in Fig. 4a and $H_p = 14.4$ cm obtained for the jet in Fig. 4b). Bubble sizes were estimated from single images by means of image processing through subsequent background subtraction, cell segmentation, bubble detection and bubble size calculation using a Hough transform based algorithm. The Sauter mean diameter was about 3 - 4 mm, in agreement with data from the literature [1].

3. Simulations

CFD calculations have been performed for the given setup. It is not possible, to resolve all physical phenomena in a practical CFD calculation. Here, the water tank dimensions are in the range of decimeters whereas the film around the jet and the breaking-up of this could only be resolved on a sub-millimeter scale. This holds also for small interface structures on the jet surface such as capillary waves or "surface roughness" due to turbulence. Therefore in the present simulations all phenomena above the water level are omitted and a jet with a given gas void fraction is injected into a liquid tank through an inlet. For simplicity a 2D-axisymmetric domain is chosen, with the inlet ($r = 3$ mm) near the axis of symmetry, a

degassing zone at the top (for the free surface) and walls at the side and at the bottom. So the simulated tank geometry is a cylinder rather than a cuboid with a quadratic base. Since all relevant phenomena occur near the jet axis, this difference ought to be negligible. The radius of the domain is 15 cm and the height is 28 cm to keep the geometry as similar to the setup of the experiment as possible. A water outlet is located at the bottom near the outer wall. Similar to the jets displayed in Fig. 4, a liquid jet with a velocity of 2.5 m/s is injected into the domain.

The calculations are performed using the ANSYS CFX-11 software. After about 3 seconds of simulated physical time, transient Euler-Euler RANS-calculations become steady. Here, the k-epsilon turbulence model is applied for the continuous liquid phase. The gas is modeled as a dispersed phase with a bubble diameter of 3.5 mm (no turbulence model). The gas void fraction fields and the velocity field of the solution are investigated with respect to the penetration depth of the plume. From the gas void fraction fields one can not identify a sharp plume edge to determine a penetration depth. However, by plotting isolines for zero vertical gas velocity, one obtains a distinct depth near the axis, below which gas is not transported in the simulation (isolines far away from the plume are meaningless, since gas is not present here). This depth is 25 cm for 5% gas (Fig. 5a) and 18 cm for 20% gas at the inlet (Fig. 5b). The simulations presented in Fig. 5 were performed using the Grace drag law, and a turbulent dispersion force according to Lopez de Bertodano with $C_{TD} = 0.5$. If the lift force [4] is included, a region of high gas void fraction develops near the axis (Fig. 5c). Gas is trapped here.

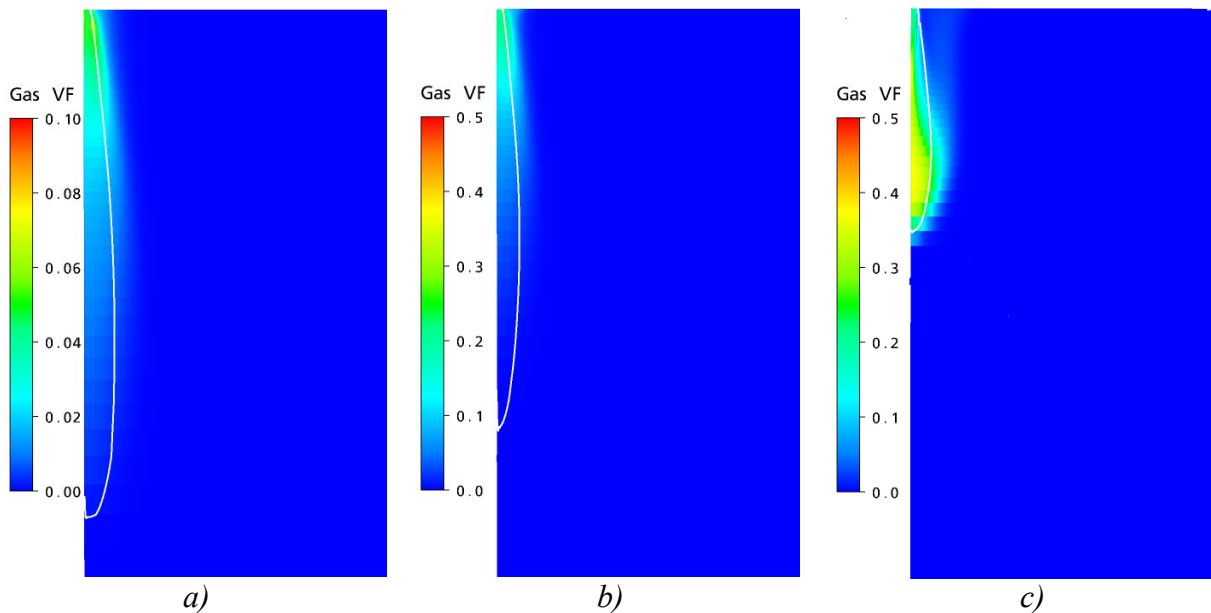


Fig. 5: Gas void fractions of two-phase jets injected in water with a velocity of $v_j=2.4$ m/s
a) 5% gas in the inlet; b) 20% gas; c) 20% gas with lift force.

White curves: isolines for zero vertical gas velocity. Note the different colour scales

This is physical to some extent, since according to Tomiyama's law bubbles with an equivalent diameter below 4 mm have a lift coefficient C_L about +0.3, and due to this positive lift coefficient they migrate in vertical shear flows into the region of faster counter-flow. In the impinging jet scenario the bubbles migrate towards the axis. In Fig. 5c the effect of the lift force seems to be overestimated. In fact, the Tomiyama law was obtained from experiments with single bubbles only and may not be valid at high gas void fractions. In addition to this, in

regions of high gas holdup, coalescence and breakup widens the bubble size distribution, i.e. the assumption of a monodisperse gas phase is no longer reasonable.

Although the penetration depths of the simulated plumes are more or less similar to those observed in the experiment, a direct comparison is not possible: In the simulation the gas void fractions of the injected two-phase jets are chosen deliberately. In the experiment neither the gas void fraction nor the velocity fields have been measured because sensors massively obstruct the jet. For example a substantial deformation of the plume is observed, if a wire-mesh sensor is installed near the plume. A non-intrusive technique for measuring gas void fractions and gas fluxes is high-speed X-ray tomography, which is currently developed at the Forschungszentrum Dresden-Rossendorf. Where the gas void fraction is low, Particle Image Velocimetry (PIV) can be used to measure the liquid velocity. Of course, tracer particles cannot be tracked optically inside dense plumes. Experiments on plunging jets with PIV are under way, so that it will be possible to compare liquid velocities with simulated values at least outside the plume. In the emergency core cooling scenario described in the introduction, physical processes on the surface of the free falling jet play an important role (e.g. heat and mass transfer). Therefore simulations related to this scenario have to include the region above the water level. One approach for controlling and modeling gas entrainment in CFD calculations of impinging jets including the water surface is discussed in [5].

4. Summary and outlook

The development of the plume of entrained bubbles below an impinging jet has been investigated in an experiment and by CFD simulations. The penetration depth of the plume decreases with increasing quantities of entrained gas in both experiments and simulations. This is due to the fact that the momentum of the liquid jet below the water level is reduced by friction with the rising bubbles. For a better comparison of the experiments and CFD calculations, non-intrusive measurements of gas void fractions and velocity fields below the jet are needed such as high-speed computer tomography.

References

- [1] A. K. Bin, Gas entrainment by plunging jets (1993), *Chemical Engineering Science* 48 (21), 3585
- [2] D. Chirichella, R. Gomez Ledesma, L.T. Kiger, and J.H. Duncan (2002), Incipient air entrainment in a translating axisymmetric plunging laminar jet, *Physics of Fluids*, 14 (2)
- [3] L. Davoust, J.L. Achard and M. El Hammoumi (2002), Air entrainment by a plunging jet: the dynamical roughness concept and its estimation by a light absorption technique, *International Journal of Multiphase Flow*. 28, 1541
- [4] A. Tomiyama, H. Tamai, I. Zun and S. Hosokawa (2002), Transverse Migration of single Bubbles in Simple Shear Flow, *Chemical Engineering Science* 57 (11), 1849
- [5] M. Schmidtke, D. Lucas (2009), CFD Approaches for modeling bubble entrainment by an impinging jet: *Science and Technology of Nuclear Installations*, article ID 148436

Acknowledgement

The NURESIM project is partly funded by the European Commission in the framework of the Sixth Framework Program (2004–2006).

MEASUREMENT OF HYDRODYNAMICS IN FIXED BEDS WITH ELECTRICAL CAPACITANCE TOMOGRAPHY AND CAPACITANCE WIRE MESH SENSOR

Marco Jose da Silva, Bartosz Matusiak*, Krzysztof Grudzień*, and Uwe Hampel

1. Introduction

Trickle bed reactors are widely used in the manufacturing of petroleum-based products and fuels, as well as in the production of various chemicals and pharmaceuticals [1]. In trickle bed reactors a gas and a liquid phase cocurrently flow downward over a bed of randomly packed catalyst particles. The process efficiency and safety in such reactors is determined by the liquid distribution and the flow regimes. An intricate problem associated with trickle bed reactor operation is liquid maldistribution, which denotes the fact that the liquid does not homogeneously flow through the bed. On one hand, liquid maldistribution is an economic issue, since only a fraction of the often expensive catalyst contributes to the overall reaction. On the other hand liquid maldistribution may lead to local runaways which may impact the safety of the reactor operation. To achieve improved utilization of the catalyst bed and better reactor performances, as well as to meet with rising environmental standards, hydrodynamics in trickle bed reactors and their coupling to chemical reaction still need examination.

Assessment of the hydrodynamics in running trickle bed reactors is very difficult due to the opaque nature of such systems [1]. In past studies, which were mostly conducted in laboratory-scale beds at moderate pressures and temperatures and for non-reactive flows, different techniques have been applied to determine hydrodynamic parameters. Among them are local void and temperature probes, differential pressure transducers, tracer methods, and colorimetric techniques. More recently, tomographic imaging modalities were introduced to investigate trickle bed reactors: Nguyen et al. [2] applied magnetic resonance imaging (MRI), Van der Merwe et al. [3] X-ray tomography and Schubert et al. [4] gamma ray tomography. Considering the complexity and costs as well as the low temporal resolution of these imaging modalities electrical imaging techniques appear to be more attractive.

One applicable and rather established imaging technique is Electrical Capacitance Tomography (ECT) [5]. ECT is based on the reconstruction of the permittivity distribution $\varepsilon(\mathbf{r})$ inside an object from multiple capacitance measurements on the surface of the same. An ECT sensor typically consists of a set of elongated electrodes placed equidistantly around the perimeter of an object. Inter-electrode capacitance is given by

$$C = \frac{Q}{\Delta\varphi} = - \frac{\oiint_A \varepsilon(\mathbf{r}) \nabla \varphi(\mathbf{r}) dA}{\Delta\varphi}, \quad (1)$$

where Q denotes the charge accumulated on the electrodes, $\varphi(\mathbf{r})$ is the potential distribution resulting from the current injection, $\Delta\varphi$ the voltage across the electrodes and A the area of the receiver electrode. Commonly the capacitance is measured by driving an AC current through a pair of electrodes and measuring the resulting AC voltage across them. This measurement

* Computer Engineering Department, Technical University of Lodz, Lodz, Poland

procedure is repeated for all possible pairs of electrodes giving $N \times (N-1)/2$ independent measurements for N electrodes. The permittivity distribution is related to the capacitance measurements in a non-linear way, which may be denoted in the form of an operator equation

$$\mathbf{C} = F \{ \varepsilon(\mathbf{r}) \}. \quad (2)$$

The reconstruction part of ECT consists in the construction of an inverse operator F^{-1} and the determination of an approximate permittivity distribution from the measured capacitance values, which are lumped in the vector \mathbf{C} , according to

$$\varepsilon(\mathbf{r}) = F^{-1} \{ \mathbf{C} \}. \quad (3)$$

There is a choice of solution strategies to solve the inverse problem, whereby the most popular is Linear Back Projection (LBP) [5]. LBP algorithms are simple and efficient and can be used for real-time reconstruction. On the other hand they are somewhat over-regularizing so that spatial resolution is not as high as with other more sophisticated inverse schemes.

Permittivity itself may be written as a product $\varepsilon = \varepsilon_0 \varepsilon_r$ of the vacuum permittivity ($\varepsilon_0 = 8.85 \text{ pF m}^{-1}$) and the dimensionless relative permittivity ε_r . The latter is a material property and typically ranges between $\varepsilon_r = 2$ (for many types of oil) to roughly $\varepsilon_r = 81$ for water at low frequencies. In contrast to electrical conductivity the dynamic range of electrical permittivity across different substances is much smaller and therefore it is much easier to distinguish between liquids and gases. When a liquid is non-conducting, as is the case with organic substances, then permittivity measurement is the only choice.

More recently wire mesh sensors, introduced by Prasser et al. [6], have found widespread application as an alternative electrical imaging modality in the study of two-phase flows. A wire-mesh sensor consists of two planes of wire electrodes stretched across the cross-section of a flow channel at an angle of 90° . An associated electronics measures the local conductivity in the gaps of the wire crossings. In contrast to tomography, image reconstruction is no longer needed, since the sensing volume is confined to the vicinity of each crossing point. The sensor was successfully employed for the visualization of gas-liquid flow in pipes. Recently, a new capacitance wire mesh sensor was developed [7] which uses a sophisticated AC based capacitance measuring electronics to measure the capacitances in the wire crossing points. This for the first time allows a fast and direct imaging of electrical permittivity distributions in a flow cross-section rather than conductivity distributions. The advantages are obvious. Gas-liquid flows can be measured for any type of liquid and the measurements are less dependent on ion concentration. Other than in ECT local permittivity values in the wire crossings can be directly determined from capacitance measurements according to

$$C = \varepsilon_r \varepsilon_0 k_G \quad (4)$$

without a reconstruction procedure. The geometry factor k_G is given by the wire geometry and distance and can be easily obtained from reference measurements on substances of known permittivity.

In this work we applied for the first time an ECT system and a wire-mesh sensor system to visualize the liquid distributions and integral liquid holdup values in a trickle bed reactor test

setup and compared their results. Thereby the ECT images were generated using a simple LBP reconstruction algorithm which facilitated fast image reconstruction.

2. Experimental setup

The experimental trickle bed reactor was built from a polyvinylchlorid (PVC) column of 100 mm internal diameter, a height of 440 mm, and a wall thickness of 3 mm. It was randomly packed with commercial porous Al_2O_3 catalyst beads. The average diameter of the beads was 4.0 mm. The relative electrical permittivity of the bed was between 2.1 and 2.6. The reactor was operated at ambient pressure and room temperature. To investigate the capability of both sensors to visualize liquid maldistributions we injected liquid from the top of the column via three individually operated inlets. As liquid we used isopropanol ($\text{C}_3\text{H}_8\text{O}$) with a relative electrical permittivity of 20.18. The ECT sensor was placed 115 mm down the top of the column where we expected that flow dispersion is not yet strong enough to fully homogenize the liquid distribution. The wire mesh sensor was mounted 15 mm underneath the ECT sensor, which is a sufficient distance to avoid cross-interferences. A scheme of the setup is shown in figure 1, the arrangement of three inlets at the top plate in figure 2a.

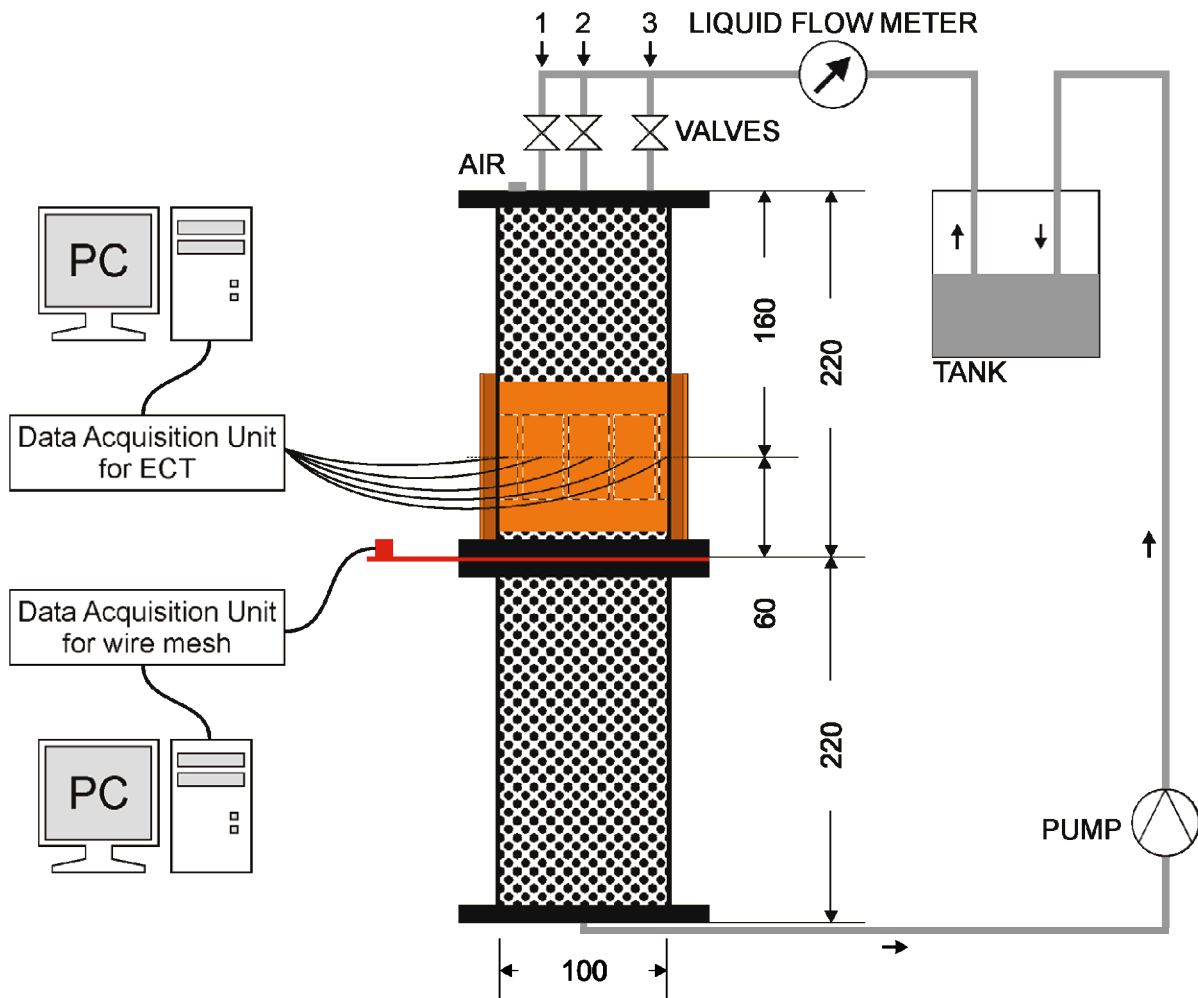


Fig. 1: Experimental setup

In most applications, the electrodes of the ECT sensors are placed on the outer wall of the vessel. However, Jaworski et al. [8] showed that if the ratio of the permittivity values of the media inside the sensor and the material of the vessel wall is too large and the wall too thick

(e.g. if the ratio is larger than 8 for a 2.5 mm thin wall), the capacitance measurement records between adjacent electrodes becomes nonlinearly related to the internal permittivity. This fact makes image reconstruction very problematic. For the present case, where the wall is comparatively thick and isopropanol ($\epsilon_r = 20.18$) has much higher permittivity than PVC ($\epsilon_r = 3.39$), we developed a special ECT sensor with isolated internal electrodes. This sensor was made as flexible printed circuit board (flex-PCB) consisting of 12 electrodes. Each electrode is 50 mm long and 23.5 mm wide. Around the electrodes a grounded shielding was placed. The flex-PCB was tightly fitted to the inside of the column wall in such a way that electrodes were in contact with the internal surface of the wall. Wire connections to the electrodes were made via holes in the column wall which after soldering were properly sealed. To prevent electrical influence from the exterior of the column, an additional external grounded shield was provided. The ECT sensor was operated from a personal computer together with an ET3 data acquisition unit. The ET3 electronics was developed at the Technical University of Warsaw and implements a charge-discharge principle for capacitance measurements [9]. Data acquisition was performed with a speed of 60 frames per second (fps). For 12 electrodes each frame contained 66 independent capacitance values, which were used for the images reconstruction process.

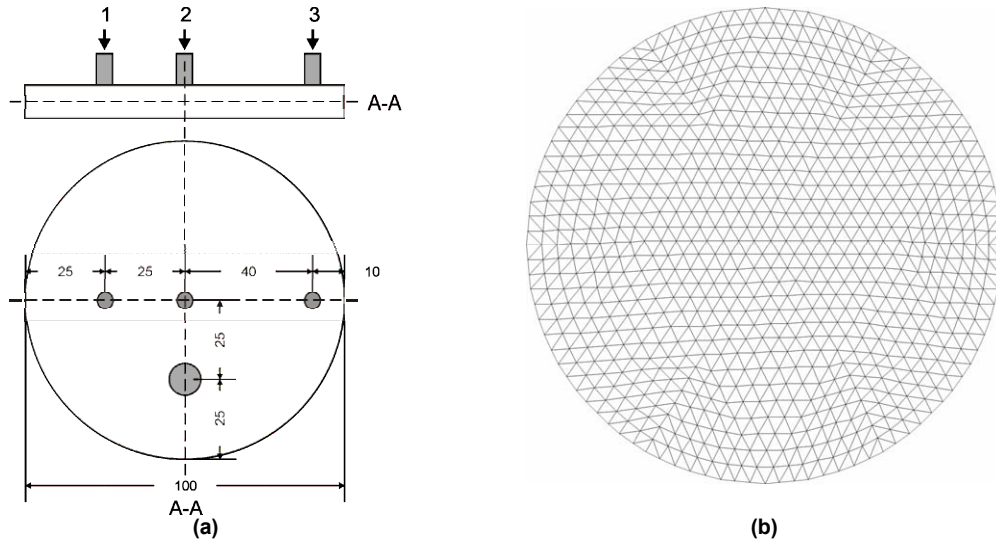


Fig. 2: (a) Top plate with three inlets. (b) Mesh for ECT image reconstruction

The wire-mesh sensor is composed of two planes of 16 stainless steel wires of 0.1 mm diameter and 6.25 mm in-plane separation. The distance between the planes is 1.5 mm and the wires from different planes are perpendicular to each other. This arrangement gives 208 sensing points inside the circular cross-section of the column. Care was given to the filling of the wire-mesh sensor volume with catalyst particles. The wire spacing was much larger than the catalyst particles, thus the particles filled the space between the wires quite well. By gently shaking the bed after filling we assured that sufficient compaction between the wires was achieved and the bed structure became as homogeneous as possible throughout the whole bed. In contrast to the applied ECT system, the wire mesh sensor utilizes an AC-based method for capacitance measurements and employs a logarithmic detection scheme for the demodulation of the alternating-current signal [8]. Therefore, the relation between the measured output voltage V of the sensor electronics and the capacitance C in a crossing-point is given by

$$V = a \ln(C) + b, \quad (5)$$

where a and b are circuit constants which are determined by proper reference measurements. Acquired measurement data are stored in the measurement computer, which is also used to control the electronics. In this study the wire-mesh sensor was operated at 100 fps.

3. Image reconstruction and analysis

Due to the fact that both techniques need some calibration for data normalization, calibration scans were performed and the data was normalized according to parallel capacitor model [10]. During each calibration, the dry bed was scanned as a reference for minimum permittivity values. Then it was completely flooded with isopropanol and scanned after 15 minutes as a reference for maximum permittivity values.

For solving the ECT inverse problem we first computed the electrical fields and resulting sensitivity distributions for dual-electrode measurements with custom-made FEM software. For this purpose, we utilized NETGEN mesh generator (Open Source under LGPL) to prepare a mesh consisting of 1536 triangle elements, which is shown in figure 2b. On the base of this mesh we calculated the electrical fields for given electrode excitation patterns by solving Poisson's equation for the electrical field and calculated the resulting sensitivity matrices for image reconstruction as described in [11].

The liquid holdups H for both tomographic methods were calculated on the base of the liquid distribution images. Every image consists of N pixels with reconstructed respectively measured permittivity values ε_i . From the permittivity values a phase fraction value is calculated using the known permittivity calibration values from the extra measurements according to

$$h_i = \frac{\varepsilon_i - \varepsilon_{gas}}{\varepsilon_{liquid} - \varepsilon_{gas}}. \quad (6)$$

The cross-sectional liquid holdup is then calculated from

$$H = \frac{\sum_{i=1}^N A_i h_i}{\sum_{i=1}^N A_i}, \quad (7)$$

where A_i denotes the area of pixel i . Note, that for the ECT images the pixels are triangles of different area and even for the wire mesh sensor the peripheral sensor pixels are non-square.

4. Experiments

All the experiments were performed simultaneously with both sensors. Liquid was supplied to the column from each of the three inlets subsequently. The volumetric flow rate was $40 \text{ l}\cdot\text{h}^{-1}$. Calculated holdups and reconstructed liquid distribution images are shown in figure 3. These images are time averaged over the 20 s. The lack of spatial resolution for the ECT images is evident from the pictures. However, the shapes of liquid distributions in the ECT images are in very good agreement with the corresponding wire mesh sensor images. In the cases of liquid supply from inlet 1 and 3, the ECT images show a liquid concentration in the centre which is too low to be physically plausible. This may be a result of an inadequate model for data normalization in this case. Nevertheless, the differences in the holdup values for the different sensors are smaller than 3%, which shows that both methods give quite similar and reliable results.

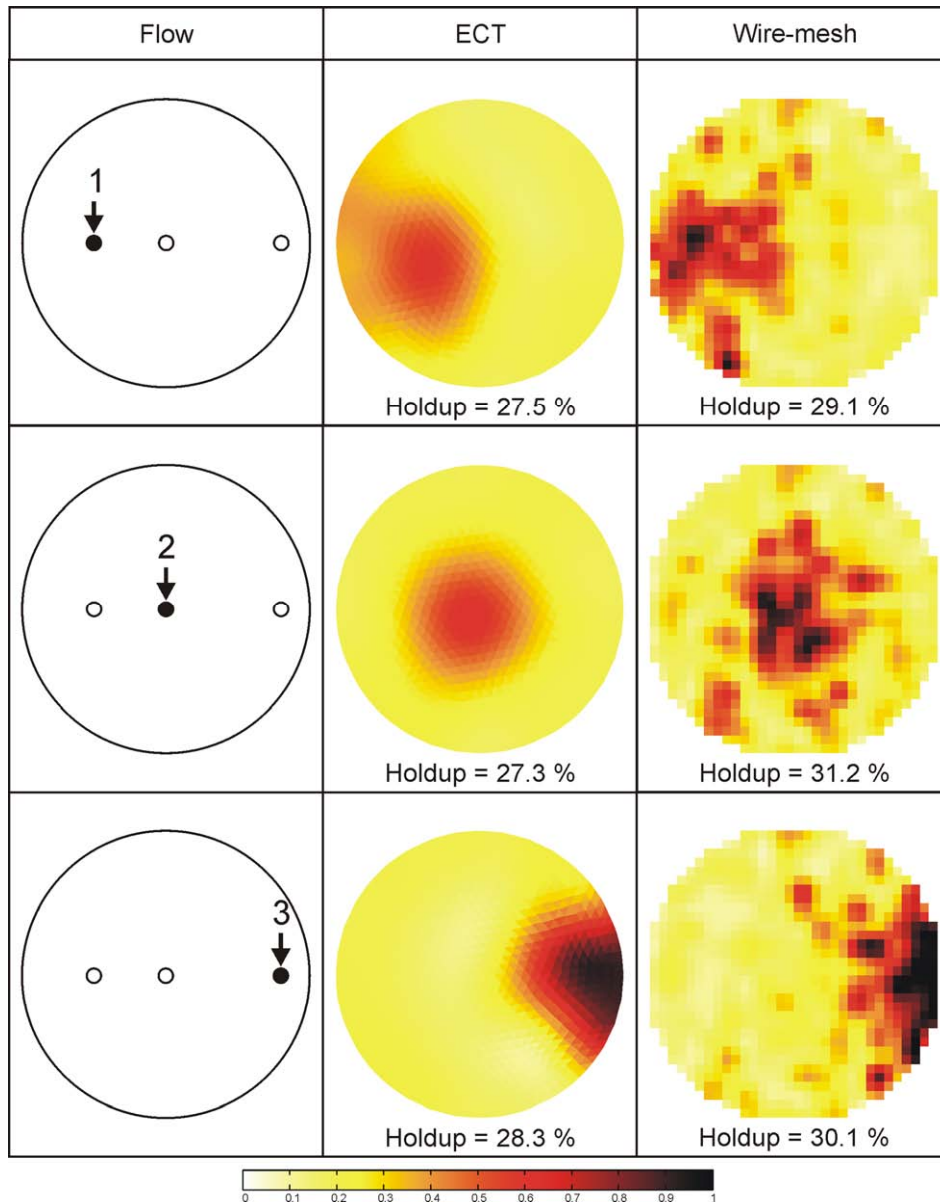


Fig. 3: Measurement results: the images show the reconstructed liquid holdup distribution measured with ECT (centre) and wire-mesh sensor (right) for different liquid supply patterns (rows)

5. Conclusions

In this paper, a capacitance wire mesh sensor has been used for the first time to acquire cross sectional images of liquid distributions in a trickle bed reactor model. It is also the first time that the capacitance wire-mesh and ECT were simultaneously operated. This gives the opportunity to compare the usability of both methods to investigate liquid distribution and holdup in trickle bed reactors. The preliminary experiments showed that both methods give qualitatively and quantitatively similar results with respect to cross-sectional liquid holdup. Obviously, the spatial resolution of ECT is much lower than for the wire mesh sensor. However, the results show that non-invasive Electrical Capacitance Tomography can give reliable information about cross sectional dynamic liquid holdups in a fixed bed, even with a simple and fast linear back projection reconstruction algorithm. As a conclusion for practical

applications, the wire mesh sensor should be used when the focus is on high spatial resolution. Nevertheless, for industrial application the chemical compatibility of the wire electrodes and their influence on the flow must be further assessed. On the other hand, if non-intrusive measurement is of primary importance, ECT may be the method of choice. Future work should focus on finding more suitable normalization schemes for ECT, since the applied parallel capacitor model obviously produces too low values in the centre of the reconstructed images.

References

- [1] M. P. Dudukovic (2000), Opaque multiphase reactors: experimentation, modeling and troubleshooting, *Oil Gas Sci. Tech.*, Vol. 54, 135-158.
- [2] N. L. Nguyen, V. Van Buren, A. Von Garnier, E. H. Hardy, R. Reimert (2005), Application of magnetic resonance imaging (MRI) for investigation of fluid dynamics in trickle bed reactors and of droplet separation kinetics in packed beds, *Chem. Eng. Sci.*, Vol. 60, 6289-6297.
- [3] W. Van Der Merwe, W. Nicola, F. De Beer 2007, Trickle flow distribution and stability by X-ray radiography, *Chem. Eng. Sci.*, Vol. 132, 47-59.
- [4] M. Schubert, G. Hessel, C. Zippe, R. Lange, U. Hampel (2008), Liquid flow texture analysis in trickle bed reactors using high-resolution gamma ray tomography, *Chem. Eng. J.*, Vol. 140, 332-340.
- [5] N. Reinecke, D. Mewes (1996), Recent developments and industrial/research applications of capacitance tomography, *Meas. Sci. Technol.*, Vol. 7, 233-246.
- [6] H. M. Prasser, A. Böttger, J. Zschau (1998), A new electrode-mesh tomograph for gas liquid flows, *Flow Meas. Instr.*, Vol. 9, 111-119.
- [7] M. J. Da Silva, E. Schleicher, U. Hampel (2007), Capacitance wire-mesh sensor for fast measurement of phase fraction distributions, *Meas. Sci. Technol.*, Vol. 18, 2245-2251.
- [8] A. J. Jawroski, G. T. Bolton (2000), The design of an electrical capacitance tomography sensor for use with media of high dielectric permittivity, *Meas. Sci. Technol.*, Vol. 11, 743-757.
- [9] T. Olszewski, P. Kleczyński, P. Brzeski, J. Mirkowski, A. Płaskowski, W. Smolik, R. Szabatin (2004), Electrical capacitance tomograph design, 3rd International Symposium on Process Tomography in Poland, Lodz, 118-123.
- [10] G. T. Bolton, W. J. Korchinsky, R. C. Waterfall, (1998), Calibration of capacitance tomography systems for liquid-liquid dispersions, *Meas. Sci. Technol.*, Vol. 9, 1797-1800.
- [11] S. Liu, W. Q. Yang, H. Wang, F. Jiang, Y. Su (2001), Investigation of square fluidized beds using capacitance tomography preliminary results, *Meas. Sci. Technol.*, Vol. 12, 1120-1125.

SYNCHRONIZED FORCE AND PIV MEASUREMENTS FOR ACTIVE FLOW CONTROL BY PERIODIC ELECTROMAGNETIC FORCES ON A NACA0015 PROFILE – EFFECTS OF EXCITATION FREQUENCY

Christian Cierpka, Tom Weier, and Gunter Gerbeth

1. Introduction

Flow separation and its control is a long standing interest in fluid dynamic research. A comprehensive and recent review can be found in [1]. Among the passive flow control methods are, e.g. shape modifications and vortex or turbulence generators. Popular active flow control methods are suction and blowing, plasma actuators [2] or any kind of momentum input in order to change flow characteristics. The addition of momentum can be done steadily or periodically in time. The most striking feature of time dependent addition of momentum is that a control goal, e.g. a specific lift increase, can typically be attained at orders of magnitude smaller momentum input compared to steady actuation.

Main driving parameters are the time averaged momentum input and the excitation frequency. For many actuators, the wave form of the excitation is fixed, although it has significant influence on the control authority. Bouras et al., Scholz et al., and Cierpka et al. [3-5] investigated effects of the wave form. Weier and Gerbeth [6] demonstrated clearly that under otherwise identical conditions the attainable lift changed up to 70% for different wave forms and Cierpka et al. [7] found that especially pulsed excitation with short duty cycles and periods without forcing in between had the ability to decrease the separation region better than a continuous input of momentum. The addition of momentum is usually accomplished by imposing mass fluxes. In the case of electrically conducting fluids, like seawater, the input of momentum can be achieved by electromagnetic, i.e. Lorentz forces without mass flux.

The Lorentz force density \mathbf{F}_L is defined by the vector product of a current density \mathbf{j} and a magnetic induction \mathbf{B} :

$$\mathbf{F}_L = \mathbf{j} \times \mathbf{B} \quad (1)$$

It appears as a body force term on the right hand side of the Navier-Stokes-Equation for incompressible flow and acts as a direct momentum source for the flow.

$$\frac{\partial \mathbf{u}}{\partial t} + (\mathbf{u} \cdot \nabla) \mathbf{u} = -\frac{1}{\rho} \nabla p + \nu \nabla^2 \mathbf{u} + \frac{1}{\rho} \mathbf{F}_L \quad (2)$$

\mathbf{u} denotes the velocity vector, t the time, ρ the fluids density, p the pressure and ν the kinematic viscosity. Ohm's law for moving conductors describes the current density:

$$\mathbf{j} = \sigma(\mathbf{E} + \mathbf{u} \times \mathbf{B}) \quad (3)$$

\mathbf{E} denotes an electric field and σ the electrical conductivity of the fluid. In liquid metal Magnetohydrodynamics ($\sigma \sim 10^6 \dots 10^7$ S/m), the Lorentz force density is strongly coupled with the flow, since the flow induces currents via the $\mathbf{u} \times \mathbf{B}$ term in equ. (3). The induced currents produce Lorentz forces strong enough to change the flow. For seawater and other electrolytes σ is rather small ($\sigma \sim 10$ S/m). Therefore, the induced currents are very low for

moderate applied magnetic fields ($B \sim 1$ T) and the induced Lorentz forces due to these currents are negligible and too weak for a noticeable influence on the flow.

An external electric field has to be applied in order to generate forces large enough to influence the flow. Since this external field can be modified in direction and time, the Lorentz force can be changed in sign and amplitude as well. The actuator is therefore an ideal tool for fundamental research in the lab frame. Its appealing features are: momentum is directly generated in the fluid without associated mass flux, the frequency response of the actuation is practically unlimited, and using a waveform generator for the signal the waveform of the excitation is completely free. The paper presented focuses on frequency effects for different angles of attack. A description of the complex interaction of the different parameters momentum input, frequency and wave form can be found in [8].

2. Experimental setup

A Lorentz force actuator, consisting of flush mounted electrodes and permanent magnets as proposed by Gailitis and Lielausis [9], was implemented at the leading edge of a NACA0015 profile (Fig. 1). The leading edge shaped magnets were eroded from a block of NdFeB in the preferred direction. Finally, they were nickel plated and magnetized. Due to the soft iron closure a mean magnetic induction of $B = 0.5$ T was measured at the surface using a Hall probe. A high power amplifier, driven by a frequency generator, has been used to feed the electrodes, which were made of thin plates of platinum to increase their durability in the sodium hydroxide solution. The Amplifier was driven by a frequency generator Agilent 33220A.

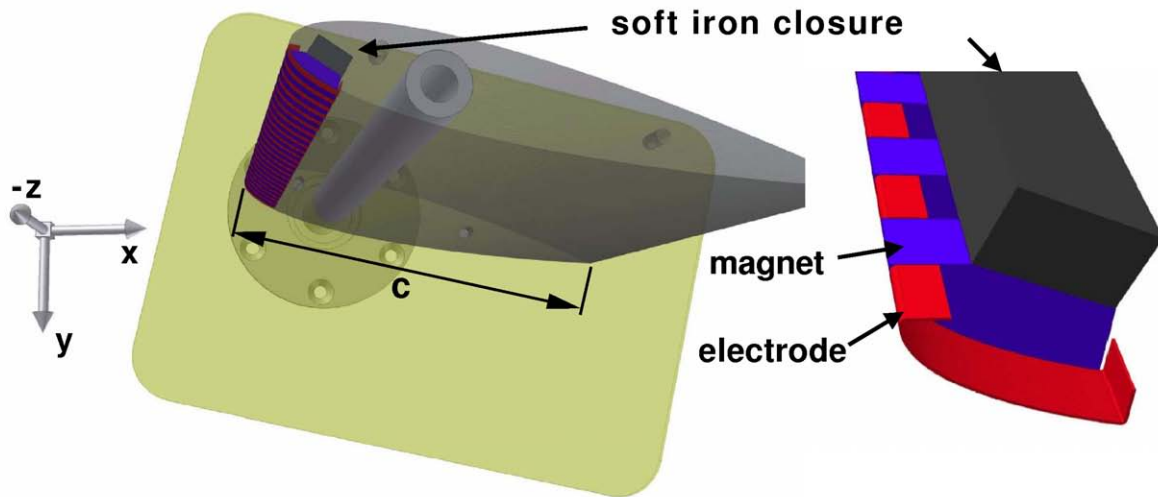


Fig. 1: NACA0015 profile with leading edge Lorentz force actuator, support for the force balance and coordinate system

By the use of alternating currents, the generated Lorentz force oscillates in streamwise direction with the frequency f_e of the applied electric field.

The normalized excitation frequency F^+ is defined with the chord length $c = 160$ mm and the free stream velocity u_∞ .

$$F^+ = \frac{f_e c}{u_\infty} \quad (4)$$

The effective momentum coefficient c_μ' is characterized by the ratio of the rms momentum added by the Lorentz force to the free stream momentum.

$$c_\mu' = \frac{1}{2} \frac{a l B_0}{c \rho u_\infty^2} \sqrt{\frac{1}{T} \int_0^T j(t)^2 dt} \quad (5)$$

The length and width of the magnets/electrodes is given by a and l , $j(t)$ denotes the time dependent current density and T the period of oscillation.

Time resolved PIV measurements were performed in a closed sodium hydroxide channel. This channel is driven by an axial pump and has been operated with a mean velocity of $u_\infty = 32$ cm/s and $u_\infty = 64$ cm/s resulting in chord length Reynolds numbers of $Re = u_\infty c / \nu = 0.5 \times 10^5$ and $Re = 10^5$, respectively. The angle of attack can be varied from outside the channel. A six components force balance was used to measure lift and drag forces. For details of the set up and the PIV system the interested reader is referred to [8].

3. Results

For the NACA0015 profile, leading edge separation occurs at $\alpha = 13^\circ$ for the smaller of the Reynolds numbers and at $\alpha = 15^\circ$ for the higher one.

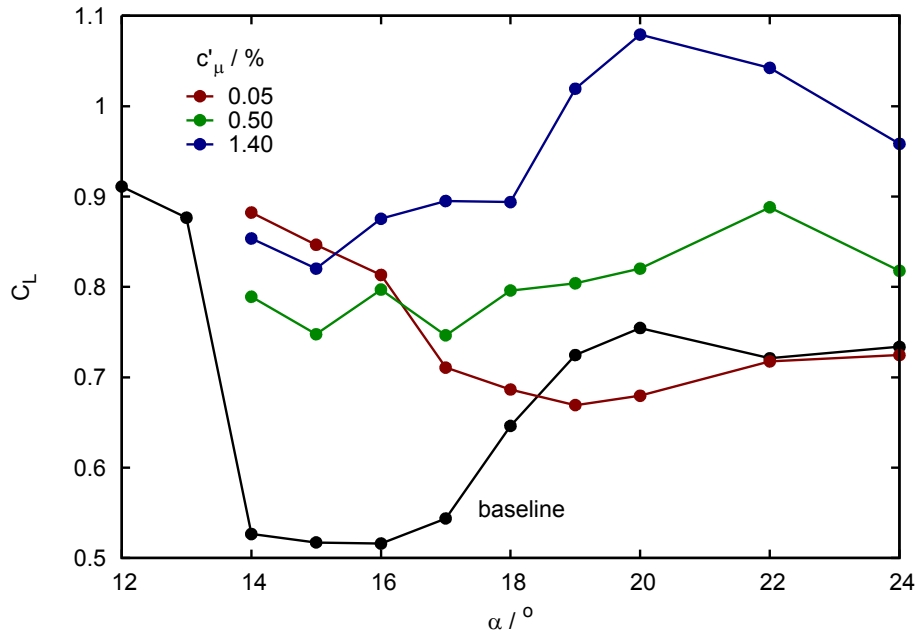


Fig. 2: Lift coefficient vs. angle of attack for sinusoidal excitation with $F^+ = 0.75$ for different momentum coefficients at $Re = 0.5 \times 10^5$

In Fig. 2 the lift coefficient is shown for $F^+ = 0.75$ and sinusoidal excitation at $Re = 0.5 \times 10^5$. There is a region for $\alpha = 14 \dots 17^\circ$ where the differences in lift for the very different momentum coefficients ($c_\mu' = 0.05 \dots 1.4\%$) is rather small. In that region the lift can almost be reestablished to the value of the former attached flow. For $\alpha > 17^\circ$ and for low c_μ' the lift drops significantly. For higher forcing amplitudes the lift can be increased above the maximum of the natural lift polar without excitation. The attainable lift increases now

monotonically with c_μ' . The effect of the excitation is obviously dependent on the angle of attack and can be separated into two regions.

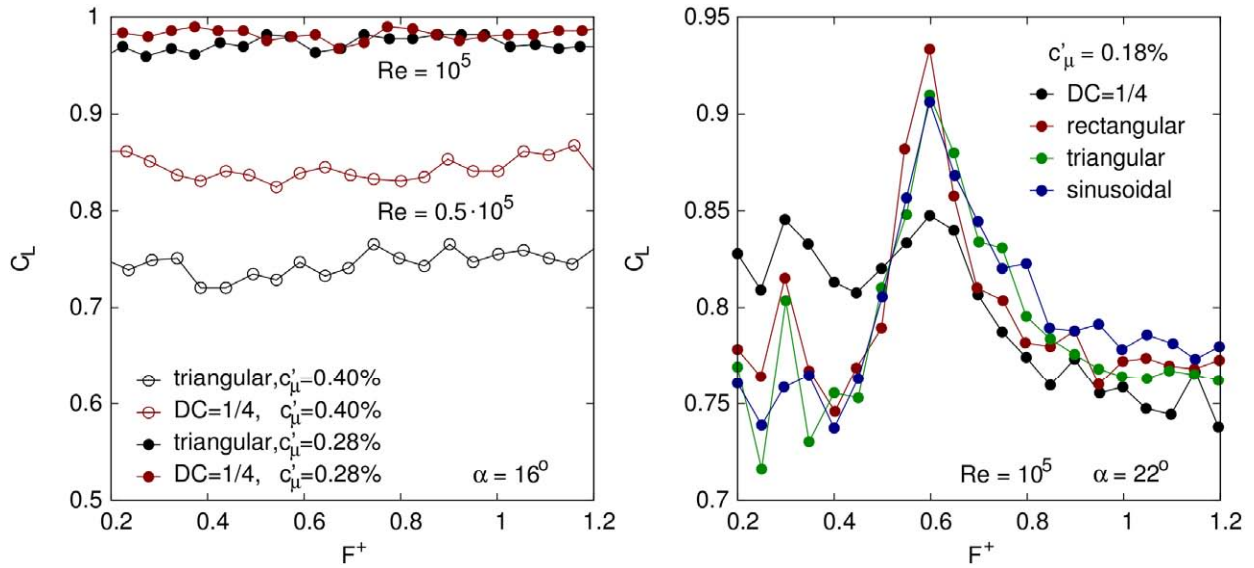


Fig 3: Lift coefficient vs. F^+ for different wave forms (DC=duty cycle) and low c_μ' . $\alpha = 16^\circ$ (left) and $\alpha = 22^\circ$ (right)

The influence of α becomes clearer in Fig. 3. On the left hand side for $\alpha = 16^\circ$ the lift coefficient is shown for different dimensionless frequencies and two different wave forms. For rectangular pulses, the duty cycle (DC) gives the ratio of the pulse duration to the pulse period. Disregarding wave form effects, which are more prominent for the lower Reynolds number, no effect of the change of F^+ is visible. Flow measurements with PIV (not presented here) showed a complete reattachment of the flow.

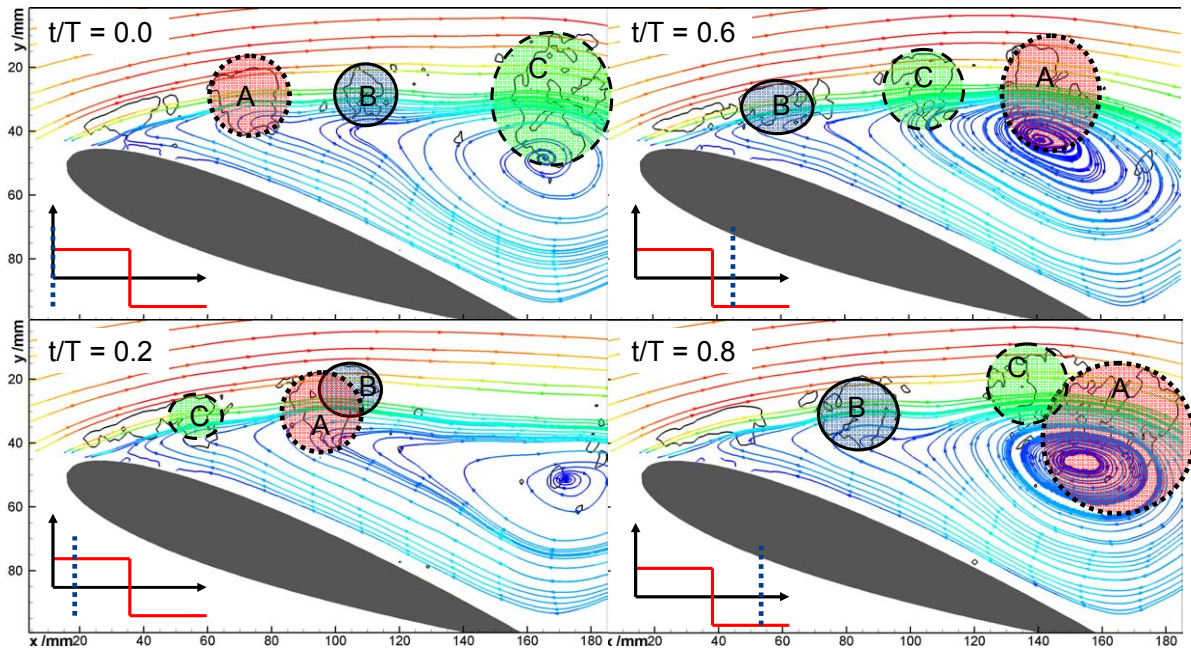


Fig. 4: Phase averaged stream lines for excitation with $DC = 1$, for $\alpha = 20^\circ$, $c_\mu' = 0.12\%$, $F^+ = 0.75$ and $Re = 10^5$. Vortices (A,B,C) are indicated by the λ_2 -criteria and highlighted by color and lines. The bottom left inserts are indicating the Lorentz force

The lift increases and the drag decreases. For the higher angle of attack of $\alpha = 22^\circ$ (on the right hand side of Fig. 3) the picture changes completely. The highest value for all investigated wave forms was measured at a dimensionless excitation frequency of $F^+ = 0.6$. There is a second maximum at the first subharmonic for $F^+ = 0.3$. Regarding active flow control systems for aerodynamics with limited frequency range, this second maximum can be used to optimize the excitation also for lower frequencies. With the increase in the lift, the drag rises as well. The mechanism for the lift is not the flow reattachment anymore, but complex vortex interaction. Since the vortex production due to the actuator and their temporal and spatial evolution is strongly dependent on the frequency, the lift signal shows this behavior, too.

The complex vortex interaction is exemplarily presented in Fig. 4 for $\alpha = 20^\circ$ and $F^+ = 0.75$, which is close to the optimum of $F^+ = 0.67$ for this angle of attack. For this frequency and the excitation with $DC = 1$, three successive vortices were shed during one period. For $t/T = 0.0$ all three vortices A, B, and C are present, where the large structure C detaches from the trailing edge. In the following phase the lift and drag decrease. A first interaction of vortices A and B, which agglomerate approximately above the mid chord, can be seen for $t/T = 0.2$. This is possible since B was produced in the phase of anti-stream-wise forcing and has a lower convection speed than A.

At the leading edge, a new vortex C forms again and due to the stream-wise forcing it will move quickly downstream and catches the former structure A at $t/T = 0.8$. This last vortex merging is also related to the highest lift during one period. A closed recirculation region directly above the suction side of the profile is established and increases the circulation around the hydrofoil. Choosing the wrong frequency (not shown here), less or even no interaction of the vortices is visible above the suction side.

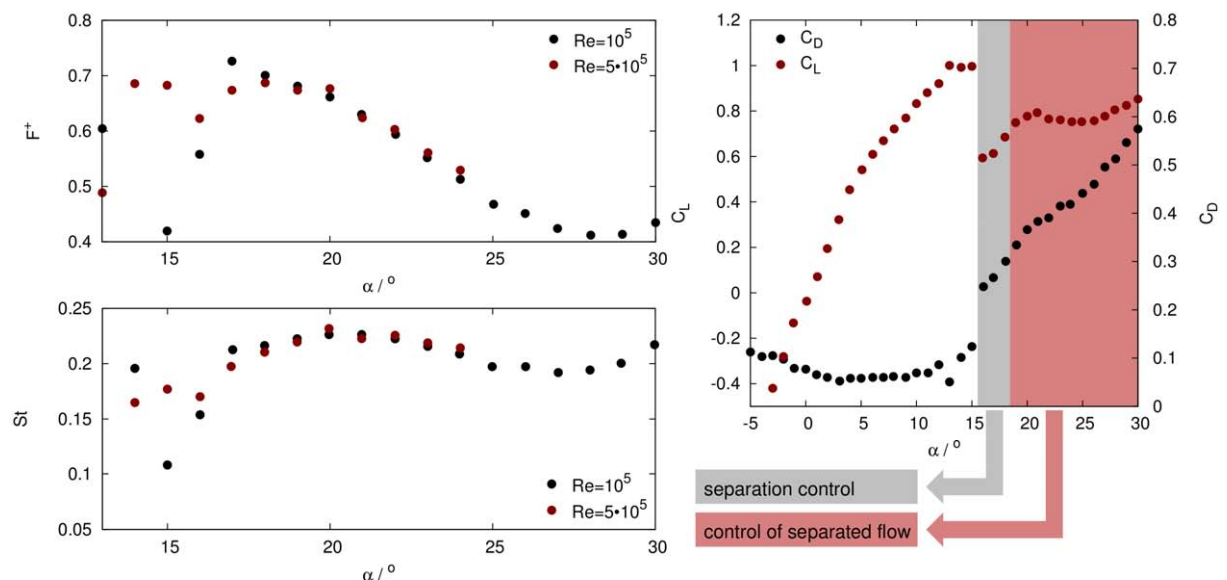


Fig. 5: Dominant frequency in the lift signal vs. α as F^+ and Strouhal number $St = fcsin(\alpha)/u_\infty$ (left). Two regions of flow control for this investigation (right)

The time dependent lift signal of the airfoil with separated flow shows a dominant frequency component even in the unforced case. This dominant frequency is plotted in the left part of Fig. 5 versus the angle of attack in two dimensionless forms differing in the length scales used for normalization. In the upper diagram, the dominant frequency is scaled with the chord length in the same way as the normalized excitation frequency in equ. (4). When the flow is

fully separated the dimensionless dominant frequency seems to be independent of the Reynolds number in the Reynolds number range investigated here. However, the dimensionless frequency changes significantly with α from $F^+ = 0.7$ at $\alpha = 18^\circ$ to $F^+ = 0.4$ at $\alpha = 29^\circ$. These values closely resemble those of the optimal excitation frequencies. To the authors knowledge, this effect was rather disregarded in the literature.

Using a characteristic wake width ($c \sin(\alpha)$) as length scale for frequency normalization results in the so called Strouhal number ($St = f c \sin(\alpha) / u_\infty$). Plotting the dominant frequency of the lift signal as Strouhal number versus the angle of attack in the bottom left part of Fig. 5, we find values of around $St = 0.2$ for $\alpha > 17^\circ$. Since such a value of the Strouhal number is quite typical for wake flows, this is a strong indication for a considerable influence of the wake on the separated flow above the airfoil.

4. Conclusion

Two different regimes (highlighted in Fig. 5 right) exist for the active flow control on a NACA0015 profile and the investigated Reynolds numbers. For α slightly above the critical angle of separation, small momentum input is sufficient to reattach the flow completely. The lift increases and the drag decreases. The Lorentz force actuator acts as a kind of turbulence generator and the turbulent shear layer evolving at the leading edge remains attached.

For higher angles of attack, a complete reattachment for low momentum input is not possible. Nevertheless vortex interactions can be triggered, using the right frequency of excitation. Due to this vortex interaction a recirculation region is stabilized above the suction side and increases the lift significantly.

It is a main result and was rather disregarded in the literature that the optimal frequency obviously changes with the angle of attack. The optimal excitation frequency within this study was always the dominant frequency in the lift signal and changes from $F^+ = 0.7 \dots 0.4$ for $\alpha = 18 \dots 30^\circ$. For higher angles of attack the wake flow becomes more and more important.

References

- [1] M. Gad-el-Hak (2000), Flow control: passive, active, and reactive flow management, Cambridge University Press
- [2] S. Grundmann and C. Tropea, (2007), Experimental transition delay using glow-discharge plasma actuator, Experiments in Fluids 42, 653-657
- [3] P. Scholz, J. Ortmanns, C.J. Kähler and R. Radespiel (2006), Leading Edge Separation Control by means of Pulsed Jet Actuators, AIAA Flow Control Conference, San Francisco, California
- [4] C. Bouras, H. Nagib, F. Durst and U. Heim (2000), Lift and Drag Control on a Lambda Wing Using Leading-Edge Slot Pulsation of Various Wave Forms, Bulletin of the American Physical Society 45(9)
- [5] C. Cierpka, T. Weier and G. Gerbeth (2007), Electromagnetic control of separated flows using periodic excitation with different wave forms, Active Flow Control, Notes on Numerical Fluid Mechanics and Multidisciplinary Design (NNFM), 95, Berlin, Springer, 27-41
- [6] T. Weier and G. Gerbeth (2004), Control of Separated Flows by Time Periodic Lorentz Forces, European Journal of Mechanics B/Fluids, 23, 835-849

- [7] C. Cierpka, T. Weier and G. Gerbeth (2008), Evolution of vortex structures in an electromagnetically excited separated flow. *Experiments in Fluids*, 45, 943-953
- [8] C. Cierpka (2009), Zeitaufgelöste PIV-Untersuchungen zur Strömungskontrolle mittels elektromagnetischer Kräfte in schwach leitfähigen Fluiden, Wissenschaftlich-Technischer Bericht, Forschungszentrum Dresden-Rossendorf
- [9] A. Gailitis and O. Lielausis (1961) On a possibility to reduce the hydrodynamical resistance of a plate in an electrolyte, *Applied Magnetohydrodynamics*, 12, 143-146.

Acknowledgements

Financial support from Deutsche Forschungsgemeinschaft (DFG) in frame of the Collaborative Research Centre (SFB) 609 is gratefully acknowledged.

FROM PROMISE 1 TO PROMISE 2: NEW EXPERIMENTAL RESULTS ON THE HELICAL MAGNETOROTATIONAL INSTABILITY

Frank Stefani, Gunter Gerbeth, Thomas Gundrum, Rainer Hollerbach¹, Janis Priede², Jacek Szklarski³, and Günther Rüdiger⁴

1. Introduction

Magnetic fields play an active role in cosmic structure formation. In 1991, Balbus and Hawley [1] had highlighted the key role of the magnetorotational instability (MRI, or Velikhov-Chandrasekhar instability [2]) for the enhanced angular momentum transport in accretion disks which is necessary to explain the mass accumulation rates of protostars and black holes.

Besides tremendous theoretical and numerical effort to understand the MRI, the last years have also seen considerable experimental activities to investigate this important instability in the liquid metal laboratory [3]. In the standard version of MRI, with only an axial magnetic field being externally applied, the azimuthal field which is also necessary for the working of the MRI, must be produced by induction effects proportional to the magnetic Reynolds number (R_m) of the flow. It is this reliance on R_m that makes standard MRI experiments so expensive since they become of the same size as dynamo experiments [4]. But why not substitute the induction process simply by externally applying an azimuthal magnetic field as well? In 2005, this apparently simple question was addressed by Hollerbach and Rüdiger [5], who showed that the MRI is then possible with far smaller Reynolds (Re) and Hartmann (Ha) numbers. First experimental evidence for this helical MRI, as we call it now, was obtained in 2006 at our liquid metal facility PROMISE (Potsdam Rossendorf Magnetic InStability Experiment) which is basically a Taylor-Couette cell made of concentric rotating copper walls, filled with GaInSn (an eutectic which is liquid at room temperatures). In [6] it was shown that the travelling MRI wave appears only in the predicted finite window of the magnetic field intensity, with a frequency of the travelling wave that was also in good accordance with numerical simulations. More results of this experiment were published later in [7].

However, a certain difficulty with these early experiments was the fact that the observed MRI wave did not travel along the entire height of the Taylor-Couette cell but ceased to exist at some position typically close to mid-height. By modifying the electric boundary conditions in radial direction, and analyzing the resulting change of the axial velocity [8], it was possible to identify this sink of the travelling MRI wave with the position of the radial jet that originates from the Ekman pumping at the upper and lower lids of the Taylor-Couette cell. The influence of this Ekman pumping on the flow structure was carefully discussed in [9].

In order to overcome this problem we have modified the PROMISE experiment by changing the axial boundary conditions, first by replacing the copper of the lower lid by insulating material, and second by splitting both the upper and lower lids into two rings (rotating with the inner and outer cylinder, respectively). Henceforth, this new version of the experiment

¹ University of Leeds, UK

² University of Coventry, UK

³ IPPT Warsaw, Poland

⁴ AIP Potsdam

will be called PROMISE 2 in order to discriminate it from the previous PROMISE 1 experiment. We will show that the minimization of the Ekman pumping makes the radial jet disappear almost completely. Consequently, the MRI wave can travel throughout the entire Taylor-Couette cell. We will investigate in detail the dependency of the MRI wave on the azimuthal field strength showing a much improved agreement with the 2D numerical predictions [9]. Further comparisons with the results of a 1D eigenvalue code [10] for the convective and the absolute instability will provide strong evidence that the observed wave represents a global instability indeed and not only a noise-triggered convective instability as argued in [11].

2. From PROMISE 1 to PROMISE 2

Apart from the modified end-caps, the PROMISE 2 set-up is more or less identical to that of PROMISE 1 which was described in detail in [6]. The basic part of it is a cylindrical containment vessel made of copper (see Fig. 1). The inner wall of the vessel is 10 mm thick, and extends in radius from 22 to 32 mm; the outer wall is 15 mm thick, extending from 80 to 95 mm. This vessel is filled with the eutectic alloy $\text{Ga}_{67}\text{In}_{20.5}\text{Sn}_{12.5}$, which has the advantage of being liquid at room temperatures.

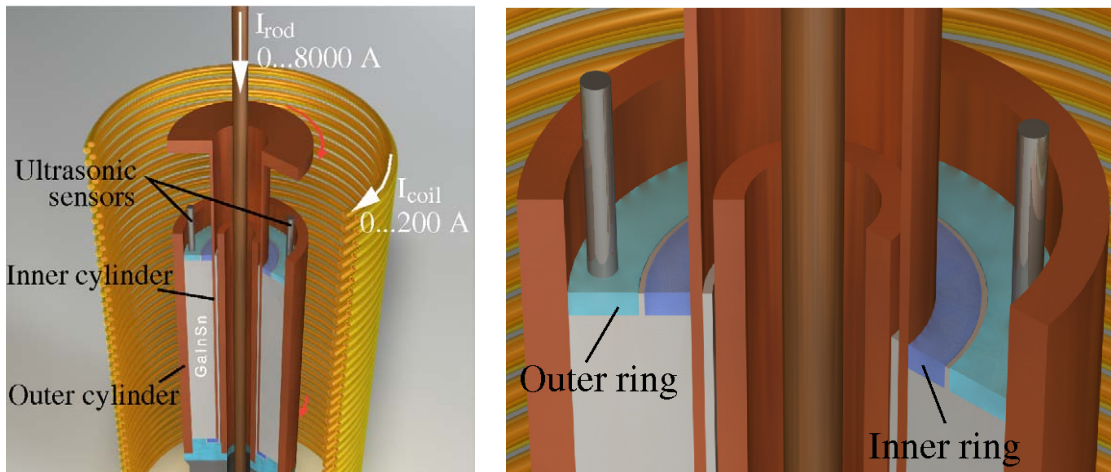


Fig. 1: The PROMISE 2 experiment, Left: General view, Right: Details of the split end-cap

The copper vessel is closed by a plastic bottom and is fixed, via a brass spacer, on a precision turntable; the outer wall of the vessel thus serves as the outer cylinder of the Taylor-Couette cell. The inner cylinder of the Taylor-Couette flow is fixed to an upper turntable, and is immersed into the liquid metal from above. It has a thickness of 4 mm, extending in radius from 36 to 40 mm. Between this immersed cylinder and the inner wall of the containment vessel there is thus a gap of 4 mm, also filled with GaInSn. It has a thickness of 4 mm, extending in radius from 36 to 40 mm, thus leaving a gap of 4 mm between this immersed cylinder and the inner wall of the containment vessel. The actual Taylor-Couette cell then extends in radial direction over a cylindrical gap of width $d = r_{out} - r_{in} = 40$ mm, and in axial direction over the liquid metal height of $0 \text{ mm} < z < 400$ mm.

While in PROMISE 1 the upper end-cap was a plastic lid fixed to the outer frame this end-cap is now split into two concentric plastic rings (see Fig. 1). The inner ring rotates with the inner copper cylinder, the outer one rotates with the outer cylinder. The choice of the splitting position at $r = 56$ mm was motivated by the simulation in [9] showing that a splitting at $0.4 d$ would minimize the global Ekman pumping. The lower end-cap is split in the same manner, so

that we have a symmetric configuration, with respect to both the rotation rate and to the electrical conductivities. This is a significant improvement compared with PROMISE 1, in which the copper bottom was simply part of the vessel which rotated with the outer cylinder.

The magnetic field configuration is identical to that of PROMISE 1, with axial magnetic fields of order 10 mT being produced by the current I_{coil} in a double-layer coil with 78 windings, and an azimuthal field of the same order being generated by a current I_{rod} through a central water-cooled copper rod of radius 15 mm. As in PROMISE 1, the measuring instrumentation consists exclusively of two high-focus ultrasonic transducers with a working frequency of 4 MHz which are fixed into the outer plastic ring, 12 mm away from the outer copper wall, flush mounted at the interface to the GaInSn. Since this outer ring is rotating, it is necessary to transfer the signal into the laboratory frame (in contrast to PROMISE 1 in which the upper lid was fixed to the frame). This is accomplished by the use of a slip ring contact which is situated below the vessel (not shown in Fig. 1).

3. Experiments and main results

The flow structure in the non-magnetic case is an important reference point for the later analysis of the helical MRI. Starting with $\mu := f_{\text{out}}/f_{\text{in}} = 0$, we expect a Taylor vortex flow whose amplitude should decrease for increasing μ . Beyond the Rayleigh point $\mu_{\text{Ray}} := (r_{\text{in}}/r_{\text{out}})^2 = 0.25$ the Taylor vortex flow is supposed to disappear completely in accordance with Rayleigh's criterion. However, in any real Taylor-Couette-cell with finite height this is far from trivial due to the existence of a meridional flow driven by the Ekman pumping at the upper and lower end-caps. Approximately at mid-height of the cell the two opposed vertical flows meet each other and produce a radial jet.

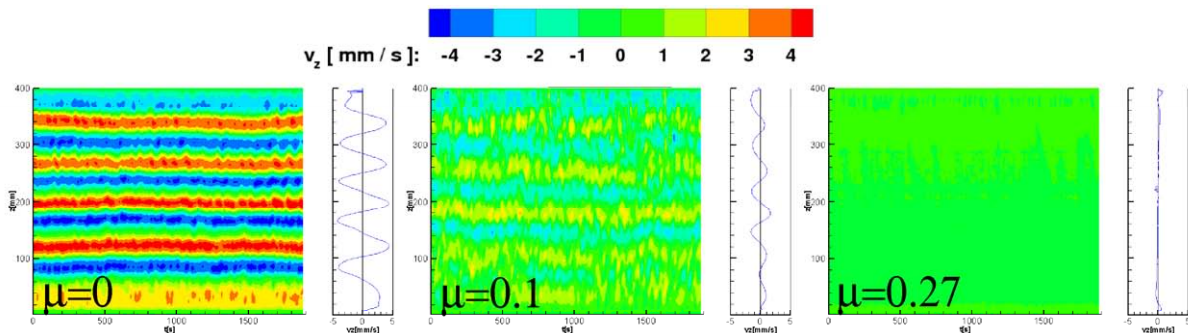


Fig. 2: Measured axial velocities in dependence on the vertical position and the time, for different rotation ratios μ . The Taylor vortex flow at $\mu=0$ becomes weaker for increasing μ and disappears completely for $\mu = 0.27$ which is beyond the Rayleigh line (at $\mu = 0.25$)

Figure 2 shows, for $f_{\text{in}} = 0.1$ Hz, the measured axial velocities for PROMISE 2. As expected, we observe a Taylor vortex flow which is getting weaker for increasing μ and then disappears completely at $\mu = 0.27$. In contrast to this, in PROMISE 1 we had observed a very steep sign change of $V_z(z)$ approximately at mid-height which indicated the existence of a narrow radial jet at this point. The absence of this structure in PROMISE 2 is due to the drastic reduction of the Ekman pumping. In the following we will see that this absence of the radial jet has important consequences for the propagation of the MRI wave.

For liquid metals, the critical Re for standard MRI (with a purely axial magnetic field) is known to be in the order of a few million. The key point of helical MRI is that by adding an azimuthal magnetic field, this number drops drastically to approximately 10^3 . In PROMISE 1, the transition to instability for increasing $\beta := B_\theta(r = r_{in})/B_z$ turned out to be not very sharp. In the following we will investigate the corresponding transition for PROMISE 2. Much more details, and dependencies on other parameters like Re , μ , and Ha , can be found in [12,13].

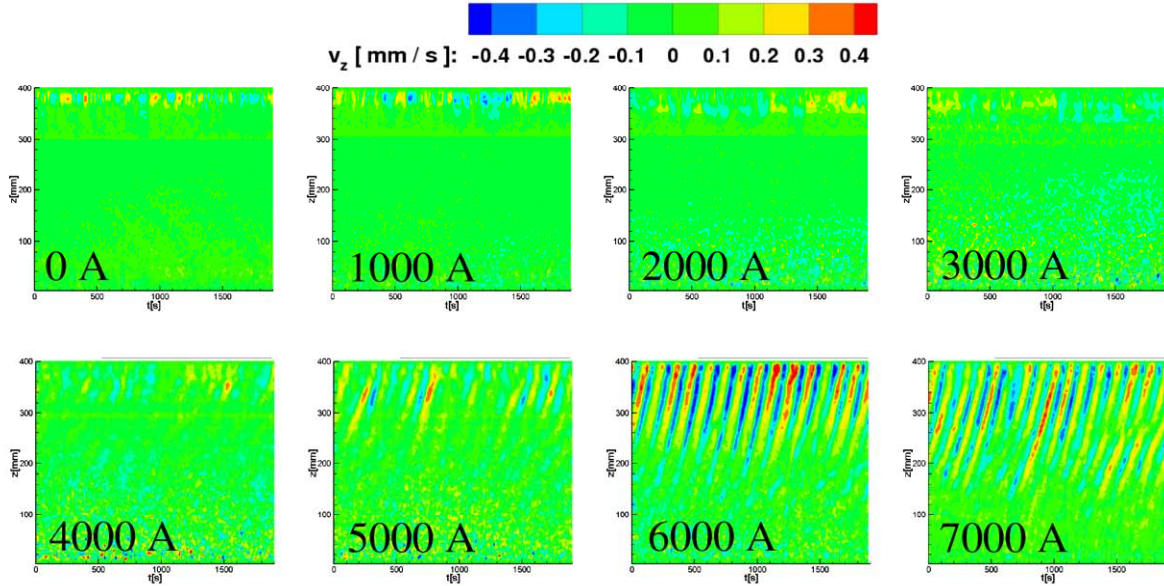


Fig. 3: Measured axial velocities in dependence on the vertical position and the time, for different values of the axial rod current

Figure 3 shows 8 panels with the measured axial velocity perturbation for $0 < I_{rod} < 7000$ A. Evidently, there is no indication of any instability for $I_{rod} < 4000$ A. The transition to MRI occurs approximately between $4000 \text{ A} < I_{rod} < 5000$ A. A more quantitative analysis is given in Fig. 4 where we show the rms of the velocity perturbation of the MRI wave in dependence on β for two different lines corresponding to $\mu = 0.26$ and $\mu = 0.27$. In addition to the results of a time-stepping 2D solver [9] we have also added the critical μ values for the convective and the absolute instability as they result from a 1D eigenvalue solver [10].

The first noticeable fact is that for $\mu = 0.26$ we obtain not only a good correspondence of the experimental results with the results of the 2D simulation, but also a good agreement of the latter with the 1D numerical prediction for the absolute instability. At the same time, the 1D prediction for the convective instability would point to much smaller values of the critical β . This is strong evidence that the observed instability is not a noise-triggered convective one as claimed in [11], but indeed a global one.

In this respect it is also remarkable that for $\mu = 0.27$ the agreement of the absolute instability of the 1D code (at $I_{rod} \sim 8200$ A) and the global instability from the 2D code (at $I_{rod} \sim 6200$ A) becomes worse. Evidently, the value $\mu = 0.27$ is very close to the upper limit of the helical MRI. In this case, the threshold of MRI will be extremely sensitive to any slight modification of the base velocity profile. This is a typical case in which we do get a global instability for the experimental axial boundary conditions, but the hypothetical use of ideal Taylor-Couette boundary conditions would make the flow stable again. This interesting case has been

observed in the numerical simulations of Liu [11]. However, as we see here the interpretation of the author is not correct: what is observed for real boundary conditions is not a noise-induced convective instability (this would start already at $\beta = 2.3$) but still a global instability, although on the basis of a flow that is slightly modified by the lids which make the flow a bit more prone to MRI than the ideal Taylor-Couette flow would be.

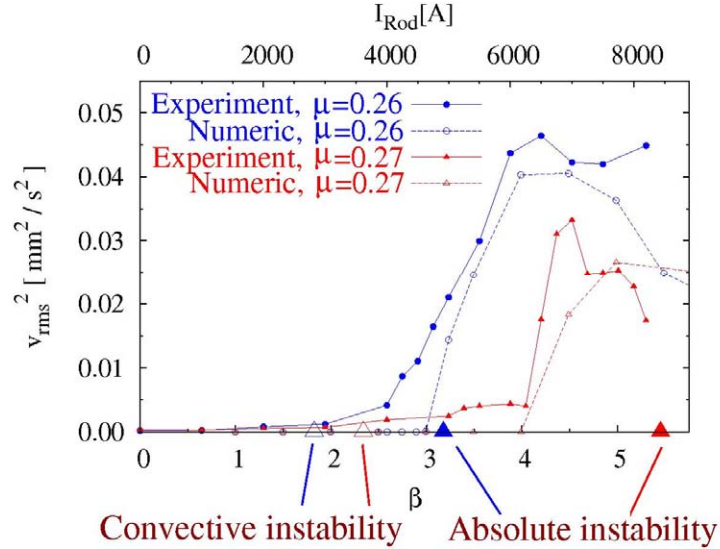


Fig. 4: Rms of the velocity perturbation for different values of the rod current. The full lines show the experimental results, the dashed lines show the predictions by a 2D code. The 1D numerical predictions for the convective and absolute instability are also shown

4. Summary and outlook

We have studied the helical MRI in an improved Taylor-Couette setup in which the Ekman pumping is significantly reduced by using split end-caps. The MRI wave, which now spreads over the whole height of the cell, appears much sharper and in better agreement with numerical predictions. We conclude that the observed helical MRI represents a self-sustained global instability rather than a noise-sustained convective one. A “promising” perspective of PROMISE would be to extend the range of parameters Re and Ha in order to investigate the continuous transition between the well-studied region of the helical MRI and the experimentally much more demanding region of the standard MRI. One way to accomplish this would be to replace the working fluid GaInSn by sodium, which is one of the central topics of the planned DRESHDYN platform. Another interesting extension is the study of various combinations of the MRI and the Taylor instability, which requires to direct electric currents through the liquid metal.

References

- [1] S. A Balbus and J. F. Hawley (1991), A powerful local shear instability in weakly magnetized disks. 1. Linear Analysis, *Astrophys. J.* 376, 214
- [2] E. P. Velikhov (1959), Stability of an ideally conducting liquid fluid between cylinders rotating in a magnetic field, *Sov. Phys. JETP* 36, 995
- [3] F. Stefani, A. Gailitis, G. Gerbeth (2008), Magnetohydrodynamic experiments on cosmic magnetic fields, *ZAMM* 88, 930

- [4] D. Sisan et al. (2004), Experimental observation and characterization of the magnetorotational instability, *Phys. Rev. Lett.* 93, Art. No. 114502
- [5] R. Hollerbach and G. Rüdiger (2005), New type of magnetorotational instability in cylindrical Taylor-Couette flow, *Phys. Rev. Lett.* 95, Art. No.124501
- [6] F. Stefani et al. (2006), Experimental evidence for magnetorotational instability in a Taylor-Couette flow under the influence of a helical magnetic field, *Phys. Rev. Lett.* 97, Art. No. 184502
- [7] F. Stefani et al. (2007), Experiments on the magnetorotational instability in helical magnetic fields, *New J. Phys.* 9, 295
- [8] F. Stefani et al. (2008), Results of a modified PROMISE experiment, *Astron. Nachr.* 329, 652
- [9] J. Szklarski (2007), Reduction of boundary effects in the spiral MRI experiment PROMISE, *Astron. Nachr.* 328, 499
- [10] J. Priede and G. Gerbeth (2009), Absolute versus convective helical magnetorotational instability in a Taylor-Couette flow, *Phys. Rev. E* 79, 046310
- [11] W. Liu (2009), Noise-sustained convective instability in a magnetized Taylor-Couette flow, *Astrophys. J.* 692, 998
- [12] F. Stefani et al. (2009), Liquid metal experiments on the helical magnetorotational instability, *Magnetohydrodynamics* 45, 135
- [13] F. Stefani et al. (2009), Helical magnetorotational instability in a Taylor-Couette flow with strongly reduced Ekman pumping, *Phys. Rev. E*, in press

Acknowledgments

This work was supported by German Leibniz Gemeinschaft, within its SAW programme. We thank Heiko Kunath for technical assistance.

THERMOELECTROMAGNETIC CONVECTION – AN ALTERNATIVE STIRRING TECHNIQUE IN METALLURGY

Andreas Cramer, Xiugang Zhang, and Gunter Gerbeth

1. Introduction

The interaction between a thermoelectric current \mathbf{j}_{TE} and an imposed magnetic field \mathbf{B} may drive thermoelectromagnetic convection (TEMC). Prerequisite for \mathbf{j}_{TE} is a temperature gradient ∇T and a spatial variation of the thermoelectric power S , both of which in combination may generate an electro-motive force (emf). For whatever the temperature distribution, simple analytical consideration shows that no current will circulate in a medium of uniform composition. This is because S is a function of T , only, a consequence of which is that the resulting Lorentz force $\mathbf{j}_{TE} \times \mathbf{B}$ is irrotational, i.e. conservative. In order to have thermoelectric current flowing, ∇S and ∇T must not be parallel. This is, in general, achieved by a spatially varying composition. The mathematically interested reader is referred to the pioneering study of Shercliff [1], who generalised Ohm's law for conducting liquids by introducing a term for the emf.

Although these basics of TEMC are known for a long time, embodiments for an effective stirring of a liquid metal pool are badly missing. This prompted us to perform an experimental study on TEMC configurations which are concerned with the case that was termed by Shercliff as “the extreme case when the composition and S vary discontinuously across an interface along which T varies [1]”. Besides thermocouples or a sound direct conversion between thermal and electric energy, thermoelectromagnetic stirring is probably a likewise attractive application of the Seebeck effect. Whenever there is a freedom to use electrically conducting walls in metallurgy, TEMC may become an efficient and cheap tool since the necessary temperature gradient is often intrinsic to the process.

2. Experimental setup

Three flow containers were built that had in common that the necessary temperature gradient ∇T in a square box was obtained by heating and cooling, respectively, of two opposing massive copper side walls. Utilising a nickel plate having the relatively high thermoelectric power of $S = -15 \mu\text{V/K}$ for the bottom established the material discontinuity with respect to the liquid metal layer in the first setup. Here, also both other side walls parallel to ∇T were made from copper to simplify matters. Some parasitic loss via current circulating through these walls is then to be expected owing to the high ratio of electrical conductivities between copper and the melt. Despite this disadvantage, it made sense to deal with this setup yet at the stage of laboratory experiments since it is a potential industrial configuration for the reason of the ease of construction. If TEMC stirring shows up to work in a downgraded setup with loss of current, it will work more than ever in an optimised configuration. In both other apparatuses, the side walls parallel to ∇T were however replaced with glass for the additional reason of being of more generic nature. It is worth noting that fused silica stands temperatures comparable to that of copper.

The task formulation of a marked TEMC may be accomplished with a strong inhomogeneity of the magnetic flux density \mathbf{B} , which was fulfilled with a $50 \times 20 \times 8 \text{ mm}^3$ permanent magnet made from cobalt-samarium in the first setup. With the direction of magnetisation along the

shortest side, it produced $B = 270$ mT at its surface. Sizes of the container were length = width = 15 cm. For a more detailed description of the experiment with the permanent magnet [2] is referred to.

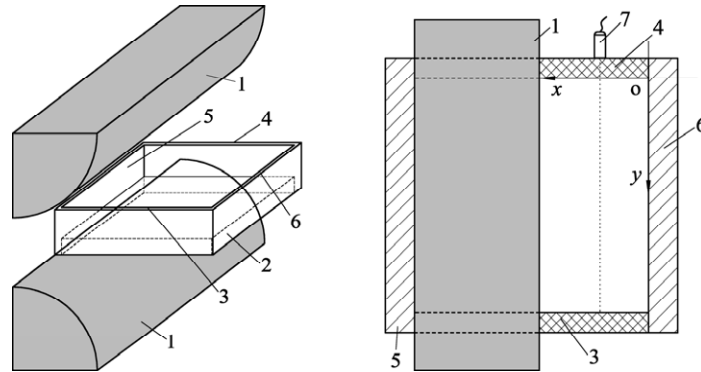


Fig. 1: Sketch of the experimental setup with the electromagnet in perspective (left) and top view (right). 1: pole shoes, 2: constantan or nichrome bottom, 3&4: front and rear insulating side walls, and 5&6: cooled and heated isothermal side walls, respectively. The ultrasonic sensor (7) can be traversed along the rear wall

The second and third quadratic containers were a little bit smaller and used in combination with an electromagnet. The length of 12 cm was accounted for by adjusting ΔT accordingly, this means that ∇T is the same in all containers. Figure 1 depicts the experimental arrangement for the setups with the electromagnet and the shape of the pole shoes. In order to enhance TEMC, bottom materials with even higher absolute values of S were employed. $S_{\text{constantan}} = -35 \mu\text{V/K}$ is probably the highest value that can be found among metals, and $S_{\text{nichrome}} = 25 \mu\text{V/K}$ provides also the complementary case. Note that these materials differ significantly from nickel, the latter being ferromagnetic, which has a significant influence onto the distribution of \mathbf{B} . The filling height of the melt was always 1.5 cm. GaInSn ($T_{\text{melt}} = 10^\circ\text{C}$) was chosen as the liquid metal under investigation mainly for the reason of its thermoemf $S_{\text{GaInSn}} = -0.55 \mu\text{V/K}$ differing not that much from $S_{\text{Cu}} = -2 \mu\text{V/K}$ of the copper walls.

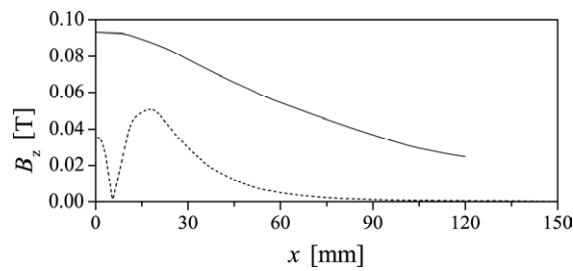


Fig. 2: Dependence of B_z at the liquid-solid interface on the position between the hot and the cold wall. Dashed line: permanent magnet, solid line: field produced by the electromagnet

Numerical simulations were performed with a commercial solver showing that \mathbf{B} was almost perpendicular to the bottom of the first container within the lower part of the metallic melt layer, as was to be expected because of the ferromagnetic nickel. The pole shoes used in the second configuration produced a field with a prominent vertical component. Measurements performed with a 3-axis Gauss meter agreed nicely with the computations. For the following considerations, it is thus sufficient to restrict to B_z . Besides observing the motion at the melt

surface, local flow measurements were performed. An ultrasonic Doppler velocimeter (UDV) was used to acquire instantaneous velocity profiles along the ultrasonic beam.

3. Results and discussion

In a first series of experiments, the permanent magnet was located with its long side aligned to the cold wall. Under the assumption of a homogeneous thermoelectric current between the isothermal walls, the Lorentz force is directed along the wall while diminishing with increasing distance to that wall. The flow structure expected to develop thus is a recirculation in the horizontal plane: driven by the force acting in the vicinity of the wall and closing elsewhere in the liquid metal volume. Characteristic velocities u obtained with UDV depended monotonously increasing on ΔT , which accords to the relative strength of TEMC

$$Te = \sigma \Delta S B \Delta T l^2 / \rho \nu^2 \quad (1)$$

proposed by Gorbunov [3]. Te , l , ρ , and ν are the dimensionless parameter aka similarity criterion, the characteristic length, density, and kinematical viscosity. A typical value for, e.g., $\Delta T = 50$ K is $u = 70$ mm/s clearly demonstrating the dominance over buoyancy, the latter producing a velocity of 5 mm/s, only. An entire velocity section along the propagation direction of the ultrasonic beam in conjunction with scanning the sensor in the perpendicular direction yields area-wide results, from which a stream function may be calculated. Such evaluation shown in the left panel of Figure 3 agreed nicely with the expected flow structure of a single convection cell penetrating the container entirely with the eye of the vortex moved off centre towards the source of motion.

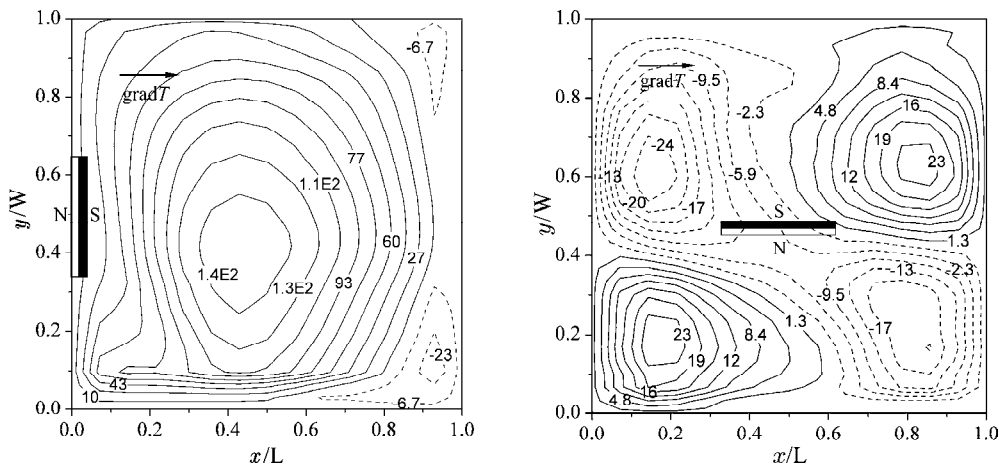


Fig. 3: Stream functions in the configuration with the permanent magnet calculated from area-wide UDV measurements. Left: single cell with magnet at the wall, right: multi-cellular pattern with centred magnet

Although the flow was relatively stable to the appearance of observation with the naked eye, velocities in the range of several cm/s indicated that the flow was not laminar. The plot of instantaneous velocities in Figure 4 clearly shows that the flow was turbulent. In the case that the magnet is located above the centre of the container, a convective pattern consisting of four cells is to be expected from the distribution of the thermoelectromagnetic force. Also in this configuration, the corresponding stream functions measured by scanning the UDV sensor in the second series of experiments fully supported the expectations of four vortices with diagonally opposing cells having the same rolling direction (c.f. right panel of Figure 3).

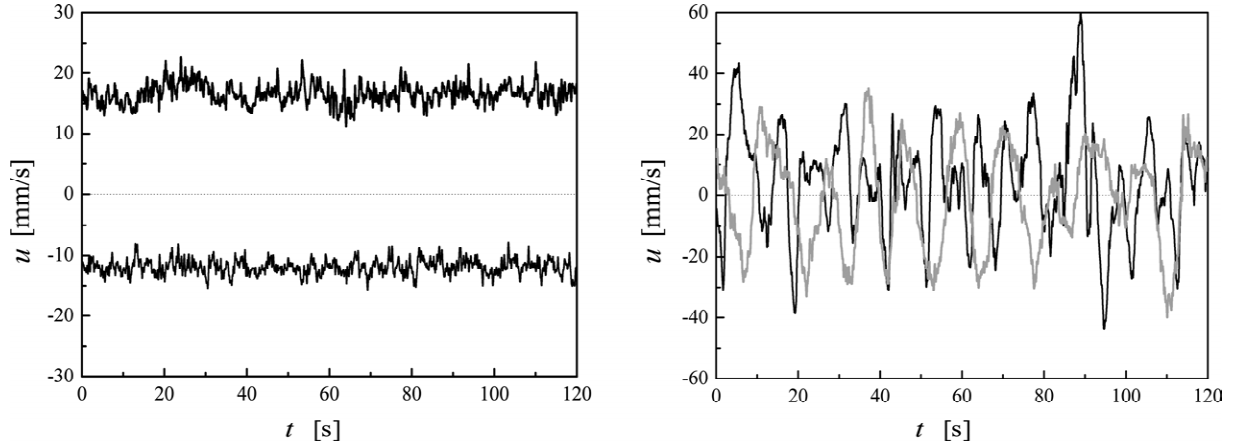


Fig. 4: Time series of the local velocity at two selected locations, each, in configuration one calculated from area-wide UDV measurements. Left: single cell with the magnet at the wall, right: multi-cellular pattern with centered magnet

Because the cell boundaries are not rigid walls, the system with the magnet above the center likely is the more unstable one. Free boundaries are potential sources of instability in many fluid-dynamical systems. Despite the temperature difference in the case of the centered magnet was 10 K higher than in the case of the single cell, mean velocities decreased distinctly whereas the turbulence was significantly intensified. The flow was characterised by oscillations of the mean flow eddies, which can be either movement of the vortices' eyes and/or growth and shrinkage of the vortices. Intermittence was, however, not observed in the investigated range of temperature differences. More results and an extended discussion of this configuration containing the permanent magnet are to be found in [2].

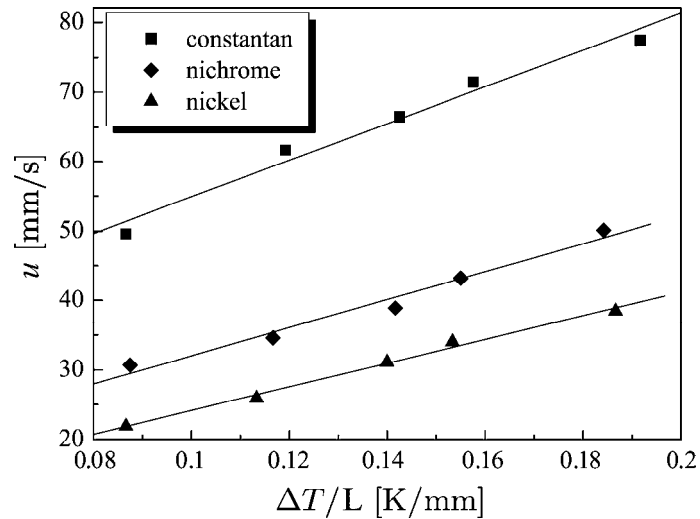


Fig. 5: Comparison of the dependence of the characteristic velocity u on the temperature drop $\Delta T/L$ with the bottom materials nickel, constantan, and nichrome as parameter. All measurements were done at the location of maximum velocity within the container

An obvious question when moving to the second setup is that about a potential mitigation of the vigour of the flow in the first container by Ohmic losses via the electrically conducting walls parallel to ∇T . The slightly different sizes are accounted for by adjusting identical $\Delta T/L$, where L is the distance between the isothermal walls. Another issue with respect to contras-

ting the experiments is the magnetic field, of which both absolute value and gradient are important. Figure 5 shows measurements for identical $B_z = 50$ mT. For not too high field strength, which is the range wherein the damping effect of the static field remains small, these results should conform to the criterion proposed by Gorbunov [3]. Since ΔS is the only parameter subject to variation, u should solely depend on the emf for any $\Delta T/L$. The points of the fit curves on the axis of ordinate are $u_{\text{Ni}} = 20.7$, $u_{\text{nichrome}} = 27.9$, and $u_{\text{constantan}} = 49.6$ mm/s. u_{Ni} has to be corrected to 32.3 mm/s for the different characteristic length. Even though there were certainly Ohmic losses in the experiments with the copper walls parallel to ∇T , the ratio $(u/\Delta S)_{\text{Ni}} = 2.2 \text{ mm}\cdot\text{K}/(\mu\text{V}\cdot\text{s})$ is much too high compared to the values of 1.1 and 1.4 for nichrome and constantan, respectively. This suggests that ∇B should be included in a scaling law since this gradient is much steeper for the permanent magnet above a ferromagnetic bottom (c.f. Figure 2).

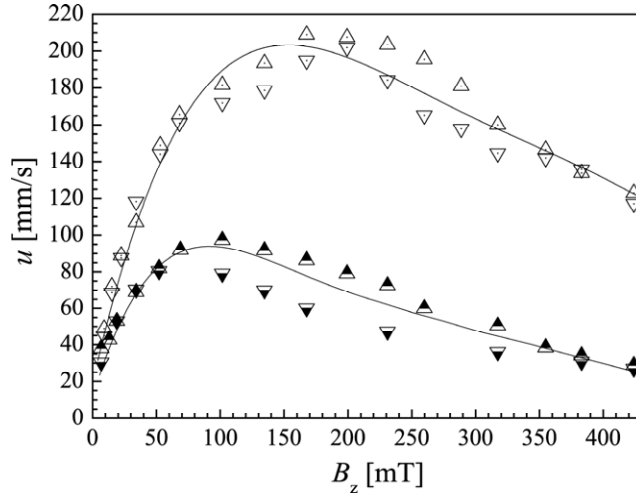


Fig. 6: Comparison of the dependence of the characteristic velocity on the vertical component of \mathbf{B} obtained in the container with constantan bottom at $\Delta T = 30$ and 60 K

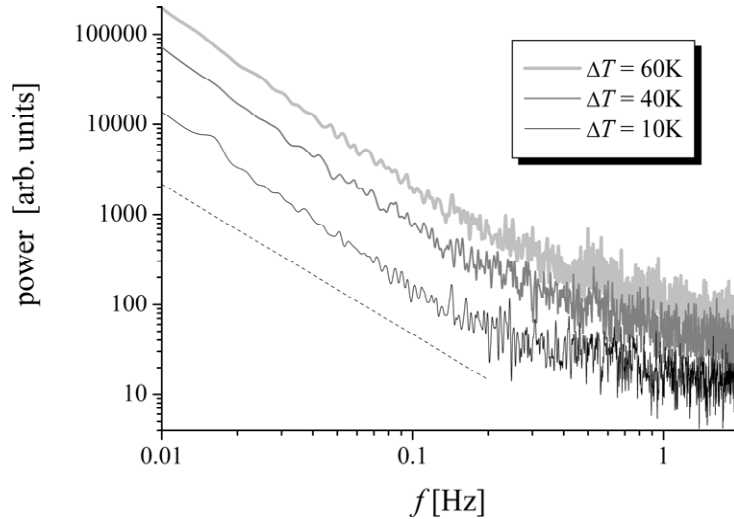


Fig. 7: Turbulence spectra for three selected temperature differences calculated from UDV measurements of u_y close to the cold wall where this velocity component is maximum. The straight dashed line represents the case of homogeneous isotropic turbulence $E(f) \propto f^{-5/3}$

Figure 6 shows four series, two for $\Delta T = 30$ and 60 K, each, wherein B_z was varied. Despite

the quite long sampling time exceeding ten minutes and comprising more than 12000 readings per single measurement, the data show a significant scatter predominantly in the range of medium field strength. Moreover, there seems to be a systematic deviation within each pair. The also damping influence of the flow driving magnetic field is however clearly demonstrated. The threshold above which braking overcomes impelling flow depends obviously on ΔT , which was not necessarily expected.

First results on the turbulence characteristics in a thermoelectromagnetically driven flow are presented in Figure 7. The series covered six equidistant measurements in the range $\Delta T = 10$ to 60 K at $B_z = 50$ mT, not all of them are shown in the graph. Those not depicted exhibit the same characteristics of an energy spectrum governed by homogeneous isotropic turbulence.

4. Summary

Thermoelectromagnetic convection (TEMC) was studied in square melt layers heated differentially in the horizontal direction. While the origin of the flow is an electro-motive force, the crux of the experiments was establishing a high differential Seebeck coefficient ΔS . Two case studies were realised: a generic one with a 2D distribution of the magnetic field \mathbf{B} having a gradient in direction of the temperature difference ΔT , only, and the other one having a full 3D distribution of \mathbf{B} . The main findings obtained with ultrasonic flow measurements are: (i) strong fluid motion suitable for metallurgical tasks is accomplishable, (ii) the vigour of the flow scales reasonably with ΔS , B , and ΔT as proposed in [3], (iii) at high values of B , the damping impact of the static field outbalances its flow driving effect, and (iv) ∇B determining the magnitude of the curl of the Lorentz force may become quite important. TEMC turbulence characteristics are seemingly classical, i.e. homogeneous and isotropic obeying the celebrated relation with its exponential $-5/3$ dependence of the kinetic energy on frequency.

References

- [1] J. A. Shercliff (1979), Thermoelectric magnetohydrodynamics, *J. Fluid Mech.* 91, 1917–1928
- [2] X. Zhang, A. Cramer, and G. Gerbeth (2009), Model experiments on macroscopic thermoelectromagnetic convection, *Magnetohydrodynamics* 45(1), 25–42
- [3] L. A. Gorbunov (1987), Effect of thermoelectromagnetic convection on the production of bulk single-crystals consisting of semiconductor melts in a constant magnetic field, *Magnetohydrodynamics* 23(4), 400–407

THE INFLUENCE OF DIFFERENT THERMAL HYDRAULIC MODELS ON THE RESULTS OF A DYN3D BORON DILUTION TRANSIENT CALCULATION

Sören Kliem, Yaroslav Kozmenkov, Siegfried Mittag, Ulrich Rohde, and Frank-Peter Weiss

1. Introduction

The strong thermal-neutron absorber Boron-10 is dissolved as boric acid in the coolant of Pressurized Water Reactors (PWR). It is used to compensate excess reactivity of the reactor core at the beginning of fuel cycle. Therefore, an unintentional, or even un-avoidable, decrease of boron concentration leads to a reactivity increase and may result in a power excursion, a so-called boron dilution transient. Slugs of under-borated, or even boron-free, coolant can be formed in the primary circuit, e.g. due to a malfunction of the chemical and volume control system, or due to a small break loss of coolant accident with partial failure of the safety injection system. When the first main coolant pump is started, or natural circulation re-establishes, that slug is shifted towards the core and introduces a certain positive reactivity there.

3D neutron kinetics core models like the reactor dynamics code DYN3D developed at Forschungszentrum Dresden-Rossendorf [1] are needed to simulate adequately the response of the reactor core to such a reactivity insertion. The code has been applied to the analysis of the core behaviour for different boron dilution transients [3,4,8].

DYN3D includes its own thermal hydraulic model called FLOCAL [2]. The code has also been coupled to the advanced thermal hydraulic system codes ATHLET and RELAP5 [5,6] which describe the interaction between the reactor core and the whole nuclear plant. For both codes ATHLET and RELAP5, the internal coupling type is available, where the thermal hydraulics of the whole system including the reactor core is modelled by the system code while only neutron kinetics is simulated by DYN3D. With this approach three options are available for the thermal hydraulic modelling of the reactor core in connection with the DYN3D neutron kinetic model. In the current paper, the influence of the use of these different thermal hydraulic models on the course and results of a boron dilution transient is investigated.

2. Boundary conditions of the analysis

The corresponding scenario is based on the start-up of the first main coolant pump (MCP) of a primary circuit loop where a slug of de-borated water has accumulated. During the transport of the slug from the cold leg to the core inlet, mixing with the higher borated coolant in the reactor pressure vessel takes place. Mixing is the only inherent physical mechanism against severe consequences of boron dilution transients. Therefore, it has been comprehensively investigated at the coolant mixing test facility ROCOM [7]. Time-dependent boron concentration curves at the inlet into each fuel assembly serving as boundary conditions for the core calculations, have been derived on the basis of experimental ROCOM data. The neutronic calculations start when the deboration front reaches the reactor core. In this state the MCP has already reached its stationary mass flow level, so that the calculations were performed at stationary flow conditions with a total core mass flow rate of 3200 kg/s.

The reactor core under consideration is a generic PWR core at the beginning of an equilibrium fuel cycle. The macroscopic cross-section library needed for the core calculations was generated using the 2D neutron transport code HELIOS. Initially, the reactor is in a hot sub-critical state with all control rods inserted. As a conservative assumption, one stuck rod cluster was assumed in the core sector with the highest deboration. The neutron kinetics model is the same in all three calculations. The same nodalisation in space and the same time steps were applied for thermal hydraulics (1 ms) and neutron kinetics (0.1 ms) calculations. The same material properties for fuel and cladding as well as the same constant heat transfer coefficient for the gas gap between fuel and cladding were used. In the calculations, a pressure of 3.0 MPa, an initial coolant boron concentration of 2200 ppm, and a coolant inlet temperature of 190 °C were assumed.

3. Results of the calculations

All three calculations resulted in the same K_{eff} -value for the initial state (Tab. 1). The 2D power distributions in the initial state show maximum differences between the solutions of 0.17 %.

At first, the influence of the numerical model for the description of the boron transport through the core was investigated. Starting from $t = 0$ s, the deboration front moves into the reactor core. Each of the codes used has its own boron transport model. Numerical diffusion within the different boron transport models can influence the results of a boron dilution transient analysis [3,8]. At the inlet into the core, the time-dependent boron concentration is identical in the three calculations. At higher core elevations, small differences develop between the calculations with growing time. Partially the differences are to be seen in the behaviour of the core average boron concentration (Fig. 1). At the outlet of the core, the differences are more significant. Theoretically, from the source-free boron transport equation, a sharp propagation of the boron dilution front without any diffusion is expected. The DYN3D calculation shows the sharpest front (Fig. 2) followed by ATHLET and RELAP5.

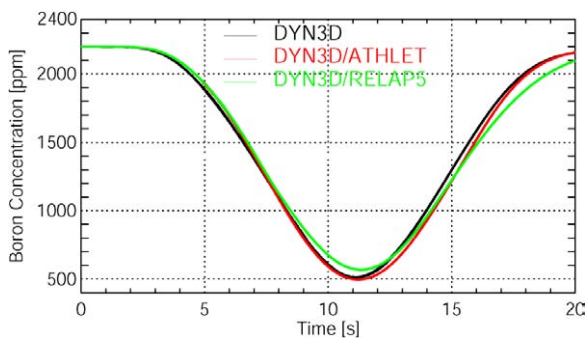


Fig. 1: Average boron concentration in the core

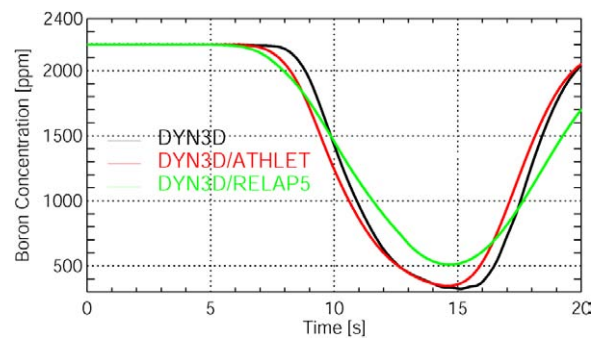


Fig. 2: Average core outlet boron concentration

The boron transport model of DYN3D is based on a particle-in-cell approach and has practically no numerical diffusion as was shown in [3]. The ATHLET model shows a smoothing of the boron front in comparison to DYN3D, but reaches nearly the same minimum value. The RELAP5 model is more diffusive. Due to the smoothing of the front the minimum value at the outlet calculated by RELAP5 is higher than in the two other calculations.

At about 5 s after the start of the calculations re-criticality of the scrammed reactor is reached, first in the calculation with the lowest numerical diffusion (DYN3D) followed by the two

others. Due to the considerable boron concentration reduction in the core even super-prompt criticality occurs (Fig. 3) which results in high power peaks (Fig. 4). Around the time of occurrence of the peak, the described differences in the movement of the boron front are still small (Fig. 1). Nevertheless differences in the time of re-criticality and height of the first power peak can be seen (Tab. 1).

Table 1: Key parameters of the calculations

	DYN3D	DYN3D/ATHLET	DYN3D/RELAP5
K_{eff} [-] of initial state	0.886819	0.886819	0.886819
Time of re-criticality [s]	5.05	5.28	5.66
Max. core power [MW]	14180	18715	20675
Full power pulse width at half maximum [ms]	15	15	15
Max. 3D power peaking factor [-]	123.2	109.2	103.9
Max. fuel centerline temperature [°C]	1261.2	1109.8	1154.2
Max. cladding temperature [°C]	256.0	278.1	267.4
Minimum DNBR [-]	1.566	1.637	2.677

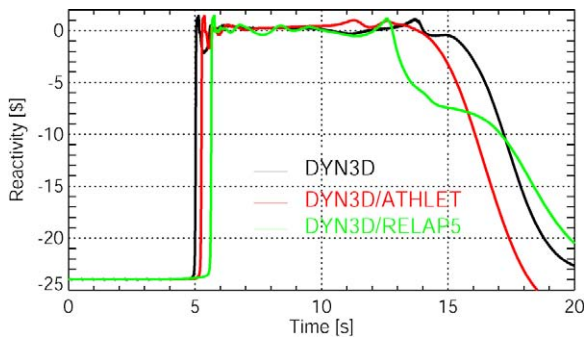


Fig. 3: Reactivity

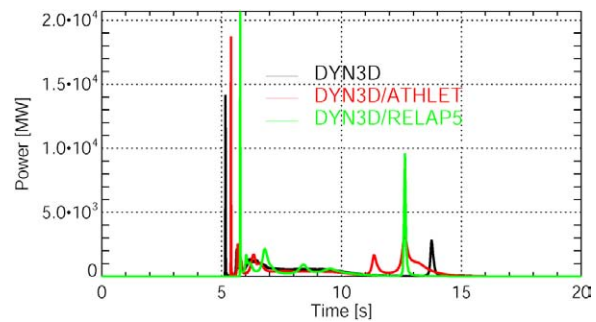


Fig. 4: Core power

Normally it could be expected that the calculation with the lowest numerical diffusion provides the highest power peak (e.g. [3,8]) as the height of the power peak is determined by the reactivity insertion rate around the time of re-criticality. This reactivity insertion rate is decreased by the numerical diffusion as explained above.

However, in the concrete case the time history of the boron concentration at the inlet into the fuel assemblies is based on experimental data. The time history of the boron concentration shows a small step, namely a temporary reduction of the decrease rate, at the fuel assembly with the highest power generation (N° 179) immediately after re-criticality (Fig. 5). This step influences the reactivity insertion rate. In the special case, the boron concentration rate in the nodes with the highest power production is the lowest in the DYN3D calculation (see Fig. 6). In the two other calculations the corresponding boron concentration gradient is higher at the time of re-criticality. Thus, the DYN3D calculation provides the lowest power maximum followed by DYN3D/ATHLET. The calculated power maximum in the DYN3D/RELAP5 calculation is about 10 % higher than the DYN3D/ATHLET value.

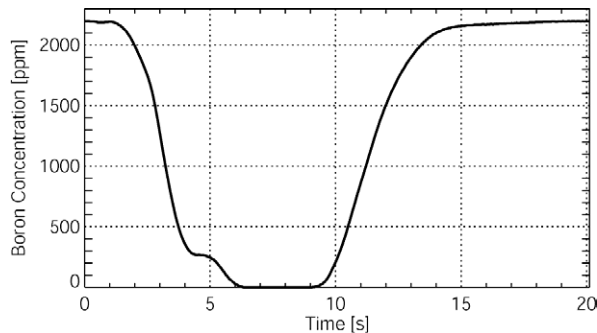


Fig. 5: Boron concentration at the inlet into fuel assembly 179

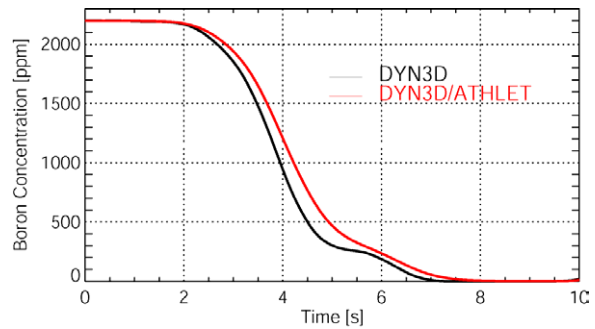


Fig. 6: Boron concentration in node 3 of fuel assembly 179

The heat insertion into the core is limited during this first power peak, because the power-peak width is very small (15 ms), due to the very effective, strongly negative Doppler feedback of the fuel temperature (identical in all three calculations). Nevertheless, boiling of coolant starts shortly after this first power peak (Fig. 7).

Secondary power peaks occur while the deboration front propagates through the reactor core. The structure of these peaks is determined by the ongoing introduction of positive reactivity resulting from lower-borated coolant and negative reactivity due to fuel temperature increase and coolant boiling. These power peaks are considerably lower than the first ones, apart from the last peak in the DYN3D/RELAP5 calculation, where super-prompt criticality is reached again (Fig. 3).

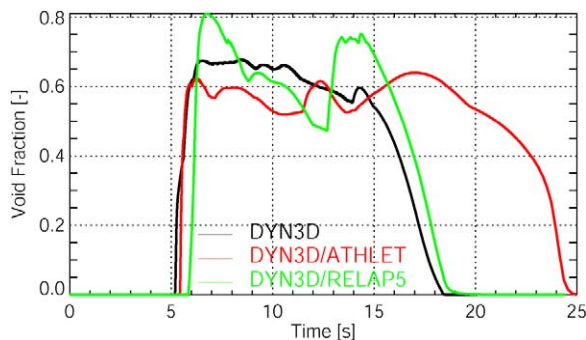


Fig. 7: Maximum void fraction in the core

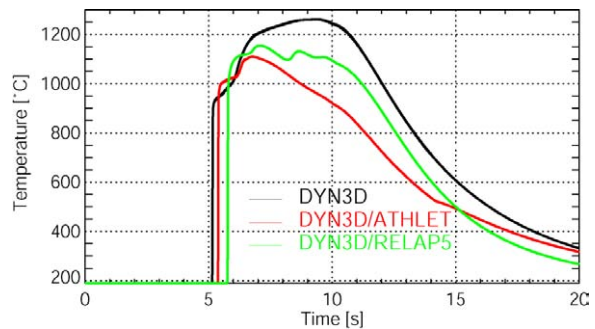


Fig. 8: Maximum fuel centerline temperature

Differences in the results of the calculations by the three different codes are caused not only by the different numerical treatment of boron transport, but also by differences in the thermal hydraulic models. Relevant models for the calculation of the vapour volume fraction being an important feedback parameter, are the boiling models, fuel rod models, and drift flux models. Because different models are used in the various codes, naturally the time course of the maximum void fraction is also different, in the three calculations (Fig. 7). The first appearance of vapour in the core in the DYN3D/ATHLET result is delayed against the DYN3D calculation due to the delay of the first power peak (0.23 s). The corresponding delay is higher in the DYN3D/RELAP5 calculation. Further, the DYN3D/RELAP5 calculation yields two pronounced void maxima which can be attributed to the high first and last power peaks. DYN3D shows a very smooth behaviour of the maximum void fraction. The last power peak produces only a small increase of the maximum void fraction. In all calculations the void fraction in the core goes down to zero shortly after the last power peak.

All three calculations result in a jump of the fuel temperature during the first power peak (Fig. 8), which is responsible for the limitation of this peak. Here the time difference between the three calculations is fully identical with the time difference of the first power peak. The absolute maximum values differ by about 150 K between the codes.

An important criterion for the cooling of the fuel is the ratio between actual and critical heat fluxes, the so-called DNB (departure from nucleate boiling) ratio. If the minimum DNB ratio from all local positions reaches values less than unity, the heat flux exceeds the critical one, and boiling heat transfer crisis occurs. This can lead to an overheating of the fuel rod cladding. The DNB ratio is calculated in the three codes with different correlations. For the considered transient in all three calculations, no heat transfer crisis is predicted (Tab. 1). Due to the absence of the heat transfer crisis the maximum cladding temperature also shown in Tab. 1 remains at low values.

4. Conclusions

The availability of three different thermal hydraulic models to be combined with the neutron kinetics core model DYN3D permitted the investigation of model influences upon the calculation results for a boron dilution transient. Quantitative differences were found in the single solutions. The different degree of numerical diffusion in the boron transport models affects the height of the first power peak. It was shown, that the rate of reactivity insertion is very sensitively affected by details of the space- and time-dependent behaviour of the boron concentration. In the considered case with use of experimental data for the coolant mixing, the power peak after criticality is the lowest one in the case of minimum numerical diffusion, which was not expected from previous investigations. Differences were also found in the heat transfer and the drift flux models. Concerning safety criteria like maximum fuel and cladding temperature as well the DNB ratio, the same conclusions can be drawn from all calculations: Safety-relevant margins are not reached. Deviations of calculated parameters have been observed, but there is no qualitative difference in the transient behaviour.

References

- [1] U. Grundmann, U. Rohde, S. Mittag (2000), DYN3D – Three Dimensional Core Model for Steady-State and Transient Analysis of Thermal Reactors, Proc. PHYSOR2000, Pittsburgh, USA
- [2] A. Manera, U. Rohde, H.-M. Prasser, T. H. J. J. van der Hagen (2005), Modeling of flashing-induced instabilities in the start-up phase of natural-circulation BWRs using the code FLOCAL, Nucl. Eng. Dsgn., 235, 1517
- [3] S. Kliem, U. Rohde, F.-P. Weiss (2004), Core response of a PWR to a slug of under-borated water”, Nucl. Eng. Design, 230, 121
- [4] S. Kliem, U. Rohde (2007), Boron dilution analyses at reactor shutdown conditions using the coupled code DYN3D/ATHLET, Proc. Ann. Mtg. Nucl. Techn. (pp. 51-57), INFORUM GmbH, Berlin
- [5] S. Kliem, U. Grundmann, U. Rohde (1997), The Coupled Code Complex DYN3D/ATHLET - Application to Main Steam Line Break Analysis, Proc. Joint International Conference on Mat. Methods and Supercomputing for Nuclear Applications (pp.1358-1366), ANS, La Grange Park, USA
- [6] Y. Kozmenkov, Y. Orekhov, U. Grundmann, S. Kliem et al. (2001), Development and Benchmarking of the DYN3D/RELAP5 Code System, Proc. Ann. Mtg. Nucl. Techn. (pp.15-18), INFORUM GmbH, Berlin

- [7] S. Kliem, H.-M. Prasser, T. Sühnel (2006), High-resolution measurements of the coolant mixing in the downcomer of the ROCOM test facility, Proc. Ann. Mtg. Nucl. Techn. (pp. 78-84), INFORUM GmbH, Berlin
- [8] U. Grundmann, U. Rohde (1994), Investigations on a Boron Dilution Accident for a VVER-440 Type Reactor by the Help of the Code DYN3D, Proc. ANS Topical Meeting on Advances in Reactor Physics: Reactor Physics Faces the 21st Century (v. 3, pp.464-471), Knoxville (Tennessee), USA
- [9] U. Grundmann, U. Rohde, S. Mittag, S. Kliem (2005), DYN3D version 3.2 - code for calculation of transients in light water reactors (LWR) with hexagonal or quadratic fuel elements - description of models and methods -, Rossendorf, Report FZR-434

ANALYTICAL TIME DEPENDENT TRANSPORT DEVELOPMENTS FOR THE ANALYSIS OF ACCELERATOR DRIVEN SYSTEM (ADS) EXPERIMENTS

Bruno Merk and Frank-Peter Weiß

1. Introduction

Different current and planned experiments (MUSE [1], Yalina [2], Guinevere [3]) are foreseen to study the zero power neutron physical behavior of accelerator driven systems (ADS). The detailed analysis of the kinetic space-time behavior of the neutron flux is important for the evaluation of these ADS experiments.

Up to now, the analysis of all these experiments has been based on the standard methods [4] known from experiments in critical reactors. These standard methods - Sjöstrand method and Slope method - are based on the point kinetics equations. This system of equations was developed from the time dependent diffusion equation by separation of space and time. However, for accelerator driven system with their strong space-time dependent external neutron source, the diffusion approximation is neither valid nor separable. Additionally, the diffusion equation is not able to represent the wave like spatial propagation of a localized perturbation.

A method to handle this problem is to solve the time dependent Telegrapher's equation [5] instead of the point kinetic equations. Solutions for the Telegrapher's equation have been provided for a pulsed external source [6], for the start up of an external source [10], [7] and for the switch-off of the external source [8]. For the development of these analytical solutions, two different mathematical strategies are used. First, the Telegrapher's equation without delayed neutron production is solved by using the Green's function method [9]. The Green's function method offers the possibility to solve the space-time dependent P_1 equation with an external source avoiding the separation of space and time. Second, a multiple-scale expansion [11] with two or three time-scales is performed to account for the delayed neutron production. The multiple-scale expansion offers the possibility to separate the prompt neutron production from the delayed neutron production due to their very different time scales. Thus, the stiffness problem, arising in a closed form solution, is avoided and the solution for the problem can be derived stepwise with significantly reduced complexity compared to a closed form.

External source problems can be handled in much more detail by using numerical simulations or more comprehensive analytical solutions, combined with intermediate steps, which are carried out numerically. These more comprehensive solutions are used for the system simulation or for the definition of analytical benchmarks.

Here, fully analytical approximation solutions are developed in contrast to the procedure mentioned before. The solutions are dedicated to the analysis of current and future ADS experiments. A fast method for the determination of integral parameters from the experimental results, comparable to those defined for critical reactors will be developed after the foreseen evaluation against ongoing experiments. Completely analytical approximation solutions even with the lower approximation are more suitable for this development and provide a deeper physical understanding of the system behavior.

2. Current Experimental Results

The significant difference between the well-known behavior of critical reactors in kinetic experiments and the kinetic behavior of a system with an external neutron source was observed for the first time in the MUSE experiments [1]. The results for a close to critical and a subcritical configuration are shown in Fig. 1. In the left figure for the close to critical configuration SC0 the signals from the different neutron detector positions decay in the same manner. This means the curves can be reproduced easily by a solution obtained by separation of space and time. Here, the point kinetics equations are a good basis for the analysis of these results. On the right hand side the detector responses are shown for a sufficiently subcritical system SC2, as it has been suggested to be representative for ADS. The slopes of the detector responses are significantly different for the different detector positions. These results cannot be represented by an analysis method based on the separation of space and time, since the separation of space and time induces an identical slope at all positions in space. This observation demonstrates the need for the development of an advanced analysis method for the analysis of ADS experiments.

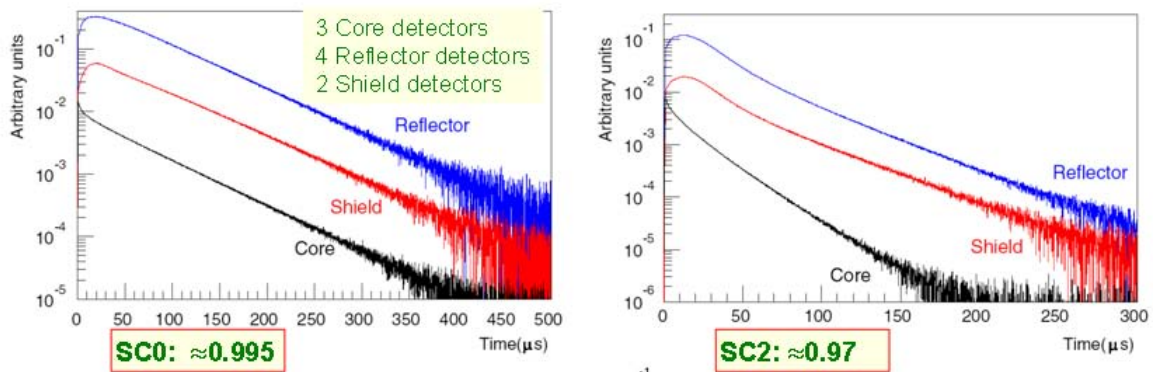


Fig. 1: Neutron detector response for 3 different positions and two different criticality states recorded in the MUSE experiments at CEA Cadarache [12]

3. Developed Analytical Solution

The multiple-scale expansion method has been used to derive closed-form, multiple-scale approximation solutions for the space-time dependent P_1 - or Telegrapher's equations with a localized external neutron source. The system consists of a homogenized multiplying system of planar one-dimensional geometry (see Fig. 2) with one energy group and delayed neutrons and a central external neutron source. The closed-form analytical multiple-scale approximation solutions are provided for the space-time dependent neutron flux as well as for the concentration of delayed neutrons precursors for the switch-on as well as for the switch-off of the external neutron source.

The development of the analytical solutions starts from the solution of the time-dependent P_1 equation without delayed neutrons with the Green's function method. This method does not rely on the separation of space and time. The analytical approximation solutions offer the possibility of a direct investigation of the space-time behavior of subcritical systems with external neutron source and the potential for a deeper understanding of the space-time dependent neutron transport effects in subcritical systems under the influence of changes in the external neutron source. Thus, these approximation solutions represent a new theoretical basis suitable for the analysis of the before mentioned operating and planned kinetic ADS experiments (MUSE, Yalina and Guinevere).

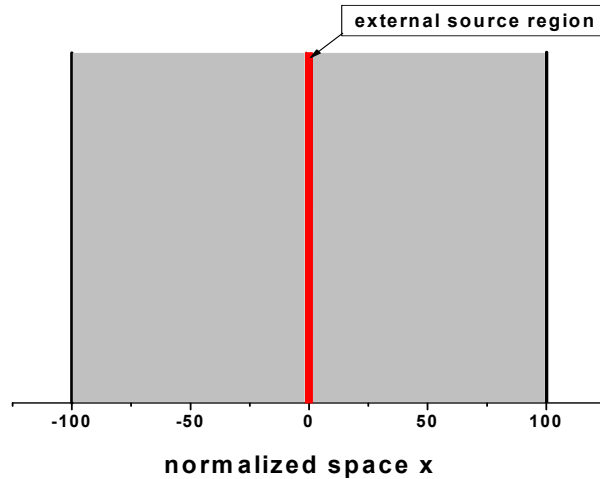


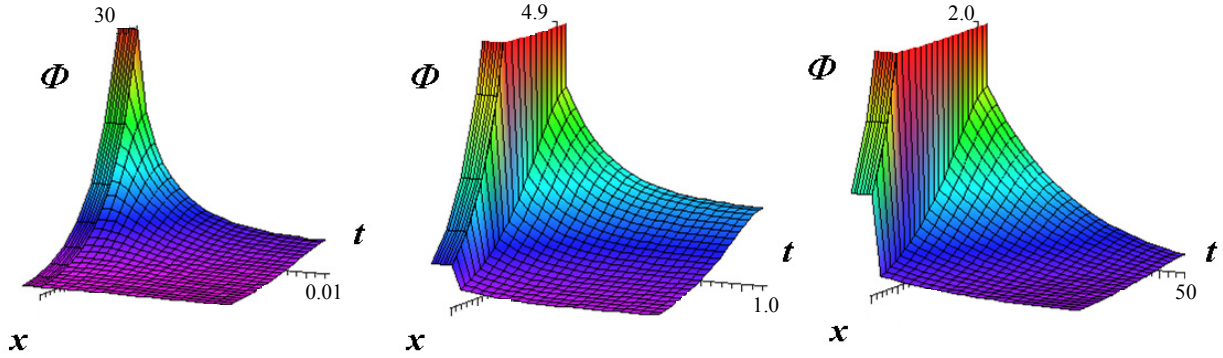
Fig. 2: Spatial view of the one dimensional slab with the external neutron source in the center

The space-time dependent neutron flux, following the switch-off of the external neutron source, is shown in three steps in Fig. 3. The solution is calculated with the developed analytical approximation for a homogenized one-dimensional subcritical system with one energy group and delayed neutron production. Only the front half of the one-dimensional homogenized system is shown with the steady state solution for negative times and the decrease of the neutron flux after the switch-off of the localized external neutron source. The spatial dimension points to the left and to the front, and the time progress points to the right. The left part of Fig. 3 shows the sudden decrease of the neutron flux due to the rapid decay of the prompt neutron flux after the switch-off of the external source. The typical steady state spatial neutron flux distribution (exponential decay with increasing distance from the source) for the described system with operating external source exists for the times lower than $t = 0$ (left side of the graph). At $t = 0$ the external source is switched-off and the neutron flux decreases very rapidly in the center of the system following an exponential function. With little time delay the effect of the switch-off of the external source spreads out like a wave through the complete system (see the first spatial grid curve after switch-off). After roughly 0.01 s the prompt neutrons have decayed and the neutron flux is reduced to the level created by the delayed neutrons of both time scales. After roughly 0.01 s (with the defined system parameters) a plateau in the space-time dependent neutron flux is reached. This plateau is determined by the much slower decaying delayed neutrons.

The central part of Fig. 3 shows the space-time dependent neutron flux during the first second on a reduced vertical time scale. On the left side, the outer part of the steady state solution is still visible. Close to $t = 0$ the sharp drop in the neutron flux due to the decay of the prompt neutrons can be seen. This sharp drop is the exponential decay, identical to the decay observed in the left hand figure, but on a shrunk time scale. The following exponential decay of the neutron flux is caused by the decay of the delayed neutron precursors, belonging to the second timescale of the multiple-scale expansion. The flux change is mostly uniform over space. After roughly one second, the neutron flux has reached a second plateau, since the delayed neutrons, which belong to the second time scale have mostly decayed. Finally, the right hand side of Fig. 3 shows the complete decay of the space-time dependent neutron flux to zero, caused by the decay of the delayed neutron precursors, which belong to the longest time scale of the multiple-scale expansion. The two shorter time scales sum up in the negative jump in the space-time dependent neutron flux at the beginning of the graph immediately after

the switch-off of the external source. In the following time-period, the remaining neutron flux fades away since the precursors of the last time scale decay. After roughly 50 s the neutron flux has nearly completely died out.

Fig. 3: Evolution of the space-time dependent neutron flux, following the switch off of the external neutron source, considering the delayed neutron production (dimensionless in space)



4. Comparison to Point Kinetics Results

Fig. 4 compares the deviation in percent:

$$dev = \left(\frac{\Delta\Phi_{transport}}{\Delta\Phi_{point\ kinetics}} - 1 \right) * 100 \quad (1)$$

of the relative change in the space-time dependent neutron flux for the P_1 transport solution compared to the point kinetics solution. The result is normalized with the point kinetics solution, since the relative change of the neutron flux in the transport solution remains zero for wide ranges in the outer part of the system at the beginning of the transient. This is a direct consequence of the wave like propagation of the perturbation. Additionally, the deviation is limited to $\pm 20\%$ in the graph, thus, the upper and lower horizontal planes represent deviations of more than 20%.

The point kinetics solution heavily underestimates the relative change in the space-time dependent neutron flux in the center at the beginning of the transient. The deviation reduces with time and drops to below 10% in the center after 0.01 s. In the outer area, the relative change in the neutron flux is significantly overestimated by the point kinetics solution, since in the point kinetics solution the perturbation is immediately spread out. In contrast to that, the perturbation propagates like a wave through the transport solution.

Thus, there is some time delay until the perturbation is ‘recognized’ in the outer area of the system. In all areas, which are not yet reached by the wave front, the deviation in the relative change in the neutron flux can be easily quantified to -100%. The consideration of the deviation demonstrates that the point kinetics solution does not give acceptable results for the analysis of such kind of transients.

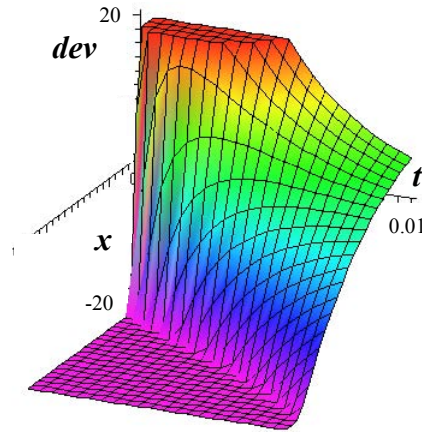


Fig. 4: Relative deviation (%) between the transport solution and the point kinetics solution in the space-time dependent neutron flux for the pure prompt system after the switch off of the external neutron source from steady state (the graph is cut at $\pm 20\%$)

5. Conclusion

The multi-scale expansion method has been used to develop closed-form solutions for the space-time dependent P_1 - or Telegrapher's equations with localized external neutron source for a homogenized multiplying system, in planar one-dimensional geometry, with one energy group and delayed neutrons. The development of this multiple-scale approximation does not rely on separation of space and time. The solution offers the possibility of a direct investigation of the space-time behavior of subcritical systems with an external neutron source. Additionally, the developed multiple-scale approximation solutions offer a deeper understanding of the space-time dependent neutron transport effects in subcritical systems and of the influence of changes in external neutron source. These approximation solutions are a new theoretical basis, suitable for the analysis of the operating and planned kinetic ADS experiments.

The results produced with the developed analytical approximation solution are compared to the results gained by solutions for the point kinetics. This comparison shows major differences from the point kinetics. These major differences prove that point kinetics methods for the analysis of kinetic experiments in nuclear reactors will not provide reliable results for the analysis of systems like ADS with strong external neutron sources.

The developed multiple-scale approximations can be used and developed for the analysis of the experiments in subcritical systems with external neutron source. Moreover, this development presents the possibility to improve the online monitoring of subcriticality during the operation of accelerator driven systems by the analysis of the transient behavior following short trips of the external neutron source.

References

- [1] R. Soule et al.: "Neutronic Studies in Support of Accelerator-Driven Systems: The MUSE Experiments in the MASURCA Facility," Nucl. Sci. Eng., 148, 124 (2004)
- [2] A.I. Kievitskaia, et al.: "Experimental and theoretical research on transmutation of long-lived fission products and minor actinides in a subcritical assembly driven by a neutron generator", 3rd Int. Conf. on Accelerator Driven Transmutation Technologies and Applications, Praha, (1999)

- [3] H.Ait Abderrahim, P.Baeten: “The GUINEVERE-project at VENUS, Project Status” ECATS meeting, Cadarache, 31.01.2008
- [4] C. Persson et. al: “Analysis of reactivity determination methods in the subcritical experiment Yalina”, Nucl. Instr. and Meth. in Physics Res. A 554 (2005) 374–383
- [5] A. M. Weinberg, E. P. Wigner: “The Physical Theory of Neutron Chain Reactors“, The University of Chicago Press, Chicago (1958)
- [6] B. Merk: “Time Dependent Analytical Approximation Solutions for a Pulsed Source Problem: P₁ Transport versus Diffusion “, IEEE Nuclear Science Symposium, Dresden (2008)
- [7] B. Merk: “An Analytical Approximation Solution for a Time Dependent Neutron Transport Problem with External Source and Delayed Neutron Production”, Nucl. Sci. Eng., 161, 1-19 (2009)
- [8] B. Merk, F. P. Weiß: “A Three Scale Expansion Solution for a Time Dependent P₁ Neutron Transport Problem with External Source”, Nucl. Sci. Eng., 163 (2009), 152-174
- [9] D. G. Duffy: “Green’s Functions with Application”, Chapman & Hall/CRC Boca Raton (2001)
- [10] B. Merk: "An Analytical Solution for a One Dimensional Time Dependent Neutron Transport Problem with External Source”, Transport Theory and Statistical Physics, 37:1–15, 2009
- [11] B. R. Merk, D. G. Cacuci: “Multiple Time Expansions for Neutron Kinetics —II: Illustrative Application to P₁ and P₃ Equations”, Nucl. Sci. Eng., 151, 194-211 (2005)
- [12] E. Gonzalez: “The MUSE4 Experimental Results”, International Workshop – October 21-22, 2004, Rome – Italy

Acknowledgement

This work was partly funded by the European Commission under Domain 2 ECATS of the integrated project EUROTRANS.

BURNING PLUTONIUM AND MINIMIZING RADIOACTIVE WASTE IN EXISTING PWR

Siegfried Mittag and Sören Kliem

1. Introduction

The main problem with nuclear power plants is the continuous production of radioactive nuclides. This material has to be contained safely during reactor operation and, after spent-fuel unloading, be disposed of in a safe and economic way. Namely, the (repeated) neutron capture by uranium-238 leads to high quantities of long-lived radioactive actinides (Fig. 1). The half-lives of the so-called minor actinides (MA) are, on the average, much longer than those of fission products, so that they will determine the radio-toxicity in the final storage a few hundred years after unloading. The production of these nuclides cannot be avoided in conventional light-water-reactor fuel, because this fuel is either low-enriched uranium (LEU) oxide or uranium-plutonium mixed oxide (MOX), containing more than 90 % uranium-238. Burning MOX is a way of reducing weapons-grade and reactor-grade plutonium stockpiles in the world. However, conventional MOX fuelling of light-water reactors (LWR) does not allow a rapid reduction of stockpiles, as fissile plutonium is re-bred from uranium-238 (Fig. 1). In order to avoid the continuous uranium – actinide conversion during reactor operation, other (“innovative”) compositions of LWR fuel are considered.

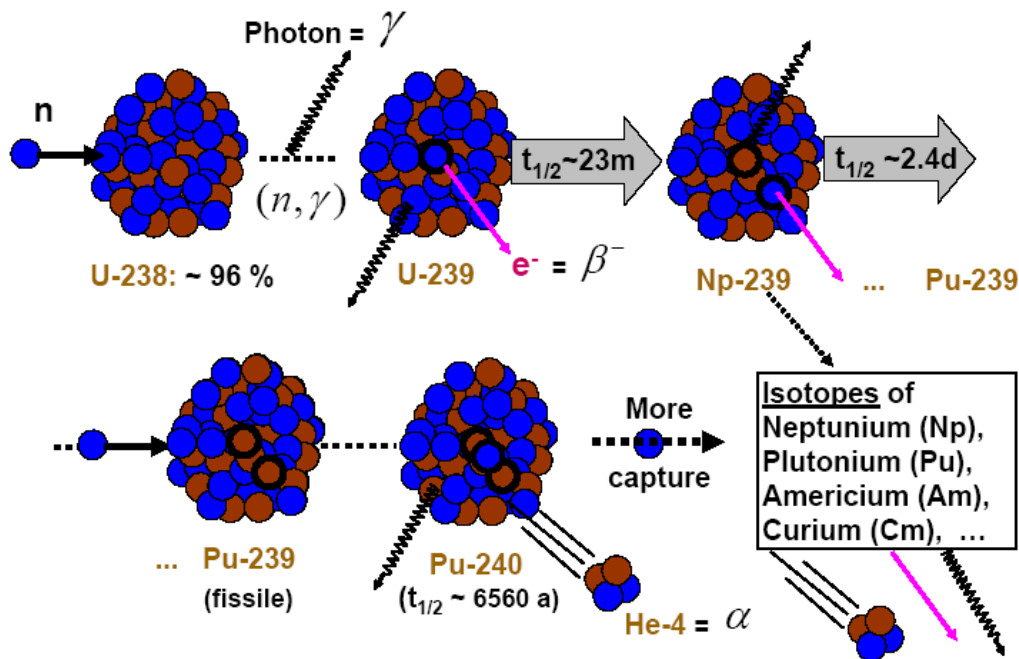


Fig. 1: Actinide breeding in LWR

2. Innovative LWR fuel

In order to avoid breeding of plutonium and long-lived minor actinides (MA), the uranium-238 carrying the fissile nuclides has to be replaced by a different fuel carrier material. However, it is mainly this uranium-238 that provides resonances in the neutron capture cross section, which produce the negative fuel-temperature feedback, i.e. a negative Doppler coefficient. This fuel feature is vitally important with respect to reactor safety. Thus innovative

carrier matrices should also have sufficient resonance absorption to ensure a strong-enough negative fuel-temperature coefficient (FTC). This fact and requirements of fuel-rod thermo-mechanical stability narrow the scope of material to be chosen as an inert matrix i.e. not breeding material, to hold fissile nuclides. Recently, so-called inert matrix fuel (IMF) is being designed, e.g. on the basis of zirconium or molybdenum, though less pronounced neutron resonance absorption is observed in the isotopes of these elements. Erbium can be added to the fuel matrix in order to introduce more (epithermal) resonances enhancing the negative FTC.

The design and study of innovative LWR fuel, for example IMF, is the main objective of the EU FP7 project LWR-DEPUTY (“Deep Plutonium burning in thermal systems”). FZD participating in this project, contributes to the investigation of alternative fuel matrices based on thorium, which is a mono-isotopic element (thorium-232). The absorption cross section of this nuclide has quite a similar resonance structure as uranium-238, making it very suitable to serve as a fuel carrier material, from the neutron-kinetics safety point of view (FTC).

Thorium-232 is, like uranium-238, a “fertile” nuclide, producing (by neutron capture and beta decay, $t_{1/2} = 22.3$ minutes) protactinium-233, which decays with a half-life of 27 days to fissile uranium-233. The chance of U-233 fission after absorbing another (thermal) neutron is about 90%, leaving 10% to build up U-234, which produces fissile U-235 by further neutron capture. The capture-to-fission ratio of U-235 is about 1/6; in the end there is very little probability for the buildup of higher long-lived radioactive actinides, a situation different to the case of U-238 fuel matrices (Fig. 1).

Compared to the well-proved uranium oxide fuel, thoria exhibits even greater chemical stability, higher thermal conductivity, and a lower coefficient of thermal expansion. Its melting point is at 3390 °C, i.e. some 500 degrees higher than that of UO₂. These facts are of key importance for a thorium-fuel application in LWR.

Prior to the real introduction of new fuel into a reactor core, performance and safety studies have to be carried out. Respective fuel-assembly and core calculations can be carried out by suitable neutronic and thermal-hydraulic computer codes.

3. Thorium fuel benchmark calculations

DYN3D is a reactor dynamic code capable of modelling LWR core transient behaviour. The lattice depletion code HELIOS is applied to produce fuel-assembly-homogenized few-group diffusion and kinetics parameters, which are needed as input data for the nodal diffusion code DYN3D. In order to verify the respective HELIOS methodology for new thorium-based fuel, as a first step, a benchmark problem set up by the IAEA [1] has been calculated. The benchmark was defined for a Westinghouse PWR 17x17-rod-array MOX fuel assembly carrying 5% reactor-grade plutonium oxide, embedded in a thorium oxide matrix (95%). Fig. 2 shows some results of the respective FZD HELIOS calculation, compared to those of other participants. The build-up of fissile U-233 is shown as a function of neutron exposure during reactor operation (burnup), the latter measured in units of produced fission energy, i.e. gigawatt-days per tonne of heavy metal (thorium + plutonium) in the fuel. There is similar good agreement between the calculations for the depletion of Pu-239, which is not shown in Fig. 2. Instead, the parameter k -infinity of the fuel assembly is depicted, which quantifies the neutron multiplication properties in the fission chain reaction.

The next and more important benchmarking step to be carried out in the project LWR-DEPUTY will be a lattice burnup calculation for an experimental thorium-plutonium rodlet that had been irradiated during four reactor cycles in the PWR core of the German NPP Obrigheim (KWO). Post-irradiation examination (PIE) and radio-chemical analysis (RCA) are under way to obtain real densities for Pu-239, U-233, and other nuclides, including some fission products. The comparison of measured and calculated nuclide concentrations will, naturally, be a more relevant validation for the accuracy of calculation methods than a code-to-code comparison.

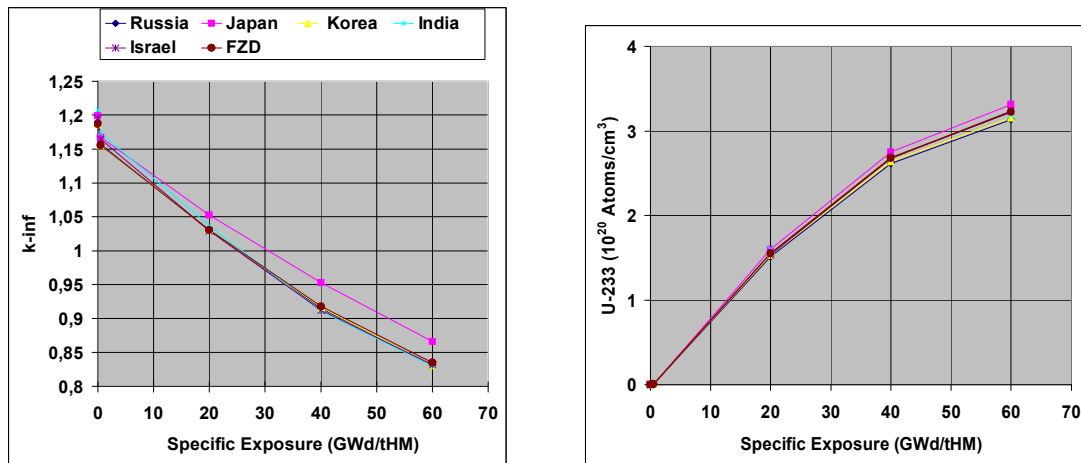


Fig. 2: IAEA benchmark calculations for Th-Pu MOX fuel assembly

4. Safety studies for a PWR core containing thorium fuel

A lot of experience has been gathered worldwide in designing and operating LWR cores using various fuel assemblies (FA) at different burnup stages. At the beginning of a PWR operation cycle, excess reactivity will be compensated by the neutron absorber boron added to the moderator. PWR cycles start with a moderator boron concentration of about 1000 ppm (at nominal power), which is continuously decreased, in line with growing core burnup. A PWR core with typical fuel loading has been studied under the conditions at the beginning of cycle (BOC).

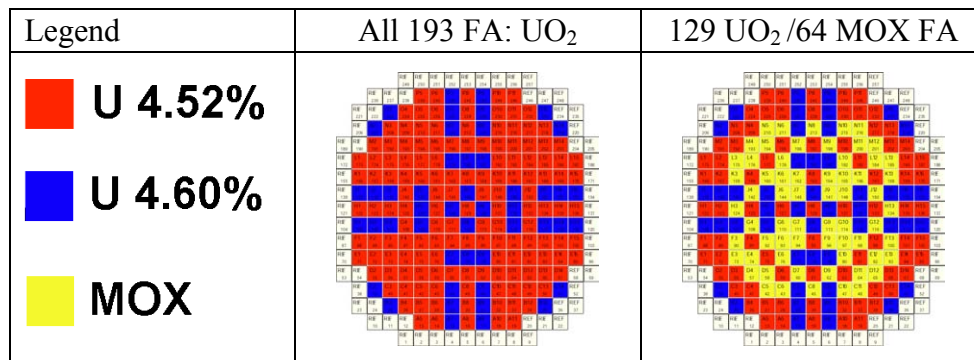


Fig. 3: Core loading patterns chosen for safety studies. MOX means either conventional mixed oxide or ThPu MOX

Fig. 3 has two core loading patterns that are applied in real PWR operation. Uranium fuel assemblies contain fissile U-235 (LEU), whereas reactor-grade plutonium gained by reprocessing spent fuel is used in MOX. In all conventional PWR fuels the fissile nuclides are

embedded in a matrix of U-238. Usually, the share of fissile material is not higher than 5 %. The results of safety analyses for the two different cores compiled of the FA types, depicted in Fig. 3, are described in [2]. In the following, an “innovative” MOX FA is introduced, in which the U-238 oxide matrix of [2] is replaced by thorium, while the original assembly and fuel-rod geometry is preserved. 64 of such thorium-plutonium oxide FA are placed in the positions of the conventional MOX FA of Fig. 3, thus forming a new core composition to be analysed.

For the three cores under consideration, all of them studied at the beginning of a PWR equilibrium cycle (BOC), Table 1 shows the most safety-relevant parameters calculated by the code DYN3D.

Table 1: Core reactivity coefficients for different core loadings

Reactivity coefficient of	U (MOX-free)	U-MOX	Th-MOX
Moderator density [pcm/kg/m ³]	+14.19	+18.77	+18.28
Moderator temperature [pcm/K]	+3.422	+3.252	+3.675
Total moderator temperature, MTC [pcm/K]	-30.14	-40.36	-38.48
Fuel temperature, FTC [pcm/K]	-2.457	-2.636	-2.773
Boron concentration [pcm/ppm]	-7.028	-5.468	-5.542

The negative core MTC (4th line of Table 1) is mainly the result of moderator density decreasing (2nd line) with growing temperature at nominal pressure. Additionally to the coefficients discussed in section 2, the boron efficiency, i.e. the effect of soluble boron in the moderator on reactivity is given in the last line. The table demonstrates that MTC and FTC are roughly the same for thorium MOX as for conventional MOX, the Th-MOX FTC being even slightly better due to the convenient resonance structure in the absorption cross section.

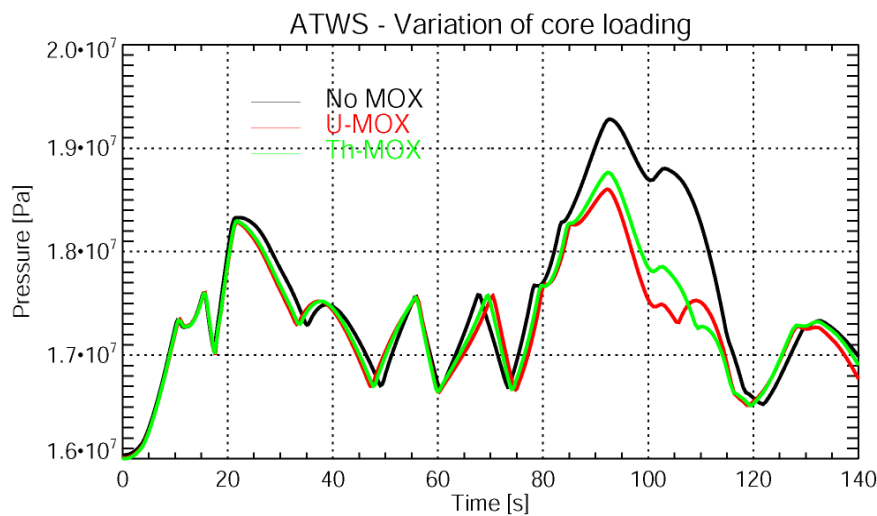


Fig. 4: PWR core with different loadings: Primary pressure during an ATWS transient, calculated by DYN3D/ATHLET

For in-depth safety considerations, also the reactor behaviour during possible transients – in fact anticipated transients without scram (ATWS), though they are very unlikely – has to be studied. As an example, the course of the safety-relevant primary-circuit pressure in an ATWS – caused by the loss of feed water supply and mechanical blockage of all control rods [2] – is depicted in Fig. 4. The calculations have been performed by the coupled codes DYN3D/ATHLET, the latter of the two modelling the thermal hydraulics of the PWR circuits influencing the core neutron kinetics that is simulated by DYN3D. In all three cores, the pressure peaks are far from the critical value of 23 MPa, above which primary-circuit lines might be damaged. The 1/3 Th-MOX core loading exhibits a similar behaviour as the respective conventional-MOX version.

5. Reactor safety and fuel resources

Thorium-based fuel will not only reduce the production of long-lived radioactive actinides. It implies breeding fissile material, uranium-233, in thermal reactors such as LWR. Thorium is about three times more abundant than uranium in the earth's crust, and could thus contribute significantly to meet the demand of nuclear fuel in the future.

With respect to better uranium-fuel utilization, fast breeders like sodium fast reactors (SFR) have been developed. Only few of them have been built and operated, though enhanced fast reactor designs are under consideration. Some of these advanced “Generation IV” fast-spectrum concepts are even designed for the incineration of long-lived actinides.

In the immediate future, however, well-established LWR, fuelled by thorium-plutonium oxide, may offer the most practicable approach for radioactive-waste minimization. This concept will be better acceptable for the public, because of:

- the current high LWR safety standard, which is being continuously improved, both in existing plants and in newly built ones, such as the European Pressurized-Water Reactor (EPR) and other “Generation III” designs,
- much experience in LWR operation worldwide,
- preserving high level of both the safety and economy, when using thorium-plutonium oxide,
- excellent resources economy by breeding fissile material,
- less “neutron wasting”, which happens in burnable poisons and IMF resonance absorbers, and
- a less reactivity swing over fuel lifetime, compared to U-238 and IMF matrices.

It should be recalled that the idea of thorium-based fuel in LWR is by no means new. The Shippingport light-water breeder reactor (LWBR), which was operated 30 years ago, produced about 2500 GWh electric energy within five years. After shutdown in 1982, its core contained 1.3% more fissile material than at the start of operation [3]. However, during the last decades, there were no real incentives to replace conventional LWR fuel. Proliferation aspects may have contributed to reluctance against thorium-based fuel. Moreover uranium-232, which is also formed to a small extent in this fuel via (n,2n) reactions, has highly radioactive daughter products, namely the hard gamma emitter thallium-208. The strong gamma radiation makes reprocessing more expensive, but on the other hand, enhances proliferation resistance.

6. Conclusions

Thorium MOX may be a promising alternative to conventional LWR fuel. It is expected that thorium MOX can satisfy both safety and economic requirements. The introduction of this fuel into existing PWR might be a first step of thorium utilization, thus reducing radioactive-waste production. However, prior to any new core loadings, be it with or without thorium, a detailed safety analysis has to be fulfilled, according to the strict requirements of the nuclear authorities in the country. Only a few of necessary safety studies have been carried out and are described in section 4, for a generic PWR core, with 1/3 of all fuel assemblies consisting of thorium-plutonium MOX. The results may contribute a little to encourage the use of such new fuel. However, a lot more analyses have to be performed before, and the core loading could then be optimized with respect to economics.

Starting with only slightly-modified core loading in existing modern PWR might “break the ice” for introducing this innovative fuel.

References

- [1] Potential of thorium based fuel cycles to constrain plutonium and reduce long lived waste toxicity, IAEA-TECDOC-1349, Vienna, 2003.
- [2] Kliem, S., Mittag, S., and Rohde U.: ATWS analysis for PWR using the coupled code system DYN3D/ATHLET. Ann. Nucl. Energy 36 (2009), 1230-1234.
- [3] Water cooled breeder program. Summary report. DOE research and development report WPD-TM-1600, USA, 1987.

FLUX DEPENDENCE OF DEFECT CLUSTER FORMATION IN NEUTRON IRRADIATED WELD MATERIALS

Frank Bergner, Uwe Birkenheuer, and Andreas Ulbricht

1. Introduction

The core-belt region of the reactor pressure vessel (RPV) of a nuclear power plant (NPP) is exposed to intense neutron irradiation, the fast neutrons causing a degradation of the mechanical properties. In order to guarantee the structural integrity of the RPV throughout operation time, surveillance programs are implemented prior to initial commissioning of a nuclear power plant. According to these programs specimens of the RPV steel are inserted into capsules and placed in special surveillance channels. At these positions, the fast neutron flux (number of neutrons per unit area and unit time) exceeds the flux at the RPV wall by a leading factor (typically between 1.5 and 12). The specimens are taken from the surveillance capsules at regular intervals in order to undergo mechanical tests. The mechanical properties are then assumed to be characteristic of the RPV material at an instant of time corresponding to the irradiation time of the specimen multiplied by the leading factor. However, this procedure is only applicable if flux effects are either completely absent, i.e. degradation depends on fluence only, or result in a conservative prediction of the behavior of the RPV material. At this point, the basic interest in the dependence of the mechanical properties and the underlying microstructure on neutron flux becomes evident.

The primary irradiation parameter governing the degradation of material properties is neutron fluence, Φ , i.e. neutron flux, φ , multiplied by exposure time, t . Neutron flux is a secondary parameter, though of primary technical importance. In order to separate flux effects from the dominant dependence on fluence, it is necessary to vary the value of flux while keeping the value of fluence constant. An appropriate pair of samples was selected from German irradiation programs.

Small-angle neutron scattering (SANS) is used to characterize the size distribution of irradiation-induced solute clusters and a rate theory model is applied to simulate cluster evolution.

2. Experiments

The material investigated is a first generation submerged weld NiCrMo1 UP (modified)/LW320, LW340 (German specification). The composition is given in table 1, the irradiation conditions and the irradiation-induced mechanical property changes are summarized in table 2. Slices of cross-section area of 10 mm x 10 mm and of 1 mm thickness were prepared for the SANS experiment.

Table 1: Composition of investigated material (wt.-%)

C	Mn	Si	Cr	Ni	Mo	V	S	P	Cu
0.08	1.10	0.15	0.74	1.11	0.60	0.001	0.017	0.015	0.22

The SANS measurements were performed at the instrument V4 of the Berlin Neutron Scattering Center of Helmholtz Zentrum Berlin [1]. Samples were placed in a magnetic field of 1.2 T perpendicular to the incident neutron beam. The SANS raw-data treatment and analysis described in [2] was performed using the BerSANS software package [3]. Further

analysis is based on the indirect transformation method [4] and provides the size distribution of scatterers without assuming a certain type of distribution. The A -ratio, originally defined as the ratio of the scattering cross-sections perpendicular and parallel to the magnetic field direction, was calculated in the size space after performing the transformation according to the relation, $A = 1 + M / N$, where M and N denote the area under the size distribution curve obtained from the magnetic and nuclear scattering contributions, respectively.

Table 2: Irradiation conditions (fluence and flux values for neutron energy, $E > 1$ MeV) and irradiation-induced changes of yield stress and brittle-ductile transition temperature (Measuring uncertainties are of the order of 10%)

Code	Fluence, Φ in cm^{-2}	Flux, ϕ in $\text{cm}^{-2}\text{s}^{-1}$	Time	Temperature in $^{\circ}\text{C}$	$\Delta\sigma_y$ in MPa	ΔT_{41} in K
I-1	2.2×10^{19}	2.1×10^{12}	122 days	285	211	119
I-2	2.2×10^{19}	6.0×10^{10}	11.6 years	288	196	111

3. Results

The coherent magnetic scattering cross-sections obtained for the RPV weld and the reconstructed volume-weighted size distributions are shown in figure 1. The scattering cross-sections of the low-flux and high-flux irradiations exhibit characteristic differences manifesting themselves in different size distributions. The results of the SANS measurements are summarized in table 3. The increase of the peak radius (marked for the green curve in figure 1b) of the volume-weighted size distribution of scatterers by a factor of about 2 is the most prominent effect of reducing the flux by a factor of 35 at constant fluence. The total volume fraction of scatterers is approximately independent of flux. The increase of size at constant volume fraction requires the number density to decrease as shown in table 3. The maximum size of scatterers (see figure 1b) increases from 2 nm for the higher flux to 4 nm for the lower flux. The size distribution obtained for the lower flux seems to consist of two overlapping components. However, these cannot be separated without assumptions on the type of distribution.

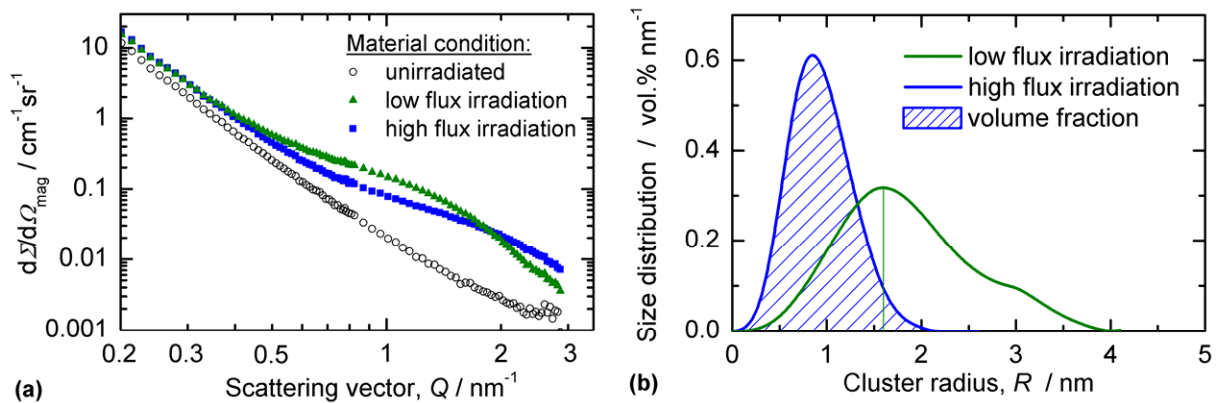


Fig. 1: (a) Coherent magnetic scattering cross sections obtained for different conditions of the RPV weld, (b) Reconstructed size distributions of irradiation-induced defects

Table 3: Parameter of irradiation-induced clusters detected by SANS

Code	Peak radius in nm	Volume fraction in %	Number density in cm^{-3}	A -ratio
I-1	0.85	0.51 ± 0.02	17×10^{17}	2.3 ± 0.1
I-2	1.6	0.53 ± 0.02	5×10^{17}	2.5 ± 0.1

4. Discussion

We have observed that the A -ratio is approximately independent of flux. This is an indication of similar compositions of the scatterers in both cases. On the one hand, the A -ratio of about 2.4 implies that the scatterers are not pure Cu, which would require a much higher A -ratio [5]. This is confirmed by the measured total volume fractions, which are significantly larger than the total Cu content. Atom probe investigations performed for similar RPV materials confirm that Cu is an important constituent of the clusters [6, 7]. These results indicate that irradiation-enhanced Cu diffusion controlled by the vacancy concentration could be responsible for the observed flux effect. In order to check this possibility, we apply a simple rate theoretical estimation below.

The constituents of our rate theory model are the balance equations for point defects (vacancies and self-interstitial atoms) and for Cu-clusters. We assume the ratio of irradiation enhanced and thermal Cu-diffusivity to be given by the ratio of steady-state and equilibrium concentration of vacancies. Based on asymptotic considerations of the equations involved in the model, we have found that there are two different flux regimes (figure. 2). In the low-flux regime, the growth rate of Cu-rich clusters is independent of flux. In this case, the dominant process causing the loss of vacancies is the disappearance at sinks like grain boundaries or dislocations. The high-flux regime with vacancy-interstitial recombination as prevailing mechanism of vacancy loss is characterized by an inverse proportionality of the growth rate with the square root of flux. The rate theory model [8] also yields an expression for the transition flux estimated to be $0.7 \times 10^{12} \text{ cm}^{-2}\text{s}^{-1}$ under the present conditions. In other words, the investigated low-flux irradiation of the weld material belongs to the flux-independent regime whereas for high-flux irradiation a reduced rate of cluster growth is expected in qualitative agreement with the experimental observation.

Although a strong flux effect on the cluster size is observed, it is important to notice that the mechanical properties essentially agree for the two irradiation conditions (see table 2). This shows that the volume fraction of the irradiation-induced clusters (which is the same for both irradiation conditions, see table 3) governs the mechanical properties whereas cluster size is secondary in the present case.

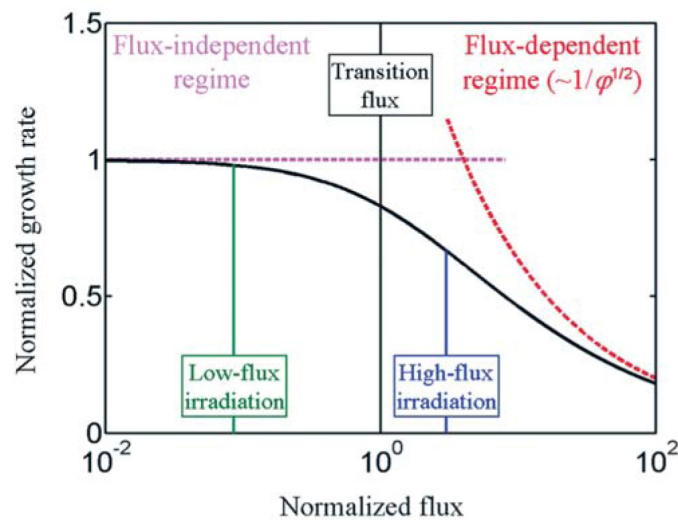


Fig. 2: Cluster growth rate normalized to the limiting rate at zero flux vs. neutron flux normalized to the transition flux

5. Conclusions

The SANS investigation of a RPV weld material irradiated at different levels of neutron flux (differing by a factor of 35) up to the same fluence shows that the clusters are substantially larger (by a factor of 2) for irradiation at low flux, whereas the volume fraction of irradiation-induced clusters is essentially independent of flux. We found that this result can be explained by the transition from a flux-independent regime of cluster growth at lower flux to a second regime, where cluster growth mediated by irradiation-enhanced Cu diffusion depends inversely on the square-root of flux.

The results indicate that the mechanical properties are mainly determined by the volume fraction of the clusters whereas cluster size seems to be of minor influence [9]. It is important to emphasize that these findings are consistent with the basic assumption of current surveillance programs.

References

- [1] U. Keiderling, A. Wiedenmann (1995), New SANS Instrument at the BER II Reactor in Berlin, Germany, *Physica B* 213/214, 895
- [2] P. Strunz, J. Saroun, U. Keiderling, A. Wiedenmann, R. Przenioslo (2000), General formula for determination of cross-section from measured SANS intensities, *J. Appl. Cryst.* 33, 829
- [3] U. Keiderling (2002), The new 'BerSANS-PC' software for reduction and treatment of small-angle neutron scattering data, *Appl. Phys. A* 74, S1455
- [4] O. Glatter (1980), Determination of particle-size distribution functions from small-angle scattering data by means of the indirect transformation method, *J. Appl. Cryst.* 13, 7
- [5] M.-H. Mathon, A. Barbu, F. Dunstetter, F. Maury, N. Lorenzelli, C.-H. De Novion (1997), Experimental study and modelling of copper precipitation under electron irradiation in dilute FeCu binary alloys, *J. Nucl. Mater.* 245, 224
- [6] M. K. Miller, K. F. Russell, M. A. Sokolov, R. K. Nanstad (2005), Atome probe tomography of radiation-sensitive KS-01 weld, *Phil. Mag.* 85, 401
- [7] P. Pareige, B. Radiguet, R. Krummeich-Brangier, A. Barbu, O. Zabusov, M. Kozodaev (2005), Atomic-level observation with three-dimensional atom probe of the solute behaviour in neutron-, ion- or electron-irradiated ferritic alloys, *Phil. Mag.* 85, 429
- [8] F. Bergner, A. Ulbricht, H. Hein, M. Kammel (2008), Flux dependence of cluster formation in neutron-irradiated weld material, *J. Phys. Condens. Matter* 20, 104262
- [9] A. Ulbricht, F. Bergner, J. Böhmert, M. Valo, M.-H. Mathon, A. Heinemann (2007), SANS response of VVER440-type weld material after neutron irradiation, post-irradiation annealing and reirradiation, *Phil. Mag.* 87, 1855

Acknowledgement

The work was founded by the German Bundesministerium für Wirtschaft (BMWi) under contract number 1501315.

FINITE ELEMENT CALCULATIONS FOR TIME-DEPENDENT THERMAL ANALYSIS OF EPOS COMPONENTS

Matthias Werner, Eberhard Altstadt, Gerhard Brauer, Klaus Noack,
and Reinhard Krause-Rehberg

1. Introduction

The positron beam technique is a unique tool to study crystal lattice defects and open-volume cavities of nanometres scale in thin samples and layers [1].

The superconducting electron LINAC **ELBE** (Electron Linac with high **B**rilliance and low **E**mittance) at Forschungszentrum Rossendorf [2] gives the unique possibility to construct an intense positron beam line for materials research. The positron beam will be bunched for positron lifetime spectroscopy by making use of the primary bunch structure of the ELBE electron beam (77 ns repetition time of 5 ps bunches, cw-mode, 40 MeV, 1 mA).

A detailed description of the ambitious intentions to realize the EPOS project has already been published [3]. However, this realization is not straightforward and sometimes several options have to be considered and tested before a reasonable solution to a certain problem is found. The present report reviews activities with respect to the thermal analysis of EPOS components. Such efforts are essential for an efficient choice of construction materials.

In particular, this report analyses the thermal behaviour of the positron moderator and the electrostatic lenses designed in such a way that a mono-energetic positron beam can be formed for transportation into the positron laboratory. Fig. 1 shows the configuration under consideration.

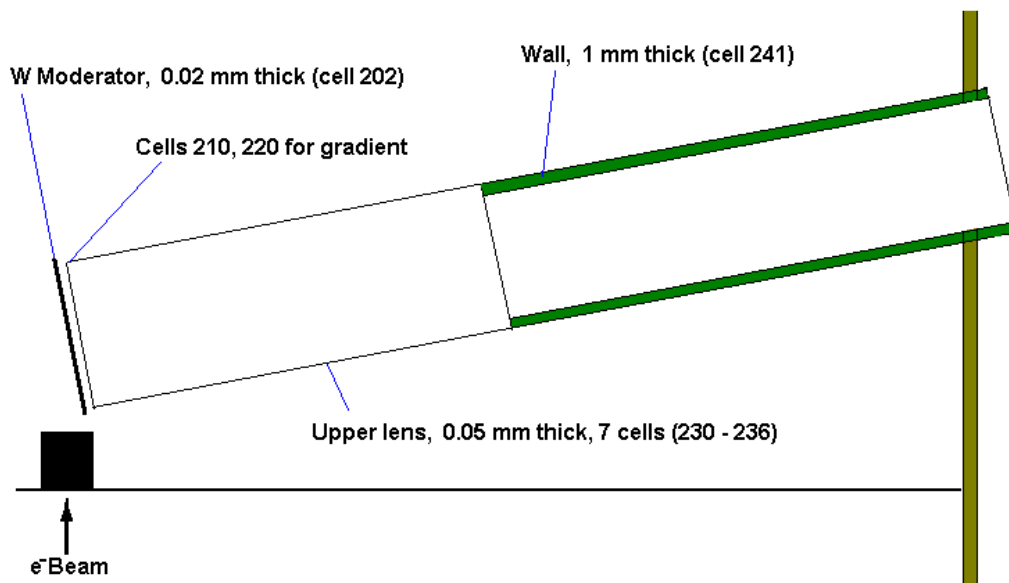


Fig. 1: Part of the EPOS configuration arrangement and the definition of the estimation volumes (MCNP cells)

In a first step, the volumetric heat generation is calculated using the code MCNP. In a second step, the time dependent temperature distributions are evaluated using the finite element code ANSYS

2. Evaluation of the heat generation rates

The heat generation rates in the moderator and lenses were calculated with the Monte Carlo code MCNP[®]-5, release 1.40 [4]. MCNP is a general-purpose Monte Carlo N-Particle code that can be used for stochastically simulating neutron, photon, electron, or coupled neutron/photon/electron transports. The code is able to treat an arbitrary three-dimensional configuration of materials.

For neutrons and photons energy pointwise cross-section data given in Evaluated Nuclear Data Libraries (such as ENDF/B-VI) are used to account for the various interactions with the materials. In case of electrons they are treated by means of a continuous-slowning-down model. The code allows the estimation of a broad range of integrals of the space-, energy- and direction-dependent particle fields together with their statistical errors. For the study presented in this report the mean values of the heat generation by photons and electrons averaged over user-defined volumes were calculated in a coupled electron/photon/neutron transport simulation. Contributions from neutrons to the heat generation are negligible.

The results of the calculation cells are listed in Table 1. The energy input values are given as integral values in the volumes V_i for one electron with an energy of 40 MeV.

Table 1: Results of the energy input calculation

Cell	Volume V_i [cm ³]	Mass [g]	Energy input E_i [MeV]	Rel. stat. error [-]	Comment
202	1.414e-2	2.714e-1	1.18e-2	0.0028	W-moderator, complete
210	3.000e-4	2.304e-3	5.77e-5	0.0223	additional cells to account for the gradient in beam direction
220	3.000e-4	2.304e-3	2.42e-4	0.0147	
230	3.919e-2	3.010e-1	9.10e-3	0.0031	ring 1, height 1 cm
231	3.919e-2	3.010e-1	4.26e-3	0.0044	ring 2, height 1 cm
232	3.919e-2	3.010e-1	2.28e-3	0.0062	ring 3, height 1 cm
233	3.919e-2	3.010e-1	1.37e-3	0.0081	ring 4, height 1 cm
234	3.919e-2	3.010e-1	8.84e-4	0.0104	ring 5, height 1 cm
235	3.919e-2	3.010e-1	6.09e-4	0.0122	ring 6, height 1 cm
236	3.919e-2	3.010e-1	4.28e-4	0.0175	ring 7, height 1 cm
241	7.389e+0	5.675e+1	1.88e-2	0.0063	lower part of the lens
243	1.461e-3	1.122e-2	5.32e-4	0.0086	grid at the top of the lens

The volumetric heat generation rate is obtained by:

$$Q_i^{\text{vol}} = \frac{E_i}{V_i} \cdot I/e \quad (1)$$

where I is the current of the electron beam and I/e equals the number of electrons per second.

3. Thermal calculations

Based on the code ANSYS® a finite element model is used to calculate the transient temperature distribution in the moderator, the grid and in the positron lens. Heat conduction within the materials and radiation heat transfer at the surfaces is considered. The heat generation density is obtained from Table 1. An axisymmetric model was chosen assuming that the temperature gradient in beam direction is negligible. To be conservative with respect to the maximum temperature, the greater value of the heat generations in the additional cells 210 and 220 was added in the upper region of ring 1 (cf. Table 1). The heat conduction and the volumetric heat input is realised by the ANSYS element type PLANE55 whereas the element type SURF151 is used for the heat radiation. Surfaces that are not meshed with SURF151 are adiabatic. The Fe model consists of 2362 elements and 2335 nodes.

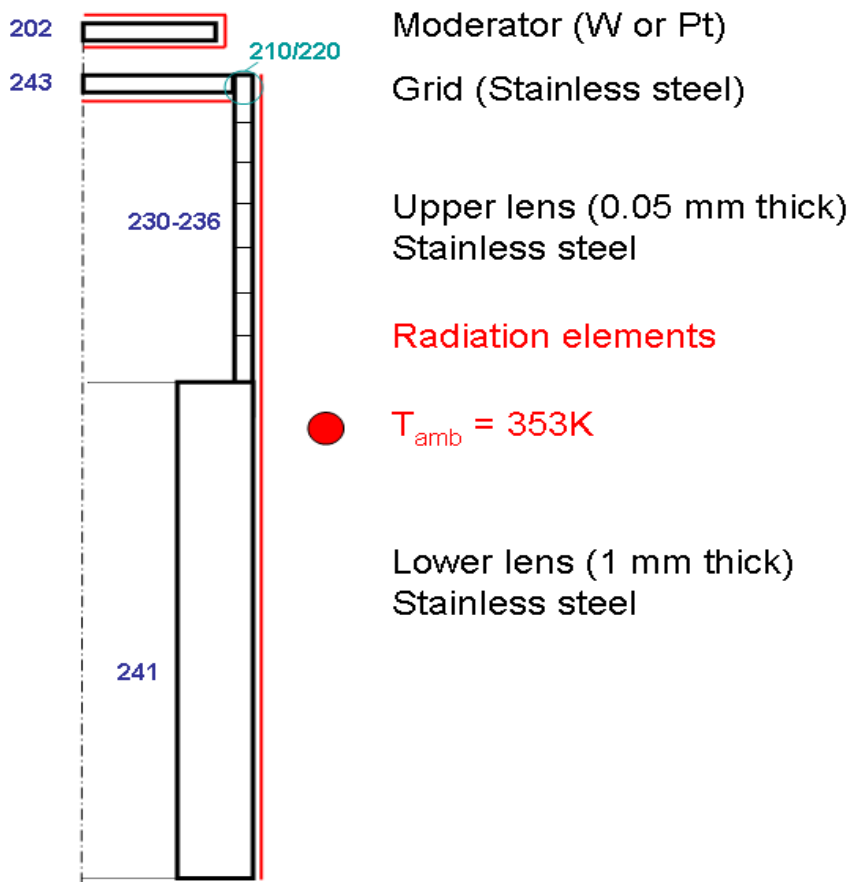


Fig. 2: Scheme of the axisymmetric FE-model with indication of the MCNP cell numbers

The lens and the grid are made from stainless steel. For the moderator two material options are considered Pt and W. In the grid range of the model reduced (or effective) material constants are used to consider the open area fraction of 90%.

Fig. 3 and 4 show the emission coefficients vs. T for tungsten and platinum respectively.

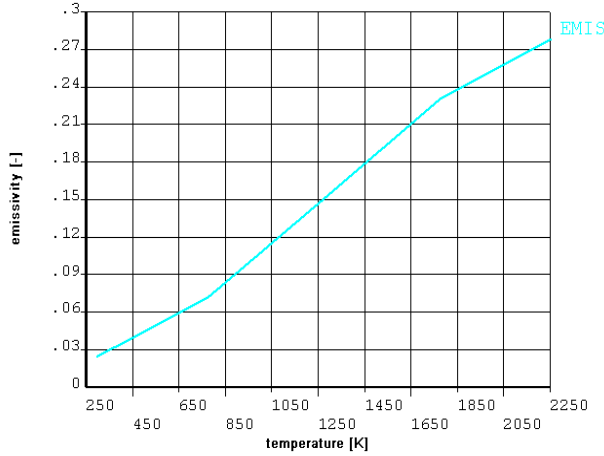


Fig. 3: Emission coefficient of tungsten vs. temperature

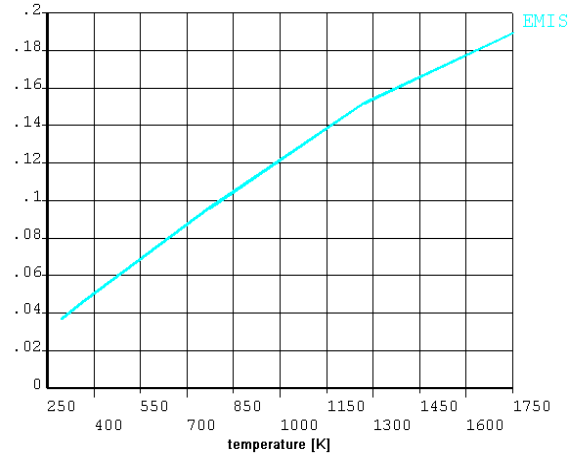


Fig. 4: Emission coefficient of platinum vs. temperature

4. Results

Transient calculations were performed for different scenarios. The following parameters were varied:

- the power of the beam (100% - full and 1% - diagnostic mode)
- the material of moderator (W or Pt)
- the thickness of the moderator
- the heat generation in the grid (100% - upper bound; 10% - realistic case).

The temperature distribution of the moderator was calculated for Pt and W with a nominal thickness of 0.04 mm at 100% beam power. It was shown that the steady state temperature is reached at about $t = 8$ s in both cases. The final temperature in W is 1144 K and in Pt 1158 K. The somewhat smaller value in W correlates to the slightly larger emission coefficient at ~ 1000 K.

In the following we investigate the influence of the moderator thickness on the maximum temperature. It is obvious that the maximum temperature will increase with increasing thickness, since the volume to surface ratio is given by:

$$\frac{V}{A_{\text{surf}}} = \frac{s}{2 + 4 \cdot s/D} \quad (2)$$

where s and D are thickness and diameter respectively of the moderator disc ($s \ll D$). The thickness should be chosen in such a way that the maximum temperature is sufficiently far from the melting temperature of the material and the maximum temperature is high enough to enable the healing of the microstructural point defects caused by the irradiation.

The thickness of the moderator was varied from 0.01 mm to 0.7 mm for W and from 0.01 mm to 0.40 mm for Pt. The dependence of T_{max} on the thickness is shown in Fig. 5. The total heat input, which is proportional to the thickness, is indicated in the upper horizontal axis.

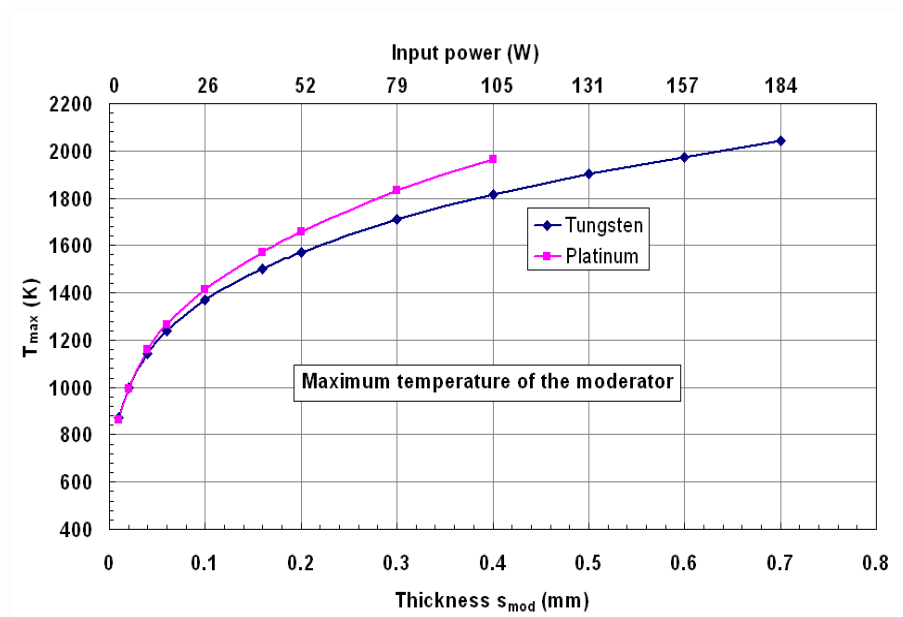


Fig. 5: Maximum moderator temperature in dependence on thickness

The temperature distributions in the lens (grid and tube) are discussed for the following situations: 100% heat generation and 1% heat generation in the tube and in the grid. For the upper bound case the influence of the emission coefficient of steel is investigated in the range $0.03 \leq \varepsilon_{st} \leq 1$ because the emission coefficient of steel strongly depends on the surface finishing. Fig. 6 shows the temperature vs. time for 100% beam power at different locations. The steady state is reached after ~ 60 s.

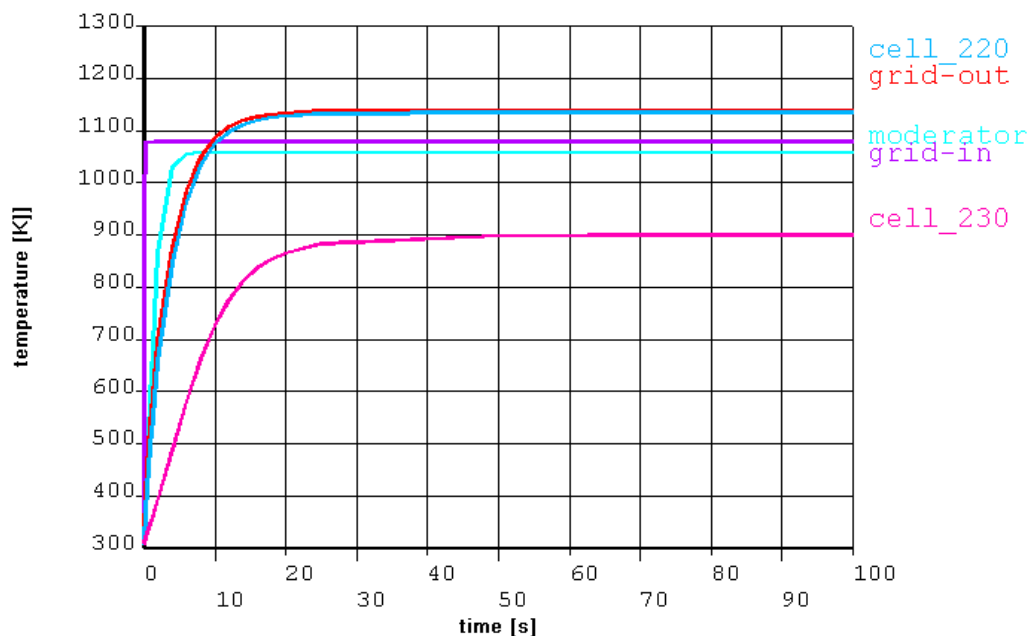


Fig. 6: Temperature vs. time for different positions; 100% beam power, emission coefficient $\varepsilon = 0.24$

The beam power of the diagnostic mode is 1% of the nominal power. The volumetric heat generation rate is reduced likewise. The temperatures vs. time are shown in Figure 7. The calculations were performed for the nominal emission coefficient of $\varepsilon = 0.24$. As expected the

temperatures are much lower than with full beam power. The overall maximum is about 409 K = 136 °C.

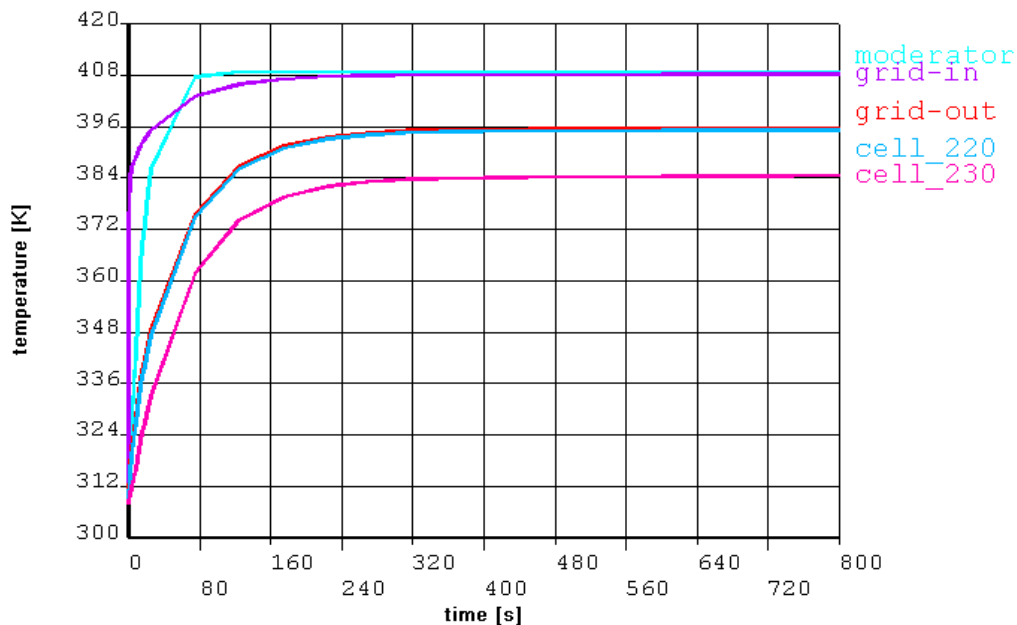


Fig. 7: Temperature vs. time for different positions in the upper part of the lens and in the moderator; 1% beam power (diagnostic mode)

5. Conclusions

We performed a time-dependent thermal analysis of the metallic parts (positron moderator and electrostatic extraction lens) of the positron source EPOS being directly exposed to the high-energetic, high –flux electron beam of the radiation source ELBE. The temperature of the moderator can be adjusted by varying the thickness of the foil. It is possible to obtain high enough temperatures to ensure defect annealing under operation conditions. This will lead to a larger positron diffusion length, and thus to a higher efficiency of the electron-positron conversion. The upper part of the extraction lens tube which is hit by the high-intense electron beam must be thinned in order to reduce the heat load. A version having a wall thickness of only 50 μm has been realized. We expect a temperature not higher than 1150 K. The mesh grid on top of the extraction tube which is also made from stainless steel will have a temperature about 1100 K at full beam power. All this parts will be at stable operation temperature after less than 60 s.

References

- [1] R. Krause-Rehberg, H. S. Leipner, Positron annihilation in semiconductors, Vol. ISBN 3-540-64371-0 (Springer-Verlag, Berlin, 1999).
- [2] <http://www.fz-rossendorf.de/ELBE/> and <http://www.positronannihilation.net/EPOS/>
- [3] R. Krause-Rehberg, S. Sachert, G. Brauer, A. Rogov, K. Noack, Appl. Surf. Sci. 252, 3106 (2006).
- [4] MCNP – A General Monte Carlo N-Particle Transport Code, Version 5, X-5 Monte Carlo Team, LA-CP-03-0284, 2003.
- [5] Table of emissivity of various surfaces. Mikron Instrument Company, Inc.

NANOINDENTATION OF ION-IRRADIATED FE-CR MODEL ALLOYS AND FERRITIC/MARTENSITIC STEELS

Cornelia Heintze, Carmen Recknagel, and Frank Bergner

1. Introduction

Ferritic/martensitic Cr-steels are candidate materials for future nuclear applications such as Generation-IV fission or fusion reactors. In these applications structural materials of some components are exposed to intense irradiation fields, high temperatures and mechanical loading, which cause degradation of the mechanical properties. To ensure the integrity and safety of these components the degradation mechanisms and their impact on the mechanical properties have to be understood.

In order to investigate the effect of irradiation on the mechanical properties self-ion irradiation was chosen to simulate the damage induced by fast neutrons. The major advantages of ion irradiation are the avoidance of activated material due to neutron irradiation, the reduction of irradiation times and improved capabilities to vary irradiation conditions. However, the limited penetration depth of the ions requires special methods to characterize the ion-induced damage. The present investigation is focused on the application of nanoindentation. The aim is to contribute to the understanding of irradiation hardening. For ferritic/martensitic Cr-steels the influence of Cr on the hardening behavior is of special interest. Therefore, Fe-Cr model alloys are investigated in addition to ferritic/martensitic steels to separate the Cr effect.

2. Experiments

The reduced activation Cr-steel, Eurofer'97, and Fe-Cr model alloys containing 2.5, 9 and 12.5 at%Cr were investigated. The chemical composition, origin and heat treatment of the materials are summarized in Tables 1 and 2. The specimens were prepared by grinding with SiC-paper (up to 2500 grit) and polishing with diamond suspension (particle size 3 μm and 1 μm). Single beam ion irradiations with Fe-ions were performed at the 3 MV-Tandatron accelerator of Forschungszentrum Dresden-Rossendorf, Institute of Ion Beam Physics and Materials Research. The irradiations were carried out at 300°C up to damage levels of 1 dpa and 10 dpa (displacements per atom).

The resulting damage profiles were calculated by means of the SRIM code version 2006.02 assuming an average displacement energy of 40 eV [1]. A one-step irradiation using a single ion energy causes a non-monotonously graded damage profile as shown in Fig. 1 for the irradiation with Fe-ions with an energy of 5 MeV. The resulting non-homogeneous damage layer considerably complicates the interpretation of the hardness results. Therefore, a three-step irradiation with different ion energies was applied to obtain a roughly rectangular damage profile (Fig. 1) which allows for more reliable hardness results compared to a one-step irradiation. The thickness of the damage layer is about 1.4 μm .

The depth-sensing nanoindentation measurements were carried out with the UNAT device (asmech GmbH) using a Berkovich indenter. Indentation loads in the range from 1 to 500 mN corresponding to a maximum indentation depth from about 100 nm to 4 μm were applied. Corrections were performed for system stiffness, indenter area function and thermal drift. The hardness values for each load were determined from at least 10 single load-depth curves

analyzed according to the Oliver and Pharr method [2]. For Fe-9at%Cr (300°C, 1 dpa) the irradiated region was characterized by means of transmission electron microscopy(TEM).

Table 1: Chemical composition (wt%)

	Cr	Ni	Mn	W	V	Ta	C	P	Si	N	Cu
Eurofer'97	8.82	0.02	0.47	1.09	0.2	0.13	0.11	0.005	0.04	0.02	0.002
Fe-2.5at%Cr	2.4	0.044	0.009	-	0.001	-	0.008	0.013	0.02	0.012	-
Fe-9at%Cr	8.4	0.07	0.03	-	0.002	-	0.02	0.012	0.09	0.015	-
Fe-12.5at%Cr	11.6	0.09	0.03	-	0.002	-	0.027	0.05	0.11	0.024	-

Table 2: Origin and heat treatment

Material	Heat treatment	Origin
Eurofer'97	Normalized (980°C/27 min/AC) & tempered (760°C/90 min/AC)	Böhler (Austria), production nr. T512, batch 249, heat 83698, plate 14.5 mm
Fe-Cr	Normalized (1050°C/3 h/AC) & tempered (730°C/4 h/AC)	SCK-CEN, Mol (Belgium)

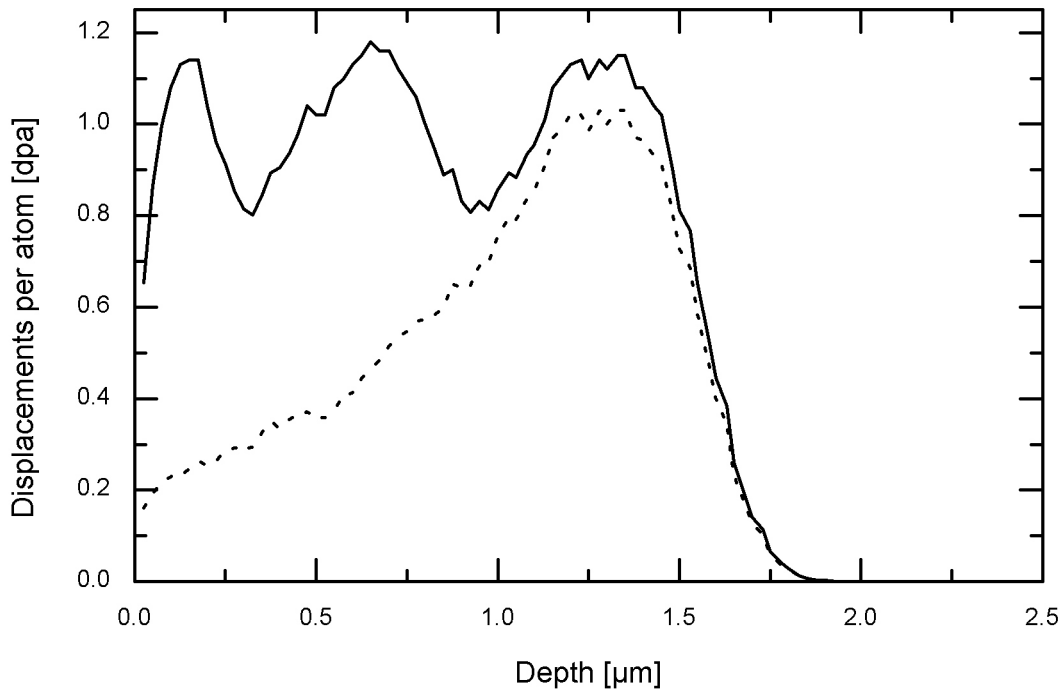


Fig. 1: Damage profile calculated by SRIM for a three-step irradiation with Fe-ions up to 1 dpa using energies of 500 keV, 2 MeV and 5 MeV and fluences of $1.8 \times 10^{14} \text{ cm}^{-2}$, $2.9 \times 10^{14} \text{ cm}^{-2}$ and $5.6 \times 10^{14} \text{ cm}^{-2}$, respectively (solid line) and for a one-step irradiation with Fe-ions of 5 MeV (dotted line)

3. Results

The load dependence of the hardness is shown in Fig. 2 for the Fe-Cr alloys and Eurofer'97 in the unirradiated condition. The curves exhibit the well-known indentation size effect (ISE) which is about the same for Cr-contents of 9 and 12.5 at% as well as Eurofer'97. A significantly stronger ISE was observed for Fe-2.5at%Cr. The ISE was discussed in detail in [3] for Eurofer'97. In the present work the load dependence of hardness for the unirradiated

conditions is taken as reference. For the Fe-Cr model alloys the hardness increases with Cr-content. As expected, Eurofer'97 shows a significantly higher hardness compared to the Fe-9at%Cr model alloys.

The load dependence of the hardness of the Fe-Cr alloys and Eurofer'97 ion-irradiated at 300°C up to 1 and 10 dpa is presented in Fig. 3. It can be seen that the load dependence is further modified by the irradiation-induced formation of a harder damage layer. The measured hardness value should be representative of the layer if the indentation depth is smaller than about 10% of the thickness of the damage layer. Otherwise, the hardness is a composite value approaching substrate hardness at large indentation depth. In case of an inhomogeneous damage layer, like the one resulting from a one-step irradiation, the interpretation is considerably more complicated.

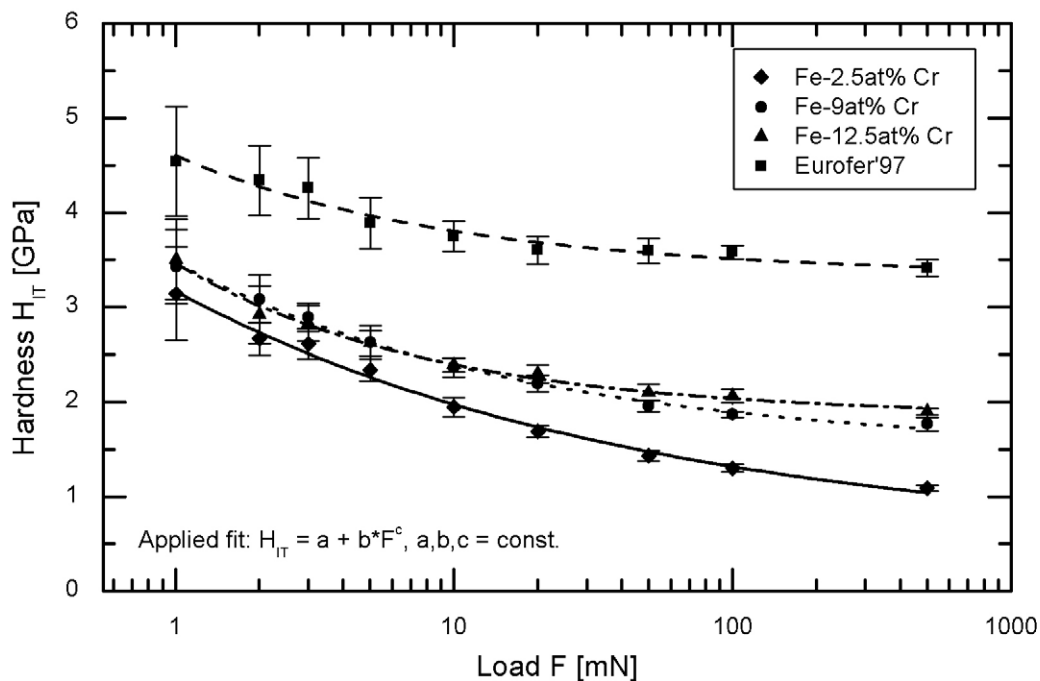


Fig. 2: Load dependence of the hardness of the Fe-Cr model alloys and Eurofer'97 in unirradiated condition

The irradiation-induced hardness change at an indentation load of 5 mN is depicted as a function of dpa in Fig. 4 at an irradiation temperature of 300°C. The indentation load of 5 mN was chosen as a compromise between the influence of the unirradiated substrate increasing with load and the uncertainty of the measured hardness values increasing with decreasing load. Each of the three Fe-Cr alloys exhibits significant hardening at 1 dpa. In the low chromium alloy (2.5 at%) the hardness further increases up to 10 dpa, while the data indicate a saturation-like behavior for the alloys with chromium contents of 9 and 12.5 at%. In contrast to Fe-9at%Cr the irradiation-induced hardening of Eurofer'97 increases up to 10 dpa. The hardening of Eurofer'97 is still lower at 1 dpa, but it exceeds the hardness change of Fe-9at%Cr at 10 dpa.

A distribution of irradiation-induced dislocation loops was observed by TEM in Fe-9at%Cr ion-irradiated at 300°C up to 1 dpa (Fig. 5) [4].

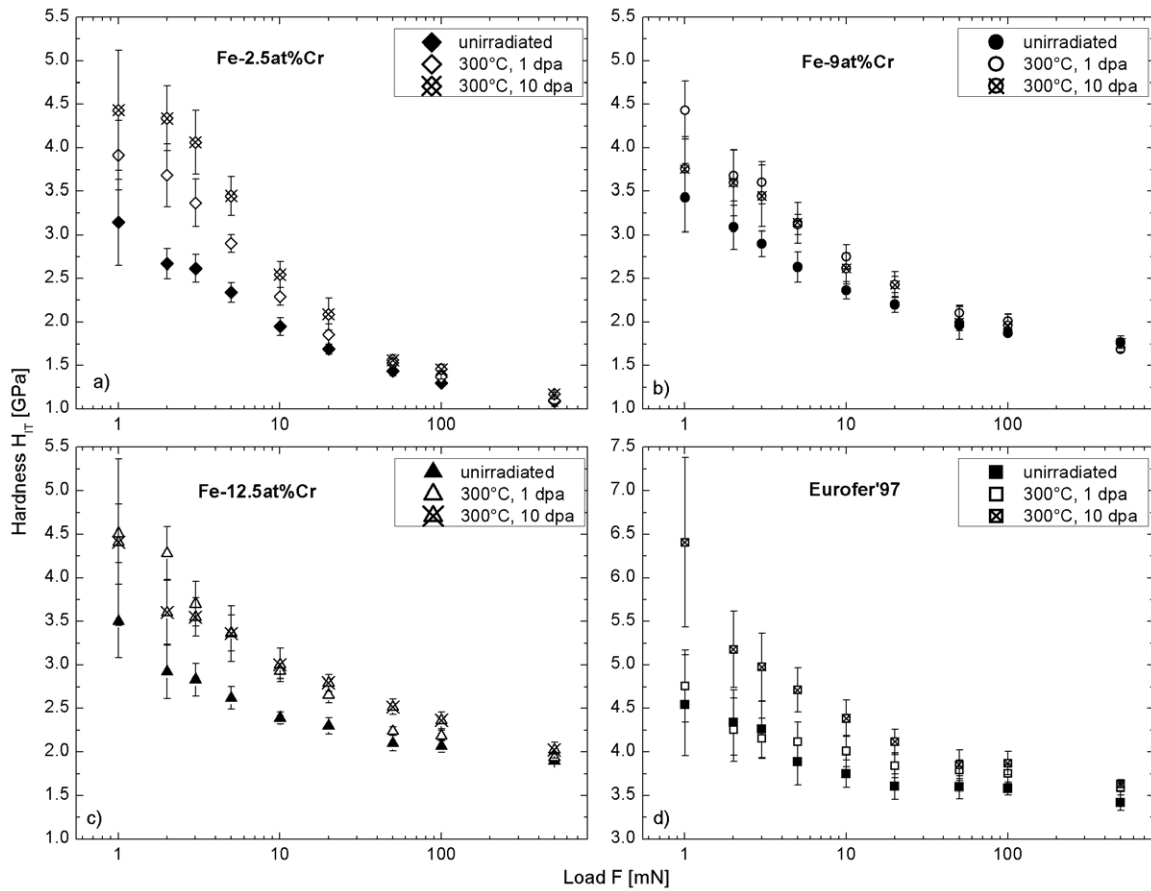


Fig. 3: Load dependence of the hardness of the Fe-Cr alloys and Eurofer'97 in unirradiated condition and irradiated at 300°C up to 1 and 10 dpa

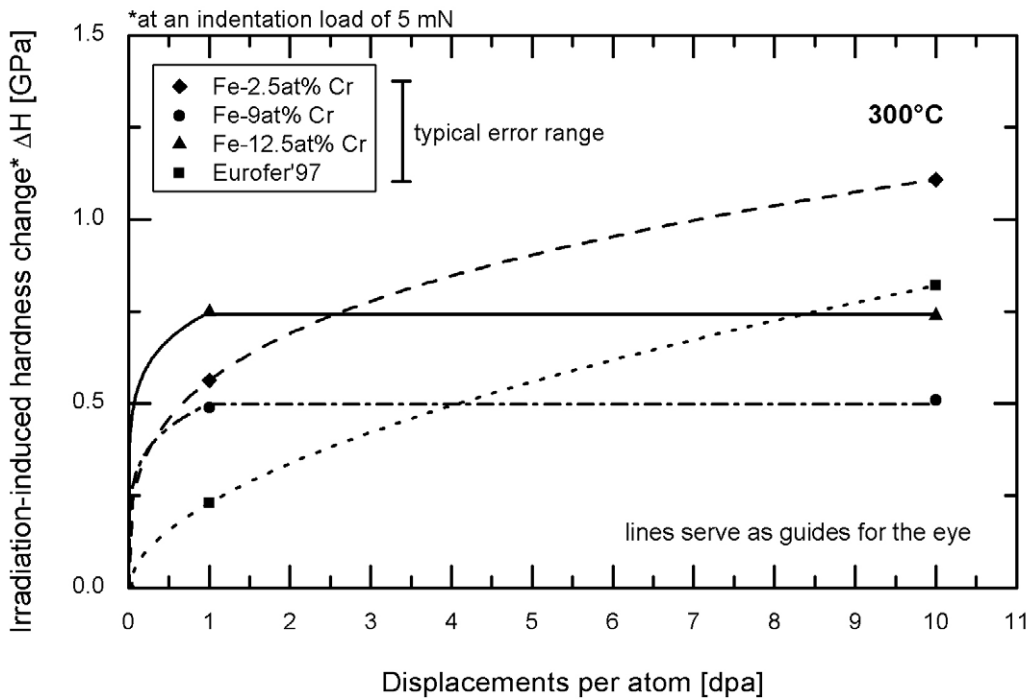


Fig. 4: Fluence dependence of the irradiation induced hardness change in the Fe-Cr alloys and Eurofer'97 at an indentation load of 5 mN

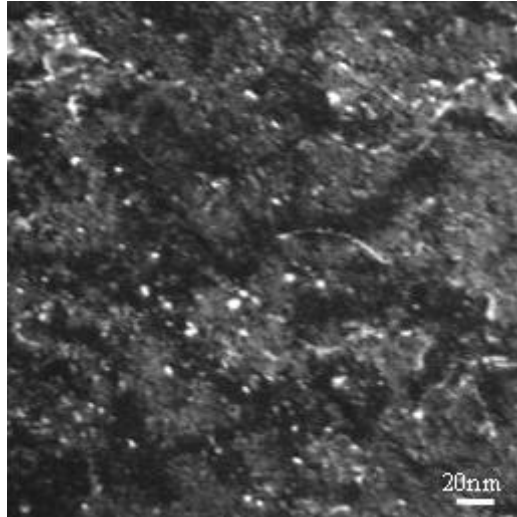


Fig. 5: TEM micrograph for Fe-9at%Cr (300°C, 1 dpa)

4. Discussion

The rectangular damage profile produced by the three-step irradiation and the measured load dependence of hardness constitute a reliable basis for the characterization of irradiation damage. The irradiation-induced hardness increase at an indentation load of 5 mN turned out to be a representative measure. Below we give a tentative mechanistic interpretation of the experimental findings.

For the present discussion we assume that the damage in units of dpa is the dominant parameter and ignore the effect of secondary parameters such as type and energy of particles or flux. This enables us to refer to microstructural data obtained from neutron-irradiated materials in order to interpret the results of the present work. Information about the size and number density of dislocation loops was gathered by TEM for the same Fe-Cr model alloys [5] and Eurofer'97 [6]. The transferability of these results is qualitatively confirmed by the observation of dislocation loops in ion-irradiated Fe-9at%Cr (Fig. 5). Precipitates such as α' -phase can be detected by means of small angle neutron scattering (SANS) which was also applied to the Fe-Cr model alloys [7, 8, 9] and Eurofer'97 [10]. As a first approximation, the hardening is assumed to be independent of the size of the irradiation-induced defects and is mainly determined by their concentration. In Table 3, reported concentrations are summarized in terms of number density of dislocation loops and volume fraction of α' -particles.

Table 3: Summary of microstructural data [5-10]

Material	Neutron exposure [dpa]	Loop number density [10^{21}m^{-3}]	Volume fraction of α' [vol%]
Fe-2.5at%Cr	0.6	2.7	0
	1.5	2.2	0
Fe-9at%Cr	0.6	1.9	<0.2
	1.5	1.7	<0.2
Fe-12.5at%Cr	0.6	1.7	4.3
	1.5	1.7	4.3
Eurofer'97	0.6	2	Similar to Fe-9at%Cr
	1.5		

According to Table 3 the number density of the dislocation loops is observed to be independent or a slightly decreasing function of the fluence for each of the materials. Therefore, the hardening contribution of the loops is expected to stay about constant as observed for Fe-9at%Cr and Fe-12.5at%Cr (Fig. 4). Another hardening contribution is caused by Cr-rich α' -particles expected for Cr contents above about 9 at% [11]. SANS results (table 3) demonstrate that the volume fraction of α' saturates for 12.5 at% Cr and is much smaller for Fe-9at%Cr. This observation is consistent with the present nanohardness data. In particular, it explains the higher saturation level of Fe-12.5at%Cr in comparison to Fe-9at%Cr at about the same loop densities. The hardness increase for Fe-2.5at%Cr compared to Fe-9at%Cr at 1 dpa is consistent with the higher loop number density. But the further hardening up to 10 dpa cannot be explained by the presence of dislocation loops only. SANS revealed the presence of small defects which were tentatively interpreted as Cr-C clusters [8].

The fluence dependence of the hardening of Eurofer'97 is different from Fe-9at%Cr (Fig. 4). The lower hardening at 1 dpa can be explained by the reduced impact on hardening of about the same loop number density as found in Fe-9at%Cr at the higher initial hardness of Eurofer'97. The additional hardening at 10 dpa might be caused by the irradiation-induced defects detected by means of SANS [10] and tentatively interpreted as microvoids. Alternatively, Cr-C clusters as for Fe-2.5at%Cr could also play a role.

5. Conclusion

The load dependence of nanohardness was measured for Fe-Cr model alloys and Eurofer'97 exposed to three-step self-ion irradiations. A saturation-like behavior of the irradiation-induced hardening was observed for Fe-9at%Cr and Fe-12.5at%Cr, but not for Fe-2.5at%Cr and Eurofer'97. A tentative mechanistic interpretation was given on the basis of dislocation loops observed by TEM and Cr-rich α' particles detected by SANS for the same materials irradiated with neutrons.

References

- [1] M. Ando, H. Tanigawa, S. Jitsukawa, T. Sawai, Y. Katoh, A. Kohyama, K. Nakamura and H. Takeuchi (2002), Evaluation of hardening behaviour of ion irradiated reduced activation ferritic/martensitic steels by an ultra-micro-indentation technique, *Journal of Nuclear Materials*, 307-311, 260
- [2] W.C. Oliver and G.M. Pharr (2004), Measurement of hardness and elastic modulus by instrumented indentation: Advances in understanding and refinements to methodology, *Journal of Materials Research*, 19, 3
- [3] C. Recknagel (2008), Depth-sensing nanoindentation and accompanying Atom Force Microscopy (AFM) on unirradiated and ion-irradiated steels, Rossendorf, Diploma thesis
- [4] C. Heintze, C. Recknagel, F. Bergner, M. Hernández-Mayoral and A. Kolitsch (2009), Ion-irradiation-induced damage of steels characterized by means of nanoindentation, *Nuclear Instruments and Methods in Physics Research, B* 267, 1505
- [5] M. Matijasevic and A. Almazouzi (2008), Effect of Cr on the mechanical properties and microstructure of Fe-Cr model alloys after n-irradiation, *Journal of Nuclear Materials*, 377, 147
- [6] M. Matijasevic, E. Lucon and A. Almazouzi (2008), Behavior of ferritic/martensitic steels after n-irradiation at 200 and 300°C, *Journal of Nuclear Materials*, 377, 101
- [7] A. Ulbricht, C. Heintze, F. Bergner, H. Eckerlebe (2008), Nature of defects formed in neutron-irradiated Fe-Cr model alloys, in P. K. Pranzas, A. Schreyer, R. Willumeit

- (Eds.): GeNF - Experimental Report 2007, GKSS Forschungszentrum Geesthacht GmbH, Geesthacht, GKSS2008/6
- [8] A. Ulbricht, C. Heintze, F. Bergner, H. Eckerlebe (2009), SANS investigation of irradiation-induced phase separation in binary Fe-Cr-alloys, in P. K. Pranzas, M. Müller, R. Willumeit, A. Schreyer (Eds.): GeNF - Experimental Report 2008, GKSS Forschungszentrum Geesthacht GmbH, Geesthacht, GKSS2009/2
 - [9] A. Ulbricht, C. Heintze, F. Bergner and H. Eckerlebe (2009), SANS investigation of a neutron-irradiated Fe-9at%Cr alloy, to be published
 - [10] R. Coppola, R. Lindau, M. Magnani, R. P. May A. Möslang J. W. Rensman, B. van der Schaaf and M. Valli (2005), Fusion Engineering and Design, 75-79, 985
 - [11] L. Malerba, A. Caro and J. Wallenius (2008), Multiscale modeling of radiation damage and phase transformations: The challenge of FeCr alloys, Journal of Nuclear Materials, 382, 112

Acknowledgement

The ion irradiations were kindly performed by the Institute of Ion Beam Physics and Materials Research, Forschungszentrum Dresden-Rossendorf.

Summaries of research activities

Accident Analysis of Nuclear Reactors

The research is aimed at the enhancement of the predictive capability of computer simulations of accident scenarios in presently operating and future nuclear reactors. This is achieved by improvements of the neutron kinetics methods and by coupling of the FZDs reactor dynamics model DYN3D to thermo-hydraulics system codes and to computational fluid dynamics (CFD) simulations. This is performed primarily within the European code platform NURESIM.

In particular, it is the objective to promote the basic understanding of coolant mixing phenomena relevant for boron dilution and pressurized thermal shock scenarios in Light Water Reactors (LWR) and to adequately simulate inherent feedback mechanisms ensuring the controllability of accidents with assumed failure of the reactor scram system.

Moreover, the field of applicability of the reactor dynamics simulations is extended to innovative reactor concepts. New code versions of DYN3D are going to be developed and validated for such designs. Analytical methods of time-dependent neutron transport theory are developed to basically understand the propagation of neutron pulses in accelerator driven sub-critical systems for transmutation of minor actinides.

*S. Kliem,
S. Mittag,
U. Rohde,
S. Baier
Y. Kozmenkov,
Y. Bilodid.
A. Gommlich,
P. Tusheva*

Development, Validation and Application of the Code Complex DYN3D - ATHLET

In the course of the continuous development of the Rossendorf reactor dynamics code DYN3D, a multi-group transport approach was implemented for the improved description of spectral effects and to overcome the limitations of the diffusion approximation.

The extended code version was integrated into the European code platform NURESIM. In the corresponding European project, a systematic validation of DYN3D against mathematical benchmarks and experimental data from research reactors was performed. Presently, DYN3D is used by 13 organisations in 7 countries, among them member institutes of the Helmholtz Society (FZ Jülich, FZ Karlsruhe).

In the frame of a PhD study, the capabilities of an advanced fuel burn-up model based on the direct solution of the nuclide balances during the burn-up process within DYN3D were demonstrated. By the help of this model, so-called history effects in burn-up and their influence on the power distribution can be described more precisely.

The development of a DYN3D code version for gas-cooled high temperature reactors was started. A specific feature of this reactor design consists of fuel particles included in hexagonal graphite blocks. Therefore, heterogeneity effects and 3D heat conduction in the graphite structures have to be taken into account, for which new modules of DYN3D are going to be developed.

The expertise of the institute on thermo-hydraulic system codes and coupled neutronics/thermo-hydraulics code complexes is increasingly appreciated by industry. For example, analyses on the efficiency of the boron injection system in Boiling Water Reactors were performed under the auspices of Vattenfall. Moreover, the code complex DYN3D-ATHLET was applied to the analysis of Anticipated Transients Without Scram (ATWS) in Pressurized Water Reactors, where the reactor behaviour is fully dominated by inherent feedback mechanisms.

*Supported by
BMW, BMU, EU,
TÜV, Vattenfall
Europe Nuclear
Energy, E.ON,
VGB*

*B. Merk ,
S. Mittag,
E. Fridman,
J. Konheiser,
S. Dürigen,
V. Glivici*

Neutronics for Innovative Reactor Concepts

In the frame of the European project LWR-DEPUTY, reactor physics calculations were done on the burn-up behaviour of Thorium fuel. These investigations are aimed at the minimisation of long-lived higher actinides content in radioactive waste.

Analytical approximation methods of the time-dependent neutron transport theory, which allow a more accurate interpretation of measurements in pulsed sub-critical systems (ADS) are developed within the European project EUROTRANS.

Capabilities of the HELIOS neutron transport code as a “working horse” for deterministic reactor physics calculations were studied. In comprehensive tests, the impact of the spatial discretisation on calculated cross section data and critical parameters was investigated. Via comparison with Monte Carlo methods (code MCNP) it was shown that critical parameters of the complex HTR fuel (fuel particles in graphite matrix) can be calculated by HELIOS with appropriate accuracy.

*Supported by
BMW and EU*

*S. Kliem,
T. Höhne,
R. Franz,
P. Apanasevich*

Investigations on Coolant Mixing

The modelling of coolant mixing is highly relevant for nuclear reactor safety, because mixing is the only decisive inherent mechanism to prevent serious consequences of boron dilution accidents. Experimental investigations on coolant mixing in PWR were performed at the ROCOM test facility and complemented by CFD simulations. Extended numerical grids comprising all relevant parts of the facility and advanced turbulence models (SST model, Detached Eddy Simulation) were used in the simulations.

The expertise in mixing phenomena was exploited within a European TACIS project on boron dilution and overcooling transients in VVER type reactors.

ROCOM was selected as the reference facility of the OECD for mixing investigations and is going to be involved in an OECD project.

*Supported by EU
and industries
(VGB)*

*H. Kryk,
E. Krepper,
A. Grahn,
G. Cartland-Glover,
W. Hoffmann*

Development of CFD Models for the Simulation of Fibre Loaded Coolant Flow

Insulating material (mineral wool) may be released from pipes and components during loss-of-coolant accidents in NPP and will be transported with the coolant towards the reactor sump. There it might lead to blockage of the sieves separating the suction chambers of the safety injection pumps from the sump leading to failure of the late phase emergency core cooling. Within a research project supported by BMWi aimed at the simulation of the behaviour of mineral wool particles in the sump pool flow, models were developed for the transport, sedimentation and re-suspension of isolation material. The work is done in co-operation with the University of Applied Sciences Zittau/Görlitz, where experiments are performed, while FZ Dresden-Rossendorf is responsible for the CFD modelling. It was shown, that an adequate description of the transport of isolation material with flowing fluid must be based on the use of a variable turbulent dispersion coefficient, which is dependent from the length and time scale of the local turbulent parameters. A

model based on the Ergun/Davies equation was elaborated to describe the differential pressure on a strainer dependent on the fibre load and the flow conditions. The model constants were adapted for the simulation of different materials based on experiments performed in Zittau. Further investigations were directed on the air entrained by a jet and its influence on the water flow field. The consequences on the preferred location of fibre deposition could be shown. In a new project that started in October 2008, the impact of corrosion products and water chemistry is investigated under realistic sump cooling conditions. For the clarification of the influence of chemical effects on strainer clogging, first analyses of isolation material probes by the help of REM/EDX were done. In these investigations, precipitations of zinc on the surfaces of the fibres were found, which are assumed to be caused by crystallisation processes on the fibres themselves.

*Supported by
BMW*

Materials and Components Safety

The change in the toughness behaviour of reactor pressure vessel materials is investigated as it results from neutron and gamma irradiation. The consequences are evaluated with respect to the safety of light water reactors (LWRs). For this purpose, material and fracture mechanical parameters of irradiated specimens have to be measured under hot cell conditions. The interpretation of the experiments is supported by finite element calculations. The microstructural reasons and mechanisms of the neutron embrittlement are studied by small angle neutron scattering and nano indentation experiments supported by nano-scaled modelling. These microstructural methods are also applied to materials which are currently developed for new reactor concepts (GEN-IV reactors).

*H.-W. Viehrig,
U. Rindelhardt,
E. Altstadt,
C. Zurbuchen,
J. Schuhknecht*

Investigation of Reactor Pressure Vessel Material of the Dismantled Greifswald NPP

The characterisation of the irradiated, annealed and re-irradiated core welding seam of unit 1 revealed a large scatter of the fracture toughness and an irregular course of the reference temperature (T_0) over the wall thickness. It could be shown that the different T_0 result from the microstructure of the multi layer welding seam rather than from the re-irradiation. In the range of the filling layers, reference temperatures between -33 °C and $+20\text{ °C}$ were found. The high values of T_0 are located in the melting zones between two layers. Nevertheless, a successful thermal recovery and low re-embrittlement can be stated.

*Supported by
BMW*

*H.-W. Viehrig,
C. Zurbuchen,
E. Altstadt*

Application of the Master Curve Concept to Irradiated Material

Within a project with the Swiss HSK (Hauptabteilung für die Sicherheit der Kernanlagen), the influence of the specimen size, pre-crack geometry and the loading rate upon the Master Curve(MC) reference temperature (T_0) is studied. Compact tensile and large scale bending specimens were manufactured from the RPV steel 22 NiMoCr 3-7. It was shown, that fracture toughness values measured with different specimen thicknesses can be mutually translated. The applicability of the MC concept with dynamic loading was proven.

Supported by HSK

*E. Altstadt,
M. Abendroth*

Analysis of VVER-440 PTS Scenario

The finite element based fracture mechanical evaluation of a VVER-440-RPV for a PTS (pressurizes thermal shock) scenario has shown, that the mechanical integrity of a RPV wall after 30 years of irradiation can only be guaranteed in case of intact cladding. Assuming contrarily a surface crack, a thermal recovery (annealing) has to be performed after about 19 full power years.

Supported by EU

*F. Bergner,
A. Ulbricht,
C. Heintze,
R. Kuchler*

Analysis of the Irradiation Induced Microstructural Changes

Within the EU project PERFECT, extended SANS experiments at model alloys were evaluated and interpreted together with TEM, atom probe and PAS analyses of the project partners. Moreover, SANS experiments were performed at material specimens of the Greifswald NPP. It could be shown, also from the microstructural point of view, that the RPVs of units 1 and 2 were successfully thermally recovered. In the EU project GETMAT, the formation of irradiation induced defect clusters in Fe-Cr alloys was investigated as a function of the neutron fluence and the Cr

*Supported by
BMW, EU*

*F. Bergner,
C. Heintze,
P. Franke*

*F. Bergner,
U. Birkenheuer,
A. Gokhman,
R. Kuchler*

content. The irradiation behaviour of alloys with up to 9% Cr on the one hand and of alloys with more than 9% Cr on the other hand is basically different.

Characterisation of Ion Irradiated Gen-IV Materials

In cooperation with the FZD Institute of Ion Beam Physics and Materials Research we continued the simulation of neutron irradiation induced damage by irradiation with ions. The diploma thesis “Depth sensing nano hardness measurements and accompanying atom force microscopy at unirradiated and ion irradiated steels” was successfully finished. An irradiation induced increase of the hardness could be proved for the ferritic-martensitic Cr steel Eurofer’97, for the austenitic steel SS 304 and for a 9%Cr model alloy.

Modelling of the Irradiation Induced Embrittlement

Within a project supported by BMW, a new modular software package which is used to evaluate RPV steel embrittlement was further developed for application to Cu-vacancy clusters. By employing the Fokker-Planck transformation a significant reduction of the computational effort could be achieved. Two dimensional dislocation simulations were started to describe the effect of defect clusters on the mechanical properties.

Thermal Fluid Dynamics of Multi-Phase Flows

The general aim of the work done in the field of thermal fluid-dynamics is the qualification of Computational Fluid Dynamics (CFD) codes for the simulation of complex two-phase flows with relevance for industrial applications. To achieve this goal, closure models are needed for the interaction between the phases, i.e. mass, momentum and heat transfer. For the special case of dispersed bubbly flow, all these transfers strongly depend on the local bubble size distribution. For this reason, the gas phase has to be split into a number of size groups in case of polydisperse flows. Transfers between these groups are amongst others determined by bubble coalescence and fragmentation. For stratified flows in horizontal components models for the transfers at the free interface and for the coupling of the turbulence fields are required. The theoretical work is based on sound experiments at the TOPFLOW test facility using advanced two-phase measuring instrumentation, which is developed in the framework of the present project.

*E. Krepper,
Y. Liao,
D. Lucas*

Qualification of CFD Models

The basic equations were derived to extend the Inhomogeneous MUSIG (**M**ulti **B**ubble **S**ize **G**roup) model to mass transfer between the bubble groups. They are ready for the implementation into the CFX code which is presently done by ANSYS.

The validation of the existing Inhomogeneous MUSIG model was continued using data from a new extensive test series for upward air-water flow in a vertical DN200 pipe at the TOPFLOW facility. The simulations confirmed the findings, that the implemented models for bubble forces are applicable for a wide range of parameters, while the transferability of the presently available models for bubble coalescence and fragmentation is still limited.

For this reason, investigations were done which focus on the improvement and generalization of these models. Based on an extended assessment of the available models for bubble coalescence and breakup, the first version of a new fundamental model was developed and implemented into a test solver. This model considers different mechanisms for bubble coalescence and breakup. First simulations for adapting and validating the model were carried out using the above mentioned TOPFLOW data from air-water flow in a vertical pipe.

*Supported by
BMW*

*Ch. Vallee,
T. Höhne,
T. Seidel*

Experiments and CFD-Simulations for a PWR Hot Leg Geometry

Air-water as well as steam-water experiments on co-current and counter-current flow were conducted in a hot leg model at the TOPFLOW facility. The experimental series included extensive investigations of the Counter-Current Flow Limitation (CCFL) phenomenon, which is important for nuclear reactor safety.

The different fluid properties in the single experimental runs (experiments were carried out for air-water at 0.3 MPa and for steam-water at 1.5, 3 and 5 MPa) allowed investigating the influence of the material parameters on CCFL. As a result a modified Wallis parameter was suggested to obtain the flooding curve.

A statistical evaluation of the experimental data was done to provide data suitable for comparison with CFD simulations. Such simulations were conducted using the newly implemented Algebraic Interfacial Area Density (AIAD) model together with an approach for turbulence

*Supported by
BMW*

damping at the interface. The AIAD model allows the application of closure models in dependency on the local flow morphology.

*M. Schmidtke,
D. Danciu,
E. Krepper*

Investigations on Bubble Entrainment by a Liquid Jet

CFD calculations were done to simulate the bubble entrainment by an impinging liquid jet as well as the bubble migration after entrainment. New experimental data which were obtained by high-speed video observation for such a flow situation in a small scale vessel were used for the validation. Characteristic parameters, such as the penetration depth of the bubbles, showed a good agreement between simulations and experimental data.

*Supported by EU
and BMW*

*U. Hampel,
E. Schleicher,
M. Bieberle,
F. Fischer*

Ultra fast X-ray Tomography

The ultrafast X-ray tomography scanner ROFEX and a DN50 test section for upward co-current steam-water and air-water two-phase flow studies at TOPFLOW were prepared for an experimental campaign. For that, the necessary radiation protection measures were implemented, the electron beam monitoring was decisively improved, and a vertical positioning unit was commissioned. Within the DFG-funded project “Ultraschnelle Röntgentomographie”, for the first time ever, a real two-phase flow was scanned in a small pipe in dual-plane scanning mode. This will allow to measure gas phase velocities in pipe flow in the future. Also for the first time, a three-dimensional scanning mode was successfully tested at 1000 volume scans per second.

*Supported by
DFG and BMW*

*U. Hampel,
A. Bieberle,
D. Hoppe,
E. Schleicher,
C. Zippe*

Optimisation of the Gamma Ray Tomography for Void Fraction Measurements in Fuel Rod Assemblies

For the measurement of steam distributions and the detection of the boiling crisis in BWR rod bundle mockups under original thermal-hydraulic conditions, a gamma ray tomography system was developed and put into operation. This system is being utilized at the KATHY thermal hydraulic test facility of AREVA NP Germany. Besides decisive improvements in the thermal stability of the scanner, dedicated data processing algorithms for radiation scatter correction and computation of local gas fraction were successfully developed and tested.

*Supported by
AREVA NP*

*M. J. Da Silva,
S. Thiele,
U. Hampel*

Comparative Experimental Studies of Gas/Water and Oil/Water Two-Phase Flow

A new capacitance wire mesh sensor measurement system with 24 x 24 measuring points was applied to study oil-gas two-phase flow in a vertical pipe of 67 mm inner diameter at the University of Nottingham. There it was for the first time demonstrated that this new sensor can be successfully operated under harsh near-industrial operating conditions. The flow structural data acquired with the wire mesh sensor were analyzed with respect to radial gas profiles and bubble size distributions as a function of the superficial gas and liquid velocities. The work was rewarded with a Best Paper Award at the PROCTOM symposium 2008 in Zakopane, Poland.

*Partly supported
by DAAD*

*M. Schubert,
H. Kryk,
G. Hessel*

Investigation of Flow Phenomena in Electrolytic Cells

Residence time distributions were measured for the first time during a running electrolysis process using Laser Induced Fluorescence (LIF) visualisation. It was found that the average residence time of the liquid is not influenced significantly by the electrolysis process. However the backmixing inside the cell is clearly improved by the electrolytically generated gas bubbles. The investigations are a basis to optimize the design of the electrolytic cell as well as the operational parameters.

*Supported by
VKTA*

Magneto-Hydrodynamics

Magneto-Hydrodynamics investigates the interaction of electrically conducting fluids (liquid metals and semiconductors, electrolytes) with magnetic fields. In various applications, the use of magnetic fields provides a comfortable contact-less possibility to control the transport processes in such melts. Moreover, problems as MHD turbulence, the homogeneous dynamo or the magnetorotational instability are the subject of intense basic research.

*A. Cramer,
I. Grants,
J. Pal,
Ch. Zhang,
S. Eckert,
G. Gerbeth*

Basics of MHD flows and Experiments at MULTIMAG

The combination of azimuthal flow driving (rotating magnetic field – RMF) and poloidal flow driving (travelling magnetic field – TMF) provides a variety of interesting flow configurations in a cylindrical cell. The most attractive feature, available in this form only at the MULTIMAG facility, consists in the free superposition of both field types. A suitable combination of RMF and TMF results in flow fields resembling the main features of tornado flows. Keeping the RMF fixed and enhancing the TMF, lead to the occurrence of an intense swirl in the cylindrical cavity. An unexpected reversal of the flow direction on the axis was observed for intermediate values of the TMF as it is also known for tornado-like flows.

Supported by DFG

*K. Timmel,
X. Miao,
S. Eckert,
G. Gerbeth*

Facility CONCAST for Steel Flow Modelling

The facility CONCAST was built up and started operation at the end of 2008. This new liquid metal loop works with a tin-bismuth alloy. It represents a model of the continuous steel casting process, in particular of the related flow in the nozzle and in the mold. In parallel, a much smaller facility using the room-temperature melt GaInSn was installed and put into operation. First tests were performed with an external steady magnetic field located at the mold and with the introduction of argon gas bubbles into the nozzle. The reconstruction of the velocity field in the mold by a fully contactless magnetic tomography was experimentally demonstrated and resulted in a patent aiming at the realistic steel case.

Supported by DFG

*S. Boden,
S. Eckert*

X-ray Analysis of Gas Bubble Motion in Metal Melts

Systematic X-ray visualizations of the gas bubble motion in a liquid metal were performed. In parallel, the same configuration was also studied in a water-gas flow. Compared to water, the injection of gas bubbles into the metal melt depends strongly on the wetting conditions at the injection nozzle. Due to the much larger surface tension of the metal melt, the bubbles tend to have a more spherical shape. For the same gas flow rate, larger bubbles arise in the metal melt compared to water and bubble coalescence is reduced.

*Supported by
DFG, Industry*

*Th. Gundrum,
F. Stefani,
G. Gerbeth*

Experiments on the Magneto-Rotational Instability (MRI)

The experiments at the improved set-up PROMISE-2 fully confirmed the theoretical figure that indeed a global magneto-rotational-instability is observed, and not only a noise-triggered convective instability. The reduced Ekman pumping by the splitted end plates resulted in a very good agreement between the measurements and the related computations.

*Supported by WGL
and DFG*

*D. Buchenau,
G. Gerbeth*

Development of New Contactless Flow Rate Sensors

Exact flow rate measurements at liquid metal duct flows and their calibration are a notorious problem for all liquid metal loops. Commercially available sensors rely on an electrode contact to the fluid which in case of liquid metal flows cannot be used due to unknown corrosion processes at the electrodes. Two fully contactless solutions have been developed. The first one works with an alternating magnetic excitation field and measures the flow induced magnetic field phase shift at two magnetic field sensors. The second one uses a rotating permanent magnet the rotation rate of which is directly proportional to the flow rate. The latter works in an equilibrium state between the rotating magnet and the duct flow, which makes the signal independent on the melt temperature. This is of particular value for liquid metal loops with strong temperature gradients as they occur, e.g., in spallation targets.

Supported by EU

Transient Two-Phase Flow Test Facility TOPFLOW

The TOPFLOW (Transient TwO Phase FLOW) test facility is one of the major research facilities at Forschungszentrum Dresden – Rossendorf. It is mainly used for the investigation of generic and applied steady state and transient two-phase flow phenomena in either steam-water or air-water mixtures. TOPFLOW has a maximum heating power of 4 MW and allows operation at pressures up to 7 MPa and temperatures up to 285°C in pipes and vessel geometries of industrial relevance. It has become the experimental reference facility of the German CFD (Computational Fluid Dynamic) Research Alliance. Since 2006, two major research projects are run at the TOPFLOW facility. One is a BMWi funded project aiming at the development and validation of CFD models for disperse and stratified two-phase flows with heat and mass transfer. Within this project a series of novel two-phase flow experiments are conducted at TOPFLOW in different test sections. Furthermore, an international consortial project is run dedicated to the investigation of thermal hydraulic phenomena in a pressurised thermal shock scenario (PTS). Additionally, a smaller industry project for the test of a steam nozzle prototype during critical steam flow was conducted.

*C. Vallee,
T. Seidel,
M. Beyer,
H. Carl*

Stratified Two-Phase Flow Experiments in the Hot Leg Model of a Pressurized Water Reactor during Loss of Coolant Accident Conditions

In 2008 the co-current and counter-current steam/water flow experiments at pressures of 1.5, 3.0 and 5.0 MPa and saturation conditions were completed. Thereby, the new pressure tank technology was successfully used. For the first time worldwide, large-scale video observation of steam/water flow up to 5 MPa and 262°C through a 0.48 m² glass window was performed with a high-speed video camera. The recorded image sequences are an important contribution to CFD code validation.

As first step frequency distributions of the water level in the reactor pressure vessel simulator were calculated, which allow a good comparison between the experiments and CFD calculations. An important result of the comparison of the flooding characteristics of the hot leg model obtained for the fluid combinations air/water and steam/water under different pressures was the conclusion that the classic Wallis parameter fails to correlate the data properly. Finally, it was found that this effect was attributed to the dynamic viscosity of the fluids and an accordingly modified parameter was proposed which provides a good correlation over all the experimental data.

*Supported by
BMW*

*D. Lucas,
M. Beyer,
H. Carl,
L. Szalinski,
P. Schütz*

Two Phase Flow Experiments in the Vertical Test Section DN200 with Heat and Mass Transfer

The modification of the test section “Variable Gas Injection” and the installation of the pressure relief pipe were completed. Furthermore, the degassing system of the electrical heater and the test section circuit was assembled. After structural and pressure tests the extended test section was accepted by the technical authority. Moreover, the installation of additional process instrumentation and the modification of the process control system for the condensation and de-pressurization experiments were finished, too.

In 2008, the assembly of two new designed high temperature wire-mesh sensors was started for the 200 mm vertical test section. Furthermore,

*Supported by
BMW*

flow metering devices for saturated water and steam in the test section circuit were partly replaced or newly calibrated in order to meet the accuracy requirements in this test series.

*U. Hampel,
F. Fischer,
M. Beyer,
E. Schleicher*

Experiments with a New Vertical Test Tube DN50 using Fast X-Ray Tomography

The ultra fast X-ray tomograph and the special DN50 test section (Ti-alloy) for the investigation of upward two-phase flows were prepared for experimental operation. For that, the required measures for radiation protection were implemented, the electron beam monitoring was improved and the vertical positioning equipment was put into operation. After a vibration check of the DN50 test section, the tube was fixed at additional positions outside the tomography area for vibration damping. By the end of 2008, an improved gas injection device, which allows the controlled generation of small bubbles, was mounted at the lower end of the vertical tube.

*Supported by
BMW*

*U. Hampel,
E. Schleicher,
M. Beyer,
H. Carl,
C. Vallee*

TOPFLOW – PTS (Thermal Hydraulics at Pressurized Thermal Shock)

In this project, thermal hydraulic phenomena are investigated occurring in an emergency core cooling scenario in pressurized water reactors during loss of coolant accidents. Therefore, comprehensive test series will be performed in the TOPFLOW pressure tank up to the maximal pressure of 5 MPa using the pressure equilibrium technology. In 2008, the basic components of the horizontal test rig were manufactured and assembled. Moreover, all special sensors, such as thermo-probe lances, wire mesh sensors, thermo-void needle probes, high speed video imaging and infrared imaging were manufactured or put into synchronous operation. The installation of the required media supply and return system between the TOPFLOW facility and the pressure tank was completed and accepted by the technical authority.

*Supported by
CEA, EDF,
AREVA NP France,
IRSN, PSI*

The technical project committee decided on the measurement configurations and the first test matrix proposals were elaborated.

*U. Hampel,
M. Beyer*

Investigation of Critical Steam Flow through a Prototype Nozzle

Within an industrial project for NAM, the experimental investigation of the thermal hydraulic characteristics of a prototype steam nozzle was carried out for critical flow of saturated steam up to 7 MPa. The obtained results showed a very good agreement with numerical pre-calculations of NAM.

*Supported by
Nederlandse
Aardolie
Maatschappij B.V.
(NAM,
Netherlands)*

Publications

Publications in journals

Abendroth, M.; Willschütz, H. G.; Altstadt, E.

Fracture mechanical evaluation of an in-vessel melt retention scenario

Annals of Nuclear Energy 35(2008)4, 627-635

Albrecht, Th.; Metzkes, H.; Grundmann, R.; Mutschke, G.; Gerbeth, G.

Tollmien-Schlichting wave damping by a streamwise oscillating Lorentz force

Magnetohydrodynamics 44(2008)3, 205-222

Altstadt, E.; Carl, H.; Prasser, H. M.; Weiß, R.

Fluid-structure interaction during artificially induced water hammers in a tube with bend – experiments and analyses

Multiphase Science and Technology 20(2008)3-4, 213-238

Beckert, C.; Grundmann, U.

Development and verification of a nodal approach for solving the multigroup SP3 equations

Annals of Nuclear Energy 35(2008)1, 75-86

Bergner, F.; Ulbricht, A.; Gokhman, A.; Erak, D.

Nature of defect clusters in neutron-irradiated iron-based alloys deduced from small-angle neutron scattering

Journal of Nuclear Materials 373(2008), 199-205

Bergner, F.; Ulbricht, A.; Hein, H.; Kammel, M.

Flux dependence of cluster formation in neutron irradiated weld material

Journal of Physics: Condensed Matter 20(2008), 104262

Bergner, F.; Ulbricht, A.; Hernandez-Mayoral, M.; Pranzas, P. K.

Small-angle neutron scattering study of neutron irradiated Fe and Fe-Ni

Journal of Nuclear Materials 374(2008), 334-337

Bestion, D.; Anglart, H.; Carraghiaur, D.; Péturaud, P.; Smith, B.; Andreani, M.; Niceno, B.; Krepper, E.; Lucas, D.; Moretti, F.; Galassi, M. C.; Macek, J.; Vyskocil, L.; Koncar, B.; Hazi, G.

Review of available data for validation of NURESIM two-phase CFD software applied to CHF investigations

Science and Technology of Nuclear Installations 2009(2008), 214512

Bezugly, V.; Albrecht, M.; Birkenheuer, U.

Comparison of three quantum chemical ab initio methods for band structure calculations: the hydrogen fluoride chain

Journal of Physics: Conference Series 117(2008), 012006

Bieberle, M.; Schleicher, E.; Hampel, U.

Simulation study on electron beam X-ray CT arrangements for two-phase flow measurements

Measurement Science and Technology 19(2008)9, 094003

Boden, S.; Eckert, S.; Willers, B.; Gerbeth, G.
X-ray radioscopic visualization of the solutal convection during solidification of a Ga-30wt%In alloy

Metallurgical and Materials Transactions A 39A(2008), 613-623

Boden, S.; Hampel, U.; Bieberle, M.
Quantitative measurement of gas hold-up distribution in a stirred chemical reactor using X-ray cone-beam computed tomography

Chemical Engineering Journal 139(2008)2, 351-362

Boden, S.; Hampel, U.; Bieberle, M.; Weickert, G.
Three-dimensional analysis of macroporosity distributions in polyolefin particles using X-ray microtomography

Powder Technology 188(2008), 81-88

Bund, A.; Ispas, A.; Mutschke, G.
Magnetic field effects on electrochemical metal depositions

Science and Technology of Advanced Materials 9(2008), 024208

Cierpka, C.; Weier, T.; Gerbeth, G.
Evolution of vortex structures in an electromagnetically excited separated flow

Experiments in Fluids 45(2008), 943-953

Cramer, A.; Gerbeth, G.
Melt extraction of short metallic filaments: fibre formation process revisited

Journal of Materials Processing Technology 204(2008), 103-110

Cramer, A.; Pal, J.; Gerbeth, G.
Electromagnetic stirring with superimposed travelling and rotating magnetic fields

Electrical Review (2008)11, 144-148

Da Silva, M. J.; Lu, Y.; Sühnel, T.; Schleicher, E.; Thiele, S.; Kernchen, R.; Diele, K.-H.; Hampel, U.

Autonomous planar conductivity array sensor for fast liquid distribution imaging in a fluid coupling

Sensors and Actuators A 147(2008)2, 508-515

Dagan, R.; Rohde, U.; Faber, W.
Sektionsberichte Jahrestagung Kerntechnik 2008 - Teil 1

atw - International Journal for Nuclear Power 53(2008)8/9, 556-567

Deendarlianto,.; Vallee, C.; Lucas, D.; Beyer, M.; Pietruske, H.; Carl, H.
Experimental study on the air/water counter-current flow limitation in a model of the hot leg of a pressurised water reactor

Nuclear Engineering and Design 238(2008)12, 3389-3402

Dorao, C. A.; Lucas, D.; Jakobsen, H. A.
Prediction of the evolution of the dispersed phase in bubbly flow problems

Applied Mathematical Modelling 32(2008), 1813-1833

Drews, A.; Beyer, H.-G.; Rindelhardt, U.

Quality of performance assessment of PV plants based on irradiance maps

Solar Energy 82(2008), 1067-1075

Fischer, F.; Hoppe, D.; Schleicher, E.; Mattausch, G.; Flaske, H.; Bartel, R.; Hampel, U.

An ultra fast electron beam x-ray tomography scanner

Measurement Science and Technology 19(2008), 094002

Fischer, M.; Stefani, F.; Gerbeth, G.

Coexisting stochastic and coherence resonance in a mean-field dynamo model for Earth's magnetic field reversals

European Physical Journal B 65(2008), 547-554

Forbriger, J.; Galindo, V.; Gerbeth, G.; Stefani, F.

Measurement of the spatio-temporal distribution of harmonic and transient eddy currents in a liquid metal

Measurement Science and Technology 19(2008)4, 045704

Frank, T.; Zwart, P.; Krepper, E.; Prasser, H.-M.; Lucas, D.

Validation of CFD models for mono- and polydisperse air-water two-phase flows in pipes

Nuclear Engineering and Design 238(2008), 647-659

Gailitis, A.; Gerbeth, G.; Gundrum, T.; Lielausis, O.; Platacis, E.; Stefani, F.

History and results of the Riga dynamo experiments

Comptes Rendus Physique 9(2008), 721-728

Giesecke, A.; Stefani, F.; Gerbeth, G.

Kinematic simulation of dynamo action with a hybrid boundary-element/finite-volume method.

Magnetohydrodynamics 44(2008)3, 237-252

Gokhman, A.; Bergner, F.; Ulbricht, A.; Birkenheuer, U.

Cluster dynamics simulation of reactor pressure vessel steels under irradiation

Defect and Diffusion Forum 277(2008), 75-80

Graefe, E.-M.; Günther, U.; Korsch, H.-J.; Niederle, A.

A non-Hermitian PT-symmetric Bose-Hubbard model: eigenvalue rings from unfolding higher-order exceptional points

Journal of Physics A 41(2008), 255206

Grahn, A.; Krepper, E.; Alt, S.; Kästner, W.

Implementation of a strainer model for calculating the pressure drop across beds of compressible, fibrous materials

Nuclear Engineering and Design 238(2008), 2546-2553

Grants, I.; Gerbeth, G.

Use of a traveling magnetic field in VGF growth: flow reversal and resulting dopant distribution

Journal of Crystal Growth 310(2008), 3699-3705

Grants, I.; Zhang, C.; Eckert, S.; Gerbeth, G.

Experimental observation of swirl accumulation in a magnetically driven flow
Journal of Fluid Mechanics 616(2008), 135-152

Günther, U.; Kirillov, O.

Homotopic Arnold tongues deformation of the MHD α^2 -dynamo
Proceedings in Applied Mathematics and Mechanics 8(2008), 10719-10720

Günther, U.; Samsonov, B.

PT-symmetric brachistochrone problem, Lorentz boosts and nonunitary operator equivalence classes
Physical Review A 78(2008), 042115

Günther, U.; Samsonov, B.

The Naimark dilated PT-symmetric brachistochrone
Physical Review Letters 101(2008), 230404

Hampel, U.; Hoppe, D.; Bieberle, A.; Kernchen, R.; Diele, K.-H.; Schleicher, E.; Da Silva, M. J.; Zippe, C.

Measurement of fluid distributions in a rotating fluid coupling using high resolution gamma ray tomography
Journal of Fluids Engineering - Transactions of the ASME 130(2008)9, 091402

Höhne, T.; Kliem, S.; Rohde, U.; Weiss, F.-P.

Boron dilution transients during natural circulation flow in PWR – experiments and CFD simulations
Nuclear Engineering and Design 238(2008), 1987-1995

Hoppe, D.

Streustrahlungskorrektur bei Gammatomographie auf der Grundlage einer Faltungsoption
Technisches Messen (2008)6, 413

Hristov, H. V.; Boden, S.; Hampel, U.; Kryk, H.; Hessel, G.; Schmitt, W.

A study on the two-phase flow in a stirred tank reactor agitated by a gas inducing turbine
Chemical Engineering Research and Design 86(2008)1, 75-81

Kiessling, N.; Bieberle, A.; Hampel, U.

Analysis of scattered radiation cross-talk in a high-resolution gamma ray tomography detector with GATE Monte-Carlo simulation
Nuclear Instruments and Methods in Physics Research A 595(2008)2, 375-380

Klaiman, S.; Günther, U.; Moiseyev, N.

Visualization of branch points in PT-symmetric waveguides
Physical Review Letters 101(2008), 080402

Kliem, S.; Prasser, H.-M.; Sühnel, T.; Weiss, F.-P.; Hansen, A.
Experimental determination of the boron concentration distribution in the primary circuit of a PWR after a postulated cold leg small break loss-of-coolant-accident with cold leg safety injection
Nuclear Engineering and Design 238(2008)7, 1788-1801

Kliem, S.; Sühnel, T.; Rohde, U.; Höhne, T.; Prasser, H.-M.; Weiß, F.-P.
Experiments at the mixing test facility ROCOM for benchmarking of CFD-codes
Nuclear Engineering and Design 238(2008), 566-576

Koncar, B.; Krepper, E.
CFD simulation of convective flow boiling of refrigerant in a vertical annulus
Nuclear Engineering and Design 238(2008), 693-706

Koundy, V.; Fichot, F.; Willschuetz, H.-G.; Altstadt, E.; Nicolas, L.; Lamy, J.-S.; Flandi, L.
Progress on PWR lower head failure predictive models
Nuclear Engineering and Design 238(2008), 2420-2429

Krepel, J.; Grundmann, U.; Rohde, U.; Weiss, F.-P.
Dynamics of Molten Salt Reactors
Nuclear Technology 164(2008), 34-44

Krepper, E.; Cartland-Glover, G.; Grahn, A.; Weiss, F.-P.; Alt, S.; Hampel, R.; Kästner, W.; Kratzsch, A.; Seeliger, A.
Numerical and experimental investigations for insulation particle transport phenomena in water flow
Annals of Nuclear Energy 35(2008), 1564-1579

Krepper, E.; Cartland-Glover, G.; Grahn, A.; Weiss, F.-P.; Alt, S.; Hampel, R.; Kästner, W.; Seeliger, A.
CFD-modelling and experiments of insulation debris transport phenomena in water flow
Nuclear Technology 167(2008)1, 46-59

Krepper, E.; Lucas, D.; Frank, T.; Prasser, H.-M.; Zwart, P.
The inhomogeneous MUSIG model for the simulation of polydispersed flows
Nuclear Engineering and Design 238(2008), 1690-1702

Krepper, E.; Ruyer, P.; Beyer, M.; Lucas, D.; Prasser, H.-M.; Seiler, N.
CFD simulation of polydispersed bubbly two phase flow around an obstacle
Science and Technology of Nuclear Installations 2009(2008), 320738

Lantzsch, R.; Grants, I.; Pätzold, O.; Stelter, M.; Gerbeth, G.
Vertical gradient freeze growth with external magnetic fields
Journal of Crystal Growth 310(2008)7-9, 1518-1522

Lucas, D.; Bestion, D.; Bodèle, E.; Scheuerer, M.; D'Auria, F.; Mazzini, D.; Smith, B.; Tiselj, I.; Martin, A.; Lakehal, D.; Seynhaeve, J.-M.; Kyrki-Rajamäki, R.; Ilvonen, M.; Macek, J.; Coste, P.

An overview of the Pressurized Thermal Shock issue in the context of the NURESIM project

Science and Technology of Nuclear Installations 2009(2008), 583259

Merk, B.

An analytical solution for a one dimensional time dependent neutron transport problem with external source

Transport Theory and Statistical Physics 37(2008)5-7, 535-549

Merk, B.; Broeders, C. H. M.

Auswirkungen von verschiedenen Brennstoffzyklusoptionen auf die anfallenden Aktinidenmengen im deutschen Reaktorpark

atw - International Journal for Nuclear Power 53(2008)6, 404-412

Merk, B.; Koch, R.

On the influence of spatial discretization in cell- and lattice calculations with HELIOS 1.9

Annals of Nuclear Energy 35(2008), 1492-1501

Moretti, F.; Melideo, D.; D'Auria, F.; Höhne, T.; Kliem, S.

CFX simulations of ROCOM slug mixing experiments

Journal of Power and Energy Systems 2(2008)2, 720-733

Müller, G.; van Ouytsel, K.; Böhmert, J.; Dolbnya, I.; Bergner, F.

Investigation of the damage around a crack tip in metals using Small Angle X-ray Scattering

MP Materials Testing 50(2008)4, 191-198

Mutschke, G.; Bund, A.

On the three-dimensional character of the magnetohydrodynamic effect during metal electrodeposition in cuboid cells

Electrochemistry Communications 10(2008), 597-601

Mutschke, G.; Cierpka, C.; Weier, T.; Bund, A.; Eckert, K.; Mühlenhoff, S.; Yang, X. G.; Hess, A.

On three-dimensional magnetic field effects during metal deposition in cuboid cells

ECS Transactions 13(2008)16, 9-13

Neuhaus, T.; Schaffrath, A.; Ronneberger, R.; Altstadt, E.

Entwicklung und Validierung des Druckstoßprogramms DYVRO Mod. 3

atw - International Journal for Nuclear Power (2008)2

Nikrityuk, P. A.; Eckert, S.; Eckert, K.

Spin-up and spin-down dynamics driven by a single rotating magnetic field pulse

European Journal of Mechanics B - Fluids 27(2008), 177-201

Noack, B. R.; Schlegel, M.; Ahlborn, B.; Mutschke, G.; Morzynski, M.; Comte, P.; Tadmor, G.

A finite-time thermodynamics of unsteady fluid flows

Journal of Non-Equilibrium Thermodynamics 33(2008)2, 103-148

Omebere-Iyari, N. K.; Azzopardi, B. J.; Lucas, D.; Beyer, M.; Prasser, H.-M.

Gas/liquid flow in large risers

International Journal of Multiphase Flow 34(2008), 461-476

Paladino, D.; Huggenberger, M.; Schäfer, F.

Natural circulation characteristics at low pressure conditions - PANDA experiments and ATHLET simulations

Science and Technology of Nuclear Installations (2008), 874969

Plevachuk, Yu.; Sklyarchuk, V.; Eckert, S.; Gerbeth, G.

Some physical data of the near eutectic liquid lead-bismuth

Journal of Nuclear Materials 373(2008), 335-342

Plevachuk, Yu.; Sklyarchuk, V.; Eckert, S.; Gerbeth, G.

Measurement of the electrical conductivity of Pb-Bi alloys in the melting-solidification region

Journal of Nuclear Materials 376(2008), 363-365

Plevachuk, Yu.; Sklyarchuk, V.; Hermann, R.; Gerbeth, G.

Thermophysical properties of Nd-, Er-, YNi- alloys

International Journal of Materials Research 99(2008), 261-264

Plevachuk, Yu.; Sklyarchuk, V.; Yakymovych, A.; Eckert, S.; Willers, B.; Eigenfeld, K.

Density, viscosity and electrical conductivity of hypoeutectic Al-Cu liquid alloys

Metallurgical and Materials Transactions A 39(2008)12, 3040-3045

Plevachuk, Yu.; Sklyarchuk, V.; Yakymovych, A.; Gerbeth, G.; Eckert, S.

Microsegregation in liquid Pb-based eutectics

Journal of Non-Crystalline Solids 354(2008), 4443-4447

Prasser, H. M.

Novel experimental measuring techniques required to provide data for CFD validation

Nuclear Engineering and Design 238(2008), 744-770

Prasser, H.-M.; Beyer, M.; Al Issa, S.; Carl, H.; Pietruske, H.; Schütz, P.

Gas-liquid flow around an obstacle in a vertical pipe

Nuclear Engineering and Design 238 (7)(2008), 1802-1819

Rindelhardt, U.; Viehrig, H.-W.; Konheiser, J.; Noack, K.; Schuhknecht, J.; Gleisberg, B.

RPV material investigation of the former VVER-440 Greifswald NPP

Nuclear Engineering and Design (2008), doi:10.1016/j.nucengdes.2008.07.018

Roelofs, F.; Jager, B.; Class, A.; Jeanmart, H.; Schuurmans, P.; Ciampichetti, A.; Gerbeth, G.; Stieglitz, R.; Fazio, C.

European research on HLM thermal hydraulics for ADS applications

Journal of Nuclear Materials 376(2008), 401-404

Schaffrath, A.; Kliem, S.

Jahrestagung Kerntechnik 2008 - Sektionsbericht Sektion: Thermo- und Fluidodynamik

atw - International Journal for Nuclear Power 53(2008)8/9, 559-561

Schleicher, E.; Da Silva, M. J.; Hampel, U.

Enhanced local void and temperature measurements for highly transient two-phase flows

IEEE Transactions on Instrumentation and Measurement 57(2008)2, 401-405

Schleicher, E.; Hampel, U.; Da Silva, M. J.; Thiele, S.; Li, A.; Wollrab, E.

Design of an optical tomograph for the investigation of single and two phase pipe flows

Measurement Science and Technology 19(2008)9, 094006

Schmidtke, M.; Lucas, D.

CFD approaches for modeling bubble entrainment by an impinging jet

Science and Technology of Nuclear Installations 2009(2008), 148436

Schubert, M.; Hampel, U.; Hessel, G.; Lange, R.; Zippe, C.

Liquid flow texture analysis in trickle bed reactors using high resolution gamma ray tomography

Chemical Engineering Journal 140(2008)1-3, 332-340

Shatrov, V.; Gerbeth, G.; Hermann, R.

An alternating magnetic field driven flow in a spinning cylindrical container

Journal of Fluids Engineering - Transactions of the ASME 130(2008), 071201

Shatrov, V.; Gerbeth, G.; Hermann, R.

Linear stability of an alternating magnetic field driven flow in a spinning cylindrical container

Physical Review E 77(2008)4, 046307

Stefani, F.; Gailitis, A.; Gerbeth, G.

Magnetohydrodynamic experiments on cosmic magnetic fields

Zeitschrift für Angewandte Mathematik und Mechanik 88(2008)12, 930-954

Stefani, F.; Gerbeth, G.; Gundrum, T.; Hollerbach, R.; Rüdiger, G.; Szklarski, J.

Results of a modified PROMISE experiment

Astronomische Nachrichten 329(2008)7, 652-658

Szklarski, J.; Gerbeth, G.

Boundary layer in the MRI experiment PROMISE

Astronomische Nachrichten 329(2008)7, 667-674

Vallee, C.; Deendarlianto,.; Lucas, D.; Beyer, M.; Pietruske, H.; Carl, H.
Counter-current flow limitation experiments in a model of the hot leg of a pressurised water reactor

atw - International Journal for Nuclear Power 53(2008)8/9, 546-549

Vallee, C.; Höhne, T.; Prasser, H.-M.; Sühnel, T.
Experimental investigation and CFD simulation of horizontal stratified two-phase flow phenomena

Nuclear Engineering and Design 238(2008), 637-646

Wagner, E.; Rindelhardt, U.

Stromgewinnung aus regenerativer Wasserkraft - Potenzialanalyse

EW : Das Magazin für die Energiewirtschaft (2008)1-2, 78-81

Weier, T.; Cierpka, C.; Gerbeth, G.

Coherent structure eduction from PIV data of an electromagnetically forced separated flow

Journal of Fluids and Structure 24(2008), 1339-1348

Willers, B.; Eckert, S.; Nikrityuk, Petr A.; Rübiger, D.; Dong, J.; Eckert, K.; Gerbeth, G.

Efficient melt stirring using pulse sequences of a rotating magnetic field: II – Application during solidification of Al-Si alloys

Metallurgical and Materials Transactions B 39(2008)2, 304-316

Xu, M.; Stefani, F.; Gerbeth, G.

The integral equation approach to kinematic dynamo theory and its application to dynamo experiments in cylindrical geometry

Journal of Computational Physics 227(2008), 8130-8144

Conference contributions and other oral presentations

Abendroth, M.; Altstadt, E.

Fracture mechanical analysis of a VVER-440 PTS scenario

Jahrestagung Kerntechnik 2008, 27.-29.05.2008, Hamburg, Germany

Altstadt, E.

Materialforschung für sichere Kernkraftwerke

Werkstofftechnisches Kolloquium der Technischen Universität Darmstadt, 12.06.2008, Darmstadt, Deutschland

Azzopardi, B.; Hernandez Perez, V.; Kaji, R.; Da Silva, M. J.; Beyer, M.; Hampel, U.

Wire mesh sensor studies in a vertical pipe

Fifth International Conference on Transport Phenomena In Multiphase Systems, HEAT 2008, 30.06.-03.07.2008, Bialystok, Poland

Bartosiewicz, Y.; Seynhaeve, J.-M.; Vallee, C.; Höhne, T.; Laviéville, J.

Modelling free surface flows relevant to a PTS scenario: comparison between experimental data and three RANS based CFD-codes - Comments on the CFD-experiment integration and best practice guideline

XCFD4NRS - Experiments and CFD Code Applications to Nuclear Reactor Safety, 10.-12.09.2008, Grenoble, France

Bechta, S. V.; Granovsky, V. S.; Khabensky, V. B.; Krushinov, E. V.; Vitol, S. A.; Sulatsky, A. A.; Gusarov, V. V.; Almiashv, V. I.; Lopukh, D. B.; Bottomley, D.; Fischer, M.; Piluso, P.; Miassoedov, A.; Tromm, W.; Altstadt, E.; Fichot, F.; Kymalainen, O.

Interaction between molten corium UO_2+X - ZrO_2 - FeO_y and VVER vessel steel

2008 International Congress on Advances in Nuclear Power Plants (ICAPP '08), 08.06.-12.08.2008, Anaheim, California, United States

Bergner, F.; Ulbricht, A.; Hein, H.

Flux dependence of cluster formation in neutron irradiated weld material

14th Meeting of the International Group on Radiation Damage Mechanisms (IGRDM-14), 20.-25.04.2008, Pittsburgh, USA

Beyer, M.; Vallee, C.; Fischer, F.; Danciu, D.-V.; Schütz, P.; Pietruske, H.; Lucas, D.; Carl, H.

Stand der experimentellen Arbeiten im Rahmen des TOPFLOW-II Projekts

CFD im Containment / CFD für Zweiphasenströmungen (Meilstein-Workshop Sommer 2008), 16.07.2008, Stuttgart, Deutschland

Beyer, R.

Transmutation with fast neutrons

3rd FZD Graduate Students Seminar, 27.-29.08.2008, Limbach-Oberfrohna, Deutschland

Bieberle, A.; Hoppe, D.; Zippe, C.; Schleicher, E.; Tschofen, M.; Suehnel, T.; Zimmermann, W.; Hampel, U.

Void measurement in boiling water reactor rod bundles using high resolution gamma ray tomography

XCFD4NRS - Experiments and CFD Code Applications to Nuclear Reactor Safety, 10.-12.09.08, Grenoble, Frankreich

Bilodid, Y.; Mittag, S.

Spectral-history modeling in DYN3D burnup calculations

18th Symposium of AER on VVER Reactor Physics and Reactor Safety, 06.-10.10.2008, Eger, Hungary

Boden, S.; Eckert, S.; Willers, B.; Gerbeth, G.

Observation of melt flow effects on dendritic growth of Ga-In alloys by X-ray radioscopy

Second International Conference on Advances in Solidification Processes, 17.-20.06.2008, Leoben, Austria

Boden, S.; Willers, B.; Eckert, S.; Gerbeth, G.

Observation of melt flow effects and dendritic growth during directional solidification of Ga-In alloys by X-ray radioscopy

IEEE 2008 - Workshop on X-Ray Micro Imaging of Materials, Devices, and Organisms, 22.-24.10.2008, Dresden, Germany

Borodkin, G.; Khrennikov, N.; Konheiser, J.; Noack, K.

Neutron dosimetry study in the region of the support structure of a VVER-1000 type reactor

13th International Symposium on reactor Dosimetry, 25.-31.05.2008, Alkmaar, Netherlands

Borodkin, P.; Borodkin, G.; Khrennikov, N.; Konheiser, J.; Noack, K.

Neutron dosimetry on the full-core first generation VVER-440 aimed at reactor support structure load evaluation

13th International Symposium on Reactor Dosimetry, 25.-31.05.2008, Alkmaar, Netherlands

Cheung, C. P.; Yeoh, G. H.; Tu, J. Y.; Krepper, E.; Lucas, D.

Numerical study on population balance approaches in modeling of isothermal vertical bubbly flows

The 5th International Conference on Computational Fluid Dynamics, ICCFD5, 07.-11.07.2008, Seoul, Korea

Cierpka, C.; Weier, T.; Gerbeth, G.

Synchronized force and PIV measurements on an electromagnetically forced separated flow

ICTAM2008 - International Congress of Theoretical and Applied Mechanics, 24.-30.08.2008, Adelaide, Australia

Cierpka, C.; Weier, T.; Mutschke, G.; Eckert, K.; Uhlemann, M.; Bund, A.

Flow structure and concentration distribution measurements in seemingly parallel magnetic and electric fields

213th ECS Meeting, 18.-23.05.2008, Phoenix, USA

Cramer, A.; Pal, J.; Gerbeth, G.

Electromagnetic stirring with superimposed travelling and rotating magnetic fields.

XVI International Congress on Electricity applications in modern world - UIE'08, 19.-21.05.2008, Krakow, Poland

Da Silva, M. J.

Advanced measuring techniques for multiphase flow at Research Center Dresden-Rossendorf

Research Seminar, Engineering School of Sao Carlos, Department of Mechanical Engineering, Universidade de Sao Paulo, 08.10.2008, Sao Carlos, Brazil

Da Silva, M. J.; Hampel, U.

Neuartige Impedanzsensoren für die Visualisierung von Mehrphasenströmungen

XXII. Messtechnisches Symposium, 11.-13.09.2008, Dresden, Germany

Da Silva, M. J.; Schleicher, E.; Hampel, U.

Novel wire-mesh sensor modalities for the investigation of single phase and multiphase flows

Sensoren und Messsysteme 2008, 11.-12.03.2008, Ludwigsburg, Germany

Da Silva, M. J.; Thiele, S.; Höhne, T.; Vaibar, R.; Hampel, U.

Experimental studies and CFD calculations for buoyancy driven mixing phenomena

XCFD4NRS, Experiments and CFD Code Applications to Nuclear Reactor Safety, 10.-12.09.2008, Grenoble, France

Da Silva, M. J.; Thiele, S.; Schleicher, E.; Hampel, U.

Field-focusing imaging sensor for visualization of multiphase flows

EUROSENSORS XXII, 07.-10.09.2008, Dresden, Germany

Eckert, S.; Boden, S.; Rübiger, D.; Willers, B.

Magnetfeldkontrollierte Erstarrungsvorgänge in metallischen Legierungen

Seminar "Struktur und Eigenschaften kondensierter Materie", 20.05.2008, Chemnitz, Deutschland

Eckert, S.; Gerbeth, G.

Velocity measurements in liquid metal flows using the Ultrasonic Doppler Method: examples and perspectives

6th. International Symposium on Ultrasonic Doppler Methods for Fluid Mechanics and Fluid Engineering, 09.-11.09.2008, Praha, Czech Republic

Eckert, S.; Rübiger, D.; Willers, B.; Nikrityuk, P. A.; Eckert, K.

Use of time-modulated AC magnetic fields for melt flow control during unidirectional solidification

Second International Conference on Advances in Solidification Processes, 17.-20.06.2008, Leoben, Austria

Eckert, S.; Willers, B.; Rübiger, D.; Dong, J.; Nikrityuk, Petr A.; Eckert, K.

Solidification of aluminium alloys under the influence of modulated magnetic fields

11th International Conference on Aluminium Alloys, 22.-26.09.2008, Aachen, Germany

Fischer, F.; Hampel, U.

Ultra fast electron beam X-ray computed tomography for two-phase flow measurement
XCFD4NRS - Experiments and CFD Code Applications to Nuclear Reactor Safety,
12.09.2008, Grenoble, France

Fischer, M.; Gerbeth, G.; Stefani, F.

Constraining the geodynamo by sequences of field reversals
7th International PAMIR Conference on Fundamental and Applied MHD, 08.-12.09.2008,
Presqu'île de Giens, France

Forbriger, J.; Galindo, V.; Gerbeth, G.; Stefani, F.

Determination of harmonic and pulsed eddy current distributions in a liquid metal
7th International PAMIR Conference on Fundamental and Applied MHD, 08.-12.09.2008,
Presqu'île de Giens, France

Frank, T.; Lifante, C.; Krepper, E.

Practical calculation of bubble column flow with CFX-11
6th FZD & ANSYS Short Course and Workshop "Multiphase Flow - Simulation, Experiment
and Applications", 24.-26.06.2008, Dresden, Germany

Gerbeth, G.; Eckert, S.; Galindo, V.; Willers, B.; Hewelt, U.; Hornung, B.

Magnetic field control of the pouring process in aluminium investment casting
11th International Conference on Aluminium Alloys, 22.-26.09.2008, Aachen, Germany

Gerbeth, G.; Eckert, S.; Weiss, F.-P.

Some new results on liquid metal measuring techniques and instrumentation
THIRS Workshop, 14.-16.04.2008, Karlsruhe, Germany

Gerbeth, G.; Grants, I.; Zhang, C.; Eckert, S.

Melt flows in combined rotating and traveling magnetic fields
79th Annual Meeting of the International Association of Applied Mathematics and Mechanics
(GAMM2008), 02.-04.04.2008, Bremen, Germany

Gerbeth, G.; Shatrov, V.; Hermann, R.

Linear stability analysis of an alternating magnetic field driven flow in a spinning container
8th World Congress on Computational Mechanics (WCCM8), 01.-05.07.2008, Venice, Italy

Giesecke, A.; Stefani, F.; Gerbeth, G.

A hybrid finite volume - boundary element method (FV-BEM) for the numerical solution of the kinematic induction equation
MHD fundamentals, from liquid-metals to astrophysics, 14.-16.04.2008, Brussels, Belgium

Giesecke, A.; Stefani, F.; Gerbeth, G.

On the axisymmetric dominance of the magnetic field in the VKS dynamo experiment.
11th MHD days, 01.-03.12.2008, Ilmenau, Germany

Giesecke, A.; Stefani, F.; Gerbeth, G.

Magnetic field reversals in nature, experiments and simulations

ICTAM2008 - International Congress of Theoretical and Applied Mechanics, 25.-29.08.2008, Adelaide, Australia

Giesecke, A.; Stefani, F.; Gerbeth, G.

Kinematic dynamos in cylindrical geometry

EURO MHD 2008, 23.-26.09.2008, Nice, France

Giesecke, A.; Stefani, F.; Gerbeth, G.

A hybrid finite volume - boundary element method (FV-BEM) for the numerical solution of the kinematic induction equation.

8th. World Congress on Computational Mechanics (WCCM8) / 5th. European Congress on Computational Methods in Applied Sciences and Engineering (ECCOMAS 2008), 29.06.-04.07.2008, Venedig, Italy

Gokhman, A.; Bergner, F.; Birkenheuer, U.

Cluster dynamics study of the binary systems in neutron irradiated iron alloys

Workshop Nucleation Theory and Applications, 12.-20.04.2008, Dubna, Russia

Graefe, E.-M.; Günther, U.; Korsch, H.-J.; Niederle, A.

Unfolding of higher order exceptional points in a PT-symmetric Bose-Hubbard model

Quantum Physics with Non-Hermitian Operators (PHHQP VII), 29.06.-11.07.2008, Benasque, Spain

Graefe, E.-M.; Günther, U.; Niederle, A.; Korsch, H. J.

The spectrum of a non-Hermitian two-mode Bose-Hubbard system

DPG Frühjahrstagung, 10.-14.03.2008, Darmstadt, Germany

Grahn, A.; Krepper, E.; Alt, S.; Kästner, W.; Weiß, F.-P.; Hampel, R.

Implementation of a pressure drop model for the CFD simulation of clogged containment sump strainers

Jahrestagung Kerntechnik 2008, 27.-29.05.2008, Hamburg, Germany

Günther, U.; Graefe, E.-M.; Korsch, H.-J.; Niederle, A.; Rotter, I.; Samsonov, B.

Spectral singularities and self-orthogonality of eigenvectors

Experimental Realizations of Self-Orthogonality, 23.-28.03.2008, Haifa, Israel

Günther, U.; Graefe, E.-M.; Korsch, H.-J.; Niederle, A.; Samsonov, B.

Spectral singularities, brachistochrone dilation and the relevance of the Hessenberg type

Quantum Physics with Non-Hermitian Operators (PHHQP VII), 29.06.-11.07.2008, Benasque, Spain

Günther, U.; Kirillov, O.

Homotopic deformations of the Arnold tongue patterns in the MHD α^2 -dynamo spectrum

79th Annual Meeting of the International Association of Applied Mathematics and Mechanics (GAMM-2008), 31.03.-04.04.2008, Bremen, Germany

Günther, U.; Kirillov, O.; Graefe, E.-M.; Korsch, H.-J.; Niederle, A.
Two models of Krein-space related physics: the MHD α^2 -dynamo and the PT-symmetric Bose-Hubbard model
8th Workshop "Operator Theory in Krein Spaces and Inverse Problems", 18.-21.12.2008, Berlin, Deutschland

Hampel, U.
Measurement techniques and experimental investigations for multiphase flows
Multiphase Flows - Simulation, Experiment and Application, 24.-26.06.2008, Dresden, Germany

Hampel, U.
Advanced two-phase flow measurement techniques at Research Centre Dresden-Rossendorf - sensors, systems and applications
Meeting der Industrial Tomography Systems Ltd., 01.04.2008, Manchester, UK

Hampel, U.
Advanced two-phase flow measurement techniques at Research Centre Dresden-Rossendorf - sensors, systems and applications
Frontier Seminar at Institute of Particle Science and Engineering, Leeds University, 2.4.2008, Leeds, UK

Hampel, U.
Advanced two-phase flow measurement techniques at Research Centre Dresden-Rossendorf - sensors, systems and applications
Research Seminar, School of Chemical, Environmental and Mining Engineering, Nottingham University, 3.4.2008, Nottingham, UK

Hampel, U.
Advanced two-phase flow measurement techniques at Research Centre Dresden-Rossendorf - sensors, systems and applications
Research Seminar, Nuclear Physics Group, Positron Imaging Centre, Birmingham University, 4.3.2008, Birmingham, UK

Hampel, U.
Computed tomography methods in flow measurement
FZD Lectures, 07.07.2008, Dresden, Germany

Hampel, U.
Ultra fast electron beam X-ray tomography at FZD
Electron Beam Tomography Meeting at BUDKERS Institute Novosibirsk, 02.09.2008, Novosibirsk, Russia

Hampel, U.; Bieberle, A.; Schleicher, E.; Hoppe, D.; Zippe, C.
High resolution gamma ray tomography and its application to multiphase flow measurement
CT2008: TOMOGRAPHY CONFLUENCE - An International Conference on the Applications of Computerized Tomography, 15.-17.02.2008, Kanpur, India

Hampel, U.; Fischer, F.

Application of CdTe and CZT detectors in ultra fast electron beam X-ray tomography
2008 Nuclear Science Symposium, Medical Imaging Conference and 16th Room Temperature Semiconductor Detector Workshop, 19.-25.10.2008, Dresden, Germany

Hampel, U.; Fischer, F.

Ultra fast electron beam x-ray tomography and its application to multi phase flow measurement

IEEE Dresden 2008 - Workshop on X-Ray Micro Imaging of Materials, Devices, and Organisms, 22.-24.10.2008, Dresden, Germany

Hampel, U.; Fischer, F.; Bergmann, R.

Electron beam CT – a potential tool for small animal imaging ?

2008 Nuclear Science Symposium, Medical Imaging Conference and 16th Room Temperature Semiconductor Detector Workshop, 19.-25.10.2008, Dresden, Germany

Hampel, U.; Fischer, F.; Bieberle, M.; Schleicher, E.

Recent progress in ultra fast electron beam X-ray computed tomography

5th International Symposium on Process Tomography, 25.-26.08.2008, Zakopane, Poland

Hampel, U.; Fischer, F.; Schleicher, E.; Hoppe, D.

Ultra fast scanned electron beam X-ray CT for two-phase flow measurement

CT2008: TOMOGRAPHY CONFLUENCE - An International Conference on the Applications of Computerized Tomography, 15.-17.02.2008, Kanpur, India

Hampel, U.; Kiessling, N.; Bieberle, A.

Application of GATE to detector optimisation in transmission gamma ray tomography

2008 Nuclear Science Symposium, Medical Imaging Conference and 16th Room Temperature Semiconductor Detector Workshop, 19.-25.10.2008, Dresden, Germany

Hernández Mayoral, M.; Bergner, F.; Almazouzi, A.; Lambrecht, M.

TEM, SANS and PAS applied to neutron-irradiated pure Fe

14th Meeting of the International Group on Radiation Damage Mechanisms (IGRDM-14), 20.-25.04.2008, Pittsburgh, United States

Höhne, T.

CFD calculation of new TOPFLOW hot leg experiments

13th Meeting, 23.-24.01.2008, Großhartpenning, Deutschland

Höhne, T.

Multiphase flows in industrial applications - experiments and CFD simulations

CFD OIL2008 - 3d Encontro Latino-Americano de CFD Aplicado à Indústria de Petróleo, 18.-19.08.2008, Rio de Janeiro, Brasil

Höhne, T.

Simulation von Experimenten am Heißstrangmodell der TOPFLOW-Anlage

Workshop Strömungssimulation, 25.09.2008, Dresden-Rossendorf, Germany

Höhne, T.; Kliem, S.; Vaibar, R.

Experimental and numerical modeling of transition matrix from momentum to buoyancy-driven flow in a pressurized water reactor

16th International Conference on Nuclear Engineering ICONE16, 11.-15.05.2008, Orlando, USA

Höhne, T.; Krepper, E.; Vallee, C.

Validation of CFD Codes and Applications in Nuclear Industry

16th International Conference on Nuclear Engineering ICONE16, 11.-15.05.2008, Orlando, USA

Höhne, T.; Moncalvo, D.

Nachrechnung von experimentell bestimmten Leistungsparametern eines Vollhub-Feder-Sicherheitsventils mit ANSYS CFX

Jahrestreffen der ProcessNet-Fachausschüsse Computational Fluid Dynamics, Gasreinigung, Mechanische Flüssigkeitsabtrennung und Grenzflächenbestimmte Systeme und Prozesse, 18.-20.02.2008, Wiesbaden, Germany

Höhne, T.; Moncalvo, D.

Analysis of safety valve characteristics using measurements and CFD simulations

Jahrestagung Kerntechnik 2008, 27.-29.05.2008, Hamburg, Germany

Höhne, T.; Moncalvo, D.; Friedel, L.; Jörgensen, B.

Nachrechnung eines Vollhub-Feder-Sicherheitsventils mit ANSYS CFX

9. Fachtagung "Anlagen-, Arbeits- und Umweltsicherheit", 06.-07.11.2008, Köthen, Deutschland

Höhne, T.; Rohde, U.; Melideo, D.; Moretti, F.; D'Auria, F.; Shishov, A.; Lisenkov, E.

CFD simulations of Hidropress mixing facility experiments in the framework of TACIS project R2.02/02

TOPSAFE 2008, 01.-03.10.2008, Dubrovnik, Croatia

Höhne, T.; Vallee, C.

Numerical prediction of horizontal stratified flows

6th International Conference on COMPUTATIONAL FLUID DYNAMICS in the Oil & Gas, Metallurgical and Process Industries, 10.-12.06.2008, Trondheim, Norway

Höhne, T.; Vallée, C.; Beyer, M.

CFD post test calculation of pressurized air / water TOPFLOW hotleg experiments

6th Workshop Multiphase Flows Simulation, Experiment and Application, 24.-26.06.2008, Dresden, Deutschland

Hollerbach, R.; Stefani, F.; Gerbeth, G.; Gundrum, T.; Rüdiger, G.

The helical magnetorotational instability in cylindrical Taylor-Couette flow

XXII International Congress of Theoretical and Applied Mechanics, 24.-29.08.2008, Adelaide, Australia

Journeau, C.; Bonnet, J. M.; Godin-Jacqmin, L.; Piluso, P.; Tarabelli, D.; Altstadt, E.; et al.
European Research on the Corium issues within the SARNET Network of Excellence
2008 International Congress on Advances in Nuclear Power Plants (ICAPP'08), 08.-12.06.2008, Anaheim, California, United States

Kirillov, O.; Günther, U.; Stefani, F.
Determining role of Krein signature for 3D Arnold tongues of oscillatory dynamos
8th Workshop "Operator Theory in Krein Spaces and Inverse Problems", 18.-21.12.2008, Berlin, Deutschland

Kliem, S.
Second dynamic AER benchmark – new results
Annual Meeting of the AER Working Group D, 31.03.-01.04.2008, Garching, Germany

Kliem, S.
A PWR boron dilution benchmark
Annual Meeting of the AER Working Group D, 31.03.-01.04.2008, Garching, Germany

Kliem, S.
AER working group D on VVER safety analysis – report of the 2008 meeting
18th Symposium of AER on VVER Reactor Physics and Reactor Safety, 06.-10.10.2008, Eger, Hungary

Kliem, S.; Höhne, T.; Rohde, U.; Weiß, F.-P.
Experiments on slug mixing under natural circulation conditions at the ROCOM test facility using high resolution measurement technique and numerical modeling
XCFD4NRS - Experiments and CFD Codes Application to Nuclear Reactor Safety, 10.-12.09.2008, Grenoble, France

Kliem, S.; Kozmenkov, Y.; Höhne, T.; Rohde, U.; Weiß, F.-P.
VVER-1000 main steam line break analysis using the coupled code system DYN3D/ATHLET
International Conference on the Physics of Reactors (PHYSOR'08), 14.-19.09.2008, Interlaken, Switzerland

Kliem, S.; Mittag, S.; Rohde, U.; Grundmann, U.; Weiß, F.-P.
Simulation von ATWS-Transienten in Druckwasserreaktoren
Jahrestagung Kerntechnik 2008, 27.-29.05.2008, Hamburg, Germany

Kliem, S.; Rohde, U.; Weiss, F.-P.
Simulation of postulated accidents in pressurized water reactors using coupled 3D neutron kinetic/thermal hydraulic code systems
IEEE Dresden 2008, 19.-25.10.2008, Dresden, Germany

Kolesnichenko, I.; Khripchenko, S.; Buchenau, D.; Gerbeth, G.
Nonstationary electrovortex flows in a long shallow channel with conducting fluid
7th International PAMIR Conference on Fundamental and Applied MHD, 08.-12.09.2008, Presqu'île de Giens, France

Kolev, N.; Donovan, J.; Spasov, I.; Royer, E.; Höhne, T.

Summary of the OECD VVER-1000 MSLB benchmark results

Annual Meeting of the AER Working Group D, 31.03.-01.04.2008, Garching, Germany

Konheiser, J.; Mittag, S.; Noack, K.; Rindelhardt, U.; Borodkin, G.; Borodkin, P.; Gleisberg, B.

Retrospective dosimetry study at the RPV of NPP Greifswald unit 1

13th International Symposium on reactor Dosimetry, 25.-31.05.2008, Alkmaar, Netherlands

Konheiser, J.; Noack, K.; Mittag, S.; Rindelhardt, U.; Borodkin, G.; Borodkin, P.; Gleisberg, B.

Efforts to verify neutron fluence calculations at pressure vessels of decommissioned reactors by means of retrospective niobium dosimetry

8.AAA Meeting Garching(München), 08.12.2008, München, Germany

Krepper, E.

Numerical and experimental investigation of temperature stratification phenomena during heating up processes of fluids in large pools

International Workshop on Thermal-Hydraulics of Innovative Reactor and Transmutation Systems – THIRS, 14.04.08, Karlsruhe, Germany

Krepper, E.; Beyer, M.

Experimental and numerical investigation of temperature stratification phenomena during heating-up processes of fluids in passive cooling systems

Multiphase Flow: Simulation, Experiment and Application, 24.-26.06.08, Dresden, Germany

Krepper, E.; Cartland-Glover, G.; Grahn, A.; Alt, S.; Hampel, R.; Kästner, W.; Seeliger, A.
Experimental investigation and CFD simulation of insulation debris transport phenomena in water flow

Multiphase Flow: Simulation, Experiment and Application, 24.-26.06.08, Dresden, Germany

Krepper, E.; Cartland-Glover, G.; Grahn, A.; Weiss, F.-P.; Alt, S.; Hampel, R.; Kästner, W.; Seeliger, A.

Experimental investigation and CFD simulation of the behaviour of mineral wool in the reactor sump

16th International Conference on Nuclear Engineering, ICONE-16, 11.-15.05.2008, Orlando, Florida, USA

Krepper, E.; Cartland-Glover, G.; Grahn, A.; Weiss, F.-P.; Alt, S.; Hampel, R.; Kästner, W.; Seeliger, A.

Experiments and CFD-modelling of insulation debris transport phenomena in water flow

XCFD4RS Experiments and CFD Codes Application to Nuclear Reactor Safety, 10.-12.09.2008, Grenoble, France

Krepper, E.; Frank, T.; Lucas, D.; Prasser, H.-M.; Zwart, P.

A population balance approach for polydispersed bubbly flows considering size dependent bubble forces

6th International Conference on COMPUTATIONAL FLUID DYNAMICS in the Oil & Gas, Metallurgical and Process Industries, 10.-12.06.2008, Trondheim, Norway

Krepper, E.; Scheuerer, G.

Interfacial heat and mass transfer models

6th FZD & ANSYS Short Course and Workshop "Multiphase Flow - Simulation, Experiment and Applications", 24.-26.06.2008, Dresden, Germany

Kryk, H.

Forschung und Entwicklung für die Verfahrenstechnik

Hochschul-Informationstag, 10.01.2008, Freiberg, Deutschland

Kryk, H.; Hessel, G.

Balance-based real-time monitoring – a tool to improve safety and efficiency of batch and semi-batch processes

9th International Conference and Exhibition on The Scale-Up of Chemical Processes, 15.-17.09.2008, Rome, Italy

Kryk, H.; Hessel, G.

Sicherheitsorientierte Regelungsstrategien für Batch- und Semibatch-Prozesse in der Feinchemie

ProcessNet-Arbeitsausschuss "Sicherheitsgerechtes Auslegen von Chemieanlagen", 19.-20.11.2008, Frankfurt a.M., Deutschland

Kuzhel, S.; Günther, U.; Albeverio, S.

J-self-adjoint operators with C-symmetries: extension theory approach

8th Workshop "Operator Theory in Krein Spaces and Inverse Problems", 18.-21.12.2008, Berlin, Deutschland

Lenk, S.; Carl, H.; Beyer, M.

Prozessautomatisierung des Versuchsstandes TOPFLOW des Forschungszentrums Dresden Rossendorf

Frühjahrstagung der Studiengruppe für Elektronische Instrumentierung, 07.-09.04.2008, Karlsruhe, Deutschland

Lucas, D.

Experimente zu Zweiphasenströmungen an der Versuchsanlage TOPFLOW

Seminar für Energieverfahrenstechnik, 15.01.2008, Dresden, Germany

Lucas, D.

Qualification of simulation tools for two-phase flows

Frédéric Joliot/Otto Hahn Summer School on Nuclear Reactors: "Physics, Fuels, and Systems", 20.-29.08.2008, Aix-en-Provence, France

Lucas, D.

Die experimentellen Versuchsanlagen des Instituts für Sicherheitsforschung

3. Workshop "Strömungssimulation" der Technischen Universität Dresden und des Forschungszentrums Dresden-Rossendorf, 25.09.2008, Dresden, Deutschland

Lucas, D.

Pressurized Thermal Shock (PTS) in the European project NURESIM

14th Meeting of the German CFD Network, 17.07.2008, Stuttgart, Deutschland

Lucas, D.; Beyer, M.; Kussin, J.

A new high-quality database for air-water flow in a DN200 vertical duct

Meeting of the German CFD Network for Nuclear Reactor Safety, 23.-24.01.2008, Grosshartenpenning, Deutschland

Lucas, D.; Beyer, M.; Kussin, J.; Schütz, P.

Benchmark database on the evolution of two-phase flows in a vertical pipe

XCFD4NRS, Experiments and CFD Code Applications to Nuclear Reactor Safety, 10.-12.09.2008, Grenoble, France

Lucas, D.; Beyer, M.; Kussin, J.; Schütz, P.

A new database on upwards air-water flow in a large pipe

46th European Two-Phase Flow Group Meeting, 28.-30.05.2008, Pisa, Italy

Lucas, D.; Beyer, M.; Vallee, C.; Krepper, E.; Höhne, T.; Al Issa, S.; Liao, Y.

Entwicklung und Validierung von Modellen für Zweiphasenströmungen

Meilenstein-Workshop zu vom BMWi geförderten Projekten der Reaktorsicherheitsforschung, 16.07.2008, Stuttgart, Deutschland

Merk, B.

Vergleich von Abbrandrechnungen mit HELIOS 1.9 und KAPROS/KARBUS mit zeitlich veränderlicher Leistung

Jahrestagung Kerntechnik 2008, 27.-29.05.2008, Hamburg, Germany

Merk, B.

A time dependent analytical approximation solution for a pulsed source problem: P1 transport versus diffusion

2008 Nuclear Science Symposium, Medical Imaging Conference and 16th Room Temperature Semiconductor Detector Workshop, 19.-25.10.2008, Dresden, Deutschland

Merk, B.

On the effect of spatial discretization in LWR calculations with HELIOS 1.9

Studsvik User Group Meeting 2008, 09.-11.04.2008, Budapest, Hungary

Merk, B.; Koch, R.

Spatial discretization in LWR cell calculations with HELIOS 1.9: influence on kinf and flux distribution

ENS TOPSAFE 2008, 01.-03.10.2008, Dubrovnik, Croatia

Merk, B.; Koch, R.

On the influence of spatial discretization on cross section preparation with HELIOS 1.9

Jahrestagung Kerntechnik 2008, 27.-29.05.2008, Hamburg, Germany

Merk, B.; Koch, R.

The effect of spatial discretization in LWR cell calculations with HELIOS 1.9

18th Symposium of AER on VVER Reactor Physics and Reactor Safety, 06.-10.10.2008, Eger, Hungary

Miao, X.; Galindo, V.; Gerbeth, G.; Ren, Z.

Numerical study of the turbulent two-phase flow in a steel mould

8th. World Congress on Computational Mechanics (WCCM8) / 5th. European Congress on Computational Methods in Applied Sciences and Engineering (ECCOMAS 2008), 30.06.-04.07.2008, Venice, Italy

Mutschke, G.; Cierpka, C.; Weier, T.; Bund, A.; Eckert, K.; Mühlhoff, S.; Yang, X. G.; Hess, A.

On three-dimensional magnetic field effects during metal deposition in cuboid cells

213th ECS Meeting, 18.-22.05.2008, Phoenix, Arizona, United States

Mutschke, G.; Cierpka, C.; Weier, T.; Eckert, K.; Mühlhoff, S.; Bund, A.

3-D magnetic field effects during metal electrodeposition In cuboid cells

7th PAMIR International Conference on Fundamental and Applied MHD, 08.-12.09.2008, Presqu'île de Giens, Frankreich

Neuhaus, T.; Schaffrath, A.; Ronneberger, R.; Altstadt, E.

Entwicklung und Validierung des Druckstoßprogramms DYVPRO Mod. 3

Jahrestagung Kerntechnik 2008, 27.-29.05.2008, Hamburg, Germany

Nikrityuk, P. A.; Eckert, K.; Eckert, S.

The impact of turbulent flow on the solidification of metal alloys driven by a rotating magnetic field

2nd International Conference on Advances in Solidification Processes, 17.-22.06.2008, Leoben, Austria

Noack, B. R.; Schlegel, M.; Pastoor, M.; Luchtenburg, M.; Mutschke, G.; Morzynski, M.; Comte, P.; Tadmor, G.; Ahlborn, B.

Shear flow compositions on the Galerkin piano: A unified theory for instabilities, strange attractors, statistical mechanics and attractor control

Workshop Industrial applications of low-order models based on proper orthogonal decomposition, 31.03.-02.04.2008, Bordeaux, France

Otahal, J.; Boden, S.; Schleicher, E.; Beyer, M.; Jicha, M.; Hampel, U.

Wire-mesh and X-ray microtomography studies of flow patterns in the mixing chamber of an effervescent atomizer

5th International Symposium on Process Tomography, 25.-26.08.2008, Zakopane, Poland

Pätzold, O.; Lantsch, R.; Grants, I.; Gerbeth, G.; Stelter, M.

VGF-Kristallzüchtung mit kombinierten AC/DC-Magnetfeldern

DGKK-Workshop „Herstellung und Charakterisierung von massiven Verbindungshalbleitern“, 09.-10.10.2008, Erlangen, Germany

Pätzold, O.; Lantsch, R.; Grants, I.; Stelter, M.; Gerbeth, G.

Vertical Gradient Freeze growth in a combined magnetic AC/DC field

7th International PAMIR Conference on Fundamental and Applied MHD, 08.-12.09.2008, Presqu'île de Giens, France

Priede, J.; Gerbeth, G.

Helical magnetorotational instability in a Taylor-Couette flow

7th International PAMIR Conference on Fundamental and Applied MHD, 08.-12.09.2008, Presqu'île de Giens, France

Priede, J.; Grants, I.; Gerbeth, G.

Tridiagonal factorization algorithm for Chebyshev-tau method with an exponential coordinate mapping

8th World Congress on Computational Mechanics (WCCM8), 01.-05.07.2008, Venice, Italy

Räbiger, D.; Eckert, S.; Gerbeth, G.

Measurements of transient flow fields driven by a discontinuously applied rotating magnetic field

GAMM 2008, 31.03.-04.04.2008, Bremen, Germany

Räbiger, D.; Eckert, S.; Gerbeth, G.

Application of the Ultrasound Doppler method for velocity measurements in an electromagnetically-stirred liquid metal

6th International Symposium on Ultrasonic Doppler Methods for Fluid Mechanics and Fluid Engineering, 09.-11.09.2008, Praha, Czech Republic

Rindelhardt, U.

Perspektiven der Kernenergie - Herausforderungen und Möglichkeiten

VDE-Bezirksverein Chemnitz, 17.01.2008, Zwickau, Germany

Rindelhardt, U.

Betriebserfahrungen mit PV-Megawattanlagen in Mitteldeutschland

Institutseminar Institut für Solarenergieforschung, 26.02.2008, Hameln-Emmerthal, Germany

Rindelhardt, U.

Kernenergie im 21. Jahrhundert

Seniorenkolleg TU Chemnitz, 27.05.2008, Chemnitz, Deutschland

Rindelhardt, U.; Dietrich, A.; Kedziora, K.; Hahn, A.

Megawatt PV plants in Germany: A south-north performance comparison

23rd European Photovoltaic Solar Energy Conference and Exhibition, 01.-05.09.2008, Valencia, Spain

Rindelhardt, U.; Viehrig, H.-W.; Konheiser, J.; Schuhknecht, J.

Weld material investigations of a VVER-440 reactor pressure vessel: results from the first trepan taken from the former Greifswald NPP

16th International Conference on Nuclear Engineering, ICONE-16, 11.-15.05.2008, Orlando, USA

Rindelhardt, U.; Viehrig, H.-W.; Schuhknecht, J.; Konheiser, J.

RPV weld material investigations of a VVER-440 NPP

10th International Conference "Material Issues in Design, Manufacturing and Operation of Nuclear Power Plants Equipment", 06.-10.10.2008, St. Petersburg, Russia

Rohde, U.; Höhne, T.; Krepper, E.; Kliem, S.

Application of CFD codes in nuclear reactor safety analysis

TOPSAFE 2008, 01.-03.10.2008, Dubrovnik, Croatia

Samsonov, B.; Günther, U.

Generalized measurements and non-Hermitian quantum mechanics

Quantum Physics with Non-Hermitian Operators (PHQP VII), 29.06.-11.07.2008, Benasque, Spain

Schleicher, E.; Da Silva, M. J.; Fischer, F.; Bieberle, A.; Bieberle, M.; Hampel, U.

Messtechnik für Mehrphasenströmungen - Sensoren, Systeme und Anwendungen

Institutskolloquium, 25.11.2008, Dresden, Deutschland

Schmidtke, M.; Bothe, D.

VOF-Simulation des freien Aufstiegs von Öltröpfen in Wasser

"Mehrphasenströmungen", Jahrestagung des ProcessNet Fachausschusses, 10.-14.03.2008, Weihenstephan / Freising, Deutschland

Shatrov, V.; Gerbeth, G.

The flow around an electromagnetically self-propelled sphere

8th World Congress on Computational Mechanics (WCCM8), 01.-05.07.2008, Venice, Italy

Shatrov, V.; Gerbeth, G.

On the efficiency of MHD drag reduction

European Drag Reduction and Flow Control Meeting, 08.-11.09.2008, Ostritz, Germany

Shatrov, V.; Gerbeth, G.; Hermann, R.

An alternating magnetic field driven flow in a spinning cylindrical container and its three-dimensional linear stability analysis

7th International PAMIR Conference on Fundamental and Applied MHD, 08.-12.09.2008, Presqu'île de Giens, France

Stefani, F.

Magnetohydrodynamic experiments on cosmic magnetic fields

79th Annual Meeting of the International Association of Applied Mathematics and Mechanics (GAMM 2008), 31.03.-04.04.2008, Bremen, Germany

Stefani, F.

Dynamo action and magnetorotational instability: cosmic magnetism in the liquid metal lab

MHD fundamentals, from liquid-metals to astrophysics, 14.-16.04.2008, Bruxelles, Belgium

Stefani, F.

Von PROMISE 1 zu PROMISE 2: Helikale MRI im Laborexperiment

Kolloquium "10000 MHD-Tage in Potsdam", 01.09.2008, Potsdam, Germany

Stefani, F.; Gerbeth, G.; Gundrum, T.; Szklarski, J.; Rüdiger, G.; Hollerbach, R.

Liquid metal experiments on the helical magnetorotational instability

7th International PAMIR Conference on Fundamental and Applied MHD, 08.-12.09.2008, Presqu'île de Giens, France

Stefani, F.; Gerbeth, G.; Gundrum, T.; Szklarski, J.; Rüdiger, G.; Hollerbach, R.
An improved experiment for the investigation of the helical magnetorotational instability

11th MHD days, 01.-03.12.2008, Ilmenau, Germany

Tusheva, P.; Reinke, N.; Hurtado, A.; Schäfer, F.

Severe accident analysis for VVER-1000/V-320 for a station blackout accident scenario with ASTEC V1.3.0

Jahrestagung Kerntechnik 2008, 27.-29.05.2008, Hamburg, Germany

Vallee, C.; Deendarlianto,.; Beyer, M.; Lucas, D.; Carl, H.

Air/water counter-current flow experiments in a model of the hot leg of a pressurised water reactor

ICONE 16 - International Conference on Nuclear Engineering, 11.-15.05.2008, Orlando, Florida, USA

Vallee, C.; Deendarlianto,.; Lucas, D.; Beyer, M.; Pietruske, H.; Carl, H.

Counter-current flow limitation experiments in a model of the hot leg of a pressurised water reactor

Jahrestagung Kerntechnik 2008, 27.-29.05.2008, Hamburg, Deutschland

Viehrig, H.-W.; Schuhknecht, J.

Fracture mechanics characterisation of the WWER-440 reactor pressure vessel beltline welding seam of Greifswald Unit 8

34th MPA-Seminar and VGB-Symposium "Materials and Components Behaviour in Energy & Plant Technology", 09.-10.10.2008, Stuttgart, Deutschland

Viehrig, H.-W.; Schuhknecht, J.; Rindelhardt, U.; Weiss, F.-P.

Investigation of the beltline welding seam of the Greifswald WWER-440 unit 1 reactor pressure vessel

24th Symposium on Effects of Radiation on Nuclear Materials and the Nuclear Fuel Cycle, 24.-26.06.2008, Denver, United States

Viehrig, H.-W.; Zurbuchen, C.

Master Curve testing of highly irradiated IAEA RPV steels JRQ and JFL

Workshop on Trend Curve Development for Surveillance Data with Insight on Flux Effects at High Fluence: Damage Mechanisms and Modelling, 19.-21.11.2008, Mol, Belgium

Wagner, M.; Da Silva, M. J.; Thiele, S.; Hampel, U.

Simulation-based investigation of spatial sensitivity distribution of wire-mesh sensors

COMSOL Conference 2008, 04.-06.11.2008, Hannover, Deutschland

Weier, T.; Cierpka, C.; Gerbeth, G.

Electromagnetic excitation of separated flows: Coherent structures and mean flow features

European Drag Reduction and Flow Control Meeting (EDRFCM 2008), 08.-11.09.2008, Ostritz - St. Marienthal, Germany

Weier, T.; Cierpka, C.; Gerbeth, G.

Elektromagnetisch getriebene Strömungen in elektrochemischen Systemen

Lehrstuhlkolloquium Professur für Magnetofluidynamik, 15.10.2008, Dresden, Germany

Weier, Tom; Cierpka, Christian; Eckert, Kerstin; Uhlemann, Margitta; Bund, Andreas

Flow structure and concentration distribution in seemingly parallel magnetic and electric fields

7th PAMIR International Conference on Fundamental and Applied MHD, 08.-12.09.2008, Presqu'île de Giens, France

Willschütz, H.-G.; Altstadt, E.; Abendroth, M.

Application of the effective convectivity model to an PWR in-vessel retention scenario

Jahrestagung Kerntechnik 2008, 27.-29.05.2008, Hamburg, Germany

Wondrak, T.; Gundrum, T.; Stefani, F.; Gerbeth, G.

Contactless inductive flow tomography: theory, experiments, perspectives

The 10th Workshop on Optimization and Inverse Problems in Electromagnetism (OIPE 2008), 14.-17.09.2008, Ilmenau, Deutschland

Zhang, C.; Eckert, S.; Gerbeth, G.

Bubble-driven liquid metal flows influenced by miscellaneous magnetic fields

7th PAMIR International Conference on Fundamental and Applied MHD, 08.-12.09.2008, Presqu'île de Giens, France

Contributions to proceedings and other collected editions

Abendroth, M.; Altstadt, E.

Fracture mechanical analysis of a VVER-440 PTS scenario

Jahrestagung Kerntechnik 2008, 27.-29.05.2008, Hamburg, Germany

Proceedings of the Annual Meeting of Nuclear Technology, Sankt Augustin: dbcM GmbH, (CD-ROM), paper No. 328, pp. 252-257

Altstadt, E.; Abendroth, M.

Fracture mechanical investigation of a thermo shock scenario for a VVER-440 RPV

34. MPA-Seminar, 09.-10.10.2008, Stuttgart, Deutschland

34. MPA-Seminar "Werkstoff- & Bauteilverhalten in der Energie- & Anlagentechnik", Proceedings (CD-ROM), paper no. 50, pp. 50.1-50.12

Azzopardi, B.; Hernandez Perez, V.; Kaji, R.; Da Silva, M. J.; Beyer, M.; Hampel, U.

Wire mesh sensor studies in a vertical pipe

Fifth International Conference on Transport Phenomena In Multiphase Systems, HEAT 2008, 30.06.-03.07.2008, Bialystok, Poland

Proceedings of the 5th International Conference on Transport Phenomena in Multiphase Systems, HEAT 2008, 405-412

Bartosiewicz, Y.; Seynhaeve, J.-M.; Vallee, C.; Höhne, T.; Laviéville, J.

Modelling free surface flows relevant to a PTS scenario: comparison between experimental data and three RANS based CFD-codes - Comments on the CFD-experiment integration and best practice guideline

Proceedings of the XCFD4NRS - Experiments and CFD Code Applications to Nuclear Reactor Safety, 10.-12.09.2008, Grenoble, France, CD-ROM, Paper HOR-01

Bechta, S. V.; Granovsky, V. S.; Khabensky, V. B.; Krushinov, E. V.; Vitol, S. A.; Sulatsky, A. A.; Gusarov, V. V.; Almiyashev, V. I.; Lopukh, D. B.; Bottomley, D.; Fischer, M.; Piluso, P.; Miassoedov, A.; Tromm, W.; Altstadt, E.; Fichot, F.; Kymalainen, O.

Interaction between molten corium $UO_2+X - ZrO_2- FeO_y$ and VVER vessel steel

2008 International Congress on Advances in Nuclear Power Plants (ICAPP 08), 08.-12.06.2008, Anaheim, California, United States. Proceedings of ICAPP'08 (CD-ROM), paper no. 8052

Bergner, F.; Al Mazouzi, A.; Hernandez-Mayoral, M.; Ulbricht, A.

Combined TEM, PAS and SANS investigation of neutron-irradiated pure iron

Structural Materials for Innovative Nuclear Systems (SMINS), 04.-06.06.2007, Karlsruhe, Germany

Workshop Proceedings: OECD 2008, 283-290

Bergner, F.; Birkenheuer, U.; Ulbricht, A.; Weiss, F.-P.

Flux dependence of cluster formation in neutron irradiated weld material – Small-angle neutron scattering experiments and rate theory simulation

IEEE Dresden 2008, 20.-24.10.2008, Dresden, Deutschland

IEEE 2008 Nuclear Science Symposium Conference Record

Bieberle, A.; Bärtling, Y.; Fleischer, A.; Sühnel, T.; Zimmermann, W.; Schleicher, E.; Hampel, U.

Implementation of temperature control into a high resolution gamma ray detector for tomography applications

Proceedings of the XCFD4NRS - Experiments and CFD Code Applications to Nuclear Reactor Safety, 10.-12.09.08, Grenoble, France, CD-ROM, Paper BOI-06

Bieberle, A.; Hoppe, D.; Zippe, C.; Schleicher, E.; Tschofen, M.; Suehnel, T.; Zimmermann, W.; Hampel, U.

Void measurement in boiling water reactor rod bundles using high resolution gamma ray tomography

Proceedings of the XCFD4NRS - Experiments and CFD Code Applications to Nuclear Reactor Safety, 10.-12.09.08, Grenoble, France, Paper No. BOI-06

Bilodid, Y.; Mittag, S.

Spectral-history modeling in DYN3D burnup calculations

18th AER Symposium on VVER Reactor Physics and Reactor Safety, 06.-10.10.2008, Eger, Hungary

Proceedings of 18th AER Symposium on VVER Reactor Physics and Reactor Safety, Budapest, 978-963-372-639-6, 467-481

Boehmer, B.; Konheiser, J.; Noack, K.; Rogov, A.; Stephan, I.; Hansen, W.; Hinke, D.; Unholzer, S.; Grantz, M.; Mehner, H.-C.

Measurements and Monte Carlo calculations of gamma and neutron flux spectra inside and behind iron/steel/water configurations

12 th International Symposium on Reactor Dosimetry, 08.-13.05.2005, Gatlinburg, United States

Reactor Dosimetry: 12th International Symposium, West Conshohocken: ASTM, 978-0-8031-3412-6

Borodkin, G.; Khrennikov, N.; Böhmer, B.; Noack, K.; Konheiser, J.

Deterministic and Monte Carlo neutron transport calculation for Greifswald-1 and comparison with ex-vessel measurement data

12 th International Symposium on Reactor Dosimetry, 08.-13.05.2005, Gatlinburg, United States

Reactor Dosimetry: 12th International Symposium, West Conshohocken: ASTM, 978-0-8031-3412-6

Büttner, L.; Shirai, K.; Voigt, A.; Neumann, M.; Czarske, J.; Weier, T.; Cierpka, C.

Anwendung des Laser-Doppler-Geschwindigkeitsprofilsensors zur Vermessung elektromagnetisch beeinflusster Elektrolytströmungen

Fachtagung "Lasermethoden in der Strömungsmesstechnik", 09.-11.09.2008, Karlsruhe, BRD, 978-3-9805613-4-1, 4.1-4.8

Cramer, A.; Pal, J.; Gerbeth, G.

Electromagnetic stirring with superimposed travelling and rotating magnetic fields.

XVI International Congress on Electricity applications in modern world - UIE'08, 19.-21.05.2008, Krakow, Poland, 83-88415-80-8, 41-42

Da Silva, M. J.; Hampel, U.

Neuartige Impedanzsensoren für die Visualisierung von Mehrphasenströmungen

XXII. Messtechnisches Symposium, 11.-13.09.2008, Dresden, Germany

Tagungsband XXII. Messtechnisches Symposium, Aachen: Shaker, 978-3-8322-7506-8, 25-34

Da Silva, M. J.; Schleicher, E.; Hampel, U.

Novel wire-mesh sensor modalities for the investigation of single phase and multiphase flows

Sensoren und Messsysteme 2008, 11.-12.03.2008, Ludwigsburg, Germany

VDI-Berichte 2011, Düsseldorf: VDI Verlag, 978-3-18-092011-5, 625-634

Da Silva, M. J.; Thiele, S.; Höhne, T.; Vaibar, R.; Hampel, U.

Experimental studies and CFD calculations for buoyancy driven mixing phenomena

XCFD4NRS, Experiments and CFD Code Applications to Nuclear Reactor Safety, 10.-

12.09.2008, Grenoble, France, MIX-02

Da Silva, M. J.; Thiele, S.; Schleicher, E.; Hampel, U.

Field-focusing imaging sensor for visualization of multiphase flows

EUROSENSORS XXII, 07.-10.09.2008, Dresden, Germany

Proceedings of EUROSENSORS XXII, Duesseldorf: VDI, 978-3-00-025217-4, 736-739

Eckert, S.; Gerbeth, G.

Velocity measurements in liquid metal flows using the Ultrasonic Doppler Method: examples and perspectives

6th. International Symposium on Ultrasonic Doppler Methods for Fluid Mechanics and Fluid Engineering, 09.-11.09.2008, Praha, Czech Republic, 1-6

Eckert, S.; Willers, B.; Rübiger, D.; Dong, J.; Nikrityuk, Petr A.; Eckert, K.

Solidification of aluminium alloys under the influence of modulated magnetic fields

11th International Conference on Aluminium Alloys, 22.-26.09.2008, Aachen, Germany, 497-502

Fischer, F.; Hampel, U.

Ultra fast electron beam X-ray computed tomography for two-phase flow measurement

XCFD4NRS - Experiments and CFD Code Applications to Nuclear Reactor Safety, 10.-12.09.2008, Grenoble, France

Proceedings of the XCFD4NRS - Experiments and CFD Code Applications to Nuclear Reactor Safety, 10.-12.09.2008, Grenoble, France, CD-ROM, Paper BOI-08

Fischer, M.; Gerbeth, G.; Stefani, F.

Constraining the geodynamo by sequences of field reversals

7th International PAMIR Conference on Fundamental and Applied MHD, 08.-12.09.2008, Presqu'île de Giens, France

Proceedings of the 7th International PAMIR Conference on Fundamental and Applied MHD, Reims: Universite de Reims Champagne-Ardenne, 225-229

Forbriger, J.; Galindo, V.; Gerbeth, G.; Stefani, F.

Determination of harmonic and pulsed eddy current distributions in a liquid metal

7th International PAMIR Conference on Fundamental and Applied MHD, 08.-12.09.2008, Presqu'île de Giens, France

Proceedings of the 7th International PAMIR Conference on Fundamental and Applied MHD, Reims: Université de Reims Champagne-Ardenne, 809-813

Gerbeth, G.; Eckert, S.; Galindo, V.; Willers, B.; Hewelt, U.; Hornung, B.

Magnetic field control of the pouring process in aluminium investment casting

11th International Conference on Aluminium Alloys, 22.-26.09.2008, Aachen, Germany

Aluminium Alloys, Eds.: J. Hirsch, B. Skrotzki, G. Gottstein: Wiley-VCH, 427-433

Giesecke, A.; Stefani, F.; Gerbeth, G.

Magnetic field reversals in nature, experiments and simulations

ICTAM2008 - International Congress of Theoretical and Applied Mechanics, 25.08.-

29.09.2008, Adelaide, Australien, 978-0-9805142-1-6

Gokhman, A. R.; Bergner, F.

Cluster dynamics simulation of mixed Cu-vacancy clusters in a neutron-irradiated Fe-Cu alloy

J.W.P. Schmelzer, G. Röpke, V.B. Priezhev: Nucleation Theory and Applications, Dubna: JINR, 2008, 978-5-9530-0199-1, 319-325

Grahn, A.; Krepper, E.; Alt, S.; Kästner, W.; Weiß, F.-P.; Hampel, R.

Implementation of a pressure drop model for the CFD simulation of clogged containment sump strainers

Jahrestagung Kerntechnik 2008, 27.-29.05.2008, Hamburg, Germany, Proceedings of the Annual Meeting of Nuclear Technology (CD-ROM), paper No. 321, pp. 91-96

Gundrum, T.; Stefani, F.; Gerbeth, G.; Szklarski, J.; Ruediger, G.; Hollerbach, R.

Liquid metal Taylor-Couette experiment on the magnetorotational instability

6th International Symposium on Ultrasonic Doppler Methods for Fluid Mechanics and Fluid Engineering, 09.-11.09.2008, Praha, Czech Republic

Proceedings of the 6th International Symposium on Ultrasonic Doppler Methods for Fluid Mechanics and Fluid Engineering, Prague, Czech Republic: Czech Technical University in Prague, 978-80-87117-05-7, 65-68

Hampel, U.; Bieberle, A.; Schleicher, E.; Hoppe, D.; Zippe, C.

High resolution gamma ray tomography and its application to multiphase flow measurement

CT2008: TOMOGRAPHY CONFLUENCE - An International Conference on the Applications of Computerized Tomography, 15.-17.02.2008, Kanpur, India

AIP Conference Proceedings 1050: American Institute of Physics, 978-0-7354-0578-3, 138-143

Hampel, U.; Fischer, F.; Bieberle, M.; Schleicher, E.

Recent progress in ultra fast electron beam X-ray computed tomography

Proceedings of the 5th International Symposium on Process Tomography, 25.-26.08.2008, Zakopane, Poland, Paper No. PT08_cr11

Hampel, U.; Fischer, F.; Schleicher, E.; Hoppe, D.

Ultra fast scanned electron beam X-ray CT for two-phase flow measurement

CT2008: TOMOGRAPHY CONFLUENCE - An International Conference on the Applications of Computerized Tomography, 15.-17.02.2008, Kanpur, India

AIP Conference Proceedings 1050: American Institute of Physics, 978-0-7354-0578-3, 144-150

Hermann, R.; Gerbeth, G.; Biswas, K.; Filip, O.; Shatrov, V.; Priede, J.

Effect of melt convection on microstructure evolution of Nd-Fe-B and Ti-Al peritectic alloys

D.Herlach: Phase transformations in multicomponent melts, Weinheim: Wiley-VCH, 2008, 245-261

Höhne, T.

Multiphase flows in industrial applications - experiments and CFD simulations

CFD OIL2008 - 3d Encontro Latino-Americano de CFD Aplicado à Indústria de Petróleo, 18.-19.08.2008, Rio de Janeiro, Brasil

CD-ROM, Webpage http://www.cfdoil.com.br/pdf/keynotes/thomas_hohne.pdf

Höhne, T.; Kliem, S.; Vaibar, R.

Experimental and numerical modeling of transition matrix from momentum to buoyancy-driven flow in a pressurized water reactor

16th International Conference on Nuclear Engineering ICONE16, 11.-15.05.2008, Orlando, USA

CD-ROM, paper 48490

Höhne, T.; Moncalvo, D.

Nachrechnung von experimentell bestimmten Leistungsparametern eines Vollhub-Feder-Sicherheitsventils mit ANSYS CFX

Jahrestreffen der ProcessNet-Fachausschüsse Computational Fluid Dynamics, Gasreinigung, Mechanische Flüssigkeitsabtrennung und Grenzflächenbestimmte Systeme und Prozesse, 18.-20.02.2008, Wiesbaden, Germany

CD-ROM

Höhne, T.; Moncalvo, D.

Analysis of safety valve characteristics using measurements and CFD simulations

Jahrestagung Kerntechnik 2008, 27.-29.05.2008, Hamburg, Germany

CD-ROM, paper 0249

Höhne, T.; Moncalvo, D.; Friedel, L.; Jörgensen, B.

Nachrechnung eines Vollhub-Feder-Sicherheitsventils mit ANSYS CFX

9. Fachtagung "Anlagen-, Arbeits- und Umweltsicherheit", 06.-07.11.2008, Köthen, Deutschland,

CD-ROM, paper 09

Höhne, T.; Rohde, U.; Melideo, D.; Moretti, F.; D'Auria, F.; Shishov, A.; Lisenkov, E.

CFD simulations of Hidropress mixing facility experiments in the framework of TACIS project R2.02/02

TOPSAFE 2008, 01.-03.10.2008, Dubrovnik, Croatia

CD-ROM, paper 063

Höhne, T.; Vallee, C.

Numerical prediction of horizontal stratified flows

*6th International Conference on COMPUTATIONAL FLUID DYNAMICS in the Oil & Gas, Metallurgical and Process Industries, 10.-12.06.2008, Trondheim, Norway
CD-ROM, paper 08-12*

Hollerbach, R.; Stefani, F.; Gerbeth, G.; Gundrum, T.; Rüdiger, G.

The helical magnetorotational instability in cylindrical Taylor-Couette flow

*XXII International Congress of Theoretical and Applied Mechanics, 24.-29.08.2008, Adelaide, Australia
Proceedings of the XXII International Congress of Theoretical and Applied Mechanics, Adelaide: IUTAM, 978-0-9805142-1-6, 11858*

Johansen, G. A.; Hampel, U.; Hjertaker, B. T.

Flow imaging by high speed transmission tomography

*7th International Topical Meeting on Industrial Radiation and Radioisotope Measurement (IRRMA 7), 22.-27.06.2008, Prague, Czech Republic
Proceedings on CD*

Journeau, C.; Bonnet, J. M.; Godin-Jacqmin, L.; Piluso, P.; Tarabelli, D.; Altstadt, E.; et al.

European Research on the Corium issues within the SARNET Network of Excellence

2008 International Congress on Advances in Nuclear Power Plants (ICAPP '08), 08.-12.06.2008, Anaheim, United States. Proceedings of ICAPP '08 (CDROM), paper no. 8047

Kliem, S.

AER working group D on VVER safety analysis – report of the 2008 meeting

*18th Symposium of AER on VVER Reactor Physics and Reactor Safety, 06.-10.10.2008, Eger, Hungary
Proceedings of the 18th Symposium of AER on VVER Reactor Physics and Reactor Safety, Budapest, 9789633726389, 307-314*

Kliem, S.; Höhne, T.; Rohde, U.; Weiß, F.-P.

Experiments on slug mixing under natural circulation conditions at the ROCOM test facility using high resolution measurement technique and numerical modeling

Proceedings of the XCFD4NRS - Experiments and CFD Codes Application to Nuclear Reactor Safety, 10.-12.09.2008, Grenoble, France, CD-ROM, Paper MIX03

Kliem, S.; Kozmenkov, Y.; Höhne, T.; Rohde, U.; Weiß, F.-P.

VVER-1000 main steam line break analysis using the coupled code system DYN3D/ATHLET

*International Conference on the Physics of Reactors (PHYSOR'08), 14.-19.09.2008, Interlaken, Switzerland
Proceedings of the International Conference on the Physics of Reactors 2008, CDROM paper 311, Villigen: Paul Scherrer Institut, 978-3952140956*

Kliem, S.; Mittag, S.; Rohde, U.; Grundmann, U.; Weiß, F.-P.

Simulation von ATWS-Transienten in Druckwasserreaktoren

*Jahrestagung Kerntechnik 2008, 27.-29.05.2008, Hamburg, Germany
Tagungsband der Jahrestagung Kerntechnik 2008, CDROM, Berlin: INFORUM GmbH*

Klyukin, A.; Grants, I.; Gerbeth, G.

Experimental study of traveling magnetic field driven instability in a thermally stratified liquid gallium cylinder

7th International PAMIR Conference on Fundamental and Applied MHD, 08.-12.09.2008, Presqu'île de Giens, France

Fundamental and Applied MHD, Reims: Université de Reims Champagne-Ardenne, 627-631

Kolesnichenko, I.; Khripchenko, S.; Buchenau, D.; Gerbeth, G.

Nonstationary electrovortex flows in a long shallow channel with conducting fluid

7th International PAMIR Conference on Fundamental and Applied MHD, 08.-12.09.2008, Presqu'île de Giens, France

Fundamental and Applied MHD, Reims: Université de Reims Champagne-Ardenne, 369-373

Krauze, A.; Priede, J.; Hermann, R.; Gerbeth, G.

Numerical modeling of the growth of small-diameter intermetallic compound crystals by a two-phase RF floating zone method

7th International PAMIR Conference on Fundamental and Applied MHD, 08.-12.09.2008, Presqu'île de Giens, France

Fundamental and Applied MHD, Reims: Université de Reims Champagne-Ardenne, 851-855

Krepper, E.; Cartland-Glover, G.; Grahn, A.; Weiss, F.-P.; Alt, S.; Hampel, R.; Kästner, W.; Seeliger, A.

Experimental investigation and CFD simulation of the behaviour of mineral wool in the reactor sump

16th International Conference on Nuclear Engineering, ICONE-16, 11.-15.05.2008, Orlando, Florida, USA, CD-ROM, contribution 48121

Krepper, E.; Cartland-Glover, G.; Grahn, A.; Weiss, F.-P.; Alt, S.; Hampel, R.; Kästner, W.; Seeliger, A.

Experiments and CFD-modelling of insulation debris transport phenomena in water flow

Proceedings of the XCFD4RS, Experiments and CFD Codes Application to Nuclear Reactor Safety, 10.-12.09.2008, Grenoble, France, CD-ROM, Paper AC-01

Krepper, E.; Frank, T.; Lucas, D.; Prasser, H.-M.; Zwart, P.

A population balance approach for polydispersed bubbly flows considering size dependent bubble forces

6th International Conference on COMPUTATIONAL FLUID DYNAMICS in Oil & Gas, Metallurgical and Process Industries, 10.-12.06.2008, Trondheim, Norway

Kryk, H.; Hessel, G.

Balance-based real-time monitoring – a tool to improve safety and efficiency of batch and semi-batch processes

9th International Conference and Exhibition on The Scale-Up of Chemical Processes, 15.-17.09.2008, Rome, Italy

Conference Proceedings: Scale-up of Chemical Processes, Chapter 18, Scientific Update Press 2008

Kryk, H.; Hessel, G.; Schmitt, W.

Safety-oriented on-line monitoring of Grignard reactions

1st European Conference on Process Analytics and Control Technology, 22.-25.04.2008, Frankfurt am Main, Germany

Book of Abstracts, P.15, S. 104

Lucas, D.

Qualification of simulation tools for two-phase flows

Frédéric Joliot/Otto Hahn Summer School on Nuclear Reactors: "Physics, Fuels, and Systems", 20.-29.08.2008, Aix-en-Provence, France

Lecture notes of the 2008 Frédéric JOLIOT & Otto HAHN Summer School

Lucas, D.; Beyer, M.; Kussin, J.; Schütz, P.

Benchmark database on the evolution of two-phase flows in a vertical pipe

Proceedings of the XCFD4NRS, Experiments and CFD Code Applications to Nuclear Reactor Safety, 10.-12.09.2008, Grenoble, France, CD-ROM, Paper BOI-001

Lucas, D.; Vallée, C.; Beyer, M.; Prasser, H.-M.; Deendarlianto,-

Experiments on the counter-current flow limitation (CCFL) in a model of a pressurised water reactor hot leg

HEAT 2008, The Fifth International Conference on Transport Phenomena In Multiphase Systems, 30.06.-03.07.2008, Bialystok, Poland

Transport Phenomena In Multiphase Systems, Volume 1, Bialystok, 325-332

Merk, B.

Vergleich von Abbrandrechnungen mit HELIOS 1.9 und KAPROS/KARBUS mit zeitlich veränderlicher Leistung

Jahrestagung Kerntechnik 2008, 27.-29.05.2008, Hamburg, Germany, Proceedings of the Annual Meeting of Nuclear Technology (CD-ROM), paper No. 110, pp. 38-42

Merk, B.

A time dependent analytical approximation solution for a pulsed source problem: P1 transport versus diffusion

2008 Nuclear Science Symposium, Medical Imaging Conference and 16th Room Temperature Semiconductor Detector Workshop, 19.-25.10.2008, Dresden, Deutschland

IEEE Conference Record, 978-1-4244-2715-4

Merk, B.; Koch, R.

Spatial discretization in LWR cell calculations with HELIOS 1.9: influence on kinf and flux distribution

ENS TOPSAFE 2008, 01.-03.10.2008, Dubrovnik, Croatia

Book of Abstracts with Proceedings CD, ISBN 978-92-95064-06-5, A1-067

Merk, B.; Koch, R.

On the Influence of Spatial Discretization on Cross Section Preparation with HELIOS 1.9

Jahrestagung Kerntechnik 2008, 27.-29.05.2008, Hamburg, Germany, Proceedings of the Annual Meeting of Nuclear Technology (CD-ROM), paper No. 109, pp. 14-18

Merk, B.; Koch, R.

The effect of spatial discretization in LWR cell calculations with HELIOS 1.9

18th Symposium of AER on VVER Reactor Physics and Reactor Safety, 06.-10.10.2008, Eger, Hungary

Proceedings of the 18th Symposium of AER, 9789633726389, 257-266

Mutschke, G.; Cierpka, C.; Weier, T.; Eckert, K.; Mühlenhoff, S.; Bund, A.

3-D magnetic field effects during metal electrodeposition In cuboid cells

7th International PAMIR Conference on Fundamental and Applied MHD, 08.-12.09.2008, Presqu'île de Giens, Frankreich, 273-277

Neuhaus, T.; Schaffrath, A.; Ronneberger, R.; Altstadt, E.

Entwicklung und Validierung des Druckstoßprogramms DYVPRO Mod. 3 Jahrestagung Kerntechnik 2008, 27.-29.05.2008, Hamburg, Germany, *Proceedings of the Annual Meeting of Nuclear Technology (CD-ROM), paper No. 205, pp. 107-117*

Nikrityuk, Petr A.; Rábiger, D.; Eckert, K.; Eckert, S.; Gerbeth, G.

Solidification of metal alloys under the influence of pulse-modulated magnetic fields

7th PAMIR International Conference on Fundamental and Applied MHD, 08.-12.09.2008, Presqu'île de Giens, France, 879-884

Ošmera, B.; Boehmer, B.; Ballesteros, A.; Konheiser, J.; Kyncl, J.; Hordosy, G.; Keresztúri, A.; Belousov, S.; Ilieva, K.; Kirilova, D.; Mitev, M.; Smutný, V.; Polke, E.; Zaritsky, S.; Töre, C.; Ortego, P.

Accurate determination and benchmarking of radiation field parameters relevant for pressure vessel monitoring. A review of some REDOS project results

12th International Symposium on Reactor Dosimetry, 08.-13.05.2005, Gatlinburg, United States, 08.-13.05.2005, Gatlinburg, United States

Reactor Dosimetry: 12th International Symposium, West Conshohocken: ASTM, 978-0-8031-3412-6

Otahal, J.; Boden, S.; Schleicher, E.; Beyer, M.; Jicha, M.; Hampel, U.

Wire-mesh and X-ray microtomography studies of flow patterns in the mixing chamber of an effervescent atomizer

Proceedings of the 5th International Symposium on Process Tomography, 25.-26.08.2008, Zakopane, Poland, Paper No. PT08_cr8

Otahal, J.; Hampel, U.; Schleicher, E.

Porovnání experimentálních technik v oblasti dvofázového proudění (Comparison of experimental techniques in two-phase flow)

Proceedings of the 27th International Conference of Fluid Dynamics and Thermodynamics Departments, 24.-27.06.2008, Plzen, Czech Republic, Paper No. SK06.

Otahal, J.; Hampel, U.; Schleicher, E.; Jicha, M.

Two-phase flow characteristics in the mixing chamber of the effervescent atomizer

ILASS Europe 2008 - 22nd European Conference on Liquid Atomization and Spray Systems, 08.-10.09.2008, Como Lake, Italy, CD-ROM

Pätzold, O.; Lantzsch, R.; Grants, I.; Stelter, M.; Gerbeth, G.
Vertical Gradient Freeze growth in a combined magnetic AC/DC field
7th International PAMIR Conference on Fundamental and Applied MHD, 08.-12.09.2008, Presqu'île de Giens, France
Fundamental and Applied MHD, Reims: Universite de Reims Champagne-Ardenne, 633-635

Plevachuk, Yu.; Sklyarchuk, V.; Yakymovych, A.; Eckert, S.; Willers, B.
Thermophysical properties of Al-Cu liquid alloys
11th International Conference on Aluminium Alloys, 22.-26.09.2008, Aachen, Germany, 1359-1360

Priede, J.; Buchenau, D.; Gerbeth, G.
Force-free and contactless electromagnetic flow rate sensors
7th International PAMIR Conference on Fundamental and Applied MHD, 08.-12.09.2008, Presqu'île de Giens, France
Fundamental and Applied MHD, Reims: Universite de Reims Champagne-Ardenne, 815-819

Priede, J.; Gerbeth, G.
Helical magnetorotational instability in a Taylor-Couette flow
7th International PAMIR Conference on Fundamental and Applied MHD, 08.-12.09.2008, Presqu'île de Giens, France
Fundamental and Applied MHD, Reims: Universite de Reims Champagne-Ardenne, 251-255

Räbiger, D.; Eckert, S.; Gerbeth, G.
Application of the Ultrasound Doppler method for velocity measurements in an electromagnetically-stirred liquid metal
6th International Symposium on Ultrasonic Doppler Methods for Fluid Mechanics and Fluid Engineering, 09.-11.09.2008, Praha, Czech Republic, 143-146

Rindelhardt, U.; Dietrich, A.; Kedziora, K.; Hahn, A.
Megawatt PV plants in Germany: A south-north performance comparison
23rd European Photovoltaic Solar Energy Conference and Exhibition, 01.-05.09.2008, Valencia, Spain
Proc. of the International Conference held in Valencia, Spain, 1-5 September 2008, München, 3-936338-24-8, 3236-3239

Rindelhardt, U.; Nitzschner, F.
Photovoltaik-Anlagen im Netzparallelbetrieb: Erfahrungen eines Regionalversorgers
Proc. 23. Symposium Photovoltaische Solarenergie, 05.-07.03.2008, Bad Staffelstein, Germany, ISBN 978-3-934681-67-5, S. 288-293

Rindelhardt, U.; Viehrig, H.-W.; Konheiser, J.; Schuhknecht, J.
Weld material investigations of a VVER-440 reactor pressure vessel: results from the first trepan taken from the former Greifswald NPP
16th International Conference on Nuclear Engineering, ICONE-16, 11.-15.05.2008, Orlando, USA, Conference-CD, contribution 48070

Rindelhardt, U.; Viehrig, H.-W.; Schuhknecht, J.; Konheiser, J.

RPV weld material investigations of a VVER-440 NPP

10th International Conference "Material Issues in Design, Manufacturing and Operation of Nuclear Power Plants Equipment", 06.-10.10.2008, St. Petersburg, Russia

The 10th International Conference (Conference CD), St. Petersburg: PROMETHEY

Rohde, U.; Höhne, T.; Krepper, E.; Kliem, S.

Application of CFD codes in nuclear reactor safety analysis

TOPSAFE 2008, 01.-03.10.2008, Dubrovnik, Croatia

CD-ROM. paper 099

Schmidtke, M.; Lucas, D.

On the modelling of bubble entrainment by impinging jets in CFD-simulations

Proceedings of the XCFD4NRS, Experiments and CFD Code Applications to Nuclear Reactor Safety, 10.-12.09.2008, Grenoble, France, CD-ROM, Paper PTS-05

Shatrov, V.; Gerbeth, G.; Hermann, R.

An alternating magnetic field driven flow in a spinning cylindrical container and its three-dimensional linear stability analysis

7th International PAMIR Conference on Fundamental and Applied MHD, 08.-12.09.2008, Presqu'île de Giens, France

Fundamental and Applied MHD, Reims: Université de Reims Champagne-Ardenne, 525-529

Stefani, F.; Gerbeth, G.; Gundrum, T.; Szklarski, J.; Rüdiger, G.; Hollerbach, R.

Liquid metal experiments on the helical magnetorotational instability

7th International PAMIR Conference on Fundamental and Applied MHD, 08.-12.09.2008, Presqu'île de Giens, France

Proceedings of the 7th International PAMIR Conference on Fundamental and Applied MHD, Reims: Université de Reims Champagne-Ardenne, 97-101

Thiele, S.; Da Silva, M. J.; Hampel, U.; Abdulkareem, L.; Azzopardi, B. J.

High-resolution oil-gas two-phase flow measurement with a new capacitance wire-mesh tomograph

5th International Symposium on Process Tomography, 25.-26.08.2008, Zakopane, Poland

5th International Symposium on Process Tomography, Lodz, Poland: Technical University of Lodz, 978-83-7283-271-9, PT08_cr7

Thiele, S.; Da Silva, M. J.; Wagner, M.; Hampel, U.

Simulation analysis of the spatial sensitivity of a wire-mesh sensor

EUROSENSORS XXII, 07.-10.09.2008, Dresden, Germany

EUROSENSORS XXII, Duesseldorf: Verein Deutscher Ingenieure e.V. (VDI), 978-3-00-025217-4, 157-160

Tusheva, P.; Reinke, N.; Hurtado, A.; Schäfer, F.

Severe accident analysis for VVER-1000/V-320 for a station blackout accident scenario with ASTEC V1.3.0

Jahrestagung Kerntechnik 2008, 27.-29.05.2008, Hamburg, Germany

Proceedings of the Annual Meeting of Nuclear Technology, Sankt Augustin: dbcM GmbH, (CD-ROM), paper No. 323, pp. 208-211

Ulbricht, Andreas; Bergner, Frank; Hein, Hieronymus; Kammel, Martin
Flux dependence of cluster formation in neutron irradiated weld material
U. Stahnke, A. Brandt, H. A. Graf: BENSC Experimental Reports 2007, Berlin: Hahn-Meitner-Institut, HMI-B617, 2008, ISSN 0936-0891, 210-210

Vallee, C.; Deendarlianto,.; Beyer, M.; Lucas, D.; Carl, H.
Air/water counter-current flow experiments in a model of the hot leg of a pressurised water reactor
ICONE 16 - International Conference on Nuclear Engineering, 11.-15.05.2008, Orlando, Florida, USA
Paper ICONE16-48374

Vallee, C.; Deendarlianto,.; Lucas, D.; Beyer, M.; Pietruske, H.; Carl, H.
Counter-current flow limitation experiments in a model of the hot leg of a pressurised water reactor
Jahrestagung Kerntechnik 2008, 27.-29.05.2008, Hamburg, Deutschland
CD-ROM: Fachsitzungen / Topical Sessions

Vallee, C.; Lucas, D.; Beyer, M.; Pietruske, H.; Schütz, P.; Carl, H.
Experimental CFD grade data for stratified two-phase flows
Proceedings of the XCFD4NRS - Experiments and CFD Code Applications to Nuclear Reactor Safety, 10.-12.09.2008, Grenoble, France, CD-ROM, Paper HOR-05

Viehrig, H.-W.; Schuhknecht, J.
Fracture mechanics characterisation of the WWER-440 reactor pressure vessel beltline welding seam of Greifswald Unit 8
34th MPA-Seminar and VGB-Symposium "Materials and Components Behaviour in Energy & Plant Technology", 09.-10.10.2008, Stuttgart, Deutschland
Proceedings 34th MPA-Seminar and VGB-Symposium "Materials and Components Behaviour in Energy & Plant Technology", Stuttgart: MPA Stuttgart

Wagner, M.; Da Silva, M. J.; Thiele, S.; Hampel, U.
Simulation-based investigation of spatial sensitivity distribution of wire-mesh sensors
Proceedings of the COMSOL Conference 2008, 04.-06.11.2008, Hannover, Germany, Paper No. 5448, <http://www.comsol.se/academic/papers/5448/>

Weier, Tom; Cierpka, Christian; Eckert, Kerstin; Uhlemann, Margitta; Bund, Andreas
Flow structure and concentration distribution in seemingly parallel magnetic and electric fields
7th International pamir Conference on Fundamental and Applied MHD, 08.-12.09.2008, Presqu'île de Giens, France, 333-337

Willschütz, H.-G.; Altstadt, E.; Abendroth, M.
Application of the effective convectivity model to an PWR in-vessel retention scenario
Jahrestagung Kerntechnik 2008, 27.-29.05.2008, Hamburg, Germany
Proceedings of the Annual Meeting of Nuclear Technology 2008 (CD-ROM), paper no. 326, 221-227

Wondrak, T.; Gundrum, T.; Stefani, F.; Gerbeth, G.

Contactless inductive flow tomography: theory, experiments, perspectives

The 10th Workshop on Optimization and Inverse Problems in Electromagnetism (OIPE 2008), 14.-17.09.2008, Ilmenau, Germany, 75-76

Zhang, C.; Eckert, S.; Gerbeth, G.

Bubble-driven liquid metal flows influenced by miscellaneous magnetic fields

7th PAMIR International Conference on Fundamental and Applied MHD, 08.-12.09.2008, Presqu'île de Giens, France, 363-368

Zhang, X.; Cramer, A.; Lange, A.; Gerbeth, G.

Model experiments on macroscopic thermoelectromagnetic convection

7th PAMIR International Conference on fundamental and applied MHD, 08.-12.09.2008, Presqu'Île de Giens, France, 495-499

Zhu, Z.; Patruno, L. E.; Dorao, C. A.; Lucas, D.; Jakobsen, H. A.

Simulation of bubble coalescence in bubble column using the least-squares method

11th International Conference on Multiphase Flow in Industrial Plant (MFIP'08), 07.-10.09.2008, Palermo, Italy, ISBN:88-88198-13-X, 643

FZD reports and other reports

Altstadt, E.; Abendroth, M.; Willschütz, H.-G.

Thermo-mechanische Finite-Elemente-Modellierung zur Schmelzerückhaltung im RDB nach Verlagerung von Corium in das untere Plenum Thermo-mechanical finite element modelling of in-vessel melt retention after corium relocation into the lower plenum

*Wissenschaftlich-Technische Berichte / Forschungszentrum Dresden-Rossendorf; FZD-503
2008*

Beckert, C.

Entwicklung des Neutronentransportcodes TransRay und Untersuchungen zur zwei- und dreidimensionalen Berechnung effektiver Gruppenwirkungsquerschnitte

*Wissenschaftlich-Technische Berichte / Forschungszentrum Dresden-Rossendorf; FZD-492
2008*

Beyer, M.; Lucas, D.; Kussin, J.; Schütz, P.

Luft-Wasser Experimente im vertikalen DN200-Rohr

*Wissenschaftlich-Technische Berichte / Forschungszentrum Dresden-Rossendorf; FZD-504
2008*

Beyer, M.; Lucas, D.; Kussin, J.; Schütz, P.

Air-water experiments in a vertical DN200-pipe

*Wissenschaftlich-Technische Berichte / Forschungszentrum Dresden-Rossendorf; FZD-505
2008*

Grundmann, U.; Beckert, C.

Entwicklung einer Transportnäherung für das reaktordynamische Rechenprogramm DYN3D

*Wissenschaftlich-Technische Berichte / Forschungszentrum Dresden-Rossendorf; FZD-497
2008*

Küchler, R.

Die numerische Auswertung von Kleinwinkelstreu曲ven

*Wissenschaftlich-Technische Berichte / Forschungszentrum Dresden-Rossendorf; FZD-496
2008*

Noack, K.; Rindelhardt, U.; Rogov, A.

Shielding and Fuel Storage Calculations for GUINEVERE

*Wissenschaftlich-Technische Berichte / Forschungszentrum Dresden-Rossendorf; FZD-490
2008*

Schmidtke, M.

Untersuchung der Dynamik fluider Partikel auf Basis der Volume of Fluid Methode

*Wissenschaftlich-Technische Berichte / Forschungszentrum Dresden-Rossendorf; FZD-502
2008*

Vaibar, R.; Rohde, U.; Höhne, T.

CFD-Modellierung von Vermischungsvorgängen in Druckwasserreaktoren in Anwesenheit von Dichtegradienten

Wissenschaftlich-Technische Berichte / Forschungszentrum Dresden-Rossendorf; FZD-500 2008

Weiss, F.-P.; Rindelhardt, U. (Editors)

Annual Report 2007 - Institute of Safety Research

Wissenschaftlich-Technische Berichte / Forschungszentrum Dresden-Rossendorf; FZD-501 2008

Werner, M.; Altstadt, E.; Jungmann, M.; Brauer, G.; Noack, K.; Rogov, A.; Krause-Rehberg, R.

Thermal Analysis of EPOS components

Wissenschaftlich-Technische Berichte / Forschungszentrum Dresden-Rossendorf; FZD-499 2008

Friedrich, H.-J.; Zaruba, A.; Meyer, S.; Kryk, H.

Planung, Errichtung und Betrieb einer kleintechnischen Anlage zur Aufbereitung von und zur Sulfatabtrennung aus schwefelsaurem Grubenwasser durch Elektrolyse am Standort der GWRA Raitzta der LMBV

Dresden: VKTA, 2008

Smith, B. L.; Bieder, U.; Graffard, E.; Heitsch, M.; Henriksson, M.; Höhne, T.; Komen, E.; Mahaffy, J.; Moretti, F.; Morii, T.; Mühlbauer, P.; Rohde, U.; Scheuerer, M.; Song, C.-H.; Zigh, G.

Assessment of CFD codes for nuclear reactor safety problems

Paris: NEA/CSNI/R(2007)13, 2008

Ulbricht, A.; Heintze, C.; Bergner, F.; Eckerlebe, H.

Nature of defects formed in neutron-irradiated Fe-Cr model alloys

Geesthacht: GeNF-Experimental Report 2007, Eds. P. K. Pranzas, A. Schreyer, R. Willumeit, GKSS Forschungszentrum, 2008

Altstadt, E.

Spannungs- und Ermüdungsanalyse für den RDB-Boden des Kernkraftwerks Krümmel

Forschungszentrum Rossendorf 2008

FZD\FWS\2008\05

Altstadt, E.

Spannungs- und Ermüdungsanalyse für den Sicherheitsbehälter des KKW Krümmel

Forschungszentrum Rossendorf 2008

FZD\FWS\2008\07

Altstadt, E.

Spannungs- und Ermüdungsanalyse für den Sicherheitsbehälter des KKW Krümmel

Forschungszentrum Rossendorf 2008

FZD\FWS\2008\07

Altstadt, E.; Werner, M.

KKW Krümmel: Spannungs- und Ermüdungsanalyse des Kernmantels für die Transiente am 28.06.2007

Forschungszentrum Rossendorf 2008

FZD\FWS\2008\06

Gerbeth, G.; Stefani, F.; Günther, U.

Untersuchung von Spektraleigenschaften kugelsymmetrischer α^2 -dynamos mit Techniken der Funktionalanalysis und Operatortheorie, Singularitätentheorie und Bifurkationstheorie

Forschungszentrum Rossendorf 2008

FZD\FWS\2008\03

Kliem, S.

Borverdünnungsanalysen beim Start der ersten HKP - Ergänzende Nachweise

Forschungszentrum Rossendorf 2008

FZD\FWS\2008\12

Krepper, E.

Simulations of DEBORA data with CFX

Forschungszentrum Rossendorf 2008

NURESIM-SP2-TH-D2.2.3.2 (January 2008)

Kryk, H.; Schubert, M.; Hessel, G.

Begleitende Untersuchungen zur Pilotierung eines Verfahrens zur elektrochemischen Aufbereitung saurer Wässer aus Tagebaurestseen / 2. Zwischenbericht

Forschungszentrum Rossendorf 2008

FZD\FWS\2008\01

Kryk, H.; Schubert, M.; Hessel, G.

Begleitende Untersuchungen zur Pilotierung eines Verfahrens zur elektrochemischen Aufbereitung saurer Wässer aus Tagebaurestseen / 3. Zwischenbericht

Forschungszentrum Rossendorf 2008

FZD\FWS\2008\04

Lucas, D.; Bestion, D.; Coste, P.; Pouvreau, J.; Morel, Ch.; Martin, A.; Boucker, M.; Bodele, E.; Schmidtke, M.; Scheuerer, M.; Smith, B.; Dhotre, M. T.; Niceno, B.; Lakehal, D.; Galassi, M. C.; Mazzini, D.; D'Auria, F.; Bartosiewicz, Y.; Seynhaeve, J.-M.; Tiselj, I.; ŠTrubelj, L.; Prošek, A.; Ilvonen, M.; Kyrki-Rajamäki, R.; Tanskanen, V.; Laine, M.; Puustinen, J.

Synthesis report on work package 2.1: Pressureized Thermal Shock (PTS)

Forschungszentrum Rossendorf 2008

Institutsbericht FZD\FWS\2008\11

Konheiser, J.; Borodkin, G.; Noack, K.

Untersuchung der Strahlenbelastung an den Auflagekonstruktionen von WWER-440 Reaktoren der ersten Generation

Forschungszentrum Rossendorf 2008

FZD\FWS\2008\10

Schmidtke, M.; Lucas, D.

Comparative simulations of bubble entrainment cases with NURESIM_CFD and CFX-11

Forschungszentrum Rossendorf 2008

NURESIM-SP2-TH-D2.1.3.3

Schmidtke, M.; Lucas, D.

Development of a modeling approach for bubble entrainment

Forschungszentrum Rossendorf 2008

NURESIM-SP2-TH-D2.1.3.2

Granted patents

Eckert, S.; Gerbeth, G.; Gundrum, T.

Verfahren zur Messung von lokalen Strömungsgeschwindigkeiten in flüssigen Schmelzen

WO 00 2008 152 025 A2 – 18.12.2008

Hampel, U.

Anordnung zur zweidimensionalen Messung des Geschwindigkeitsfeldes in Strömungen

DE 10 2007 019 927 B3 – 25.09.2008

Hermann, R.; Gerbeth, G.; Filip, O.; Priede, J.; Schultz, L.

Verfahren und Vorrichtung zur schmelzmetallurgischen Herstellung von Magnetlegierungen auf Nd-Fe-B-Basis

DE 103 28 618 B4 – 24.04.2008

J. Priede, G. Gerbeth, R. Hermann, O. Filip

Verfahren zur Herstellung von leitfähigen Legierungen in einem rotierenden Schmelztiegel

Europapatent EP 1 641 947 B1, 07.05.2008

J. Priede, D. Buchenau, G. Gerbeth, S. Eckert

Verfahren und Anordnung zur kontaktlosen Messung des Durchflusses elektrisch leitfähiger Medien

DE 10 2006 018.623 B4, 15.05.2008

Ch. Kunert, S. Eckert, G. Gerbeth, Th. Gundrum

Verfahren und Verwendung einer Messanordnung zum Messen der Strömungsgeschwindigkeit in einer zur Glas- oder Floatglasherstellung verwendeten Glas- oder Metallschmelze

DE 10 2007 027 362 B3, 04.12.2008

Prasser, H.-M.; Hampel, U.

Anordnung zur Röntgentomographie mit einem elektronisch abgelenkten Elektronenstrahl

DE 103 56 601 B4 – 27.11.2008

Schleicher, E.; Sühnel, T.; Boden, D.; Fischer, F.; Fatterschneider, H.

Gittersensor

DE 10 2007 019 926 A1 – 06.11. 2008

Schleicher, E.; Sühnel, T.; Boden, D.; Fischer, F.; Fatterschneider, H.

Gittersensor

WO002008131730A1 – 06.11. 2008

PhD and diploma theses

PhD theses

André Bieberle

Räumlich hoch auflösende Computertomografie mit Gammastrahlung zur Untersuchung von Mehrphasenströmungen
Technische Universität Dresden

Martin Schmidtke

Untersuchung der Dynamik fluider Partikel auf Basis der Volume of Fluid Methode
Universität Paderborn

Marco da Silva

Impedance Sensors for Fast Multiphase Flow Measurement and Imaging
Technische Universität Dresden

Roman Vaibar

Numerical and experimental approach of turbulent buoyancy driven flow in reactor safety research
Universität Plzen

Diploma theses

Nicole Kießling

Streustrahlungsberechnung für eine Gammastrahlen-Tomographieanordnung mittels der Simulationssoftware GATE/GEANT
Hochschule Zittau/Görlitz

Tobias Seidel

Aufbereitung der Experimente zur Heißstrang-Gegenstrombegrenzung an der Versuchsanlage TOPFLOW für die Simulation mit CFD-Codes
Technische Universität Dresden

Martin Franke

Untersuchung von Zweiphasenströmungen mittels ultraschneller limited-angle Elektronenstrahltomographie
Technische Universität Dresden

Stephan Brendler

Entwicklung und Aufbau eines Strömungsmikroskops für den Einsatz in einem Polymerisationsreaktor bis 60 bar Druck und 110°C Umgebungstemperatur
Hochschule Zittau/Görlitz

Carmen Recknagel

Registrierende Nanohärtemessung und begleitende Atomkraftmikroskopie an unbestrahlten und ionenbestrahlten Stählen
Technische Universität Dresden

Ling Yu

Vervollständigung, Erweiterung und in Betriebnahme eines optischen Tomographiesystems zur Untersuchung von Mehrphasenströmungen
Technische Universität Dresden

Awards

Christophe Vallée

Winner in the Student Paper Competition

Air/water counter-current flow experiments in a model of the hot leg of a pressurised water reactor

16th International Conference on Nuclear Engineering (ICONE 16), Orlando/Florida, USA, 2008

Date of award: May 2008

Frank Stefani (FZD), Günther Rüdiger (Astrophysikalisches Institut Potsdam)

„Society needs Science 2008“ award of “Stifterverband für die Deutsche Wissenschaft”

First experimental prove of the Magneto-Rotational Instability (MRI) effect

Date of award: 27 November 2008

Marco da Silva, Sebastian Thiele

Best Paper Award

High-resolution oil-gas two-phase flow measurement with a new capacitance wire-mesh tomograph

5th International Symposium on Process Tomography, Zakopane (Poland) 2008

Date of award: August 2008

Frank Bergner, Andreas Ulbricht

Forschungspreis des Forschungszentrums Dresden-Rossendorf 2008

Analysis of irradiation induced aging effects in reactor pressure vessel steels

Date of award: März 2009

Guests

Al-Asqalani, Ahmed Tamer

01 September 2008 – 30 November 2008
Assuit University, Faculty of Science Asiut / Egypt

Bojarevics, Andris Dr.

22 September 2008 – 26 September 2008
Institute of Physics, Riga / Latvia

Borodkin, Pavel

27 April 2008 – 25 May 2008
ROSTECHNADZOR / Russian Federation

Buceniaks, Imants Dr.

22 September 2008 – 26 September 2008
Institute of Physics, Riga / Latvia

Gokhman, Oleksandr Prof.

01 August – 27 October 2008
Southukrainian State University of Education, Odessa / Ukraine

Grants, Ilmars Dr.

19 July 2008 – 26 July 2008
17 December 2008 – 19 December 2008
Institute of Physics, Riga / Latvia

Ieremenko, Maksym

07 December 2008 – 13 December 2008
Scientific-Technical Centre for Nuclear and Radiation Safety Kiev / Ukraine

Kosner, Jan

01 June 2008 – 30 September 2008
University Brno / Czech Republic

Kozmenkov, Yaroslav

14 April 2008 – 14 September 2008
Institute of Physics and Power Engineering Obninsk / Russian Federation

Kuzhel, Sergeii

16 January 2008 – 08 February 2008
01 August 2008 – 30 August 2008
21 November 2008 – 21 December 2008
Institute of Mathematics of the National Academy of Sciences of Ukraine / Ukraine

Lakehal, Djamel Dr.

09 November 2008 – 23 November 2008
ETH Zürich and ASCOMO GmbH / Switzerland

Lizal, Frantisek

04 August 2008 – 19 September 2008

03 November 2008 – 14 November 2008

University Brno / Czech Republic

Matusiak, Bartosz

01 Juny 2008 – 31 July 2008

01 September 2008 – 30 November 2008

University Lodz / Poland

Matveev, Yury Dr.

16 July 2008 – 14 September 2008

Institute of Physics and Power Engineering Obninsk / Russian Federation

Otahal, Jan

01 Juny 2008 – 31 October 2008

University Brno /Tschechien

28 January 2008 – 01 February 2008

University Brno / Czech Republic

Ovdiienko, Iurii

07 December 2008 – 13 December 2008

Scientific-Technical Centre for Nuclear and Radiation Safety Kiew / Ukraine

Pivovarov, Valeriy Dr.

16 July 2008 – 14 September 2008

Institute of Physics and Power Engineering Obninsk / Russian Federation

Priede, Janis Prof.

20 July 2008 – 02 August 2008

Coventry University / United Kingdom

Svajlenkova, Daniela

01 Juny 2008 – 31 August 2008

University Brno / Czech Republic

Taniguchi, Shoji Prof.

31 July 2008 – 03 August 2008

Tohoku University Sendai / Japan

Wang, Fang

15 May 2008 – 27 July 2008

Northeastern University Shengyang / China

Meetings and workshops

ANSYS-FZD-Workshop: Multiphase Flow – Simulation, Experiment and Application

114 participants

Dresden-Rossendorf, 22-26 Juni 2008

International Symposium Computational Electro-Magneto-Hydro-Dynamics

70 participants

Venice/Italy, 30 Juni-05 July 2008

Workshop Strömungssimulation

44 participants

Dresden, 25 September 2008

Gießerei-Anwendertag

Messung und kontaktlose Beeinflussung von Metallschmelzen – Anwendung in

Gießereiprozessen

20 participants

Dresden, 12 December 2008

Seminars of the institute

St. Boden, B. Willers, Dr. S. Eckert

Radioskopische Erstarrungsprozesse

10 January 2008

Dr. T. Bauer (TU Dresden)

Prozessintensivierung heterogen-katalysierter Gas/Flüssig-Reaktionen mit Monolithreaktoren

22 January 2008

Dr. F. Schäfer

Störfallanalysen für deutsche Kernkraftwerke – Erfahrungen mit ATHLET

21 February 2008

Dr. M. Schubert, Dr. H. Kryk, G. Hessel

Untersuchungen zur Hydrodynamik in Elektrolysezellen

06 March 2008

Dr. R. Oertel (Dow Olefinverbund GmbH)

Prozesssicherheit in der chemischen Industrie

27 March 2008

Dr. J. Kussin, M. Beyer, Dr. D. Lucas

Neue Luft-Wasser-Experimente in vertikalen DN200-Rohren

03 April 2008

Dr. A. Cramer

Maßgeschneiderte Induktionsheizungen für die Extraktion metallischer Fasern

17 April 2008

Dr. E. Krepper, M. Beyer

Numerische und experimentelle Untersuchungen von Temperaturschichtungsphänomenen in passiven Sicherheitssystemen zur Restwärmeabfuhr

22 May 2008

Dr. E. Altstadt, M. Abendroth

Bruchmechanische Untersuchung eines Reaktordruckbehälters bei einem Thermoschock

05 June 2008

Prof. S. Taniguchi (Graduate School of Environmental Studies, Tohoku University Sendai/Japan)

Some applications of EPM to make environment friendly material processing

31 July 2008

Dr. U. Birkenheuer

Ratentheoretische Modellierung der Entwicklung bestrahlungsinduzierter Defekte in Reaktorstählen

11 September 2008

Dr. G. Laczko (Vattenfall Europe)

Simulation des Boreinspeisesystems und seiner Reaktivitätswirksamkeit in einem Siedewasserreaktor (SWR)

25 September 2008

I. Clifford (Pebble Bed Modular Reactor Pty. Ltd., South Africa)

Overview on the Pebble Bed Modular Reactor Project with regards to analysis software requirements

29 September 2008

Dr. U. Rohde, T. Höhne

Entwicklung von Analysetools für WWER-1000 Reaktortransienten mit räumlicher Veränderung der Temperatur bzw. Borkonzentration am Kerneintritt

09 October 2008

St. Wissel (IER Stuttgart)

Die Bedeutung der Kernenergie im Hinblick auf eine nachhaltige Energieversorgung und in liberalisierten Energiemärkten

23 October 2008

Dr. D. G. Schowalter (Alden Research Laboratory)

On the coupling of CFD computed debris transport and experimental sump strainer head loss tests for nuclear power plant ECCS performance evaluation

03 November 2008

Dr. D. Lakehal (Lecturer at ETH Zürich, General Manager ASCOMP GmbH Zürich)

State of the art in the simulation of multi-phase and complex fluid dynamics

12 November 2008

Prof. T. Schulenberg (Forschungszentrum Karlsruhe)

Flüssigmetall in der Kerntechnik: Ergebnisse aus dem KALLA-Labor)

20 November 2008

K. Ozanyan (University of Manchester)

Tomography Imaging at THz Frequencies

08 December 2008

Dr. M. Schmidtke, V. Danciu

Experimente und Modellierung zum Impinging Jet

18 December 2008

Lecture courses

Frank-Peter Weiß

Zuverlässigkeit und Sicherheit technischer Systeme
TU Dresden, Fakultät Maschinenwesen
Summer semester 2008 and winter semester 2008

Matthias Werner

Zuverlässigkeit und Sicherheit technischer Systeme
TU Dresden, Fakultät Maschinenwesen
Summer semester 2008 and winter semester 2008

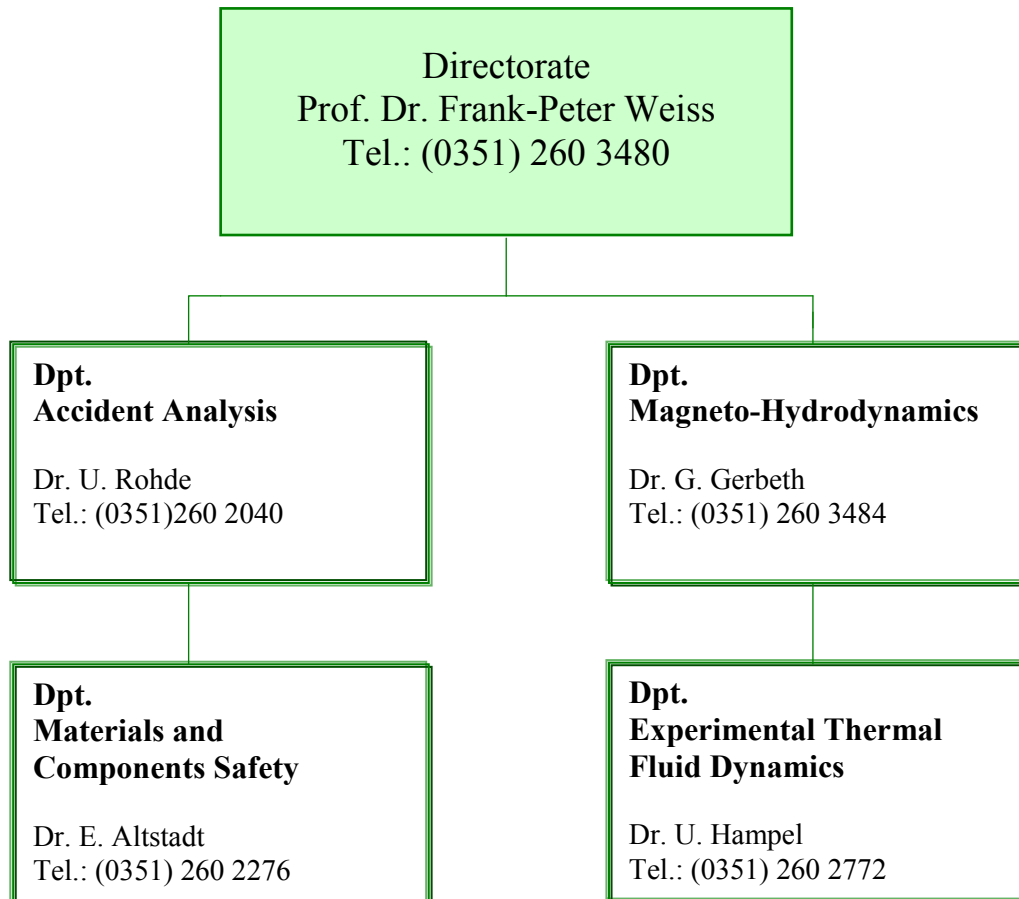
Udo Rindelhardt

Erneuerbare Energien I und II
Technische Universität Chemnitz, Fakultät für Elektrotechnik/Informationstechnik
Summer semester 2008 and winter semester 2008

Uwe Hampel

Computertomographie in der Medizin und Prozessdiagnostik
TU Dresden, Fakultät Elektro- und Informationstechnik
Summer semester 2008 and winter semester 2008

Departments of the institute



Forschungszentrum Dresden-Rossendorf e.V.
Institut für Sicherheitsforschung
Postfach 51 01 19
D- 01314 Dresden

Personnel

Director: Prof. Dr. Frank-Peter Weiß

Scientific Staff

Altstadt, Eberhard Dr.
Apanasevich, Pavel
Arora, Kanwer Shing
Baier, Silvio Dr.
Bergner, Frank Dr.
Beyer, Matthias
Bieberle, André Dr.
Birkenheuer, Uwe Dr.
Boden, Stephan
Carl, Helmar Dr.
Cartland-Glover, Gregory Dr.
Cramer, Andreas Dr.
Eckert, Sven Dr.
Fridman, Emil Dr.
Galindo, Vladimir Dr.
Gerbeth, Gunter Dr.
Giesecke, Andre Dr.
Grahn, Alexander Dr.
Günther, Uwe Dr.
Gundrum, Thomas
Hampel, Uwe Dr.
Hoffmann, Wolfgang Dr.
Hoppe, Dietrich Dr.
Höhne, Thomas Dr.
Kliem, Sören
Konheiser, Jörg
Krepper, Eckard Dr.
Kryk, Holger Dr.
Küchler, Roland Dr.
Laczko, Gabor Dr.
Leonhardt, Monika
Lucas, Dirk Dr.
Merk, Bruno Dr.
Miao, Xingcheng
Mittag, Siegfried Dr.
Pal, Josef Dr.
Rindelhardt, Udo Prof. Dr.

Rohde, Ulrich Dr.
Schäfer, Frank Dr.
Schleicher, Eckhard
Schmidtke, Martin Dr.
Schubert, Markus Dr.
Schuhknecht, Jan
Shatrov, Viktor Dr.
Silva da, Marco Dr.
Stefani, Frank Dr.
Talati, Minaben Dr.
Thiele, Sebastian
Ulbricht, Andreas Dr.
Vallee, Christophe
Viehlig, Hans-Werner Dr.
Weier, Tom Dr.
Werner, Matthias Dr.
Zurbuchen, Conrad
Zhang, Chaojie
Zhang Xiugang
Zippe, Cornelius Dr.

PhD Students

Al-Asqalani, Ahmed-Tamer
Bieberle, Martina
Bilodid, Yuri
Buchenau, Dominique
Cierpka, Christian
Danciu, Dana-Veronica
Dürigen, Susan
Fischer, Frank
Glivici, Varvara
Liao, Yixiang
Räbiger, Dirk
Timmel, Klaus
Tusheva, Polina

Technical Staff

Berger, Torsten
Bombis, Doris
Borchardt, Steffen
Erlebach, Stephan
Franz, Ronald
Futterschneider, Hein
Gommlich, André
Hessel, Günther
Kunadt, Heiko
Lindner, Klaus
Losinski, Claudia
Müller, Gudrun Dr.
Nowak, Bernd
Paul, Sebastian
Pietzsch, Jens
Pietruske, Heiko
Richter, Annett
Richter, Henry
Roßner, Michaela
Rott, Sonja
Rußig, Heiko
Schleißiger, Heike
Schneider, Gisela
Schütz, Peter
Skorupa, Ulrich
Tamme, Marko
Tschofen, Martin
Vetter, Petra
Webersinke, Wolfgang
Weichelt, Steffen
Weiß, Rainer
Zimmermann, Wilfried